INDIAN JOURNAL OF PHYSICS

VOL. XIX

AND

PROCEEDINGS

OF THE

Indian Association for the Cultivation of Science, Vol. XXVIII

(Published in Collaboration with the Indian Physical Society)

(With Twelve Plates)

PRINTED BY NISHITCHANDRA SEN, SUPERINTENDENT (OFFG.), CALCUTTA
UNIVERSITY PRESS, 48, HAZRA ROAD, BALLYGUNGE, CALCUTTA, AND
PUBLISHED BY THE SECRETARY, INDIAN ASSOCIATION FOR
THE CULTIVATION OF SCIENCE
210, Bowbazar Street, Calcutta.

1945

Price Rs. 12 *or* £1-2-6

INDIAN JOURNAL OF PHYSICS

VOL. 19

1945

PART I

	Title	Author	Page
1.	Calculation of *f*-Values Potassium Atom	J. N. Nanda	1
2.	Relative *f*-Values of Potassium Atom	J. N. Nanda	8
3.	Study of the Absorption Spectra of Mercury Vapour with Varying Temperature and Pressure	D. K. Bhattacharya and Jagat Murary	20
4.	On the Raman Spectra of Ethylene Dibromide and Dichlorethylene in the Solid State	S. C. Sircar and B. M. Bishui	24

PART II

	Title	Author	Page
5.	Sound-absorption Characteristics of Indian Materials. Part II	S. C. Chatterjee and N. Dutta	35
6.	Sound Velocity and Inter-Molecular Action in Liquids	Ram Parsad	47
7.	Magnetic Studies on Curpic Ions in Crystals	A. Mookherji	63

PART III

	Title	Author	Page
8	On the production of Mesotrons by Neutral Particles	P. S. Gill and Mela Ram	71
9.	A New Pulse Generator Circuit	B. M. Banerjee	75
10.	Electrical properties of Indian Mica, II. The Effect of Varying Relative Humidity	P. C. Mahanti, M. K. Mukherjee and P. B. Roy	83
11	On the Crystal Structure of Phthalimide. Part I. Determination of Space Group	S. N. Bagchi and M. A. Hasem	93
12	The theory of 180° Magnetic Focussing type of Beta-ray Spectrometer	Ajit Kumar Saha	97

PART IV

	Title	Author	Page
13.	Capture of Electrons by Positive Ions while passing through gases	M. N. Saha and D. Basu	121
14.	Note on Emission bands of the Silver Iodide Molecules	C. R. Sastry and K. R. Rao	136

	Title	Author	Page
15.	On the Theory of Diffusion Pump	K. Ray and N. D. Sen Gupta	138
16.	The Scattering of fast Electrons by Atoms	K. C. Kar	146
17.	Measurement of High Rotational Speed	S. Dutta Majumdar	153

PART V

18.	Wave-treatment of Propagation of Electromagnetic waves in the Inosphere	M. N. Saha and B. K. Banerjea	159
19.	High-pressure Carbon bands and their relation to the Swan System	N. L. Singh	167
20.	On the Hyperfine structure and analysis of the Complex $3S;2\ Sp^{33}D_3-5P^5P_2$ in the first spark spectrum of Arsenic in the Ultra-violet region	S. K. Mukherji	180
21.	Some Nuclear Disintegration	M. F. Soonawala	185
22.	True Relative Intensity distribution from Microphotograms	J. N. Nanda	190
23.	The effect of Transverse Magnetic Field on the Longitudinal Joule-magnetostriction effect in Nickel	O. P. Sharma	202

PART VI

24.	On the Spontaneous Emissions of Neutrons from Uranium Nucleus	S. D. Chatterjee	211
25.	X-ray Diffraction study of Dyed, Mercerised and intensively Delignified Jute fibres	N. G. Banerjee, B. B. Basak and R. K. Sen	217
26.	The effect of Temperature on the Absorption and Fluorescent spectra of Impurity Crystals	S. C. Ganguly	222
27.	Magnetic anisotropy of Molybdenite at different temperatures	A. K. Dutta	225
28.	A Spectroscopic study of an Uncondensed Spark between Copper electrodes in Three different gases at various Pressures	J. Singh and S. Ramulu	235
29.	Electron density map of Anthraquinone Crystals	S. N. Sen	243

AUTHOR INDEX

Author	Subject	Page
Bagchi, S. N. and Kasem, M. A.	Study of Absorption Spectra of Mercury Vapour with Varying Temperature and Pressure	93
Banerjee, B. M.	A new Pulse-Genertor circuit	75
Banerjee, N. G, Basak, B. B. and Sen, R. K.	X-ray Diffarction study of Dyed, Mercerised and intensively Delignified Jute-fibres	217
Bhattacharyya, D. K. and Jagat Murari	Study of Absorption Spectra of Mercury Vapour with Varying Temperature and Pressure	20
Chatterjee, S. and Dutta, N.	Sound Absorption Characteristics of Indian Materials. Part II	35
Chatterjee, S. D.	On the spontaneous Emission of Neutrons from Uranium Nucleus	211
Dutta, A. K.	Magnetic anisotropy of Molybdenite at different Temperatures	225
Dutta Mazumdar, S.	Measurement of High Rotational Speed	153
Ganguly, S. C.	The effect of Temperature on the Absorption and Fluorescent spectra of Impurity Crystals	222
Gill, P. S. and Ram, M.	On the production of Mesotrons by Neutral particles	71
Kar, K. C.	The Scattering of fast Electrons by Atoms	146
Mahanti, P. C., Mukherjee, M. K. and Ray, P. B.	Electrical properties of Indian Mica, II. The effect of varying Relative Humidity	83
Mookherji, A.	Magnetic studies on Cupric Ions in Crystals	63
Mukherji, S. K.	On the Hyperfine structure and analysis of the Complex 3842 $Sp^3\,{}^3D_3 - 5P^3P_2$ in the first spark spectrum of Arsenic in the ultra-violet region	180
Nanda, J. N.	Calculation of *f*-values of Potassium Atom	1
,, ,,	Relative *f*-values of Potassium Atom	8
,, ,,	True relative Intensity distribution from Microphotograms	190
Prashad, R.	Sound velocity and Intermolecular action in Liquids	47
Ray, K. and Sen Gupta, N. D.	On the Theory of Diffusion pump	138

Author	Subject	Page
Saha, A. K	The Theory of 180° Magnetic focussing type of Beta-ray spectrometer	97
Saha, M. N. and Basu, D.	Capture of Electrons by Positive Ions while passing through Gases	121
Saha, M. N. and Banerjea, B. K.	Wave-treatment of propagation of Electromagnetic waves in the Ionosphere	159
Sastry, C. R. and Rao, K. R.	Note of Emission bands of the silver Iodide Molecules	136
Sen, S. N.	Electron density maps of Anthraquinone Crystals	243
Sharma, O. P.	The effect of Transverse Magnetic field on the Longitudinal Joule-magnetostriction effect in Nickel	202
Singh, J. and Ramula, S.	A Spectroscopic study of an Uncondensed spark between Copper electrodes in Three different gases at various Pressures	235
Singh, N. L.	High pressure Carbon Bands and their Relation to the Swan system	167
Sirkar, S. C. and Bishui, B. M.	On the Raman spectra of Ethylene dibromide and Dichlorethylene in the Solid state	24
Soonawala, M. F.	Some Nuclear Disintegrations	185

SUBJECT INDEX

Subject	Author	Page
Absorption Spectra of Mercury vapour with varying temperature Study of,	D. K. Bhattacharyya and Jagat Murari	20
Absorption and Fluorescent Spectra of Impurity crystals, The effect of Temperature on	S. C. Ganguly	222
Beta-ray Spectrometer. The Theory of 180° Magnetic focussing type of,	A. K. Saha	97
Capture of Electrons by Positive Ions while passing through Gases	M. N. Saha and D. Basu	121
Carbon bands and their relation to the Swan system, High Pressure	N. L. Singh	167
Crystal structure of Phthalimide, On the, Part I. Determination of Space Group	S. N. Bagchi and M. A. Kasem	93
Diffusion Pump. On the Theory of	K. Ray and N. D. Sen Gupta	138

Subject	Author	Page
Electromagnetic waves in the Ionosphere, Wave treatment of Propagation of	M. N. Saha and B. K. Banerjea	159
Electron density map of Anthraquinone	S. N. Sen	213
Electrical properties of Indian Mica, II. The effect of varying Relative Humidity	P. C. Mahanti, M. K. Mukherjee and P. B. Ray	83
f-values of Potassium Atom. Calculation of	J. N. Nanda	1
f-values of Potassium Atom. Relative	,, ,,	8
Hyperfine structure and analysis of the Complex 3842 $Sp^{33}D_3-5P^3P_2$ in the first Spark Spectrum of Arsenic in the Ultra-violet region	S. K. Mukherji	180
Intensity distribution from Microphotograms. True relative	J. N. Nanda	100
Joule-Magnetostriction effect in Nickel. The effect of Transverse magnetic field on the	O. P. Sharma	202
Magnetic anisotropy of Molybdenite at different temperatures	A. K. Dutta	225
Magnetic Studies on Cupric Ions in Crystals	A. Mookherji	63
Mesotrons. On the production of, by Neutral Particles	P. S. Gill and Mela Ram	71
Neutrons from Uranium Nucleus. On the Spontaneous emission of	S. D. Chatterjee	211
Nuclear Disintegration. Some	M. F. Soonawala	185
Pulse Generator Circuit A new	B. M. Banerjee	75
Raman Spectra of Ethylene Dibromide and Dichlorethylene in the solid states. On the	S. C. Sirkar and B. M. Bisilui	24
Rotational Speed, Measurement of high	S. Dutta Majumdar	153
Scattering of fast Electrons by Atoms	K. C. Kar	146
Silver Iodide Molecules, Note on the Emission bands of	C. R. Sastry and K. R. Rao	136
Sound absorption characteristic of Indian Materials. Pt. II	S. Chatterjee and N. Dutta	35
Sound Velocity and Intermolecular Action in Liquids	Ram Parshad	47
Spectroscopic study of Uncondensed Spark between Copper electrodes in three different gases at various pressures	J. Singh and S. Ramulu	235
X-ray Diffraction Study of Dyed, Mercerised and intensively Delignified Jute Fibres	N. G. Banerjee, B. B. Basak and R. K. Sen	217

ERRATA

" Sound Velocity and Jutes Molecules Action in Liquids " by Ram Parshad, Ind. J. Phys., Vol. 10, p. 47, 1915.

Page 48, line last but one. Read " For examples see p. 57 " instead of " For example see p. 56 ".

Pages 40, 50, in formula for V and E, the index of powers of R is 6.

Page 54, line 20 from top. Read " One example of above is that of waters " instead of " The above is the example of water ".

,, 58, table of example on p. 50 have come on p. 58, under the Rule " Increase of magnitude of diamagnetic susceptibility......".

CALCULATION OF *f*-VALUES OF POTASSIUM ATOM

BY JATINDER NATH NANDA

ABSTRACT. Employing the empirical and the Hartree fields, the *f*-values of potassium atom have been determined. The Schroedinger equation was integrated by Stoermer's numerical method using close-type formula given by Milne. (A simple interpolation formula for altering the argument interval is also given.) A striking feature of the calculation is that the *f*-value of the first line is greater than unity.

Demands of the sum rule suggest that contribution fowards *f*-value by the continuous absorption at the head of the series limit must be .05, *i.e.*, much larger than the expected value of .0002 from the monotonic curve obtained theoretically by Miss Phillips (1932). It appears, therefore, that the extrapolation of this curve is not warranted Ditchburn's recent experiments showing marked increase in atomic absorption on high frequencies seem to support this view.

Hargreaves (1929) has shown that the oscillator strengths of any absorption line due to a transition from the level *s* to the excited level *r*, is given by

$$f_{rs} = \tfrac{1}{3}(\nu_{rs}/Rca^2)\frac{1}{g_s}\Sigma|I_{rs}|^2 \qquad \ldots \quad (1)$$

where ν_{rs} is the frequency of the radiation, R the Rydberg constant and a the Bohr radius of one quantum orbit of Hydrogen, I_{rs} is the matrix amplitude of the transition *s* to *r*. Summation is for any degeneracy in the levels, which can be neglected here as the determination is to be for the doublets as a whole. Matrix amplitude is known from the eigen-functions of each level. The eigenfunctions for potassium can be calculated following the work of Trumpy (1929) on lithium and of Prokofjew (1929) on sodium. The advantages and limitations of the method have been discussed by the latter. The method with some modifications is given below.

For the case of an atom with centrally symmetrical field, the eigenfunctions (neglecting spin and relativity effects) are represented as

$$\psi_{n,l,m} = X_{n,l}(r)Y_{l,m}(\theta)e^{im\phi}$$

where $Y_{l,m}(\theta)$ are the Legendre functions. The function $X_{n,l}(r)$ satisfies the equation

$$\frac{d^2X_{n,l}}{dr^2} + \frac{2}{r}\frac{dX_{n,l}}{dr} + \frac{8\pi^2m}{h^2}\left[E_{n,l} - V - \frac{l(l+1)}{r^2}\right]X_{n,l} = 0 \qquad \ldots \quad (2)$$

where V is the potential energy in the central field and E is the eigen-value of the state in question. To solve this equation a knowledge of the eigen-values and potential functions is required for which the equations have continuous, finite and single-valued solutions. For the purposes of the present study it is important to use the observed, actual term values and make any required adjustments only in the theoretical field to be used, say Hartree field. But for the empirical field as given earlier by the author (Nanda, 1944) any special corrections are not needed. Thus, for $E_{n,l}$ we may put $-W_{n,l} = -hc\nu_{n,l}$ where $\nu_{n,l}$ is the term-value for n_l in wave numbers. It is possible, then, by a numerical method to solve the equation for any term-value.

Due to the finite interval in numerical integration, and also due to any slight inaccuracy of the field, the eigen-functions may not exactly fulfil the boundary conditions, especially rX may not come out exactly zero at $r=0$. This can be achieved by very slight modification of the field, and in fact, the magnitude P at $r=0$ was never larger than 1% of the largest amplitude.

To solve the wave equation (2) substitute $r=a\rho$ and $P=\rho X_{n,l}$; ρ being r/a, and $V=\frac{Q}{\rho^2}$ where Q is the field function obtained elsewhere in the form $\alpha\rho^2+\beta\rho+\gamma$. The wave equation becomes

$$\frac{d^2P_{n,l}}{d\rho^2}+\left[2\alpha+\frac{\nu_{n,l}}{R}+\frac{2\beta}{\rho}+\frac{2\gamma-l(l+1)}{\rho^2}\right]P_{n,l}=0 \qquad \dots \quad (3)$$

R is the Rydberg constant. At large ρ where the wave function assumes an asymptotic form, we can write the solution as follows :

$$P_{n,l}=e^{-\frac{1}{2}x}x^k\left\{1+\frac{\mu^2-(l+\frac{1}{2})}{x}+\frac{[\mu^2-(l+\frac{1}{2})^2][\mu^2-(l-\frac{1}{2})^2]}{1.2.x^2}+\dots\right\} \qquad \dots \quad (4)$$

where $x=2\rho\sqrt{\frac{\nu_{n,l}}{R}-2\alpha}$; $k=\frac{\beta}{\sqrt{\frac{\nu_{n,l}}{R}-2\alpha}}$; $\mu^2=\frac{1}{4}-[2\gamma-l(l+1)]$

writing equation (3) in the form

$$\frac{d^2P_{n,l}}{d\rho^2}=f(P_{n,l},\rho) \qquad \dots \quad (5)$$

we can construct the table (I) for

$$P_{n,l} \text{ and } \xi_i=h^2f(P_{n,l},\rho_i) \qquad \dots \quad (6)$$

where $h=\rho_i-\rho_{i-1}$; and their backward differences, given by the relation $\Delta^i\nu_i=\Delta^{i-1}\nu_i-\Delta^{i-1}\nu_{i-1}$. The accuracy is not appreciably increased by extending the table beyond $\Delta^4\xi_i$.

TABLE I

ρ_i	$P_{n,l,i}$	ΔP_i	Δ^2P_i	ξ_i	$\Delta\xi_i$	$\Delta^2\xi_i$	$\Delta^3\xi_i$	$\Delta^4\xi_i$
ρ_1	P_1			ξ_1				
ρ_2	P_2	ΔP_2		ξ_2	$\Delta\xi_2$			
ρ_3	P_3	ΔP_3	Δ^2P_3	ξ_3	$\Delta\xi_3$	$\Delta\xi_3$		
ρ_4	P_4	ΔP_4	Δ^2P_4	ξ_4	$\Delta\xi_4$	$\Delta\xi_4$	$\Delta\xi_4$	
ρ_5	P_5	ΔP_5	Δ^2P_5	ξ_5	$\Delta\xi_5$	$\Delta\xi_5$	$\Delta\xi_5$	$\Delta\xi_5$
...	...	...	...	...	...	...	...	...
...	...	...	...	...	...	...	...	...
ρ_i	P_i	ΔP_i	Δ^2P_i	ξ_i	$\Delta\xi_i$	$\Delta^2\xi_i$	$\Delta^3\xi_i$	$\Delta^4\xi_i$

After putting down a few values from asymptotic expression at large distances, the integration ahead towards lesser distances is carried out in the following manner. Stoermer's formula gives a trial value of $\Delta^2 P_i$ by the relation

$$\Delta^2 P_i = \xi_{i-1} + \tfrac{1}{12}(\Delta^2 \xi_i + \Delta^3 \xi_i + \tfrac{19}{20}\Delta^4 \xi_i + \ldots) \qquad \ldots \quad (7)$$

Simple addition or subtraction in the first two columns of the table yields a trial value of $P_{n,l}(\rho_i)$. Using this value of $P_{(i)}$ and the field Q we get ξ_i from equation (6) and right hand side of the table is completed as a trial value. Now a check is applied by the closed type formula (Milne, 1933) which requires

$$\Delta^2 P_i = \xi_{i-1} + \tfrac{1}{12}(\Delta^2 \xi_i - \tfrac{1}{20}\Delta^4 \xi_{i-1} + \ldots) \qquad \ldots \quad (8)$$

Thus, the trial value is altered till the formula (8) is satisfied.

The starting point in this computation is so chosen that the value of P is very small, below significance so far as the main body of the P column is concerned. To save labour, the value of the interval for ρ may be as large as unity in the region $\rho > 2$, since the field function Q is same in the region greater than $\rho = 6.31$ and further, between $\rho = 1.90$ and $\rho = 6.31$ it is given by a single expression. It is only between $\rho = 0$ to $\rho = 1.9$ that there are five different expressions for Q, and so below $\rho = 1.9$ the interval should be small, say .1. To interpolate P between the interval ρ_i and ρ_{i-1} for a small fraction $x/h = p/10$ (let) above the ith point, the formula that can be best used is given below:

$$P_{i-p/10} = P_i - \left(p.\frac{\Delta P_i}{10} + \frac{p(10-p)}{|\underline{2}}\,\frac{\Delta^2 P_i}{10^2} + \frac{p(10-p)(20-p)}{|\underline{3}}\,\frac{\Delta^3 P_i}{10^3} + \ldots\right). \quad (9)$$

The values at $\rho = 2.4$, 2.3, 2.2, 2.1 are known and further integration can be

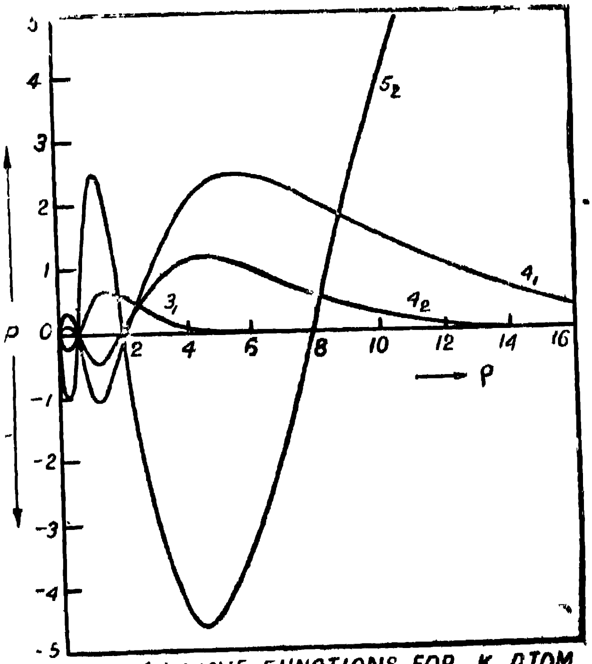

FIG 1(a) WAVE FUNCTIONS FOR K ATOM
(UNNORMALISED)

carried out for $h'=.1$. In this manner, the eigen-functions $P(\rho_i)$ have been determined for the levels 4_0, n_1 (n from 2 to 8). See figure I(a) and I(b).

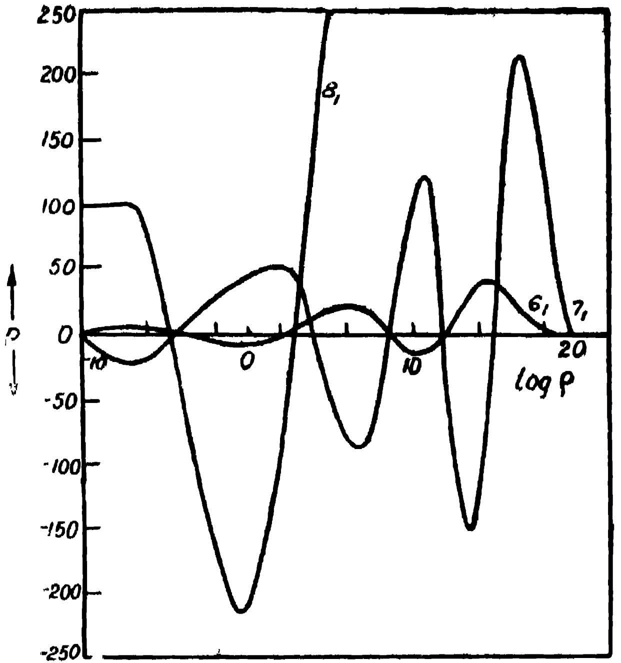

FIG. 1(b) WAVE FUNCTIONS FOR K ATOM (UNNORMALISED)

It can be shown that the square of the matrix amplitude $|I|^2$ for the transition 4, 0 to n, 1 is given by the relation

$$|I|^2 = a^2 \left\{ \frac{\left(\int_0^\infty \rho P_{n,1} P_{4,0}\, d\rho\right)^2}{\int_0^\infty P_{n,1}^2\, d\rho \int_0^\infty P_{4,0}^2\, d\rho} \right\} = a^2 S_{n,1;\,4,0} \qquad (10)$$

substituting the above in (1), we get

$$f(4,0 \rightarrow n,1) = \frac{1}{3}\,\frac{\nu_{n,1\rightarrow 4,0}}{R}\,S \qquad \ldots \quad (11)$$

where ν is the absorbed frequency in wave numbers. The integrals for knowing S were found graphically. For higher levels, the integration may be done numerically by well-known Durand's rule or Simpson's rule.

The calculated f-values are given in Table II. In order to study the effect of any change in the field, the calculations were repeated with the Hartree field and the values with this field are given in column four of the table. However, since the boundary conditions for P at $\rho=0$ were much better observed by the use of the empirical field than with the uncorrected Hartree field (1934), the empirical field values should command greater reliance.

TABLE II

No.	Transition n,l to n,l	f-value empirical field	f-value Hartree field
1	4,0 to 4,1	1.08	1.02
2	4,0 to 5,1	1.18×10^{-2}	$1,33 \times 10^{-2}$
3	4,0 to 6,1	2.5×10^{-3}	3.1×10^{-3}
4	4,0 to 7,1	3.1×10^{-3}	3.2×10^{-3}
5	4,0 to 8,1	6.6×10^{-6}	6.0×10^{-6}
6	4,0 to 2,1	-3.55×10^{-3}	-2.83×10^{-3}
7	4,0 to 3,1	-14.5×10^{-2}	-10.7×10^{-2}

The inverse transitions (6) and (7) are calculated on the assumption that the wave functions are separable.

DISCUSSION

1. A striking feature of the calculations is that the f-value of the first line is greater than unity. This is not against the sum rule of Thomas and Kuhn, since the inverse transition 4.0 to 3,1 is quite strong. It will be of interest to verify this point experimentally by a new determination of the absolute f-value of this line. The value observed by Weiler (*loc. cit.*) from observations on anomalous dispersion by Hook method is 1.00.

2. Ratio of f-values for the first two lines is 91·5 (empirical field) and 76.7 (Hartree field). The experimentally observed value from the Hook method is 111.5 (Prokofjew and Gamow (1927), and 98.5 Weiler (1929). Only the first two lines have been studied in this manner. There is no experimental data on observations in total absorption. Experiments, however, are in progress in this Laboratory to study the total absorption of these lines on infra red photographic plates.

3. Ratio of the third line to the fourth is slightly less than unity. Experiments of the author in total absorption (to be described in a subsequent paper) show them to be of the same order of intensity. In fact, the lines in total absorption show that the ratios do not follow a rational scheme. After some lines have shown a steady decrease in intensity, there is a pair of lines of almost same intensity, and the experimental errors are such that we cannot definitely say which is the stronger and which the weaker of the two.

4. An interesting point from the calculations appears to be the extreme weakness of the line (5). The ratio of f-values of fourth and fifth lines is more than 500. There appears to be no chance for its verification. The experimental value from absorption is even less than two. The theory will have to be modified in the fundamentals, and probably exchange effects will lead to the right order results. So far as the theory outlined above goes, the consistency of the work will be apparent from the following argument.

Hargreaves (*loc. cit.*) has shown that the f-value of a line ending at a higher level with large n can be approximately determined if we know the rate of variation of the f-value at the series limit.

$$f_{n' \to n} = \frac{C}{n^3}\left(\epsilon_0 - \frac{1}{n^2}\right) \qquad \ldots \quad (12)$$

where n' is the ground state, and ϵ_0 is the term-value in hcR units. C is given by the relation

$$C = \frac{2}{\epsilon_0}\left(\frac{df}{d\epsilon}\right)_{\text{series limit.}} \qquad \ldots \quad (13)$$

Miss Phillips has calculated $\left(\frac{df}{d\epsilon}\right)$ at series limit for potassium atom to be .0024.

Substituting this in above, we get

$$f_{n' \to 8} = \frac{2 \times .0024}{.319} \frac{(.319\text{-}1/64)}{8^3} = 8.9 \times 10^{-6}.$$

which compares favourably with the theoretical value 6.6×10^{-6}.

5. The calculated f-values suggest a very large continuous absorption from the requirements of the f-sum rule. The rule states for Potassium atom in the normal state :—

$$\sum_{n=4}^{\infty} f_{4,\,0 \to n,\,1} + (f)_{\text{cont}} - f_{4,\,0 \to 2,\,1} - f_{4,\,0 \to 3,\,1} = 1 \qquad \ldots \quad (14)$$

lines 4, 0 to 4, 1 to 4, 0 to 8, 1 have been evaluated. The sum for the remaining lines

$\sum_{n=8}^{\infty} f_{4,\,0 \to n,\,1}$ can be found from the $\frac{1}{n^3}$ law and its value is 2.6×10^{-5}.

Substituting in above we get, $(f)_{\text{cont}} = {}^{\cdot}05$ (empirical field) and it is still larger for Hartree field. But the value obtained from integration of the curve obtained by Miss Phillips is only .0002. This might mean that extrapolation of this curve showing monotonic decrease is not warranted. The experimental observations of Ditchburn recording this increase in continuous absorption support this view. But regarding the explanation of the increase being in a region far beyond the series limit, further calculation including exchange effects are needed.

CONCLUSION

The f-values of few members of the principal series lines of potassium have been determined and f-value for continuous absorption inferred. A glance at these values shows the arbitrary relation between the f-ratios and the line numbers. The calculations are, however, for a single atom. In order to examine the theory critically, the experiments must be carried on at very low vapour pressures and with no disturbing foreign gases. But it is not easy to conduct such experiments, since quartz windows on the absorption tube are attacked by potassium vapour and so the ends of the tubes have to be kept cold. This necessitates the use of some foreign gas to guard against rapid distillation of the metal to the cooler portions. Further at low vapour pressures and low foreign gas pressures the lines are very fine and their photometric measurements are very difficult. For quantitative measurements we, therefore, need broad lines. How far the broadening agents effect the f-values, has yet to be investigated in detail.

My thanks are due to Dr. P. K. Kichlu, who suggested this problem, for continual interest and help, and to Mr. B. M. Anand for his invaluable advice and criticism.

PHYSICAL LABORATORY,
GOVERNMENT COLLEGE,
LAHORE.

BIBLIOGRAPHY

Ditchburn (1942), *Proc Roy. Soc.*, **181**, 386.
Hargreaves (1929), *Proc. Camb. Phil. Soc.*, **25**, 75.
Hartree (1934), *Proc Roy, Soc.*, **143**, 506.
Milne (1933), *Bull. Nat. Re. Council Amer.*, **92**, 83
Nanda (1944), *Ind. Jour. Phy.*, **18**, 172.
Phillips (1932), *Phy. Rev.*, **39**, 905.
Prokofjew (1929), *Zeits. fur. Phy.*, **58**, 255.
Prokofjew and Gamow (1927), *Zeits. fur. Phy*, **44**, 887.
Trumpy (1929), *Zeits. fur. Phy.*, **57**, 787.
Weiller (1929), *Ann. Der. Phy.*, **1**, 361

2

RELATIVE *f*-VALUES OF POTASSIUM ATOM

By JATINDER NATH NANDA

(Plate I)

ABSTRACT Principal series lines of potassium have been studied in absorption. Construction details for the high intensity hydrogen discharge tube as a source for ultraviolet light, and a sensitive intensity reducing device are given. On account of uncertainty in the number of absorbing atoms due to the presence of foreign gas and cold ends in the absorption tube, relative *f*-values alone have been worked out.

f-value of the first line relative to the second varies with the conditions of experiment from 16.1 to 6.4; the theoretical value is 91.5 and experimental value from anomalous dispersion Hook method is 98.5. Extremely low values obtained from the present direct method need clarification. On the photographic plates, in addition to the atomic lines, strong molecular bands also appear, though the expected number of K_2 molecules is only 3 to 4% of the total vapour present.

There is no sudden drop of intensity from the fourth to fifth lines as given by theory. However the intensity does not decline smoothly with the series number. Some lines show slightly greater intensity than the preceding ones (*e.g.*, 10th and 13th). The continuum at the head of the series limit shows a broad minimum at about 2700 Å, the absorption increasing towards shorter wave lengths. This anomaly has also been reported by others.

1 INTRODUCTORY

The study of intensity of spectral lines have assumed great importance due to astrophysical and theoretical significance. Absorption spectra are preferred on account of comparative ease in controlling the conditions for obtaining these. Alkali aborption spectra have received considerable attention on account of their simple structure. Various methods have been developed to measure the line intensities (Mitchell and Zemansky, 1934).

Besides other methods the direct method, that of measuring the area under the graph for absorption coefficient with frequency, has been employed by Trumpy (1925, 1927) for evaluating relative *f*-values of lithium and sodium. A modification of the method, employing the area under the absorption contour itself (Total absorption method) has been extensively used by King and others (1940) for *f*-values of copper, etc. Continuous absorption at the head of principal series has been studied by the direct method for lithium, sodium, potassium and caesium by various authors, *e.g.*, Trumpy, Bott, Ditchburn and co-workers.

For the last few years experiments on absorption spectra of potassium under varying conditions of temperature and foreign gas pressure have been conducted in this laboratory. Potassium was selected since its line absorption has not been studied by absorption methods. The results and the methods employed are given as follows :

2 ABSORPTION TECHNIQUE

The experimental set up for observing photographically the absorption of an alkali vapour consists of the following four parts (Fig. 1).

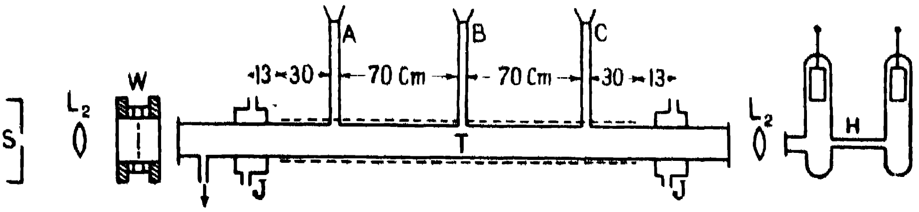

Experimental Arrangement

FIG. 1

(*i*) The source for continuous background (H).
(*ii*) The absorption tube (T) where the alkali metal is vaporized.
(*iii*) An intensity reducing device (W) to calibrate the photographic plates.
(*iv*) The spectrograph (S)

A brief description of each is given below :—

(*i*) The background source.—The principal series of potassium extends from infra-red to near ultraviolet, the resonance line having a wavelength about 7700 Å and the limit being at 2850 Å. For the first and the second member (4046 Å) a straight filament tungsten in glass lamp (10 Volts 5 Amps.) was used as the source. It was fed by a transformer from A.C. mains. The current was seen to remain constant in any exposure. The photographs were taken on Kodak infra-red plates.

For the region of second line onwards a high power water-cooled hydrogen discharge tube gave an intense ultraviolet background illumination. The photographs were obtained on Ilford process plates. The tube was constructed especially for the purpose. We may here mention briefly its method of preparation since the tube is practically indispensable for ultraviolet quantitative photometry. It possesses all the prerequisites of such a source namely, intensity, steadiness, and almost continuous spectral distribution of intensity.

The discharge tube was entirely made of pyrex excepting the quartz window which was wax-jointed at one end. The conditions of discharge in a similar tube have been studied by Bay and Steiner (1927). For special requirements the intricate designs suggested by Lawrence and Eldefassen (1930) and Kistiakowsky (1931) may be followed. The discharge tube, employed in these experiments is shown in Fig. 2. It consists of a long tube L (50 cms. long and 5 mms. bore) connecting two upright tubes G (20 cms. long, 3 cms. wide) in which hollow cylindrical aluminium electrodes (E) are sealed by tungsten pyrex seals.

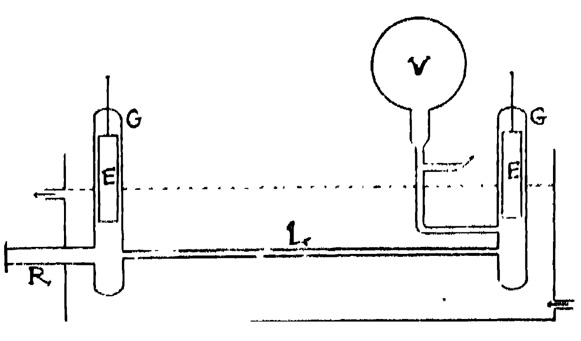

Hydrogen Discharge Tube

FIG. 2

The electrodes do not touch the glass walls, being of slightly (2 mms.) less diameter than the tubes G. One of the side tubes is connected to a large flask (2 litres capacity) which does not allow changes in pressure due to discharge. The tube is to be viewed end on for getting large intensity. A side tube R (12 cms. long 2 cms. wide) carrying the quartz window at one end is sealed on to one of the side tubes exactly in line with the discharge tube. The whole tube dips up to the middle of the electrodes in water renewed continously in a galvanized iron tank. The tube R projects out of an opening in one of the side walls of the tank. The tube is held in position by a strong wooden frame supported on four legs fixed on the support of the tank. In this position the tube has stood for months without giving the least trouble.

Pure and dry hydrogen is introduced by the side capillary C which is later sealed off at the required pressure (about 1 mm.) inside the tube. Hydrogen was prepared by electrolysis over nickel electrodes, of barium hydroxide solution in distilled water. The gas entered the tube through a calcium chloride tower and a liquid air trap in succession. The collecting tube could be isolated by a vacuum stopcock. The whole apparatus could be evacuated to very low pressures by a mercury diffusion pump, the pressure being read on a McLeod gauge. First the apparatus was rinsed with hydrogen by repeated fillings and evacuations. Later it was exhausted continuously while individual parts of the tube were gently heated by flame to remove any loose traces of gas. Finally after it had been again alternately filled with hydrogen and exhausted, the stopcoks were closed when the pressure inside was 1 mm. On observing the discharge, first various bands appear on the plate, but when purifying action of the discharge has continued for some time (about ten hours) the spectrum consisted of a beautiful continuum practically free from any structure. The tube was then sealed off. The tube gives very intense light and consumes more than a thousand watts at 3000 volts.

Due to the length of the tube, the collimating lens must be of large focal length so that it has a greater depth of focus. A quartz lens L_1 of 86 cms. focal length was placed at distance of 50 cm. from the end of tube. The parallel beam of light passed through the quartz windows enclosing the absorption tube, and converged through a lens L_2 of 50 cm. focal length on to the slit of the spectrograph. The focal length of this lens was large so that the light image on the slit is of some size. The optical system is clear from Fig. 1.

(*ii*) The absorption tube T was of three meters length and 2.5 cm. internal diameter. It was constructed by end to end welding of short lengths of thin steel tubing. The ends were closed by pyrex glass caps carrying annular discs of brass with groves to support plane quartz windows of 1 cm. free aperture. All the joints at the ends were made by sealing wax. Three iron tubes A, B, C each 30 cms. long and having one cm. bore were welded to the main tube at regular intervals. Alkali metal could be introduced directly into the absorption tube through these side tubes in the beginning of the experiment. Later pyrex glass tubes carrying iron-constantan thermocouples were introduced in each of the tubes. In the working position the side tubes were kept inclined to the vertical so that the ends were not heated up by the heat from the heating coils on the main tube ; and the thermocouple tubes could be held in position by rubber corks and plasticene. The hot junction of the thermocouples was kept well into the main tube, the cold junction was kept at room temperature and the temperature differences were read on a Crompton potentiometer.

Since the glass or quartz windows are attacked rapidly by the alkali vapour, the ends of the tube had to be kept cold by circulating water in the end jackets J. A side tube F connected the absorption tube through a short length of rubber tubing to various gas reservoirs (He, A, N_2), a McLeod gauge, a mercury manometer, and the evacuation pump. The whole assembly must be leak tight.

The greater part of the length of the absorption tube could be heated by a heating coil of nichrome wire (divided into 8 segments in parallels drawing up to 20 amps. in all) insulated from the tube by asbestos sheet and heavily lagged by asbestos rope. The temperature could be fairly kept constant by altering the resistance in series with the heating coils.

(*iii*) Since the intensity of the source varies over the photographed region and the photographic plate has different response at different wavelengths, a simple relation between the intensity and the ensuing blackening cannot be employed everywhere. It is therefore necessary to use some calibration marks on the plate. Intensity is reduced in a known ratio and a calibration exposure is obtained, keeping the time of exposure same as that used for absorption or background exposures. Out of various intensity reducing devices, the wire screen type has been selected on account of its simplicity and greater sensitivity. Ditchburn's (1927) rotating sector device has not been used since it cuts off the available intensity to one half.

A screen is formed by stretching a number of metallic strips of uniform width on a wooden ring. From the mean diameter of the strips and their total length inside the ring, the area obstructed by the scren is calculated. Each of such screens thus transmits a certain percentage of light falling on it.

The ring supporting the screen is fitted in the wooden tube capable of rotation in ball bearings at the ends. The tube is rotated by a low power motor. The screens are to be rotated to produce randomness of the transmitted pattern on the collimating lens of the spectrograph. It also averages out any radial variation in the beam of light. The screen is placed in the optical path near the absorption tube within the focal distance of the condensing lens. Many calibration spectra can be obtained by crossing any two of such screens. To avoid diffraction effects the breadth of the wires or the openings should not be less than 1 mm.

Sensitivity (S) may be defined for such a device by

$$\frac{1}{S} = \frac{1}{I} \cdot \frac{dI}{dN}$$

where I is the transmitted intensity and N the number of equidistant wires of breadth a in a square mesh (for simplicity) of length L.

$$\therefore \quad \frac{1}{S} = \frac{1}{I} \cdot \frac{a}{L} \quad \text{or} \quad S = I \cdot \frac{L}{a}.$$

If L = 1 cm, a = 1 mm. then S = 101 which is larger than that for any other device. A possible drawback in the device is that the calibration points are fixed, whereas in other devices the transmitted intensity can be altered to suit the exposure under investigation. But in study of line absorption this is not important due to wide variations in any line.

Actually four such meshes were constructed and by combining some in pairs, in all seven distinct calibration spectra could be taken corresponding to following transmissions 23.0, 53.5, 76.5, 85.5, 65.4, 40.9, 28.5.

(*iv*) A Hilger medium size E 2 quartz spectrograph was used. It has a dispersion of about 12 Å in the ultraviolet and about 100 Å in the near infra-red region. Due to relatively low dispersion of the instrument only first two of the potassium doubles could show a measurable separation of the components and that too only under conditions of low temperature and low foreign gas pressure. But since the intensities were to be compared for the doublets as a whole a larger dispersion was not considered necessary.

Slit width was kept at 3 μ and it was verified, now and then by measurement with a high power microscope, to remain canstant. Since special thin plates could not be had, the curvature inside the plate-holder was slightly reduced so that 4″ × 10″ plates, cut out of commercial 10″ × 12″ plates on fitting in the holder, do not break by the pressure of the springs.

3. EXPERIMENTAL PROCEDURE

(*a*) *Manipulation of the metal—*

Outer layers of the oxide on the metal balls are scraped off under kerosene oil and the metal is cut into thin pieces. It is then put into the sides tubes after removing the oil by dipping the pieces in ether. The pieces of metal are dispersed in the absorption tube by shaking them with long iron needles which can be introduced through the side tubes. To avoid oxidation, the whole operation must be carried out quickly. As soon as the required quantity of potassium has been put the thermocouples are introduced and fixed in position. The closed side tubes are now tilted to the vertical, and the absorption tube is evacuated by an oil pump. Then a few mms. pressure of foreign gas is introduced to safeguard against rapid distillation of the metal to cooler parts on heating The extra purification of the metal has been found to be not necessary.

(*b*) *Order of exposures—*

A background exposure through the cold absorption tube and with no calibration screen in the path is now taken. The tube is heated by the heating

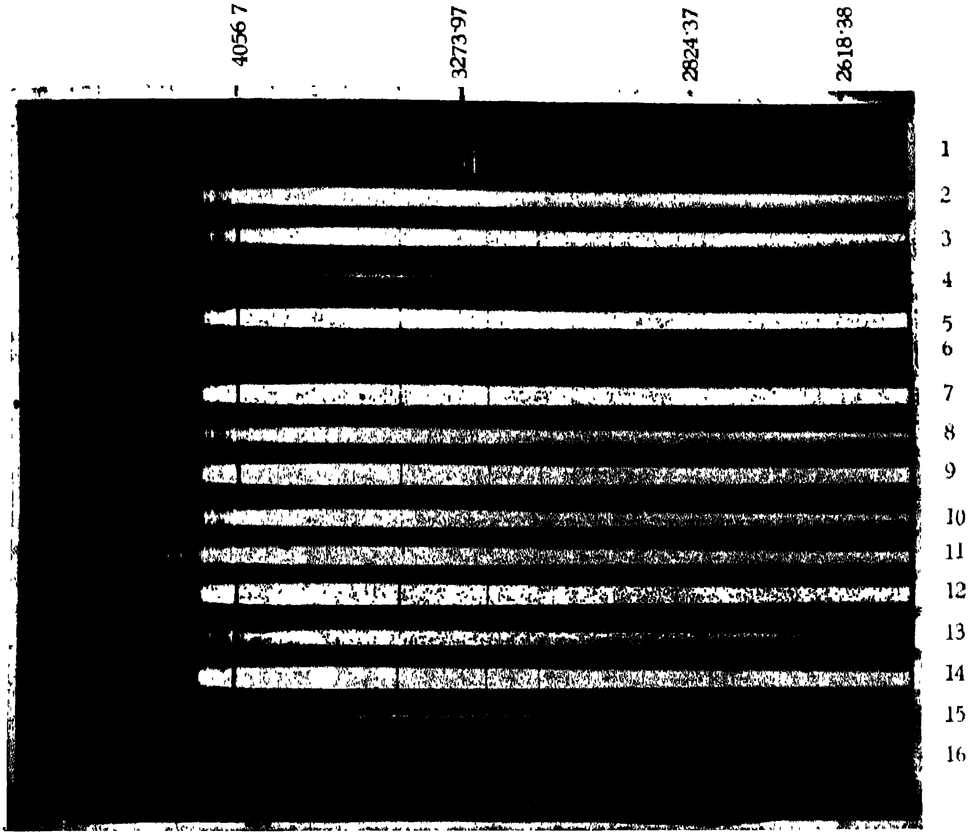

Fig. 1

An Absorption Photograph

Exposure Nos. 2, 11 :—Background exposures

Exposure Nos. 3, 5, 7, 9, 12, 14 :—Absorption under foreign
gas pressures ·7, 1·3, 2·7, 5·4, 8·0, 10·5 cms

Exposure Nos. 4, 6, 8, 10, 13, 15, 16 :—Calibration spectra

Exposure No. 1 :—Copper line spectrum for reference

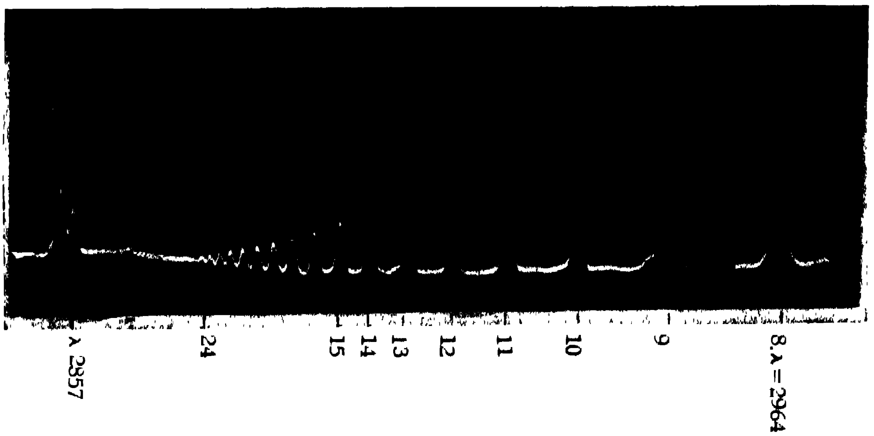

Fig. 2. Microphotogram of Exposure No. 12, Table I
Series lines 8-24.
Doublet near limit 2857 is due to Sodium impurity

coil. After waiting for at least half an hour, so that steady conditions have been reached, the first absorption exposure is obtained. Few more such exposures with varying conditions of temperature or foreign gas pressure (one remaining constant) are also taken on the same plate. Sufficient time is allowed between two exposures. The current in the heating coils and the current in the primary of the transformer feeding the hydrogen discharge tube is kept constant by hand control during any exposure. Exposure time was kept at 10 minutes for the process plates and 5 minutes for the infra-red plates. Three observations of temperature difference for each of the three thermocuples A, B and C. Room temperature and pressure were noted during each exposure. The tube is now allowed to cool and a background exposure and the calibration exposures are obtained. A reference line spectrum of copper for the ultraviolet and of neon for the infra-red region is taken on each plate. Any plate thus contained three or four absorption spectra, two background spectra, and six or seven intensity calibration spectra besides the reference spectrum (Plate 1 A).

(c) *Developing the plates*—

Care is taken to develop the plates evenly. The plate is put in developing solution in such a way that points along any line parallel to the breadth are immersed at the same time. The dishes are rocked gently. After developing and fixing, the plates are thoroughly washed in running water for several minutes. The plates are then quickly dried in a horizontal position under a fan.

(d) *Microphotometry of the plates*—

Plates were microphotometered on a Siegbahn photo-voltaic type microphotometer with wedge coupling. Magnification ratios 7, 15, 20 were used. Higher ratios were not used due to very slow speed of the work on account of lack of a string instrument. Only those lines were selected for microphotometry which did not show completely absorbed centres because the direct method is applicable only to such lines. After getting the microphotogram for the absorption line, the deflections corresponding to calibration exposures at intervals of about 200 Å were recorded. Microphotometer readings for continuous absorption beyond the series limit, some of the calibration deflections, and clear plate readings were taken visually.

(e) *Reading the microphotograms*—

Average of clear plate readings, if they do not show any marked changes, is subtracted from all microphotograph readings. To read the microphotogram accurately, it is mounted in a vertical plane between two glass plates. The readings are taken by a travelling microscope capable of moving in a horizontal as well as a vertical direction. Thus ordinates to correspond to photometer deflections are read against the distance along wavelength scale. Those points are especially read where the absorption contour shows a peak or leaves the base lines or is cut by calibration deflections.

4. METHOD OF CALCULATION

The microphotogram trace for the densest exposure (due to background) corresponds to 100% transmission. The ordinate corresponding to it from the clear plate deflection as zero is noted. Similarly ordinates for other calibration spectra for any wave length region are noted. A graph is drawn between these magnitudes and the percentage transmission. The transmission can then be read off for any point on the absorption contour (Fig. 3).

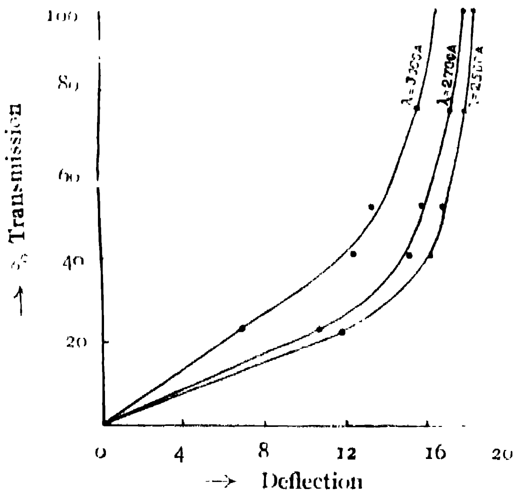

Calibration Curves

FIG. 3

Let T_ν be the % transmission at any ν, then

$$T_\nu/100 = e^{-lk},$$

where k_ν is the absorption coefficient at ν (wave numbers) and l is the length of the absorbing vapour. k_ν evidently $\propto (2-\log_{10}T_\nu)$. Thus for any line the area G under the graph $(2-\log_{10}T)$ against ν is proportional to integrated absorption $\int k_\nu d\nu$. And since $\int k_\nu d\nu \propto Nf$, the area G is a measure of f-values of lines in the same absorption spectrum. Actually the graph was not drawn for ν but for distance x along the records, so G was obtained by multiplying the area under the actual graph by $\frac{d\nu}{dx}$ at the position of the line.

For calculation of absolute f-values we know that

$$\int k_\nu d\nu = \frac{1}{l}\left\{\int \log_e 10\,(2-\log_{10}T_x)\,dx\right\}\cdot\frac{d\nu}{dx} = \frac{G}{l}\log_e 10$$

and also

$$\int k_\nu d_\nu = \frac{\pi c^2}{mc} Nf$$

where N is the number of absorbing atoms per c.c.

$$\therefore f = \frac{mc^2 G \log_e 10}{Nl\pi c^2}$$

N is obtained from the vapour pressure data as follows:

If p is the vapour pressure at T°C then $p_0 = p.\frac{273}{273+T}$ is the reduced pressure and $N = N_0 p_0$ where N_0 is the Avogadro number reduced to one c.c. and 1 cm. pressure, *i.e.*, $N_0 = \frac{A}{22{,}400 \times 76}$. However, since the temperature is not constant along the length of the tube, a simple mean of either temperatures or of vapour pressure is not reliable. Assuming thermodynamic equilibrium a better approximation is to plot the vapour pressure p from known temperature data along the length of the tube, and to reduce the resulting curve to 0°C on the same graph. The area of this curve now gives the product $p_0 \times l$ to be used in the formula (Fig. 4). But due to the presence of cold spots on the tube and due to the disturbing effect of the foreign gas, actual vapour pressure can not be assumed to be given by the vapour pressures at those temperatures. Hence absolute f-values from this arrangement cannot be determined with any accuracy.

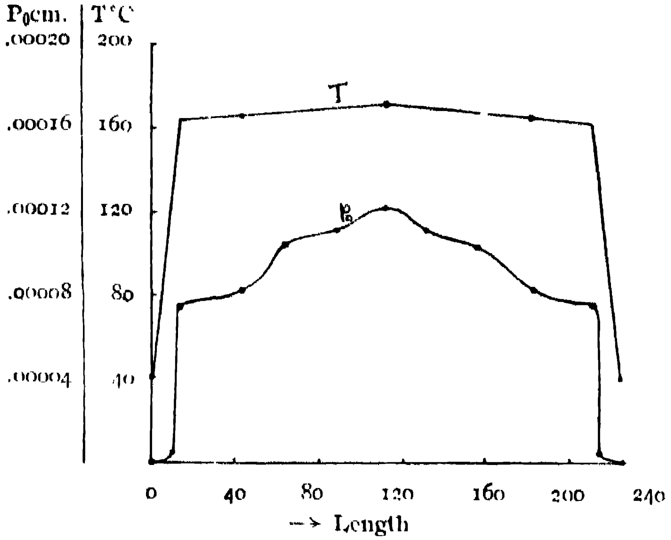

Graph to get number of absorbing atoms (Area p₀b)

FIG. 4

5. ACCURACY OF THE METHODS ADOPTED

(*i*) *Measurement of absolute f-values.*—Besides the errors to be treated under relative measurements an important error in the measurement of absolute values originates in temperature measurement. An error of two or three degrees in knowing the temperature alters the vapour pressure and so the results by about 10%. The partial pressure of the atoms in the vapour is also uncertain by a factor of about 3%.

The greatest error comes in if we assume the vapour pressure at any point along the axis to correspond to the temperature at that point. With this assumption the calculation of the f-value for the second line was attempted. In the case when foreign gas pressure was about 50 cm. the f-value came out to be 100 times that when the pressure was only 7 mm. The bigger value itself was only one-third the value given by theory (.012). Extremely low values for low foreign gas pressures appear to show that the actual quantity of vapour giving absorption is much less than that assumed on vapour pressure data. Ditchburn, Tunstead and Yates (1942) have studied this problem of dynamic equilibrium of a vapour assuming the foreign gas to remain stationary. Though their results in the form given cannot be applied to the present shape of the tube, yet these amply show that the amount of vapour increases progressively with foreign gas pressure. These considerations restrict the utility of the method to determination of relative *f*-values only, where a knowledge of the exact amount of absorbing vapour is not needed.

(*ii*) *Errors affecting relative f-values as well.*—Systematic errors which may come up due to progressive changes in intensity of the sources or systematic variations in the developed plates have been reduced to minimum by intermixing at random the absorption and calibration spectra on the plates and by careful developing.

(*a*) *Errors due to variations of sources.*—By adjusting the pressure inside the hydrogen discharge tube to a value slightly higher than that required for least damping, the tube is made self-stabilizing. Changes of current cause compensating changes in pressure. The tube runs with practically no change in intensity unless it has been standing idle for long when it requires about half an hour to come to stable conditions. Fluctuations in the primary current due to supply mains have to be controlled by hand. The ammeter reading fluctuations averaged over the time of exposure do not exceed .25%.

The light of the photometer bulb shows 1% variations. It was lighted from the mains with a stabilizing circuit given by Potter (1934). Accumulators are not used since they are apt to run down which necessitates repetition of photometry of calibration spectra before and after the absorption is studied.

(*b*) *The unevenness of the plate.*—There can be three types of errors, due to grain of the plate, variations due to uneven development and non-uniformity of the sensitive film. These errors are least in fresh fine grain process plates. Any exposures near the edges of the plates are rejected. Under average conditions contribution from such errors may sum up to 2%, but with special care it is reduced to less than 1%.

(*c*) By far the largest errors arise from the photographic intensity measurements. On average a mistake of about 5% here causes the exponent to vary by ±.05 independent of its magnitude. This causes an error of about 3% in bigger absorption coefficients and a greater error in relatively weak absorption. Greater error thus comes in from the nature of graphical methods employed. Lines showing strong absorption give much more reliable figures than those showing weak absorption. An estimate of accuracy was made by repeating a number of times the microphotometry of two lines, one about 10 times stronger than the other. The maximum divergence of the figures for stronger lines was 2% and for weaker 10%. But as any two neighbouring lines are generally of less intensity ratio and are microphotometered for the same setting of the photometer, the error in the ratio is correspondingly less. Thus for large ratios the probable error in all is about 10% and for ratios between lines of small intensity variation the errors vary between 5% and 8%.

6. OBSERVATIONS AND RESULTS

It was expected that better comparison with theory would be possible if low temperature and low foreign gas pressure were employed. In majority of cases the foreign gas pressure was only a few millimeters just to guard against distillation of the metal to cooler portions. Temperatures were between 200°-400° C and effective concentration of vapour corresponded to still lower temperatures on account of rapid diffusion of the metal. In all about 400 exposures were given, out of which 150 were absorption spectra and others intensity and wavelength calibration spectra. About 30 absorption exposures were on infra-red plates and the rest on process plates. The observations are listed below.

(1) On increase of pressure of foreign gas it appears as if a greater amount of vapour begins to absorb; the intensity of lines as well as their number increases (Plate IB), which shows that a larger foreign gas pressure makes the vapour tend to accumulate and build up the vapour pressure corresponding to the temperature at that place. This should also explain similar observations of Bhattacharya and Sinha (1943). Difficulties in calculation of absolute *f*-values arising from this uncertainty in the amount of absorbing vapour has been already dicussed in 5(*i*).

(2) The experimental data for the exposures selected for photometry is given in the first 5 columns of Table I(*a*) and in the rest of the table the areas (G) proportional to *f*-values are given. The areas are also reduced on a scale of *f*-value for the second line as unity (figures in brackets). The table is completed for higher numbers on some of the plates in the part I(*b*). The mean results are tabulated in Table II. The theoretical values (Nanda, 1945) reduced to the same scale are given in brackets. The *f*-ratios are also seen to be affected by the conditions of excitation.

(3) Lines 16 to 24 were not clearly resolved. Due to limited dispersion of the spectrograph, these lines overlap and an apparent continuous absorption before the series limit results (Plate I(*c*). This explanation has been given by Trumpy (1928) in connection with his observations on absorption of sodium vapour. The values of the individual lines have been calculated assuming arbitrary symmetrical distributions in the lines, giving the observed curve as their sum.

(4) Continuous absorption shows a minimum at about 2700 Å. The results are analogous to those of Ditchburn and others (*loc. cit.*) After a weak maximum at the series limit the absorption diminishes and then rises again towards the shorter wavelengths.

(5) Band absorption is very marked. The expected small percentage of molecules present at these temperatures appears to be very effective. Bands on both sides of the atomic series lines were present and the position of these was unaffected by the nature of filling gas. The strength of the band system $C^1\pi \rightleftharpoons A^1\Sigma$(6280 Å–6925 Å) on the above *f*-value scale is given in the Table I(*a*).

TABLE I(*a*)

No	Filling Gas		Temp. °C			Rel. Absorption in lines etc.				
	Nature	Pressure	A	B	C	1	2	3	4	5
1	N_2	3 mm.	222	228	228	78.5 (16 06)	4·9 (1.0)	(Band 91.8)		
2	N_2	14 mm	222	228	228	142 (9 28)	15·3 (1.0)	(Band 38.4)		
3	A	11 mm.	238	249	237	12.9 (6.45)	2.0 (1.0)			
4	A	11 mm.	266	281	267	38 6 (6.43)	6 0 (1.0)			
5	A	11 mm.	297	314	298	162.0 (13.84)	11.7 (1.0)			
6	N_2	10.8 cm.	163	171	167		3·15 (1.0)	.98 (.311)		
7	N_2	59 cm.	164	171	168		8.83) (1.0)	3.16 (358)		
8	A	7 mm.	264	282	265		4.64 (1.0)	1 77 (.382)		
9	A	7 mm.	300	314	300		11.4 (1.0)	4 67 (.410)	2.84 (.249)	1·51 (.132)
10	A	9·4 cm.	290	309	302			5·78 (,410)	4.03 (.286)	1·95 (.138)
11	A	7 mm.	358	381	352					
12	A	7 mm.	394	412	381					

TABLE I(*b*)

Line No.	Plate No. 11	Plate No 12	Line No.	Plate No 11	Plate No. 12
5	9·10 (.135)		15	·77 (011)	4·0 (011)
6	6.77 (.098)		16	61 (.009)	3 4 (.009)
7	3·98 (.058)		17	·49 (.007)	3·3 (.009)
8	2.38 (.034)	13·0 (.034)	18	.40 (.006)	2.6 (.007)
9	1 73 (.025)	10 4 (.028)	19	·35 (.005)	2·5 (.007)
10	2.07 (.030)	9.8 (.026)	20	.28 (,004)	2.3 0(006)
11	1.95 (.028)	7.9 (.021)	21	.20 (.003)	2.1 (.006)
12	1.38 (.020)	6.3 (.017)	22		1.9 (.005)
13	1.48 (025)	5·1 (.014)	23		1.7 (.004)
14	0.92 (.013)	4·4 (.012)	24		1.6 (.004)

TABLE II

Line No.	Relative *f*-value	Line No.	Relative *f*-value	Line No.	Relative *f*-value
1	6.4 to 16.1 (91.5)	9	026	17	.008
2	1.0 (1.0)	10	.028	18	.006
3	·365 (.2 2)	11	.025	19	.006
4	.268 (.263)	12	018	20	.005
5	.135 (.0006)	13	.018	21	.005
6	098	14	.012	22	.005
7	.058	15	.011	23	.004
8	.034	16	.009	24	.004

(6) Continuous molecular absorption overlaps the first few members of the principal series. The line strength was calculated by assuming the lines to be imposed on continuous absorption, thus altering the magnitudes of calibration transmissions.

7. DISCUSSION OF RESULTS

The chief points needing careful investigation emerge to be the nature of foreign gas effects on the intensity ratios; and the ratio of the first line to the second line being only between 6.4 and 16.1 whereas the theoretical value as well as that obtained from experiment on anomalous dispersion is about 100.

The ratios have been calculated by the direct method, regrded as applicable since the records show pointed peaks in the centres much below complete absorption range. It would not be out of place to mention that the apparent width of these lines under a high power miscroscope was for the narrowest lines about four times the width of the microphtometer slit image (12μ). The lines were obtained by a spectrograph slit of width 3μ which covers a range of about .04 Å on the photographic plate in the ultraviolet region and .3 Å in the infra-red region. The lines therefore fairly represent true distributions. The microphotometer slit had a fixed width, but a finer slit would be preferable. Other problems are regarding the great intensity of the bands and anomalous continuous absorption.

In the end I wish to thank Dr. P. K. Kichlu for suggesting the problem and for his continued interest and encouragement during the course of these experiments. I am indebted to Mr. B. M. Anand for discussions bearing on problems connected with photographic photometry. My thanks are also due to Mr. Kundan Lal, M.Sc., and Mr. C. L. Arora, M.Sc., for help in taking some of the absorption photographs.

The author is very much indebted to Prof. M. N. Saha, F.R.S., of the University of Calcutta for allowing the author to use the microphotometer of his laboratory in the earlier stages of the work.

PHYSICS LABORATORY,
GOVERNMENT COLLEGE,
LAHORE.

REFERENCES

Bay and Steiner (1927), *Zeits. f. Phy.*, **45**, 337.
Bhattacharya and Sinha (1943), *Ind. J. Phy.*, **17**, 131.
Ditchburn (1927), *Proc. Camb. Phil. Soc.*, **27**, 959.
Ditchburn, Tunstead and Yates (1942), *Proc. Roy. Soc.*, **181**, 386.
King and Stockbarger (1940), *Astrophy. J.*, **91**, 488.
Kistiakowsky (1931), *Rev. Sci. Inst.*, **2**, 549.
Lawrence and Eldefassen (1930), *Rev Sci Inst.*, **1**, 45.
Nanda (1945), *Ind J. Phy.*, **19**, 1.
Petter (1934), *J. Sci. Inst.*, **11**, 95.
Trumpy (1925), *Zeits. f. Phy.*, **34**, 715.
,, (1927), ,, ,, ,, **44**, 575.
,, (1928), ,, ,, ,, **47**, 804.
Weiler (1929), *Ann. Der. Phy.*, **1**, 361.

STUDY OF THE ABSORPTION SPECTRA OF MERCURY VAPOUR WITH VARYING TEMPERATURE AND PRESSURE

By D. K BHATTACHARYYA AND JAGAT MURARI

(Plate II)

ABSTRACT. The absorption spectra of mercury vapour with varying conditions of temperature and pressure were studied using an absorption chamber of fused quartz and a hydrogen continuum as the background. Progressive broadening of the absorption line λ2537 Å both with increasing temperature and pressure was observed. Also a few new bands near the absorption line λ 2537 Å were observed. The absorption bands between 2311 Å and λ 2341 Å were observed to develop and grow clearer with increasing pressure at 560° C and 800° C, while they did not appear at all at 250°C.

INTRODUCTION

The spectrum of mercury vapour both in emission and absorption has been studied in detail by Rayleigh (1927) and by Walter and Barrat (1929). They have ascribed quite extensive band systems to the spectrum of mercury vapour in absorption and the troublesome task of photographing them has been accomplished by Rayleigh in his excellent spectrograms published in his paper quoted above.

The origin of these spectra in absorption, however, is a bit controversial point. They do not appear if mercury is heated in a carefully evacuated sealed quartz tube at any temperature. Rayleigh used an arrangement in which mercury boiled under imposed air pressure which could be varied from about three atmospheres to any fraction of one atmosphere. The significant point is that the bands appear only in the presence of air. In the present investigation arrangements were made for varying the imposed pressure from zero to one atmosphere. A series of spectrograms were taken with gradually varying pressures at any particular room temperature. The superimposed pressures were due to the gases nitrogen and oxygen. No marked change, however, was observed in the spectrograms with nitrogen and with oxygen, pointing to the conclusion that the spectrum is probably due to diatomic mercury molecules and not due to association of a mercury atom with a gas atom. The presence of gas merely favours the formation of mercury molecules.

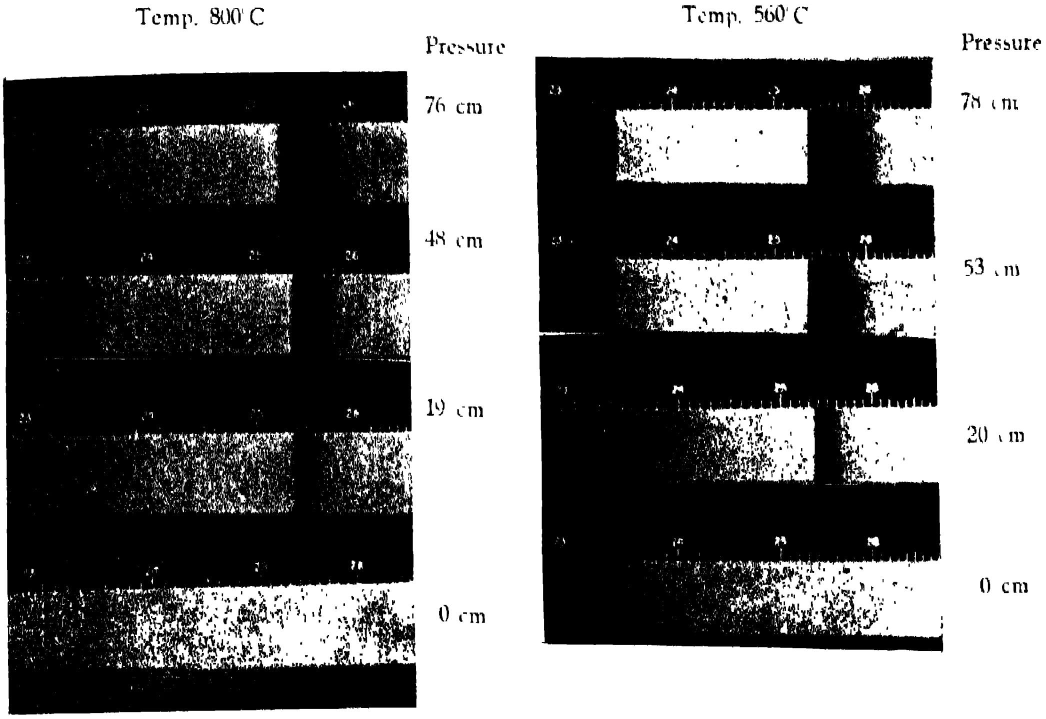

Absorption Spectra of Mercury Vapour with Varying Temperature and Pressure

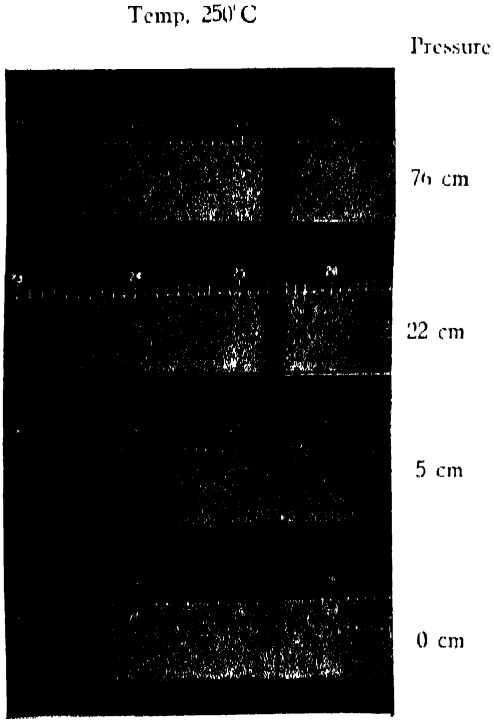

The present investigations differ from that of Rayleigh inasmuch as that the investigations of Rayleigh were made at higher pressures of imposed gas and with much longer absorption chamber. Observations with smaller pressures, however, have revealed a few new bands near the absorption line $\lambda = 2537$ Å, while the extensive spectrum observed by Rayleigh between $\lambda = 2943$ Å and $\lambda = 2614$ Å did not appear at all. This is due to the fact that with increasing external pressures the absorption spreads to longer wavelength side.

Further a systematic study of the absorption with varying pressures and temperatures as described in this paper has revealed certain behaviour of the absorption spectrum, which does not appear to have been recorded before.

EXPERIMENT

Figure 1 shows the experimental arrangement. A tube of fused quartz T with windows of fused quartz sealed on to it was used as the absorption chamber. The length of the tube was 25 cms and diameter 4 cms. The tube communicated with a large test tube B which was cooled with water in a beaker C, and served to condense any vapourised mercury. The chamber could be evacuated and dry nitrogen introduced with the help of three stopcocks A_1, A_2, A_3. The pressure was recorded by the manometer M. The chamber was surrounded by a silica tube wound with nichrome wire and covered with asbestos. This served as a furnace and different temperatures up to 1000° C could be obtained by varying the heating current. Hydrogen continuum run by a Foster transformer giving a maximum voltage of 2000 volts was used as a continuous source. An Adam Hilger Intermediate spectrograph was used for recording the spectrum. The chamber was made completely leak-tight, so that on evacuation the manometer remained perfectly steady for 24 hours.

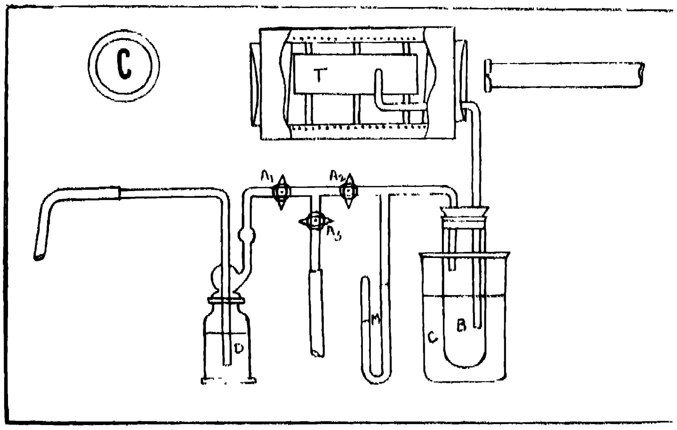

FIG. 1

The experimental procedure consisted in heating the chamber containing mercury to a definite temperature and then photographing the spectrum. Now some nitrogen, dried by passing through a sulphuric acid tower D, was introduced and the spectrum photographed with varying pressures of nitrogen.

EXPERIMENTAL RESULTS

Absorption spectra for the temperatures of 250° C, 560° C and 800° C are reproduced. The widening of the absorption line with increasing temperature and pressure is very clearly seen. Let us consider the photographs (Plate II) one by one.

Lowest Temperature 250° C. This photograph shows banded structure near the resonance line very clearly. With zero pressure the absorption line is very sharp. As the pressure is increased to 10 cms. another thin line appears at $\lambda = 2540$ Å. With further increase of pressure increasing number of diffuse bands appears and the extent of absorption increases. A noteworthy point is that the longer wavelength edge of the absorption at $\lambda = 2540$ Å remains practically fixed and only the shorter wavelength edge is extended towards still shorter wavelengths with increasing pressure. This behaviour is altered at higher temperature.

Temperature 560° C. This photograph shows the same general behaviour as the last, absorption line getting wider with increasing pressure of nitrogen. But a remarkable difference is that at this temperature the structure is practically absent and another very important difference is that in this case it is the short wavelength edge at $\lambda = 2333$ Å nearly, which remains fixed and very sharp with increasing pressure of nitrogen. The widening with increasing pressure takes place with forcing the longer wavelength edge towards still longer wavelength side.

Temperature 800° C. This photograph also does not show so much structure as the first one and is more akin to the second photograph. But a difference appears at the maximum pressure where the short wave length edge which was so far very sharp, becomes diffuse and some bands appear.

Some of the absorption edges read from the plate are recorded below.

Temp 250° C	Temp 800° C
$\lambda = 2538.5$ Å	
$\lambda = 2533$ Å	$\lambda = 2533$ Å
$\lambda = 2526$ Å	$\lambda = 2527$ Å
	$\lambda = 2524$ Å
	$\lambda = 2522$ Å
	$\lambda = 2519$ Å
	$\lambda = 2514$ Å

Besides the behaviour of the absorption about the resonance line the absorption between $\lambda = 2311$ Å and $\lambda = 2341$ Å also shows some peculiarity. They do not appear at all at the temperature of 250° C. They appear at the temperature of 560°C but here also only when the pressure is increased to 20 cms. of Hg and becomes clearer with increasing pressure of nitrogen. Similar behaviour is observed at the still higher temperature of 800° C.

Our thanks are due to Professor S. P. Prasad for giving us every facility in conducting this piece of work.

DEPARTMENT OF PHYSICS,
SCIENCE COLLEGE, PATNA,
16th April, 1945.

REFERENCES

Finkelnburg (1933), *Phys. Zeits.*, **34**, 529.

Rayleigh (1927), *Proc. Roy. Soc.*, **116**, 702.

Walter and Barrat (1929), *Proc. Roy. Soc.*, **122**, 201.

ON THE RAMAN SPECTRA OF ETHYLENE DIBROMIDE AND DICHLORETHYLENE IN THE SOLID STATE

By S. C. SIRKAR* and B. M. BISHUI

(Plate III)

ABSTRACT. The Raman spectra of ethylene dibromide and mixture of *cis* and *trans* dichlorethylene in the solid state at -170 C have been studied and these Raman spectra have been compared with those for the liquid state. The polarisation of the Raman lines of ethylene dibromide in the liquid state has also been studied. It is pointed out that two of the intense Raman lines of liquid ethylene dibromide which ought to have been polarised according to the hypothesis put forward by Mizushima and Morino (1938*a*) are actually depolarised. A new explanation that the liquid state of ethylene dibromide consists of pairs of cis molecules forming a configuration having a symmetry C_{2v} is offered and its advantages over the former one are discussed. It is assumed that in the solid state the configuration changes to have the symmetry of the point group D_{2h} and the observed variation of the permanent electric moment with change of state is also explained on this hypothesis.

INTRODUCTION

It was first observed by Mizushima, Morino and Noziri (1936) that some of the Raman lines of ethylene dichloride and ethylene dibromide observed in the liquid state disappear when the liquids are solidified at low temperatures. They pointed out that the lines observed in the solid state correspond to the oscillations of the molecules of *trans* configuration and those observed in the liquid state are due to a mixture of *cis* and *trans* types of molecules. Morino (1938) calculated the frequencies of oscillations of the *trans* configuration of the molecules of these two substances and assigned the frequencies 188 cm^{-1}, 656 cm^{-1}, 1056 cm^{-1}, 1254 cm^{-1}, 1440 cm^{-1} and 2970 cm^{-1} to the six total symmetric oscillations of *trans* ethylene dibromide molecule. Mizushima and Morino (1938*a*) adduced further evidence in support of this assignment by observing the changes which these frequencies undergo when the hydrogen atoms of the molecule are replaced by deuterium atoms. According to the assignment made by Mizushima and Morino (1938*a*) all the lines mentioned above should be highly polarised. The polarisation of the Raman lines of ethylene dibromide had been studied by Trumpy (1935) and Anantha Krishnan (1937). According to Trumpy the line 1440 cm^{-1} is completely depolarised while the value of ρ for the line 1056 cm^{-1} was observed by him to be 0.7. According to Anantha Krishnan on the other hand both these lines are completely depolarised. Thus there is a discrepancy between the values of ρ of these two lines actually observed and those expected according to the assignment made by Mizushima and Morino, and this discrepancy was not explained by them. The problem was therefore considered to be worth reinvestigation.

---

* Fellow of the Indian Physical Society.

In the present investigation the Raman spectra of ethylene dibromide in the solid state at about -170°C and in the liquid state at the room temperature and the polarisation of the Raman lines of the liquid have been studied. In order to compare the results obtained with ethylene dibromide, which is supposed to consist of a mixture of *cis* and *trans* molecules in the liquid state, with those obtained with a mixture of similar but stable *cis* and *trans* molecules, the Raman spectra of a mixture of *cis* and *trans* dichlorethylene in the solid state at about -170°C and in the liquid state at the room temperature have also been studied.

EXPERIMENTAL

The apparatus used in the present investigation for the study of the Raman spectra at the low temperatures was the same as that used in a previous investigation (Sirkar and Bishui, 1943). Kahlbaum's pure ethylene dibromide distilled in vacuum was put in a double walled cylindrical container of Pyrex glass held in a vertical position inside another transparent Dewar vessel. The interspace between the two walls of the container was evacuated with a Cenco Hyvac oil pump, so that on pouring liquid oxygen into the outer Dewar vessel to fill it up to a certain height from the bottom of the container, the temperature of the liquid was lowered only slowly, and consequently the process of solidification was very slow. The frozen mass thus produced was transparent. Dry air was slowly introduced afterwards into the interspace of the double walled container and the temperature of the solid finally reached a steady value of about -170°C within an hour. A Fuess glass spectrograph having a dispersion of about 14 A.U. per mm. in the region of 4046 A was used to photograph the Raman spectra. The substance was illuminated by light from two vertical mercury arcs condensed by two glass condensers placed on opposite sides of the container. Cobalt glass filters were placed in the path of the incident rays to cut off continuous background in the blue-green region of the spectrum.

The polarisation of the Raman lines of ethylene dibromide was studied by photographing the horizontal and vertical components of the lines simultaneously on the same plate with the help of a double image prism as usual. The liquid was contained in a horizontal Wood's tube provided with a plane window. Light from a horizontal mercury arc focussed with a glass condenser served as a cone of incident light with its axis perpendicular to that of the Wood's tube. The semivertical angle Ω of the cone of the incident light was about 20°, so that owing to the convergence of the incident beam the apparent value ρ' of factor of depolarisation is given by the relation

$$\rho' = \{\rho + (1-\rho)\psi\}/\{1-(1-\rho)/2\}\psi \qquad \ldots \quad (1)$$

where ρ is the real value of the factor of depolarisation, and $\psi=\frac{1}{3}(2-\cos\Omega-\cos^2\Omega)$ (see Bhagavantam, 1940). When $\rho=6/7$, $\rho'=0{\cdot}94$ in the present case. Owing to the loss of intensity of the vertical component by reflection at the surfaces of the prisms and lenses of the spectrograph the value of ρ' increases still further. Hence lines having ρ' almost equal to unity may be assumed to be totally depolarised under the arrangement mentioned above. This conclusion is further confirmed by the fact that the values of ρ' for some of the highly polarised lines photographed in the same spectrogram along with these depolarised lines were observed to be less than 0·2 which corresponds to a value of ρ equal to 0.05 according to (1).

The Raman spectrum of dichlorethylene (mixture of *cis* and *trans*) in the solid state at about −170°C was studied with the same arrangement as used in the case of solid ethylene dibromide and that of the liquid was also photographed for comparison with the spectrogram due to the solid. The results are discussed in the following section.

RESULTS AND DISCUSSION

The Raman lines observed at different temperatures in the case of ethylene dibromide are listed in Table I. The results obtained by Mizushima and Morino (1938*a*) in the case of the solid and liquid states of the substance and by Anantha Krishnan (1937) in the case of the liquid state are also included in the table. The numbers in parentheses placed immediately after the wavenumber shifts of the lines indicate approximate relative intensities of the lines and the letters e, k, etc., indicate the exciting lines according to Kohlrausch's notation. The letters P and D indicate that the lines are polarised and totally depolarised respectively.

The results obtained with a mixture of *cis* and *trans* dichlorethylene are given in Table II and those obtained by Cabannes (1938) for pure *cis* and pure *trans* dichlorethylene are also included in the table. In order to understand the nature of changes which the Raman lines of a mixture of *cis* and *trans* types of molecules undergo with the freezing of the mixture we shall first discuss the results obtained with the mixture of *cis* and *trans* dichlorethylene.

DICHLORETHYLENE

It can be seen from columns 1 and 2 of Table II that almost all the Raman lines of the mixture of *cis* and *trans* dichlorethylene in the liquid state are also present in the solid state. The following changes are, however, observed to occur with the solidification of the mixture. The line 563 cm^{-1} which is of moderate intensities in the liquid state becomes very feeble in the solid state. The line 1584 cm^{-1} which is very intense in the liquid state becomes broader and weaker in the solid state. The lines 852 cm^{-1} and 874

TABLE I

Ethylene dibromide

Liquid state			Solid state	
Present authors	Anantha Krishnan (1937)	Mizushima and Morino (1938a)	at −40° C Mizushima and Morino (1938a)	at −170° C Present authors
			41 (4) k ±	35 (3) k
			53 (3) k ±	52 (2) k
92 (2b) ; e, k ; D	92 (2b) D	92 (2b) e ± k ±	v	
133 (2) e ; ?		132 (2) e		125 (1) e, k
190 (8) e ±, k − ; P	189 (10) P	190 (10) e ±, k ±	187 (7) e+k+.	188 (0) e, k
232 (2) e ; P	228 (1b) P	231 (3) e	v	
325 (0) e ; ?	320 (0) ?	325 (1) e		
354 (3) e ; D	358 (2) D	355 (5) e, k	v	
470 (1) e, k ; ?	470 (0) ?	469 (1) e, k		
551 (7) e ±, k, i , P	551 (8) PP	551 (8) e ±, l, g, i, k	v	
582 (4b) e, k, i ; D	580 (2b) D	583 (6b) e ±, k, i	v	581 (0) k
660 (10b) e, k, i ; P	659 (15b) P	660 (10b) e ±, k, i	656 (10) e, k, i, f, g	656 (10) e, k, i, f
	790 (0) ?			
836 (2) e , D	834 (½) D	836 (2) e		
892 (2) e, k , P	895 (1) P	899 (3) e, k		
935 (0) e k , ?	930 (1b) P (?)	930 (2) e, k	933 (0) k	
		1019 (1) e, k		
1052 (8) e, k, i , D	1051 (6) D	1053 (9) e, k, i	1056 (5) e, k, i	1056 (5) e, k, i
1170 (2) e, k ; D	1169 (½) D	1169 (3) e, k	1157 (1) e	
	1187 (0) D			
1258 (10b) e, k ; P	1256 (10b) P	1255 (10b) e, k	1254 (8) e, k, i	1254 (8) e, k
	1295 (1s) P	1276 (3) e, k	v	
1421 (2) e, k ; D	1419 (1) D	1419 (3) e, k	b	
1438 (4) e, k ; D	1436 (2) D	1440 (5) e, k	1436 (3) e, k	1435 (2) e, k
2837 (3) e, k ; P	2852 (1) PP	2859 (4) e, k	2848 (2) e, k	2848 (0)
2950 (8) e, k, i ; P	2950 (6) PP	2953 (8) e, k, i	v	
2975 (10b) e, k, i ; P	2970 (8) PP	2972 (10) e, k, i,	2968 (8) e, k, i	2971 (7) e, k
3012 (4b) e, D	3012 (2b) D	3013 (4b) e, (k)	3020 (2) e, (k)	3017 (1) e

TABLE II

1, 2-Dichlorethylene

Present authors		Cabannes (1938)	
Liquid (mixture of cis and trans)	Solid at −170° C	Liquid (cis)	Liquid (trans)
	60 (2b) k	ρ	ρ
171 (8) e, k	173 (3b) e	174 (16) 0.52	351 (20) 0.29
351 (5) e, i	360 (3b) e	406 (10) 0.85	
407 (5) e	410 (2b) e	564 (6) 0.89	
563 (4) e, k	567 (0) e	711 (20) 0.06	766 (4) 0.70
712 (10) e, i, k	712 (4b) e, k	809 (1) P	
760 (2) e, k	760 (0) e	875 (2) D	848 (7) 0.09
852 (3) e, k	860 (1) e	1179 (12) 0.69	
874 (3) e, k			1271 (14) 0.21
1179 (10) e, i, k	1180 (3) e, k	1586 (16) 0.19	1576 (11) 0.10
1274 (5) e, k	1274 (1) e	1688 (4) P	1630 (½) P
			1693 (1) P
1584 (20) e, k	1584 (4b) e, k	3077 (20) 0.27	3070 (12) 0.20
1695 (3) e			
3075 (20) e, k, q	3082 (6b) e, k	3178 (2) D	3142 (2) D ?
3170 (2) e, k	3170 (0) k		

cm^{-1} observed in the liquid state coalesce to form a broad line at 860 cm^{-1} in the solid state. The lines 351 cm^{-1}, 407 cm^{-1} and 3075 cm^{-1} also ungergo slight changes in position with the solidification of the substance and a new band at 60 cm^{-1} is observed in the solid state. The spectrograms are reproduced in Plate I (Figs. 1 and 2).

Most of the lines observed in the liquid state have been assigned by Cabannes (1938) to the particular modes of vibration of the *cis* and *trans* types of the molecule. The *trans* configuration of the molecule has the symmetry of the point group C_{2h} and has according to group theory five total symmetric and one antisymmetric oscillations allowed in Raman effect. The five polarised lines 351 cm^{-1}, 848^{-1}, 1271 cm^{-1}, 1576 cm^{-1} and 3070 cm^{-1} are assigned to the total symmetric oscillations, and of these the most intense lines 351 cm^{-1} and 1271 cm^{-1} are supposed to be due to the deformation oscillations of the C–Cl and C–H bonds respectively. According to Cabannes the Raman line due to the mode of oscillation antisymmetric to the plane of the molecule is too weak to be observed and the line 766 cm^{-1} is not identified with this oscillation, because it is not totally depolarised, the value of ρ being 0·7 and definitely less than 6/7. This line is supposed to be an overtone of the deformation oscillation antisymmetric to the centre of symmetry, the fundamental being forbidden in Raman effect.

In the case of the *cis* configuration of dichloroethylene which has the symmetry C_{2v} five total symmetric and seven antisymmetric oscillations are allowed in the Raman effect according to the group theory. The five total symmetric modes are identified by Cabannes (1938) with the lines 174 cm^{-1}, 712 cm^{-1}, 1179 cm^{-1}, 1586 cm^{-1} and 3077 cm^{-1} which are all polarised. Of the seven totally depolarised lines expected from the theory only four are actually observed. These are 406 cm^{-1}, 564 cm^{-1}, 875 cm^{-1} and 3178 cm^{-1}. The last one is, however, assumed by Cabannes to be due to an overtone of 1586 cm^{-1}, but this assumption is not justified, because the line is totally depolarised while all overtone modes should give polarised Raman lines. Again, the line 1688 cm^{-1} is assumed by him to be an overtone of 875 cm^{-1} but since both these lines are almost equally intense, one of them cannot be the overtone of the other. In the mixture of *cis* and *trans* dichlorethylene in the liquid state only a single line at 1695 cm^{-1} is observed in the present investigation in place of the three lines 1630 cm^{-1}, 1688 cm^{-1} and 1693 cm^{-1} due to the two constituents and the line is too weak to be observed in the solid state. Also another line at 3170 cm^{-1} is observed in place of the lines 3142 cm^{-1} and 3178 cm^{-1} observed by Cabannes in the case of *cis* and *trans* configurations respectively. These facts indicate the influence of van der Waals forces on the frequencies of the corresponding vibrations. Probably some sort of association disturbs slightly the centre of symmetry of pure *trans* dichloroethylene molecule in the liquid state and when mixed with the *cis* type this symmetry is restored. The line 3142 cm^{-1} is probably due to the antisymmetric C-H valence oscillation and it has thus a feeble intensity in the pure state and disappears in the

Fig 1

Fig 2

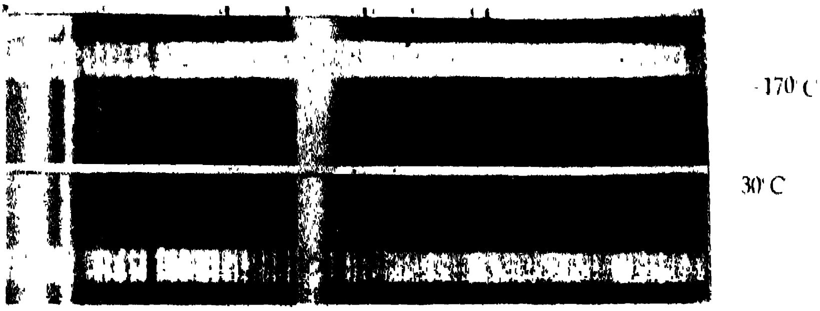

Fig. 3

Fig. 4

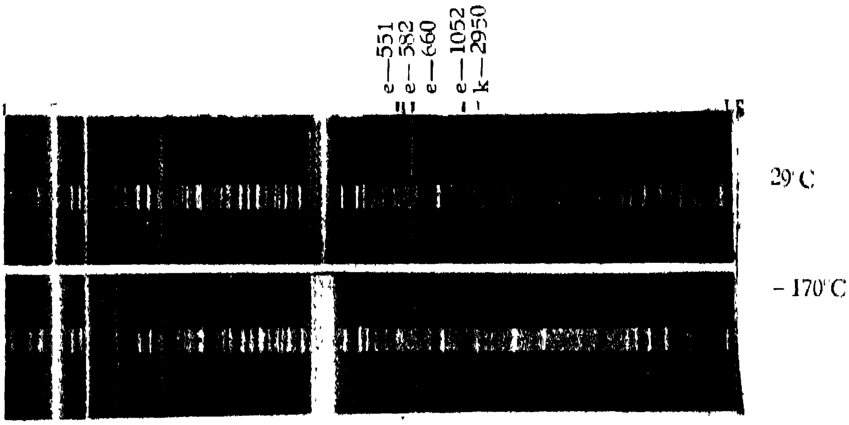

Fig. 5

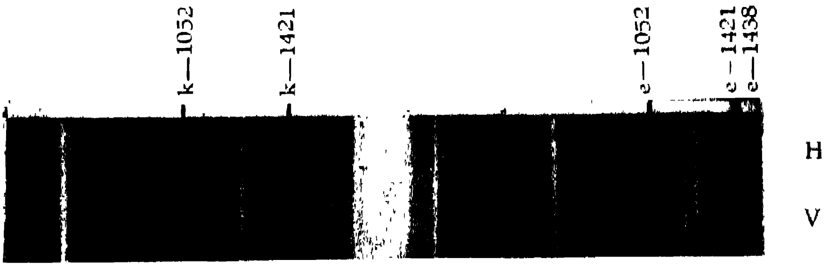

Raman Spectra

Fig. 1 Dichlorethylene, solid at 170°C
Fig. 2 „ „ liquid „ −30°C
Fig. 3 Ethylene dibromide liquid at −29°C
Fig. 4 „ „ solid „ −170°C
Fig. 5 „ „ liquid, polarisation

mixture because of restoration of the centre symmetry of the molecule. The new line at 60 cm^{-1} is due to some intermolecular oscillation, because the single molecule cannot have any mode of vibration of such a low frequency. The line is broad and feeble and it is difficult to say whether it is due to pure lattice oscillation or due to some vibration in associated molecules.

It is therefore seen from the above discussions that in the case of both *cis* and *trans* molecules all the total symmetric oscillations yield intense Raman lines and the antisymmetric oscillation in the case of the *trans* type as well as some of similar oscillations in the case of the *cis* type are absent in the Raman spectra.

ETHYLENE DIBROMIDE

It can be seen from Table I that many of the lines observed in the case of liquid ethylene dibromide are absent in the solid state at the low temperature. This can also be seen from the spectrograms reproduced in Plate I (Figs. 3 and 4). The results are in general agreement with those reported by Mizushima and Morino (1938a), but there are a few minor discrepancies. The lines 581 cm^{-1} does not disappear compeletely in the solid state at -170° C, but it becomes definitely much feebler in the solid state. This statement is based on the fact that a very weak Raman line at λ 4143.8 has been observed in the present investigation in the case of the solid state at -170°C, although Mizushima and Morino did not record any such line in the case of the solid at −40°C. The Raman line 551 cm^{-1} excited by λ4358 almost coincides with the line 656 cm^{-1} excited by λ4339 and the same line excited by λ4047 coincides with the Hg line λ4140. Hence although a faint line is actually observed at λ4466.5 it cannot be said definitely whether it is solely the line 656 cm^{-1} excited by λ4339 or the line 551 cm^{-1} excited by λ4358 is also superposed on it with a very feeble intensity. It can, however, be stated with certainty that even if the line 551 cm^{-1} be superposed on the line 656 cm^{-1} excited by λ4339 the intensity of the former line is almost negligible in the solid state in comparison with that in the liquid state.

The lines 933 cm^{-1} and 1157 cm^{-1} observed by Mizushima and Morino (1938*a*) at −40°C have not been observed in the spectrogram due to the solid at −170°C obtained in the present investigation, but a line at 125 cm^{-1} observed in this spectrogram has not been observed by them at −40° C. The results regarding polarisation of the Raman lines of the liquid obtained in the present investigation agree with those reported by Anantha Krishnan (1937). According to these results the lines 1056 cm^{-1} and 1440 cm^{-1} are totally depolarised. It is difficult to reconcile this fact with the assignment made by Mizushima and Morino (1938*a*) that these lines are due respectively to the total symmetric C-C valence and C-H deformation oscillations of the single molecule of *trans* configuration, because we have already seen that in the case of similar molecule of *trans* dichlorethylene the corresponding Raman lines are observed to be polarised and they appear with undiminished intensity in the solid state.

According to Mizushima and Morino the solid state of the substance consists entirely of single molecules of trans configuration. This molecule has six total symmetric and three antisymmetric modes of oscillation allowed in Raman effect according to the group theory. The fact that more than nine lines are observed in the solid state and of the six lines which are expected to be polarised two are totally depolarised, probably indicates that the solid state consists not of single molecules but of larger molecules formed by association of single molecules. The line 92 cm^{-1} observed in the case of the liquid state cannot be due to any mode of oscillation of the single molecule, and Mizushima and Morino (1938*b*) have pointed out that this line may originate from some oscillation of the conglomerate of molecules, such conglomerates being present only in the liquid state. It is, however, difficult to believe that if conglomerates are present in the liquid state they can dissociate into single molecules in the solid state. On the contrary, there is every possibility of the strengthening of the intermolecular bonds in such conglomerates with the solidification of the substance. The two new lines 41 cm^{-1} and 53 cm^{-1} observed in the solid state may also be due to some vibration in such associated groups of the molecules. All these facts indicate that we may have to assume that solid ethylene dibromide consists of associated pairs of molecules. An attempt will be made now to explain the polarisation of the Raman lines of the liquid on the basis of this assumption. It has to be pointed out, however, that the polarisation of the lines in solid state may not be the same as that of the corresponding lines in the liquid state.

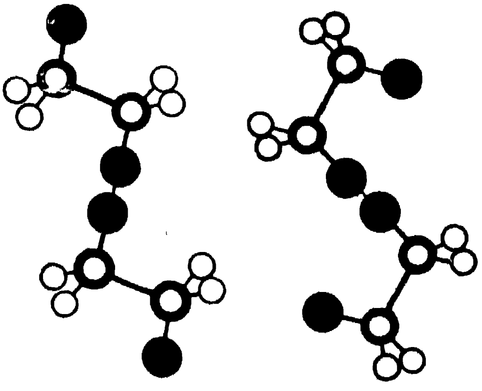

(*a*) (*b*)

FIG. 6

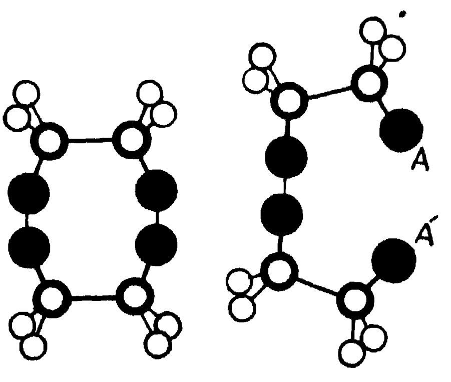

(*a*) (*b*)

FIG. 7

If two molecules of ethylene dibromide become associated by some virtual bond between two bromine atoms one belonging to each molecule, we can have two different configurations as shown in figures 6 and 7. The configuration shown in figure 6 is centrosymmetrical and may be formed by two molecules, both being either of *cis* or of *trans* type. The symmetry of the configuration is C_{2h}. The character table of this point group as well as the number of Raman lines allowed for the configuration are given in Table III in which n_i denotes the total number of times the particular irreducible representation is contained in the reducible representation and n', the number of oscillations represented by the irreducible representations excluding pure translations and pure rotations. The number of Raman lines allowed are given in the column under "Raman effect" and the nature of polarisation of the lines is also indicated in the last column by the letters P and D.

TABLE III

Symmetry C_{2h}

	E	C_2	σ_h	i	n_i	T & R	n'_i	Raman effect	Polarisation
Γ_1	1	1	1	1	14	1	13	13	P
Γ_2	1	−1	−1	1	10	2	8	8	D
Γ_3	1	1	−1	−1	10	1	9	f	—
Γ_4	1	−1	1	−1	14	2	12	f	—
U_R	16	0	8	0			21 Raman lines		
$h_j\chi'_j$	48	0	8	0					
$h_j\psi'_j$	42	2	8	0					

The other configuration is formed by two molecules of the *cis* type as shown in figure 7(*a*) and has the symmetry D_{2h}. The corresponding character table is included in Table IV.

TABLE IV

Symmetry D_{2h}

	E	C_2	C'_2	C''_2	σ_h	σ_v	σ'_v	i	n_i	T&R	n'_i	Raman effect	Polarisation
Γ_1	1	1	1	1	1	1	1	1	7	0	7	7	P
Γ_2	1	1	−1	−1	1	1	−1	−1	7	1	6	f	—
Γ_3	1	−1	1	−1	1	−1	1	1	7	1	6	f	—
Γ_4	1	−1	−1	1	1	−1	−1	1	7	1	6	6	D
Γ_5	1	1	1	1	−1	−1	−1	−1	5	0	5	f	—
Γ_6	1	1	−1	−1	−1	−1	1	1	5	1	4	4	D
Γ_7	1	−1	1	−1	−1	1	−1	1	5	1	4	4	D
Γ_8	1	−1	−1	1	−1	1	1	−1	5	1	4	f	—
U_R	16	0	0	0	8	0	0	0			21 Raman lines		
$h_jx'_j$	48	0	0	0	8	0	0	0					
$h_jy'_j$	42	2	2	2	8	0	0	0					

It can be seen from the Tables III and IV that both the configurations yield the same number of Raman lines, but in the case of that shown in figure 6, thirteen of the twenty one Raman lines are polarised and the remaining eight are totally depolarised. In the case of the other configuration shown in figure 7(*a*) there should be seven polarised and fourteen depolarised Raman lines. It has been observed in the case of *cis* and *trans* dichlorethylene that most of the depolarised Raman lines are either feeble or absent. Since we do not observe more than twelve lines in the Raman spectrum of solid ethylene dibromide any of the configurations shown in figure 6 cannot be supposed to be responsible for the origin of these Raman lines, because such a configuration ought to have given thirteen polarised Raman lines. We can, however, explain the origin of the observed Raman lines by assuming that they are due to the configuration shown in figure 7(*a*) and that seven of the twelve Raman lines observed in the solid state are polarised and five are depolarised. The remaining depolarised lines may be too feeble to be observed, as in the case of dichlorethylene.

In the case of the liquid state the virtual bond between one of the two pairs of bromine atoms may be absent thus producing a configuration having a symmetry C_{2v} as shown in fig. 7(*b*). This should yield forty two Raman lines of which thirteen should be polarised and the rest depolarised. The maximum number of lines observed in the liquid state is twenty-four and of these nine are definitely polarised and three of these polarised lines being broad, each may consist of two lines. Thus almost all the polarised lines expected for the configuration indicated above are actually observed. As regards the depolarised lines ten definitely depolarised lines are observed of which three are broad and there are three more faint lines which also may be depolarised. This may account for altogether sixteen out of twenty-nine depolarised lines expected. Some of the depolarised lines should be absent as observed in the case of *cis* and *trans* dichlorethylene According to the hypothesis put forward by Mizushima and Morino that the liquid may consist of a mixture of *cis* and *trans* molecules we shall also expect twelve polarised and fifteen depolarised Raman lines in the case of the liquid state. But the present hypothesis has the following advantages over that put forward by them. :

(*a*) According to the present hypothesis the line 1051 cm^{-1} due to the liquid may be totally depolarised, because it can be identified with the C – C valence oscillation antisymmetric to the plane of reflection possessed by the associated pair of molecules having the symmetry C_{2v}, but according to the previous hypothesis the line ought to have been polarised although it is actually not so. The line 1056 cm^{-1} observed in the solid state may be due to the symmetric C – C valence oscillation of the model shown in figure 7(*a*).

(*b*) The lines of frequencies less than 190 cm^{-1} cannot originate from any mode of oscillation of either *cis* or *trans* ethylene dibromide molecules and so according to the previous hypothesis conglomerates of molecules were postulated to be present in the liquid state and absent in the solid state. The present hypothesis can explain the origin of these lines by assuming that they are due to oscillations of associated pair of molecules present both in the solid and liquid states.

(*c*) In order to explain the behaviour of the new lines in the low frequency region observed in the solid state Mizushima and Morino (1938*b*) assumed that the molecules of ethylene dichloride can rotate freely about the Cl-C-C-Cl axis above −95°C, although the rotation about the C-C bond is stopped by freezing the substance. In the explanation offered in the present paper no such assumption, which seems to be hardly tenable, has been made. The lines in the low frequency region may be due to some oscillations of the pair of molecules as stated before.

Besides explaining the discrepancies between the observed facts and the predictions of the hypothesis put forward by the previous authors mentioned above, the configurations of pairs of molecules assumed to be present in the liquid and solid states of ethylene dihalides can also explain the permanent electric moments of the molecules observed in the two states. The configuration of the pair having the symmetry C_{2v} will possess a permanent electric moment and that present in the solid state and possessing the symmetry D_{2h} should have no electric moment, as observed by White and Morgan (1937).

The gradual diminution in the observed value of the permanent electric moment of the molecule with the lowering of the temperature may be due to the gradual diminution in the distance between the two bromide atoms marked A A′ in configuration shown in figure 7(*b*). As the temperature is lowered probably the opening in the ring is gradually narrowed down and finally the gap is closed, and the configuration becomes a centro-symmetrical one with the solidification of the substance. With the approach of the symmetry of the configuration to the centro-symmetrical one there is a diminution in the change in polarisability of the molecule taking place during some modes of oscillations which become antisymmetric to centre of symmetry in the case of the centro-symmetrical configuration. Thus the weakening of the intensity of some of the Raman lines, *e.g.*, the lines 551 cm^{-1} and 581 cm^{-1} and 2950 cm^{-1} with the lowering of the temperature can be explained.

Attempts to explain on these lines the results observed with other similar molecules will be made in later communications.

ACKNOWLEDGMENT

The authors are indebted to the authorities of the Indian Association for the Cultivation of Science for providing facilities for carrying out the experimental portion of the investigation in the Laboratories of the Association and for the award of a scholarship to one (B. M. B.) of them.

Physics Department
University College of Science,
Calcutta.

REFERENCES

Anantha Krishnan, R., 1937, The Raman Spectra of some simple molecules, *Proc. Ind. Acad. Sc. A.*, **5**, 285.

Bhagavantam, S., 1940, *Scattering of light and the Raman Effect*, p. 303.

Cabannes, J., 1938, The *cis trans* Isomerism, *J. Chimie Physique*, **35**, 1.

Mizushima, S. and Morino, Y. 1938*a*, Raman Spectra and molecular configurations of solid ethylene dihalides, *Proc. Ind. Acad. Sc. A.*, **8**, 315.

Mizushima, S. and Morino, Y., 1938*b*, The motion of ethylene halide molecules in crystals, *Bull. Chem. Soc.*, Japan, **13**, 182.

Mizushima, S. Morino, Y. and Noziri, 1936, Raman Effect and free rotation, *Sci. Papers, Inst. Phys. Chem. Research* (Tokyo), **29**, 63 and 188.

Morino, Y., 1938, The normal vibrations of ethylene halides, *Bull. Chem. Soc., Japan*, **13**, 189.

Sirkar, S. C and Bishui, B. M., 1943, Raman Spectra of some Alkyl sulphides in the solid state, *Proc. Nat. Inst. Sc.*, **9**, 287

Trumpy, B., 1936, Polarisation of Raman lines, *Z. f. Phys.*, **98**, 672.

White and Morgan, 1937, *J. Chem. Phys.*, **5**, 655

5

SOUND-ABSORPTION CHARACTERISTICS OF INDIAN MATERIALS: PART II

By S. CHATTERJEE and N. DUTT

ABSTRACT. This paper is a continuation of a previous one by the authors [Chatterjee and Dutt (1944)] and presents a theoretical investigation of the sound-absorption characteristics of rigid porous materials based on the treatment given by Lord Rayleigh. The nature of variation of sound-absorption coefficient with angles of incidence as well as frequencies of sound wave incident on rigid porous surfaces of various characteristics has been studied. The condition of total absorption has also been incorporated. The absorption coefficient of a sample of jute suface has been calculated theoretically from the dimensions and properties of the sample and a comparison has been made with the results obtained experimentally.

INTRODUCTION

Sound waves striking on a plane surface forming the boundary between two different media are generally divided into reflected and transmitted portions, the amplitudes of which depend on the relative physical properties of the two media. If the boundary presents an unbroken solid or liquid surface, the amplitude of the reflected beam will predominate and only a minor portion of the energy will be found in the transmitted portion. If the surface is the boundary between air and a porous material a portion of the incident sound wave would penetrate into the pores of the second medium. Assuming the pores to be capillary channels there will be degradation of sound energy due to the viscous action of the air inside the pores. Thus in the case of porous bodies the amplitude of the reflected beam will be smaller due to the process of absorption.

The equation showing the relation between the absorption coefficient at any angle of incidence for a sound of definite frequency on a porous surface with pores of definite radius and a definite ratio between unperforated and perforated area and the kinematic viscosity of gas in the pores and ratio of sp. heats of the gas has been shown in Paper I to be as follows :

$$\alpha_\theta = \frac{8M\{(2M^2+1) \pm \sqrt{4M^4+1}\}\cos\theta}{\{(2M^2+2M\cos\theta+1) \pm \sqrt{4M^4+1}\}^2} \qquad (1)$$

Variation of Absorption with Angle of Incidence

A graphical plot showing the relation between α_θ, θ and M is given in Fig. 1. The factor M involves not only the characteristics of the surface but also the effect of different frequency of the sound wave. As the angle increases from normal incidence value ($\theta=0°$), the absorption increases slowly, at first, and then more rapidly, it passes through a maximum value of unity and finally drops down rapidly to zero at the grazing incidence ($\theta=90°$).

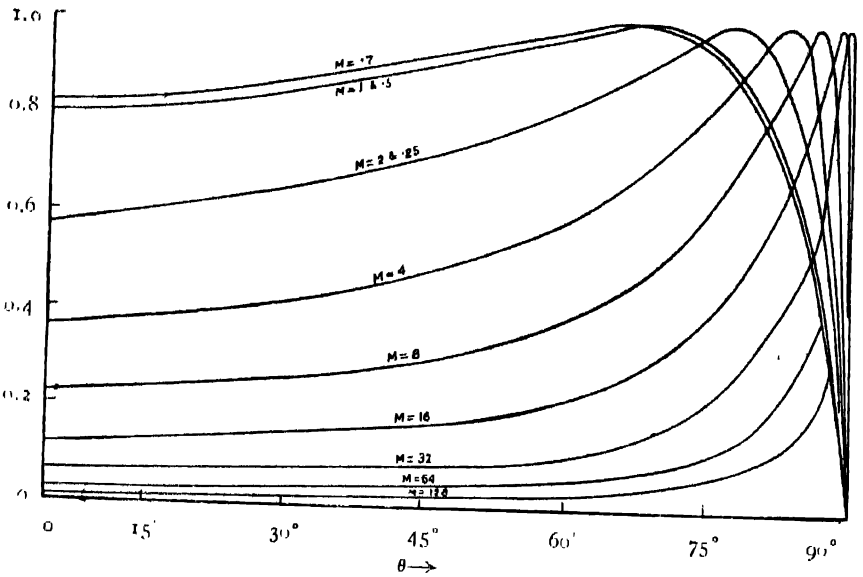

FIG. 1

The Case of Total Absorption

From Fig. 1, it is noted that for a particular value of M there is always some angle of incidence θ at which the absorption is complete. This optimum value of θ is found as follows :

Since $$a_\theta = 1 - \left\{\frac{(1+g)\cos\theta - x}{(1+g)\cos\theta + x}\right\}^2 \quad \ldots \quad \text{[Paper I, } \textit{loc. cit.}\text{]}$$

a_θ will be unity when the terms inside the bracket reduce to zero.

i.e. $$(1+g)\cos\theta - x = 0$$

or $$\cos\theta = x/1+g.$$

Substituting the value of x ... [Paper I, *loc. cit.*]

$$\cos\theta = \frac{(2M^2+1) \pm \sqrt{4M^4+1}}{2M} \quad \ldots \quad (2)$$

From (2) one gets $$M = \frac{(\cos^2\theta+1) \pm \sqrt{(\cos^2\theta+1)^2 - 8\cos^2\theta}}{4\cos\theta} \quad \ldots \quad (3)$$

For any value of θ, it is seen that corresponding to the positive and the negative signs preceding the term under the root, M will have two values at which the absorption would be unity.

When the term under the root sign becomes zero, M shall have only one value given by

$$M = \frac{\cos^2\theta + 1}{4\cos\theta}$$

and the value of the angle θ for which there is only one value of M at which absorption is unity is given as follows :

$$(\cos^2\theta+1)^2 - 8\cos^2\theta = 0\,; \quad \text{or} \quad \cos\theta = 0{\cdot}414\,; \quad \text{or} \quad \theta = 65°31'.$$

For the angle of incidence 65°31′, the numerical value of M at which unity absorption takes place is given by

$$M=\frac{\cos^2\theta+1}{4\cos^2\theta}=1/\sqrt{2}=0.707.$$

Fig. 2 shows the variation of the values of $(\cos^2\theta+1)^2-8\cos^2\theta$ with θ. It is noted from the curve that only for angles of incidence greater than 65°31′ the term under the root sign in equation (3) is positive, and consequently there will be two real values of M at which the absorption will attain unity. For angles of incidence θ less than 65°31′ the term $(\cos^2\theta+1)^2-8\cos^2\theta$ becomes negative and consequently M becomes a complex term, but from the definition, M is real and condition of unity absorption has been deduced by taking M to be real. So for any angle θ less than 65°31′ absorption can never attain unity value, but it attains a peak value lower than unity for a particular value of M which can be determined by differentiating the expression (1) indicating the relation between a_θ and M and equating the result to zero.

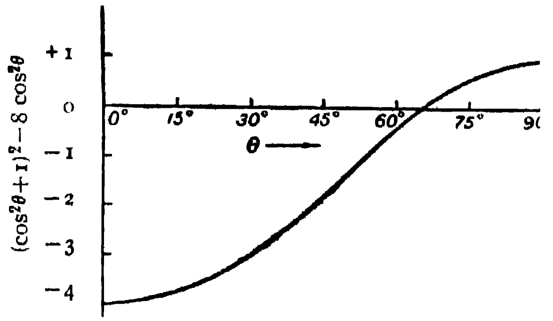

FIG. 2

Differentiating equation (1)

$$\frac{da_\theta}{dM}=\{(2M^2+2M\cos\theta+1)\pm\sqrt{4M^4+1}\}^2$$

$$\left[8\cos\theta\{(2M^2+1)\pm\sqrt{4M^4+1}\}+8M\cos\theta\{4M\pm\frac{16M^3}{2\sqrt{4M^4+1}}\right]-$$

$$8M\cos\theta\{2M^2+1)\pm\sqrt{4M^4+1}\}\times 2\{(2M^2+2M\cos\theta+1)\pm\sqrt{4M^4+1}\}$$

$$\left\{4M+2\cos\theta\pm\frac{16M^3}{2\sqrt{4M^4+1}}\right\}\Big/$$

$$\{(2M^2+2M\cos\theta+1)\pm\sqrt{4M^4+1}\}^4.$$

This reduces to

$$\frac{d\bar{a}_\theta}{dM}=8\cos\theta\left[4M^3\cos\theta+1\pm2\sqrt{4M^4+1}\pm(4M^4+1)\pm\frac{16M^5\cos\theta}{\sqrt{4M^4+1}}-\right.$$

$$\left.4M^4-2M\cos\theta\mp2M\cos\theta\sqrt{4M^4+1}\mp\frac{16M^6}{\sqrt{4M^4+1}}\mp\frac{8M^4}{\sqrt{4M^4+1}}\right]\Big/.$$

$$\{(2M^2+2M\cos\theta+1)\pm\sqrt{4M^4+1}\}^3.$$

Putting $\frac{da_\theta}{dM} = 0$ one finds

$$8\cos\theta\left[4M^3\cos\theta + 1 \pm 2\sqrt{4M^4+1} \pm (4M^4+1) \pm \frac{16M^5\cos\theta}{\sqrt{4M^4+1}} - \right.$$

$$\left. 4M^4 - 2M\cos\theta \mp 2M\cos\theta\sqrt{4M^4+1} \mp \frac{16M^6}{\sqrt{4M^4+1}} \mp \frac{8M^4}{\sqrt{4M^4+1}}\right] = 0$$

or

$$(2M^2-1)\left\{2M\cos\theta - (2M^2+1) \mp \frac{2(4M^4+2M^2+1)}{\sqrt{4M^4+1}} \mp (2M^2+1) \pm \right.$$

$$\left. \frac{2M\cos\theta\,(2M^2+1)}{\sqrt{4M^4+1}}\right\} = 0$$

or

$$(2M^2-1) = 0.$$

$$\therefore \qquad M = \frac{1}{\sqrt{2}} = 0.707.$$

Thus for angles of incidence lower than 65°31′ absorption coefficient attains a peak value for a value of $M = 1/\sqrt{2}$ at which absorption just attains unity at the critical angle of incidence of 65°31′.

Variation of Absorption with the value of M

In order to examine the nature of absorption for different values of M, a graph has been plotted to indicate the relation of absorption and M. Here one finds a family of curves for different angles of incidence. Since the values of M extend over a very large range it was thought fit to plot the values of M on a logarithim scale. This is shown in Fig. 3.

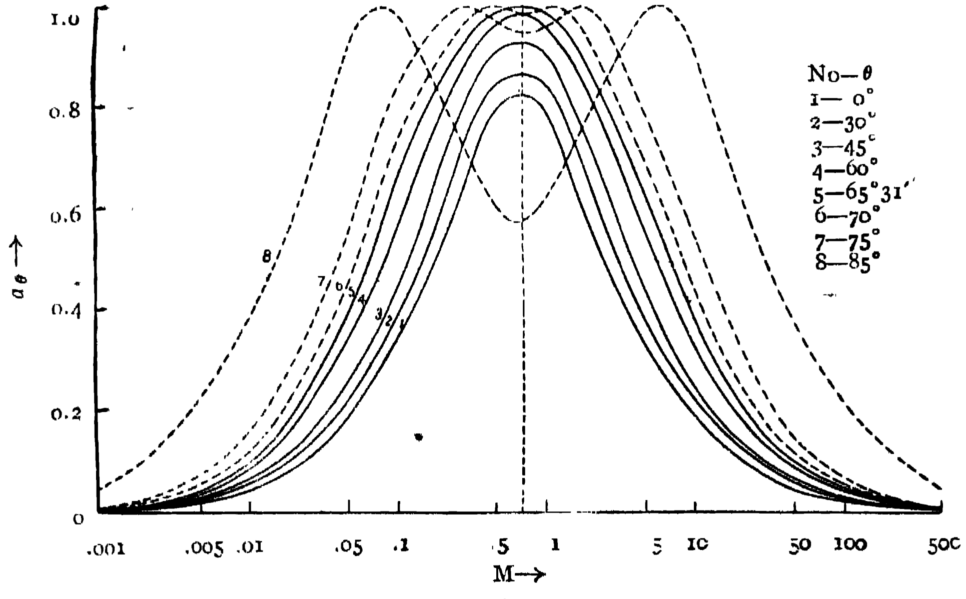

FIG. 3

The Fig. 3 shows that the absorption factor α_θ is related to the value of M, such that for the same angle of incidence there are two values of M at which equal values of absorption is attained and these two values are symmetrical with respect to the value of M at which peak absorption is found.

Taking $M_1=M_0/n$ and $M_2=nM_0$ and substituting the value of M_0 as $1/\sqrt{2}$ one finds for M_1

$$\alpha_\theta=\frac{\frac{8M_0}{n}\left\{\left(2\frac{M_0^2}{n^2}+1\right)\pm\sqrt{\frac{4M_0^4}{n^4}+1}\right\}\cos\theta}{\left\{\left(2\frac{M_0^2}{n^2}+2\frac{M_0}{n}\cos\theta+1\right)\pm\sqrt{\frac{4M_0^4}{n^4}+1}\right\}^2}$$

and for M_2

$$\alpha_\theta=\frac{8nM_0\{(2n^2M_0^2+1)\pm\sqrt{4n^4M_0^4+1}\}\cos\theta}{\{(2n^2M_0^2+2nM_0\cos\theta+1)\pm\sqrt{4n^4M_0^4+1}\}^2}.$$

Both these expressions reduce to

$$\frac{4\sqrt{2}\,n\{(n^2+1)\pm\sqrt{n^4+1}\}\cos\theta}{\{(n^2+\sqrt{2}\,n\cos\theta+1)\mp\sqrt{n^4+1}\}^2}.$$

The peak value of absorption is found to be at M_0 for angles of incidence less than that of the critical value of θ, *i.e.*, 65°31′.

For angles higher than that of the critical value of θ the peak values are attained for two other values of M. In these cases, a depression of absorption is shown at M_0 value. As the angle of incidence increases the peaks are separated further apart and the depression is more marked. At the grazing incidence the entire range of value for M reduces to zero.

It may be pointed out in this connection that when the dissipation is negligible one would get a simplified expression for total absorption as has been shown by Rayleigh (1920).

In this case taking amplitude of reflection to be B one gets

$$\frac{B-1}{B+1}=\frac{\sigma}{\sigma+\sigma'}\;\frac{1}{\cos\theta}$$

and then the condition of unity absorption, *i.e.*,

$$B=0$$

gives

$$\cos\theta=\frac{\sigma}{\sigma+\sigma'}=\frac{1}{1+g}.$$

A graphical plot of $\alpha_\theta=1-B^2$ for different values of θ and g is given in Fig. 4.

This shows that even for normal incidence one would get total absorption which is not realised in practice. Paris (1927) from the consideration of acoustic impedance has shown that under no condition one would get maximum absorption at normal incidence.

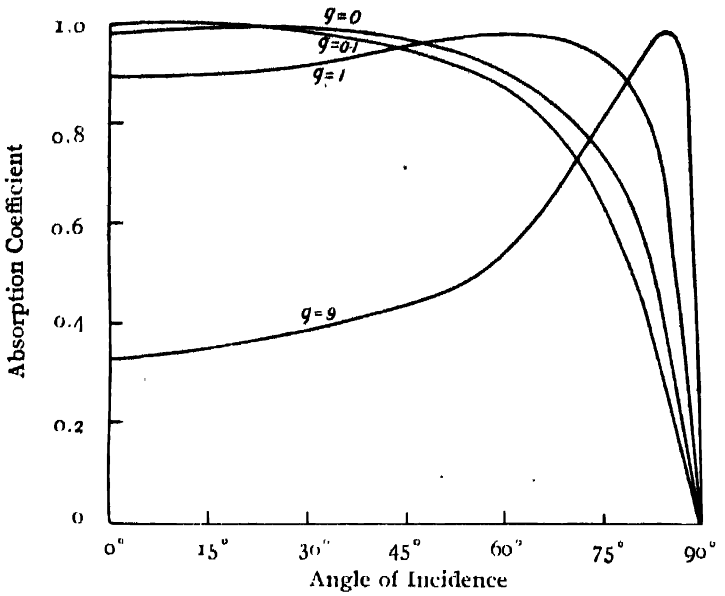

FIG. 4

Variation of α_θ with Frequency of Sound Wave and Physical Properties of the Sample

The general equation (1) does not give a direct relation between α_θ and frequency of the sound wave f. A direct relation between α_θ and f, can be obtained as follows :

We have
$$M=\frac{2(1+g)\sqrt{\nu\gamma}}{r\sqrt{2\pi f}}=\frac{S}{\sqrt{f}},\text{ say,}$$

where S is the factor depending on the surface condition of the sample.

Therefore
$$S=\frac{2(1+g)\sqrt{\nu\gamma}}{r\sqrt{2\pi}}.$$

Substituting the values of ν and γ for air we have

$$S=0\cdot36\frac{1+g}{r}.$$

Thus S depends only on the nature of the surface of the sample that is on porosity and radius of the pores, and is constant for a particular sample. Let S be termed the 'Surface factor' of the sample.

Substituting $\frac{S}{\sqrt{f}}$ for M in equation (1) we have

$$\alpha_\theta=\frac{\frac{SS}{\sqrt{f}}\left\{\left(\frac{2S^2}{f}+1\right)\pm\sqrt{\frac{4S^4}{f^2}+1}\right\}\cos\theta}{\left\{\left(\frac{2S^2}{f}+\frac{2S}{\sqrt{f}}\cos\theta+1\right)\pm\sqrt{\frac{4S^4}{f^2}+1}\right\}^2}$$

Simplifying

$$a_\theta = \frac{8S\sqrt{f}\{(2S^2+f)\pm\sqrt{4S^4+f^2}\}\cos\theta}{\{(2S^2+2S\sqrt{f}\cos\theta+f)\pm\sqrt{4S^4+f^2}\}^2} \tag{4}$$

For normal incidence θ equals 0°, this reduces to

$$a_0 = \frac{4S\sqrt{f}}{2S^2+2S\sqrt{f}+f}$$

Eq. (4) gives a direct relation between absorption and surface condition of the sample and frequency and angle of incidence of the sound wave.

The Nature of S

The minimum value of the "Surface factor" S, which a substance can have, occurs when the value of g of the substance is minimum and r, the radius of the pores, is maximum. Let us assume the minimum value of g to be 0.1, *i.e.*, when about 90% of the surface is perforated. (As the Rayleigh's equation was deduced with the assumption that the pores were moderately small, less than 0·025 cm. diameter, to allow complete dissipation of sound energy into heat through viscous action in channels into which the sound waves penetrate), one can accept the maximum value of r to be about 0.012 cm. The minimum value of surface factor S comes near about 33.

When the pores are very small (say $r = 0.001$ cm.) and the area of the unperforated surface is comparatively larger than that of the perforated surface (say $g = 10$), so that 90% of the surface is unperforated, S has fairly large value near about 4000.

In practice porous surface can be obtained having surface factor varying from 33 to values more than 4000.

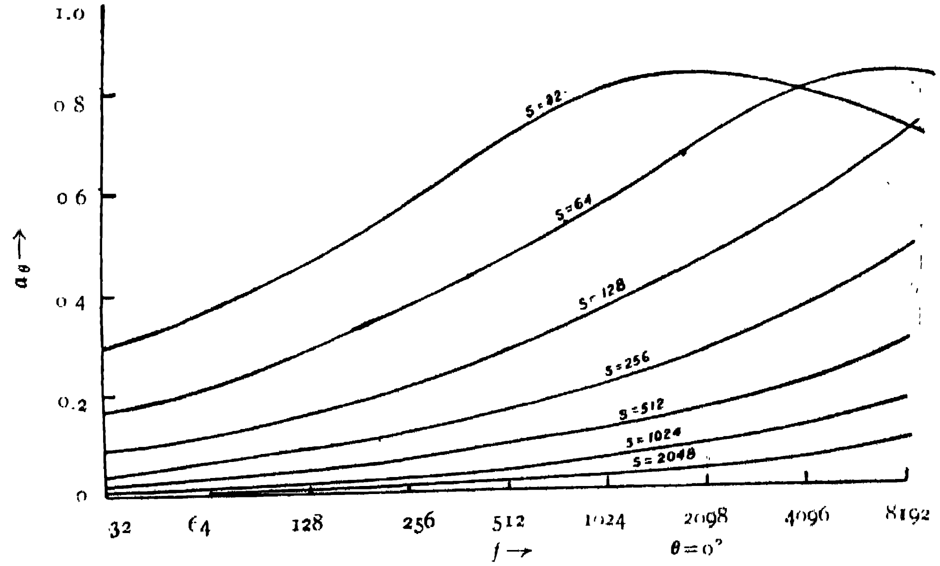

FIG. 5(a).

Fig. 5 (*a*, *b*, *c*, *d* and *e*) show the variation of a_θ with f, for substances of different values of S at various angles of incidence. It is seen that for all angles of incidence, substances having moderate values of S have a region of maximum absorption within the audio frequency band. As the value of S gradually increases the region of maximum absorption gradually shifts towards higher frequency till it is beyond the audio frequency band. Thus substances having high value of S show no selective absorption within audio frequency

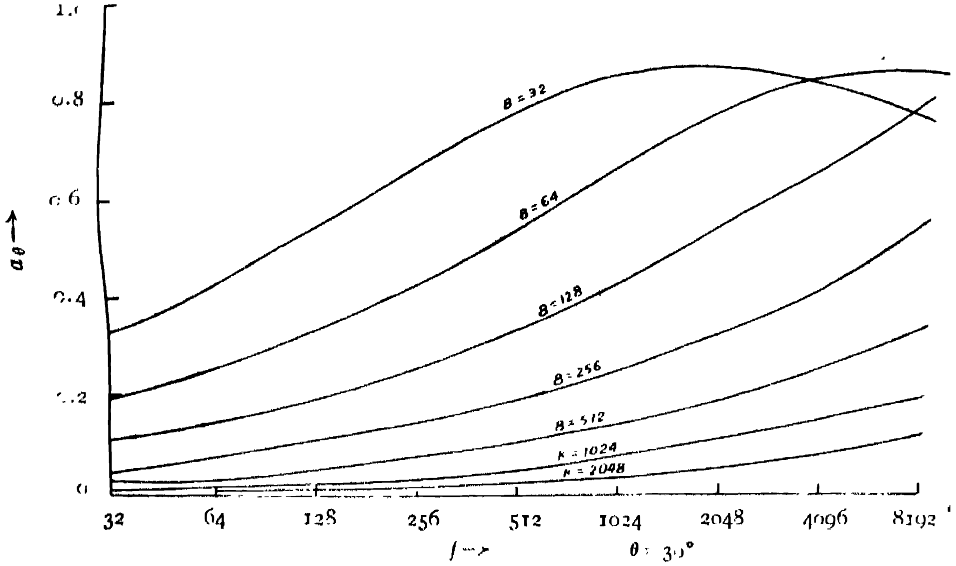

FIG. 5(b)

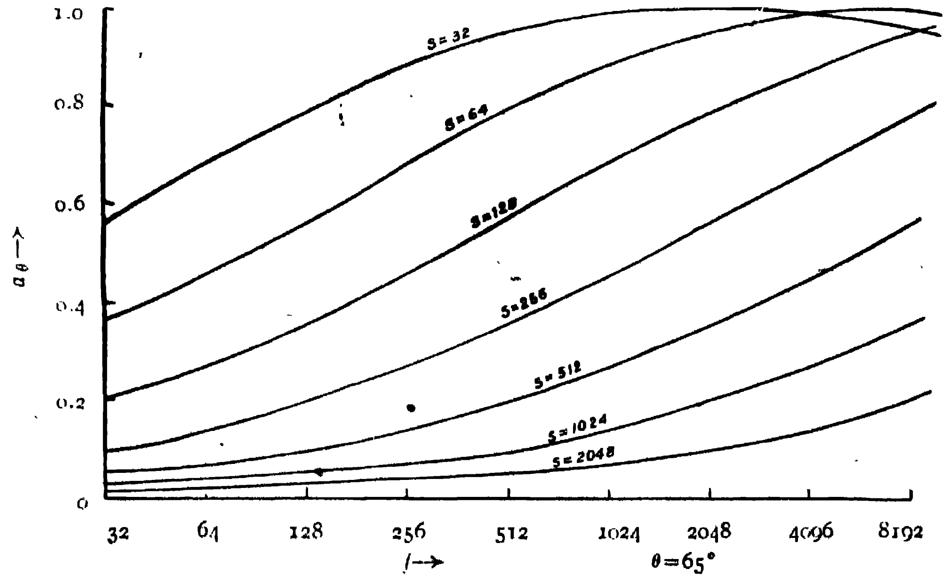

FIG. 5(c)

band and their absorption simply goes on increasing with frequency. For a particular value of S, the frequency at which maximum absorption takes place is constant for all angles of incidence less than 65°31′ and for angles greater than 65°31′ minima takes place at that frequency.

It is seen from the curves that in general the lower the value of S, the greater is its absorbing power. In other words the sound absorption coefficient is higher when the diameter of pores lies within a certain prescribed limit and the proportion of the perforated area of the surface is higher.

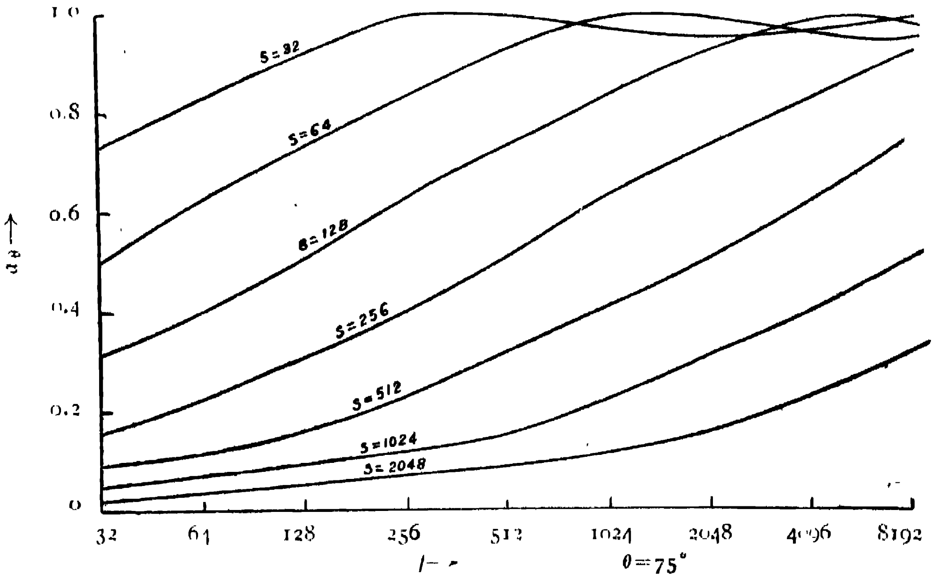

FIG. 5(*d*)

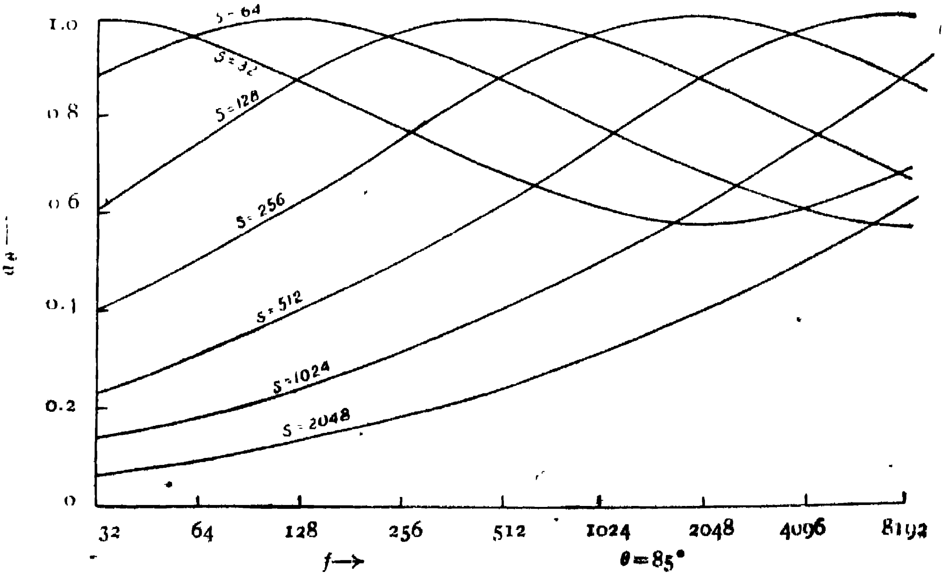

FIG. 5(*e*)

EXPERIMENTAL VERIFICATION

The absorption coefficients of some porous materials at different angles of incidence and frequencies of sound wave have been experimentally determined (See Paper I).

The variation of absorption coefficient with θ for one of these materials (Jute surface) at different frequencies is shown in Fig. 6. The nature of the curve agrees with the curves theoretically deduced as shown in Fig. 1.

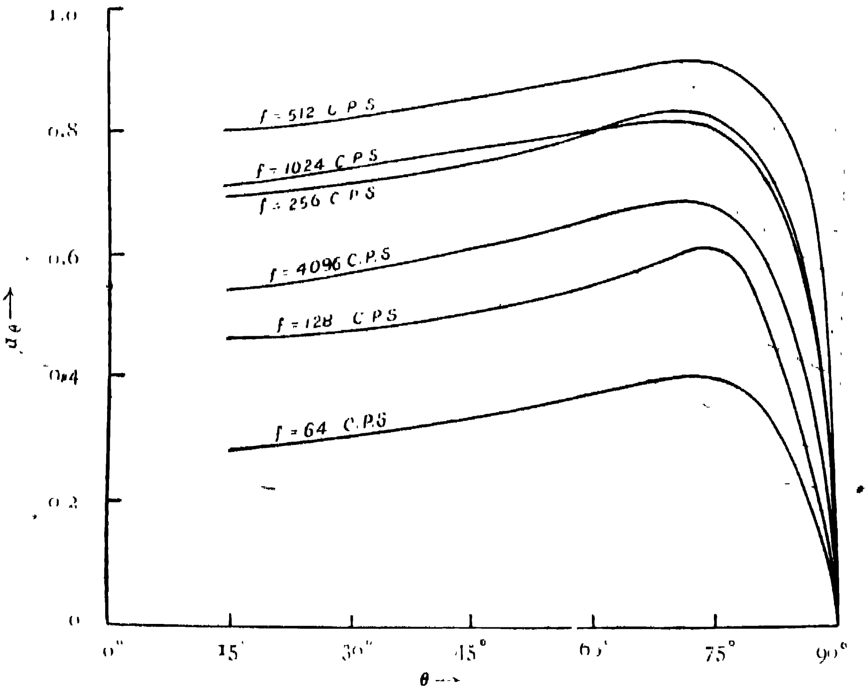

FIG. 6

In order to determine the absorption coefficient of any sample from the theoretical formula, a knowledge of the surface factor S of the sample is essential. S involves the determination of 'r' the radius of the pores and 'g' the ratio of the unperforated to the perforated surface of the sample.

The values of 'r' and 'g' of the sample formed by jute fibres were found from a microscopical study of the surface; 'r' was measured directly by means of the miscroscope and the value of 'g' was calculated from a measurement of the diameter of the fibres and the number of fibres per unit area. As the values of 'r' and 'g' are slightly different at various portions of the surface a mean of a large number of readings was taken.

The average values of r and g for the jute sample were found to be approximately ·01 cm. and ·1 respectively so that the surface factor of the jute sample came out to be about 40. In order to compare the deductions of the theoretical formula with the observational data the relation of the absorption coefficient of jute sample at an angle of incidence of 30° for various frequencies has been considered. On plotting the data in Fig. 7 one finds that for lower

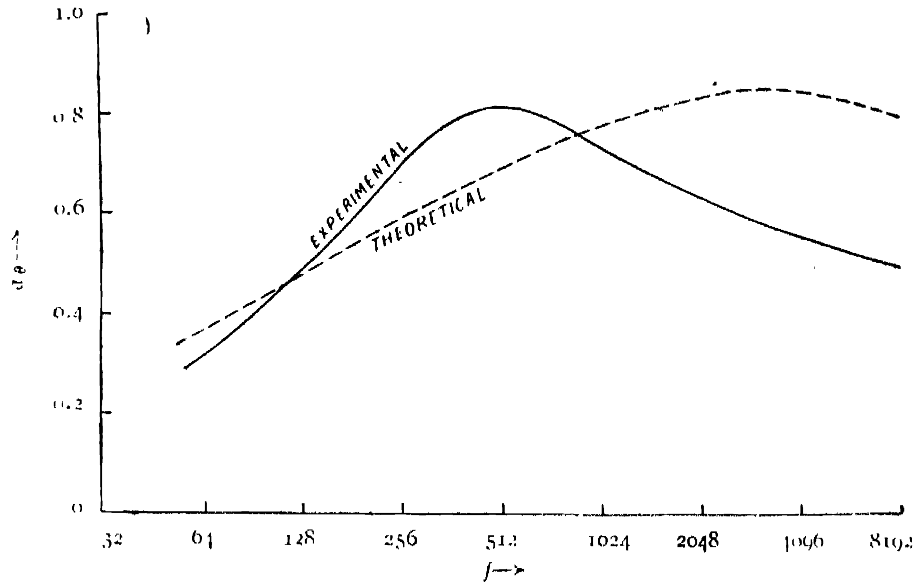

Fig. 7

values of frequencies there is a very fair degree of agreement between the theoretical value and the experimental results. But for the higher frequencies it is noted that the experimental curve of absorption is lower than the theoretical one. Further one finds that the maximum value of 0.88 is attained at 3000 c.p.s. according to the theoretical calculations. The experimental result, however, shows the maximum at a much lower frequency, namely 512 c.p.s., and the peak value of absorption is 0·83.

Such a divergence for higher frequencies requires an explanation. It may be remarked in this connexion that our theoretical formula was deduced from the consideration namely that the unperforated portion of the surface consists of rigid elements indicating that energy incident on this portion is definitely reflected at the solid boundary. But if these boundaries are of a resilient nature it is quite possible that some portion of energy is transmitted at this boundary before they are reflected. For low frequencies this time element does not play a significant role, but for higher frequencies the yielding nature of the fibre has a tendency to absorb the incident energy and the absorption will be affected by the reflected portion occurring after a definite interval. In that case the experimentally determined value of absorption will be lower for higher frequencies and the peak value of absorption will attain for the value of frequency at which the time lag factor is minimum. So absorption coefficient attains a reduced value at a lower frequency.

This aspect of the fibre regarding its yielding nature requires a closer study.

Here one may also expect certain variation between the phases of the incident and reflected waves due to yielding nature of the fibre.

ACKNOWLEDGMENT

The authors desire to express their best thanks to Prof. P. N. Ghosh, Head of the Department of Applied Physics, for his kind interest and valuable discussions throughout the progress of the work and to Mr. A. K. Sengupta for some helpful suggestions.

APPLIED PHYSICS LABORATORIES,
UNIVERSITY OF CALCUTTA.

REFERENCES

Chatterji and Dutt (1944), *Ind. J. Phys.*, **18**, 135
Paris (1927), *Proc. Roy. Soc.*, **115**, 407.
Rayleigh (1920), *Phil Mag.*, **39**, 225

6

SOUND VELOCITY AND INTER-MOLECULAR ACTION IN LIQUIDS

By RAM PARSHAD

ABSTRACT. Attempt is made to explain and discuss Parthasarathy's empirical rules between sound velocity and constitution of pure organic liquids, On the basis of the theory of intermolecular attractive forces, it is shown how cohesion and sound velocity depend upon the molecular structure of liquids. Some further rules, especially between diamagnetic susceptibility and velocity are introduced. Effect of association on compressibility and factors giving rise to cohesion and viscosity are also discussed.

INTRODUCTION

Parthasarathy (1937) has given some interesting rules relating sound velocity in liquids and their chemical constitution. They are all empirical rules. Attempt is made in the following to discuss and explain the rules on the basis of the molecular structure and theory of intermolecular forces. Some other rules are also introduced and discussed.

The rules given by Parthasarathy may be summarised as below, along with examples given by him :

(1) Aromatic compounds have usually higher velocities than the aliphatics. Benzene has velocity 1310 m/s and ethyl alcohol 1207.

(2) Among aromatic compounds, the ortho substituents have usually the greatest velocities and para the least. The effect, however, is small and may be swamped out by some opposite considerations.

Examples :—

Liquid	Velocity Meters/Sec.	Compressibility $\beta_{adiabatic} \times 10^6$	Temp. °C
o.dichlorobenzene	1246	49·7	28.0°
m-dichlorobenzene	1232	51·2	28°
o-xolene	1352	62.4	22°
m-xylene	1328	65.9	22°
p-xylene	1330	65.9	22°

(3) For paraffins, aliphatic alcohols and ketones the velocity increases as chain length increases.

Liquid	V	Compressibility $\beta \times 10^6$	Temperature C°
Hexane	1113	122.7	23
Heptane	1165	108.1	23
Ethyl Alcohol	1207	87.3	23
Propyl Alcohol	1234	81·3	23
Acetone	1203	87·4	22.5
Diethyl ketone	1314	71.2	24

(4) As the chain length of ester or ether in increased velocity decreases.

Liquid	V	$\beta \times 10^6$	Temp. C°
Methyl acetate	1211	73.5	24
Ethyl acetate	1187	79.0	23·5
Propyl acetate	1182	80·3	26
Amyl acetate	1168	83·0	26

(5) Viscous liquid have greater velocities :—Viscosity and velocity increase in the direction ethyl alcohol, ethylene glycol and glycerine. Compressibility decreases in the same order.

(6) Liquids whose molecules have dipole moments show enhanced velocities.

	V	$\beta \times 10^6$	Temp C°
Benzene	1310	66.8	23
Nitrobenzene	1455	37.6	28
Cyclonexane	1257	81.9	23
Cyclonaxanone	1441	50.8	23·5

Other examples are paraffins and their corresponding alcohols

(7) Introduction of a heavier atom into the molecule brings down the velocity. Also the introduction of a greater number of the same heavy atom tends to lower the sound velocity.

For example see p. 56.

(8) Usually the introduction of a double bond favours lowering of sound velocity.

Liquid		$\beta \times 10^6$	Temp. C°
(*a*) Acetylene dichloride $CHCl : CHCl$	1045	75.4	25
Tetra chloroethane $Cl_2HC.CHCl_2$	1155	48.6	28
(*b*) Tetra-chloroethane	1155	48.6	28
Tetra-chloroethylene $Cl_2C : CCl_2$	1027	58.4	28

(9) Among isomers, if isomerism is not of the optical kind, there is difference in sound velocity. The xylenes, α and β picolines, butyl and isobutyl alcohol show such difference. But the optical isomers, the *d* and *l* pinens possess identical velocity.

DISCUSSION AND EXPLANATION OF RESULTS

1. Now the fundamental factor with regard to the structure of liquids is not the velocity of sound waves in them but their compressibility (pointed out by Bergmann also), adiabatic or isothermal, given by

$$V = \frac{1}{\sqrt{d\beta}},$$

where V is velocity, *d* density and β the adiabatic compressibility.

The author (Parshad, 1941) has shown previously how to link up compressibility with molecular forces and only big points may be presented again.

Among molecules three kinds of forces have been recognised. (1) General forces, or dispersion or London forces.

They act among all kinds of molecules. The simplified, and approximate, formula as given by London is

$$U = -\frac{3}{4} \cdot \frac{\alpha^2 V}{R^6}, \qquad \dots (1)$$

where α is polarisability of one molecule,
V is ionisation or excitation potential,
R is distance between the two interacting molecules.

2. Orientation forces or keesom forces.

These forces, as first shown by Keesom (1916), act between dipoles only. At moderate temperatures the energy of interaction U between two molecules is given by

$$U = -\frac{2}{3} \cdot \frac{\mu_1^2 \mu_2^2}{KTR^6}, \qquad \dots (2)$$

where μ_1 and μ_2 are the dipole moments of the interacting dipoles and R is the distance between them.

Other symbols have their usual meaning.

3. Induction forces or Debye forces.

It was shown first by Debye (1921) that there can be attraction between a polar molecule and a non-polar molecule in virtue of the non-polar molecule being induced upon by the polar, prior to attraction. These forces are the least important but are independent of temperature.

The expression for the interaction energy is

$$U = -\frac{\mu_1^2\alpha_2 + \mu_2^2\alpha_1}{R^6}, \qquad \ldots \quad (3)$$

where α_1, α_2 are the polarisabilities of the molecules. Other symbols have the meanings given above.

Apart from these attractive forces functioning in molecular organic liquids under consideration, there are also found to be repulsive forces coming into importance at very small distances, and in fact varying inversely as 9th or 10th power of the distance. Their source was not clear on classical ideas, but now has been cleared up on quantum mechanical considerations. Generally then we may have interaction energy E between two molecules where E is given by

$$E = \frac{C_r}{R^n} - \frac{C_a}{R^6},$$

where n is of order 9 to 12, R is intermolecular distance, C_r is constant for repulsive fields and C_a for attractive fields.

The molecules would be in positions of minimum free energy or approximately minimum potential energy. Now it is easy to visualise that the greater the attractive constant C_a, the nearer will the molecules be to each other till the separating influence of repulsive fields and temperatures bring them to a stop. At that the cohesive energy will be the greatest.

Note.—Minimum potential energy corresponds to greatest cohesive energy since the latter is of negative sign.

Now it can also be seen that with cohesive energy great, compressibility will be small. The nearer are the molecules to each other, the greater will be the change in energy for each small progressive displacement as it will be a greater proportion of the existing intermolecular distance the smaller the latter distance already is. In other words the smaller the distance between molecules, the greater the rate of change of energy, and hence lower the compressibility. This idea can be put as below :

$E \; \alpha \; \frac{1}{R}$, where the power of R is not mentioned

$$\frac{\partial^2 E}{\partial R^2} \; \alpha \; \frac{1}{R^3} \; \alpha \; \frac{1}{R}.$$

$\frac{\partial^2 E}{\partial R^2}$ is of course related to modulus of elasticity (neglecting the temperature effect) and inverse to compressibility.

Hence

$$\text{Compressibility} \propto \frac{1}{E} \propto \frac{1}{C_a}$$

The exact evaluation of compressibility, considering the entropy and temperature, involves difficulties and has not been done satisfactorily to date. The calculation is however particularly easy, considering only two molecules and their displacement in their mutual direction, neglecting the temperature effect, *i.e.*, using only the equation (3).

By means of the above findings, the empirical rules about velocity can be explained easily. The rules for discussion will not be taken in the order presented.

Rule.—Presence of dipole moments enhances the velocity.

In terms of dipole orientation or Keesom forces (eq. 2), the rule is self-explanatory. But there are many other factors to be taken into consideration in this connection. We observe that the attractive forces are very short range forces (varying inversely as 7th power of the distance) and, so much so, that in an accurate analysis, the length and shape of molecules has to be taken into account, and interaction between parts of molecules considered, instead of molecules as a whole. Again the relative position and the nature of a dipole or dipoles in a molecule play a tremendous part in deciding the mode of molecular interaction. A dipole which is hidden in the rest of the molecule will not be as effective as that which is more open. The individual cases will be more fully discussed in the course of the analysis.

Associations.—Another phenomenon which must be taken into account, when considering effect of dipoles, is that of associations. It has been established from many evidences, *e.g.*, electron diffraction, dielectric polarisation. Raman and infra-red spectra that many so-called abnormal liquids like water, normal paraffin alcohols, carboxylic acids exhibit the tendency of their molecules to join, or associate in the form of clusters of two or more molecules. The molecules in any cluster are hard knit up among themselves, being directly under electric dipole forces, but are loosely attached to those outside, through only the residual forces. Now in sound vibrations in a liquid, we may approximately take any cluster to move as a whole, *i.e.*, not to have comparatively so much phase difference among its constituents as with respect to molecules outside. Hence the cohesive energy relevant in our case of sound velocities will be that between one group or association and other molecules or associations outside it. Now if associations are broken up while other things, *i.e.*, temperature, pressure, etc., remain the same, the great cohesive energies looked up in different associations will be released and molecules all round will be knit up more closely, due to the freed dipoles, with subsequent lowering of compressibility. Hence we have, taking the reverse, that, on forming associations, compressibilty will increase. This picture of association and its relation to compressibility is a rough one, but we do not yet know enough of liquid structure to be more defiinite in the circumstances. Another interpretation of associations is that the co-ordination number is low, *i.e.*, the number of neighbours round a molecule in a liquid is less than what would be if random distribution of molecules existed. The presence of directed dipole forces gives an open structure to the liquid. When associations are broken, the cohesive energy rises, due to closer distribution of molecules.

The effect of association in increasing the compressibility is best seen in the case of water. The velocity goes on increasing and compresibility decreasing with temperature up to a certain limit. This is due to associations breaking with increase of temperature which affect the liquids in the manner opposite to that done by expansion and increase of intermolecular distance.

To discuss the rule of dipoles we take a few cases where the simple rule breaks down. Now nitrobenzene, chlorobenzene and aniline have dipole moments of 3.80, 1.56 and 1.55 Debye units, and yet their velocities are 1490, 1302 and 1682 m/s, and their compressibilities 37.6, 53.6 and 34 7 relative units. Considering the details mentioned above, this fact is not unexpected. The dipole NO_2 of nitrobenzene is well shielded by the big O atoms on one side and the benzene nucleus on the other and has very unfavourable condition for great intermolecular approach and formation of associations. Measurements of dielectric polarisation and infra-red spectroscopic data have well testified to this fact of the absence of any prominent associations. Due to large moment and absence of associations the compressibility is sufficiently low, and indeed much less than that of chlorobenzene. In chlorobenzene, the dipole is again inhibited from close intermolecular approach due to massive Cl atoms. Again, dielectric polarisation measurements reveal that the molecules form a so-called non-polar association, which means that the associating dipoles are not head-on (indeed they cannot do so from steric reasons) but interact in a way, so that their resultant dipole is nearly zero. With all these factors of unfavourable configuration of the dipole, low dipole moment, and the fact of formation of associations the compressibility is highest and velocity the least. Aniline has been found to be almost unassociated, from studies on infra-red spectra. Now the NH_2 dipole has H atoms which, being of small size, can approach very near to other molecules, thus causing intense intermolecular action. These two factors together contribute to the lowest value of compressibility of aniline.

Again acetone has a dipole moment of 2.1D and of water 1.5D, yet in the latter the compressibility is much lower and velocity much higher than in the former (compressibility 87 and velocity 1200 m/s). In acetone the dipole is shielded from one side, so that only the negative end O is outside on the surface of the molecule. In water the dipole is open on all sides. Again ether and acetone have higher dipole moments (2.1D and 1.50D) than the moment of chloroform (.8D), yet the compressibility of the last compound is the least. This is due to the dispersion forces among Cl atoms becoming important in magnitude. Alcohols and water have nearly the same dipole moment, yet there is great disparity in compressibilities and velocities.

Similarly numerous other cases can be quoted, stressing the need for not regarding the dipole action as represented only by the dipole moment as found from dielectric polarisation measurements.

Rule of viscosity :—Viscous liquids have higher velocities.

Viscosity is the temporary resistance offered to shearing of liquid molecules. Now it is evident that the greater the intermolecular field between molecules the more difficult it will be to displace them relative to one another. Hence we have, that greater the cohesive energy or less the compressibility, the greater the viscosity or less the fluidity, that latter being the reciprocal of viscosity. Of the numerous formulae set up for viscosity by Andrade, Frenkel, Raman and others, the general form is

$$\eta = Ae^{\frac{U}{KT}}$$

where A is a constant, K, T the usual symbols, and U an activation energy. This activation energy is the energy supposed to be parted to the molecules in order that they may overcome the potential barriers or be able to move from the pits of minimum potential energy. This U can be taken as a function of the cohesive energy, or inverse of compressibility. In fact Datta (6) (1943) has formulated the following :—

$$\eta = AT^{\frac{1}{2}}e^{\frac{b}{\chi}}$$

where η is viscosity and χ the compressibility.

The fact that viscosity and cohesion go together, and therefore viscosity and velocity, is also shown by their change with temperature. With rising temperature, the chaotic motion and the intermolecular distance increase. Due to the former, the frequency of relative position of molecules in the position of greatest cohesive-interaction decreases, and due to the latter, the cohesive energy directly decreases by the increase of R in (3). Hence on these accounts viscosity and cohesive energy both decrease, the latter lowering the sound velocity.

Parthasarathy's rule about viscosity is covered by the above, but again, on analysing closer, we find that the rule is only approximate, like the rule of dipoles.

Now the fundamental difference between fluidity and compressibility is that the former is an irreversible or inelastic phenomenon of intermolecular action while the latter is an elastic one. The molecules displaced by shear have no tendency to come back, but the compressed molecules return to their original positions and configurations when the compressing pressure is removed. Again viscosity is concerned with the shearing of molecules, *i.e.*, movement of one molecule or molecular plane at right angles to the other, while the compressibility with the movement of molecules in their line of centres. Thus the viscosity, so to say, deals with the anisotropic behaviour and compressibility with symmetric behaviour of molecules. The anisotropic molecules will have a viscosity that may not in cases be compatible with their value of cohesive energy or compressibility, and on the other hand the condition will be reversed when the molecules are more or less symmetric. Again viscosity and compressibility are very significantly related to association. While the compressibility increases with association, so does also viscosity, although by our approximate rule it should decrease. Due to association a bridge or mesh-like structure is produced which and the anistropy produced by it increase the shearing resistance and so the viscosity, while the cohesive energy is decreased due to decrease of immediate neighbours and other consideration given above.

EXAMPLE OF DEVIATION OF THE RULE

Carbon tatrachloride has more viscosity than chloroform, but the velocity and compressibility considerations are in the reverse order. Isobutyl and isopropyl alcohols have higher viscosities than the normal alcohols, thus not following Parthasarathy's rule. The velocity of water increases with increase of temperature in the ordinary range due to decrease of compressibility while the viscosity decreases. With increase of pressure to some range on water, its viscosity falls while velocity increases. Viscosity and compressibility behave oppositely for formation of hydrogen bonds. The viscosity increases with formation of hydrogen bonds, while sound velocity decreases and compressibility increases. The above is the example of water.

Rule.—Aromatic compounds have higher velocities than aliphatic compounds

The difference in these compounds which concerns our purpose lies in the following :—

Anisotropy of polarisability.—Aromatic compounds have their maximum polarisability axis at right angles to the plane of the molecule and aliphatic compounds have it along the molecular chain axis.

Two molecules in interaction will tend to set themselves in their maximum mutual force-field, *i.e.*, along their axis of maximum polarisability. The aromatic molecules along their axes of maximum polarisability will have their planes parallel. In this position, the atoms at corners of the planes will come in close proximity, and exert extra strong interaction due to individual dispersion or London forces. In the case of aliphatic compounds, the considerations are just the reverse. Not only is the cohesive energy less due to lower polarisability but also because end-to-end configuration brings in the least number of atoms in close proximity.

The difference in question between aromatic and aliphatic compounds may be shown from some kinds of experimental evidence, *e.g.*, heat of mixing of ethyl alcohol in benzene and carbon tetrachloride, or heptane; dielectric polarisation of alcohol in the above solvents, and the compressibility of alcohol-heptane and alcohol-benzene mixtures (Parshad, 1942; Wolf, 1937).

Rule.—Ortho compounds have highest velocity and para the least.

The polarisability and vector sum of dipole moments decrease in the order of ortho, meta to para, producing corresponding gradation in cohesive energy. Hence the rule on compressibilities and velocities. Now it must be borne in mind that the difference in question is small, and might be upset by any new factor, for example, by association, if any. In para compounds vector sum of zero dipole moments does not mean no dipole action. The dipoles are so far away, that they act nearly singly.

Rule.—Velocity increases as chain length of paraffin, aliphatic alcohols and ketones increases.

Chain length and alcohols.—Now the alcohols are associated liquids, and as has been shown the association decreases the cohesive energy. The increase of chain length would affect the intermolecular configuration in two ways :

(1) There would be more chain to chain aggregation. In fact the chain aggregation in long chain alcohols and paraffins is well known. Due to number of atoms increasing with increase of chain the end-to-end tendency will be overcome. The total dispersion forces between atoms in an increasing chain will also be increasing.

(2) The association of alcohol dipoles is in the direction of chain length. With increasing chain, therefore, the tendency of forming association is decreased. Badger and Bauer (1937) found that the association band of alcohols (in infra-red) decreases in intensity as chain length increases. This decrease or removal of associations leads to higher cohesional energy. In the case of paraffins the dispersion energy will increase with chain length, due simply to the increase in the number of atoms in a molecule.

In ketones, although the dipole moment may be thought to remain the same, the dispersion energy will increase with increase in the size of the molecule. And due to the shielding of the positive end of the dipole in ketones, the dispersion energy is quite appreciable relatively.

Rule.—Velocity decreases as chain length in ethers and esters increases.

(1) *Dipole moments.*—As chain length increases, the dipole moment decreases.

Methyl ether	...	dipole moment		1.29 D.
Ethyl ether	...	,,	,,	1.12 D.
Propyl ether	...	,,	,,	0.86 D.

The rule is self-explanatory.

Rule.—Unsaturated compounds have lower velocity.

The rule does not seem to be general. Ethyl bromide has the velocity and the compressibility of 892 m/s and 88.1 × 10^{-6} Ab units at 28°C while ethylene bromide has the respective values of 1014 and 44.7 × 10^{-6}. The same behaviour is expected of ethyl chloride and ethylene chloride, but their values are not given in literature.

The following considerations support the rule :—

(1) *Double bonds and polarisability.*—A double bond has polarisability (Denbigh, 1940) slightly larger than a single bond, but considering that in any molecule the double bonds are formed at the cost of two single bonds, the total polarisability of a molecule with single bond is greater than that of a molecule of corresponding chemical class with double bonds.

(2) Due to residual valency forces, the unsaturated compounds form associated products, and this may tend to lower their velocity though we cannot push this conclusion far, as this association may have different grounds and other factors than those already considered.

(3) With removal of double bonds more atoms come into the molecule which can exert additional dispersion and other forces and so enhance cohesion, lower compressibility and increase velocity.

The following is against the rule :-

Dipole action.—It has been shown by Smyth that the dipole moment of double bond between atoms of different elements is much more than twice the moment for a single bond, and similar is the case for a triple bond. For example the cyanide moment is eight times that of the single carbon-nitrogen bond, and double bonds between carbon and oxygen and between carbon and sulphur have moments slightly less than three times those of the single bond. The consideration seems to go against Parthasarthy's rule. But Parthasarthy studied the compounds $CHCl=CHCl$ and $CHCl_2.CHCl_2$; $CCl_2=CCl_2$, and $CHCl_2.CHCl_2$ and in these compounds the bonds are between similar atoms and so Smyth's conclusions are not strictly applicable here.

Rule.—Introduction of a heavier atom in the molecule decreases the velocity.

The rule seems just fortuitous as has been pointed out by Bergmann also. It seems to hold more with velocities than with compressibilities. As a matter of fact it seems just the reverse for compressibility.

In the table below R.H. denotes ' Rule held ' and R.N.H. denotes ' Rule not held.'

The table has been taken at length, due to many points involved. We note that Parthasarthy's rule about velocities is held in most of the cases, with exceptions here and there. What is more important to note is that the rule does not hold at all with regard to compressibilities except for the pair carbon-tetrachloride-chloroform.

Note.—Parthasarathy's rule about compressibility may be taken as meaning a decrease of compressibility where increase of velocity is indicated.

SUBSTITUTION OF A HALOGEN BY A HALOGEN

No.	Compound	Temp.	Velocity m/s		Compressiblity × 10 absolute units	
1	Butyl bromide	25.5	1016	R.H.	76.2	R.N.H.
	Butyl iodide	28.0	959		67.3	
2	Acetylene tetrachloride	28.0	1155	R.H	48.6	R.N.H.
	Acetylene tetrabromide	28.0	1007		33.3	
3	Chloroform	23.5	1001	R.H.	67.1	R N.H.
	Bromoform	24 0	929.8		40 0	
4	Methylene chloride	23.5	1064	R.H.	66 2	R.N.H,
	Methylene bromide	24.0	971 2		43 2	
	,, iodide	24	977.0	R.N.H.	31.5	R.N.H.
5	Ethylene chloride	23.0	1240.0	R.H.	51.8	R.N.H.
	,, bromide	24 0	1014		44.7	
6	Butyl bromide	28.0	1016	E.H.	76 2	R.N.H.
	,, iodide	28.0	959		67.3	
7	Chlorobenzene	23.0	1302	R.H.	53.6	R.N.H.
	bromobenzene	28 0	1134		52 0	

ADDITION OF HALOGENS

1	Monobromo-ethane	28	892	R.H	88.1	R.N.H
	Dibromoethane	24	1014		44.7	
	Tetrabromoethane	28	1007		33.3	
2	Methylene bromide	24	971	R.H.	43.2	R N H.
	Bromoform	23,5	929		40 0	
3	Chlorobenzene	23	1302	R.H.	53.6	R N H.
	Dichlorobenzene meta	28	1232		51.2	
	,, para	25	1246		49.7	
4	Chloroform	23 5	1001	R H.	67.1	R.H.
	Carbon tetrachloride	23 0	928.5		72 6	

The rule about velocity comes to be held for the reason that with increase of the mass of the halogen content the compressibility does not decrease so rapidly as the density increases, so that velocity on the whole decreases.

The following points may be offered relevant to the problem. As a heavier halogen atom is introduced, the following changes take place:—

(1) The dipole moment decreases. This consideration will decrease the velocity and increase the compressibility.

(2) The polarisability increases; the atomic number increases and so does the polarisability, as this depends upon the number and square of radii of different shells of electrons. This factor will tend to increase the cohesive energy.

(3) *Steric hinderance.*—As a bigger atom is substituted, it will be difficult for other molecules to approach it as near as before when the atom was smaller.

On this consideration, cohesive energy will decrease from chlorine to iodine. Actually it is the polarisability consideration which is the most outstanding and so compressibility falls when a heavier halogen is substituted for a lighter one, or when the halogen content is increased. We have seen in Eq. (1) and (3), how polarisability increases intermolecular cohesive energy.

The consideration of steric hinderance is hinted at by examining more closely the case of aliphatic and aromatic liquids. In aliphatic liquids, the decrease in compressibility is relatively more than in aromatics and this may be significantly due to the different molecular structures of the two classes of liquids.

In aliphatic compounds, the question of steric hinderance is not expected to be much as the interaction is mainly end to end. But in aromatics, however, the consideration is different. We have seen before, that interaction in aromatic compounds is in the direction at right angles to the hexagonal planes and is on this account quite intense also. The presence of bigger atoms will debar the other C-H groups of the planes to come in the same close proximity as before and so interaction will be effectively decreased with the consequent increasing of compressibility from what it would be otherwise. The above explanation with regard to aliphatic and aromatic compounds throws additional light on the different modes of interaction in these compounds

Rule.—Velocity in isomers is different.

With regard to the consideration outlined in the beginning for establishing relations among cohesive energy, compressibility, molecular fields, etc., it is not difficult to see that different isomers should have different velocities and compressibilities. Isoalcohols have in general lower velocities and higher compressibilies than the normal alcohols as the dipole O-H, by coming in within the structure of the molecule, is unable to take as much an active part in interaction as when it is outside in normal alcohols. Of course in isomers of the optical kind, the molecules are identical as far as intermolecular action is concerned.

Other rules.

Besides the above rules of Parthasarthy, we introduce some further rules relating to compressibility and moleculer structure.

(1) *Rule.*—Increase of magnitude of diamagnetic susceptibility tends to increase sound velocity and decrease the compressibility.

Ortho substituted benzene have the greatest susceptibility and decrease in passing to meta and then, para, while velocity also in general varies in the same way.

The rule about diamagnetic susceptibility is also approximate and incidentally holds more for velocities than compressibilities.

(2) *Rule.*—Liquids having higher boiling points have higher velocities.

Examples are self-evident but still those of alcohols and hydrocarbons may be mentioned. Increasing chain length increases both the boiling point and velocity.

(3) *Rule.*—Liquids having greater heat of vaporisation have higher velocities.

(4) Increasing size of molecules show increasing velocity.

(5) The presence of many OH's in the molecules and situated distantly from each other, enhances sound velocity.

Example.—Velocity rises greatly and compressibility falls as we proceed from monohydric alcohols to polyhydric alcohols.

EXAMPLES

Liquid	Temp. C°	Velocity	Compressibility × 10⁶	Susceptibility.
(1) Methyl Alcohol	23·7	1130	98·9	—·65 (at – 3·0°C)
Ethyl ,,	23·5	1207	87·3	—·01 (at –20°C)
Propyl ,,	24·0	1234	81·9	—·766
Butyl ,,	23·9	1315	71·5	—·743
(2) Methyl acetate	24·0	1211	73·5	—·500
Ethyl acetate	23·5	1187	79·0	—·581
(3) Chloroform	23·5	1001	67·1	—·488
Bromoform	24·0	929·8	40·0	—·316
Carbon tetrachloride	23·0	828·5	72·6	—·429
(4) Methylene chloride	23·5	1064	66·2	—·549
Methylene bromide	24·0	971·2	43·2	—·379
Methylene iodide	24·0	973·7	31·5	—·349
Eethylen chloride	23·0	1240	51·8	—·602
Ethylene bromide	24·0	1014	44·7	—·422
(5) Cyclonexanone	23·5	1411	50·8	—·648
Cyclohexanol	24·0	1622	40·2	—·727

DISCUSSION

Rule concerning diamagnetic susceptibility.

(1) Diamagnetic susceptibility and intermolecular energy.—Susceptibility is related to polarisability through the expression—

$$\frac{h^2 a}{8Mc^2\chi} = \Sigma r^2,$$

where χ is susceptibility, a the polarisability, r the distance of the electron from the nuceleus, the other symbols having their usual meanings. The expression for polarisability is approximate.

Kirkwood (1937) has given an empirical relation :

$$-\chi = \frac{I_{,}e^2 a_0^{\frac{1}{2}} \sqrt{Na}}{4mc^2},$$

a_0 is the value of 1 Bohr radius ;
and Buckingham (1937) gives the formula

$$\chi = \frac{-2e^2\alpha_0^2}{6mc^2} \cdot v_0 < r^2 >_0,$$

where α_0 is the polarisability of the ring of electrons v_0 in number and of radius r_0.

London gives U the inter molecular energy between two molecule, as

$$U = -\frac{1}{R'} \cdot \frac{6mc^2}{N_l} \cdot \frac{\alpha_k \alpha_p}{\frac{\alpha_k}{\chi_k} + \frac{\alpha_p}{\chi_p}};$$

k and p pertain to the two interacting molecules.
The above expression is for only a simple system of molecules having one strong frequency.

(2) Angus and Hill (1940).—They conclude by investigating the susceptibility of associating substances like benzoic acid in solvents like benzene and ethyl acetate that as association increases, susceptibility decreases. We have already seen how association increases the compressibility, and hence our rule of diamagnetic susceptibility. However Anantkrishnan and Varadachari (1944) criticise the conclusions of Angus and Hill. But as far as pure liquids are concerned decrease of association does seem to be reflected in increase of susceptibility. Thus Sibaiya (1935) finds that susceptibility of ice is considerably less than that of water, and Varadachari (1935) finds that susceptibility of water rises with temperature. Rao and Sriraman (1938) finds that molecular susceptibility of formic acid is 20.53 and that of the formate ion is 17.3. The two values should have been identical if formic acid molecule were monomeric and which we know to be mostly dimeric.

Rule.—Velocity increases with increase of heat of vaporisation and boiling point.

The exact mechanism of boiling, like that of melting, is yet obscure, but it can be roughly seen that before a liquid can boil, a molecule has to gain enough kinetic energy, so as to be able to overcome the force of cohesion that bind it to other molecules. The greater the cohesive energy, the greater the heat of vaporisation. The boiling point will also rise with heat of vaporisation for boiling point is an indication of the heat of kinetic energy of a single molecule which has to counteract its cohesive energy. In fact according to Trouton's rule ML/T is constant for unassociated liquids where L = heat of vaporisation and T the boiling point and M is molecular weight. Lennard Jones (1939) gives the approximate formula

$$kT_b = \tfrac{3}{4}\,\phi_0,$$

where T_b is the boiling point and ϕ_0 the total attraction energy between a pair of molecules of the liquid. Now boiling is insensitive to the kind of molecular force of attraction holding the molecule before its escape, *viz.*, whether the molecule is associated or not. If it is not associated, it has to overcome the general sort of cohesion of other molecules upon it. If it is associated through a hydrogen bond or otherwise, it has to overcome mainly the attachment with its associated molecule or group. Due to these considerations, the relation between heat of vaporisation and compressibility is sometimes distorted.

Rule.—The size of molecule.

As the size of the molecule increases, there can be greater dispersion energy between the molecules leading to lower compressibility. It can be seen that as the size of the molecule increases, the state of any kind of molecule changes from the gas state to the liquid and then to the solid state. There is not much need here to labour the point further.

Rule.—Presence of many OH's in the molecule.

The greater the OH's in the molecule, the more will be the dipole interaction. The intensity of general cohesive interaction will be favoured by the placing of the OH's far from each other in the molecule. Then any steric hindrance of one OH for the other OH, in bringing other molecules for close interaction, decreases. By their acting independently, the OH's make the whole molecule active rather than some part of it, if the dipoles occur together. But we must note that in accordance with our previous treatment of the problem, it will be the viscosity that will increase at a more rapid rate than cohesion. The case in point is of polyhydric alcohols.

Similarly many other rules relating to surface tension, refractive index, dielectric constant, etc., may be formulated because all of them arise in general from foctors causing cohesion.

I thank Dr. A. K. Dutta and Dr. P. K. Kichlu for helpful advice and discussions.

PHYSICS LABORATORY,
GOVT. COLLEGE,
LAHORE.

REFERENCES

Anant Krishnan and Varadachari, 1944, *Proc. Ind. Acad. Sc.* **20,** 128.

Angus and Hill, 1940, *Trans. Farad Soc.* **38,** 923.

Badger and Bauer., J., 1937, *Chem. Phys.* **5,** 839.

Buckingham, 1937, *Proc. Roy. Soc.* **94,** 160.

Datta, A. K., 1943, *Nature*, **1823,** 445.

Debye, 1921, *Phys. Zeits.* **22,** 302.

Denbigh, 1940, *Trans. Farad. Soc.* **66,** 936.

Keeson, 1916, *Proc. Amst.* **18,** 635.

Kirkwood, quoted in Buckingham (1937).

Lennard Jones, 1939, Interatomic forces, Indian Association for the Cultivation of Science, Calcutta

Parthasarthy, 1937, *Curr. Sci.*, **6,** 322.

Parshad, 1941, *Ind. J. Phys.*, **15,** 323; 1942, **16,** 1.

Rao and Sriraman, 1938, *J. Annamalai Univ.* **7,** 187.

Sibaya, 1935, *Curr. Sci.* **3,** 421 , **4,** 41.

Smyth, Dielectric constant and molecular structure.

Varadachari, 1933, *Proc. Indi. Acad. Sci.*, **2,** 168.

Wolf, 1937, *Trans Farad. Soc.* **33,** 179.

MAGNETIC STUDIES ON CUPRIC IONS IN CRYSTALS

By A. MOOKERJEE

ABSTRACT. Magnetic anisotropy and principal susceptibilities of few alkali cupric halides have been measured and the results are discussed in relation to crystal structure and Van Vleck's theory. The relative orientations of the paramagnetic units in cupric Tutton salts have been calculated.

I. INTRODUCTION

The magnetic behavior of cupric ions in single crystals of $CuSO_4.5H_2O$ has been studied by K. S. Krishnan and the present writer (1936, 1938). It was shown that the electric field in the neighbourhood of the Cu^{++} ion has tetragonal symmetry, imparting on the crystal a uniaxial magnetic symmetry. The magnetic data combined with the known fine structure of the crystal reveals that the magnetic moment for directions normal to the axis of symmetry of the paramagnetic unit has the spin-only value, while the moment for direction along the axis of symmetry gets some contribution from the orbital angular momentum over the spin-only value.

Cupric alkali halides, for which X-ray data are available will provide interesting magnetic studies of single crystals as there is the possibility of calculating the directional magnetic properties of the paramagnetic unit in these crystals and compare them with those of copper sulphate pentahydrate. In this communication are presented the results of a systematic study of some of these crystals as well as of cupric acetate monohydrate as it is a less hydrated crystal, is therefore magnetically more concentrated than the other copper salts and thus may show interesting magnetic behavior quite different from the above salts and the cupric Tutton salts.

II. EXPERIMENTAL

The method adopted for the measurement of the anisotropy is that of Krishnan and Banerji (1934). The crystal is suspended at the end of a calibrated quartz fibre in the centre of a homogeneous magnetic field with known directions vertical. The direction in the crystal which sets along the field and the difference between the maximum and the minimum susceptibility in this plane were determined.

By suspending the crystal separately in any convenient vertical direction and allowing it to take up its natural orientation in a non-homogeneous magnetic field, one of the principal susceptibilties of the crystal was determined by the magnetic balancing method of Krishnan and Banerji (1937), which, combined with the anisotropy measurements, gave the principal susceptibilities.

III. RESULTS

Results of measurements are collected in Tables I and II and expressed in the usual units, *i.e.*, 10^{-6} of a c.g.s. electromagnetic unit. For the tetragonal crystals the gram molecular susceptibilities along the axis of symmetry of the crystal and for directions normal to it are denoted by $\chi_{\parallel}$ and $\chi_{\perp}$ respectively; for monoclinic crystals χ_3 is the gm. mol. susceptibility along the 'b' axis, while greater of the two in the (010) plane is denoted by χ_1 and the smaller by χ_2. θ is the angle which the 'a' axis makes with the χ_2 axis. Effective magnetic moments (μ_i) are calculated by using the expression $\mu_i = 2.84\sqrt{x'_i T}$ where $i = 1, 2, 3$ or $\perp$ and $\parallel$: x'_i is the principal susceptibility corrected for diamagnetism (for both cation and anion). Mean effective moment ($\bar{\mu}$) is given by $\sqrt{\frac{\mu_1^2+\mu_2^2+\mu_3^2}{3}}$ or $\sqrt{\frac{\mu_{\parallel}^2+2\mu_{\perp}^2}{3}}$. The diamagnetism of Cu^{++} ion was calculated to be -14.8×10^{-6} by the method of Slater as modified by Angus (1932). The following diamagnetic correcrions for the different groups as given in Stoner's book (" Magnetism and Matter," page 470) were adopted.

NH_4	K^+	Rb^+	Cs^+	Tl^+	Cl^-	SO_4^{--}	SeO_4^{--}	$CH_3(COO)_2$
−22.1	−18.5	−27.2	−41	−40	−20.1	−33.6	−41.4	−28.6

TABLE I

Temperature = 30° C

Crystal	Crystallographic data	Mode of suspension	Orientation in the field	Magnetic Anisotropy 10^6 CGS. Units
$CuCl_2.2NH_4Cl.2H_2O$	Tetragonal $z = 2$ $a = 7.58$ $c = 7.95$	Tetragonal axis horizontal	Tetragonal axis normal to the field.	$\chi_{\perp} - \chi_{\parallel} = 258$
$CuCl_2.2KCl.2H_2O$	Tetragonal $z = 2$ $a = 7.45$ $c = 7.88$	Tetragonal axis horizontal.	Tegragonal axis normal to the field	$\chi_{\perp} - \chi_{\parallel} = 263$
$CuCl_2.2RbCl.2H_2O$	Tetragonal $z = 2$ $a = 7.81$ A $b = 8.0$ A	Tetragonal axis horizontal.	Tetragonal axis normal to the field	$\chi_{\perp} - \chi_{\parallel} = 262$
$Cu(CH_3COO)_2.H_2O$	Monocl. prism $z = 8$ $a = 13.18$ $b = 8.46$ $c = 13.89$ $\beta = 117°6'$	'b' axis vertical. 'a' axis vertical. (001) pl. horiz.	$\theta = 2.2$ 'b' normal to the field. 'b' ax. par^l to the field.	$\chi_1 - \chi_2 = 198$ $\chi_1 - \chi_3 = 132$ $\chi_3 - \chi_2 = 66$

TABLE II

<table>
<tr><th rowspan="2">Crystal</th><th rowspan="2">Direction along which susceptibility was measured</th><th rowspan="2">Temp. °C</th><th rowspan="2">Density of the crystal</th><th rowspan="2">Vol. susceptibility (10^{-6}C G.S. units)</th><th rowspan="2">Gm. mol. susceptibility (10^{-6} C.G.S. units)</th><th rowspan="2">Mean susceptibility at 30°C</th><th colspan="4">Effective moment at 30°C</th></tr>
<tr><th>$\mu_\parallel$</th><th colspan="2">$\mu_\perp$</th><th>μ</th></tr>
<tr><td>CuCl$_2$ 2NH$_4$Cl. 2H$_2$O</td><td>Along $\chi_\perp$ axis</td><td>28.7</td><td>2.004</td><td>0 980</td><td>1,380</td><td>1,290</td><td>1·77</td><td colspan="2">1 94</td><td>1.88</td></tr>
<tr><td>CuCl$_2$.2KCl. 2H$_2$O</td><td>Along $\chi_\perp$ axis</td><td>31 3</td><td>2.430</td><td>10 16</td><td>2,340</td><td>1,250</td><td>1·73</td><td colspan="2">1.91</td><td>1.85</td></tr>
<tr><td>CuCl$_2$.2RbCl. 2H$_2$O</td><td>Along $\chi_\perp$ axis</td><td>30 0</td><td>2.504</td><td>8.074</td><td>1,330</td><td>1,240</td><td>1·74</td><td colspan="2">1.92</td><td>1.86</td></tr>
<tr><td rowspan="2">Cu(CH3COO)$_2$. H$_2$O</td><td rowspan="2">Along 'b'axis</td><td rowspan="2">32 5</td><td rowspan="2">1.968</td><td rowspan="2">7·355</td><td rowspan="2">748</td><td rowspan="2">770</td><td>μ_1</td><td>μ_2</td><td>μ_3</td><td rowspan="2">1.41</td></tr>
<tr><td>1·54</td><td>1.25</td><td>1.43</td></tr>
</table>

IV. MAGNETIC ANISOTROPY IN RELATION TO CRYSTAL STRUCTURE

We proceed to discuss the results obtained in the previous section in relation to X-ray data concerning the paramagnetic unit in the crystal.

$CuCl_2.2KCl.2H_2O$—This crystal has been analysed by X-ray methods by Hendricks and Dickinson (1927) and Chrobak (1934). It is assigned a space group D_{4h}^{4} with two molecules in the unit cell. Chrobak finds after detailed Fourier analysis that Cu^{++} ion is at the centre of an octahedron formed by two oxygen atoms at opposite corners and four chlorines, the diagonal joining the two oxygens being along 'c' axis. The two oxygen distance (Cu-O) from the central Cu^{++} ion is 1.97A°. Two chlorines are in the same plane as Cu^{++} ion and oxygens are at a distance ($Cu\text{-}Cl_I$) of 2·32A°. The other two chlorines which are located centrally above and below this plane are at a distance ($Cu\text{-}Cl_{II}$) of 2.95A°. There are two such groups in the unit cell of the crystal and are parallel to each other. Let the gm. mol. susceptibility along ($Cu\text{-}Cl_{II}$) be represented by $K_\parallel$ and that along (Cu-O) by $K_\perp$; $K_\parallel$ should be greater than $K_\perp$. Evidently $\chi_\parallel$ along the 'c' axis of the crystal should be equal to $K_\perp$ and $\chi_\perp$ equal to $K_\parallel$. As a result $\chi_\perp$ should be greater than $\chi_\parallel$ which is observed experimentally. We have then $K_\parallel - K_\perp = \chi_\perp - \chi_\parallel = 265 \times 10^{-6}$ and $\frac{K_\parallel + K_\perp}{3} = \frac{\chi_\parallel + 2\chi_\perp}{3} = 1250 \times 10^{-6}$ at 30°C. Hence the anisotropy of the individual group is about 21% as against 40% for that in the crystal of $CuSO_4.5H_2O$ (Krishnan and Mookherjee, 1938).

$CuCl_2.2NH_4Cl.2H_2O$—This crystal has also been studied in detail by Chrobak (1934). Two alternative structures are proposed. According to the first Cu^{++} ion is at the corners of a an octahedron formed by two oxygens at opposite corners and four chlorines similar to the potassium salt, 'c' axis being parallel to the diagonal joining the two oxygens. According to the second structure Cu^{++} ion should be at the centre of a cube formed by eight chlorine atoms. The centres of opposite faces are occupied by oxygen atoms and the line joining them is parallel to 'c' axis.

From the available X-ray data it was not possible to decide between the two. Krishnan and Mookherjee (1938) showed that magnetic anisotropy measurements favoured the first structure, *i.e.*, same as the potassium salt. Since the two paramagnetic units in the unit cell of the crystal are parallel to each other $\chi_\perp$ should be greater than $\chi_\parallel$ as before. This was also observed.

Evidently $\chi_\perp - \chi_\parallel = K_\parallel - K_\perp = 258 \times 10^{-6}$ and $\frac{2\chi_\perp + \chi_\parallel}{3} = \frac{K_\parallel + 2K_\perp}{3} =$ 1290 at 30°C ; so that the anisotropy of the unit is about 20%, almost the same as the potassium salt.

$CuCl_2\,2RbCl.2H_2O$—For this salt no detailed X-ray data are available. There are two molecules. If the disposition of the chlorine and oxygen atoms about the Cu^{++} ion is the the same and if the orientation of the groups is the same which is very much to be expected the anisotropy of the paramagnetic unit will be about 21%, almost the same as the other two halides.

Cupric Tutton Salts—Krishnan and Mookherji (1937) made measurements on a large number of Tutton salts at room temperature. The distribution of the oxygen atoms surrounding the cupric ion if taken to be the same as in $CuSO_4.5H_2O$ crystal, *i.e.*, four of the oxygens contributed by four water molecules, form a square with Cu^{++} ion at the centre ; the other two which are contributed by the SO_4^{--} groups lie centrally above and below the square, but at a much larger distance than the other four oxygens, one should expect the anisotropy of the paramagnetic unit to be at most the same as $CuSO_4.5H_2O$. Tutton salts have been studied by X-ray methods by Hofmann (1931). There are two molecules in the unit cell of the crystal. Let the symmetry axes of these two units be represented by Z_1 and Z_2. All the crystals are monoclinic and the (010) plane is a symmetry plane ; so the principal magnetic axes and susceptibilities of one of the units can be obtained from those of the others by reflection in the (010) plane of the crystal. Since the paramagnetic unit possesses uniaxial magnetic symmetry χ_2 should be the direction normal to the plane containing Z_1 and Z_2 ; χ_1 should be the internal bisector of the angle 2ψ between Z_1 and Z_2.

Evidently $\chi_1 = K_\parallel \cos^2\psi + K_\perp \sin^2\psi$; $\chi_2 = K_\perp$; $\chi_3 = K_\parallel \sin^2\psi + K_\perp \cos^2\psi$.

$$\cos 2\psi = \frac{\chi_1 - \chi_3}{K_\parallel - K_\perp} \qquad \text{and } (\chi_1 + \chi_2 + \chi_3)/3 = (K_\parallel + 2K_\perp)/3.$$

Using the above equations we have calculated the relative orientations (2ψ) of the two paramagnetic units and their principal susceptibilities $K_\parallel$ and $K^\perp$ as shown in Table III. It is found that the values of $(K_\parallel - K_\perp)$ compare well with that of $CuSO_4.5H_2O$ $(K_\parallel - K_\perp = 550)$. The variation of $K_\parallel - K_\perp$ from 640 to 500 is very much to be expected as the distances of oxygen atoms from the Cu^{++} ion should not be exactly the same in all cases.

Unlike $CuSO_4.5H_2O$ Tutton salts have six oxygen atoms from six water molecules for the formation of the octahedron hence one might say that these octahedrons should be regular and not drawn-out ones as is supposed. But this dissymmetry in the unit is very much to be expected because of the well known Jahn-Teller Theorem (1937).

Table III

Data refer to 30°C

Crystal	$K_\parallel - K_\perp$	2ψ	$K_\parallel$	$n_\parallel$	$n_\perp$	$\bar{n}$
$CuRb_2(SO_4)_2\,6H_2O$	600	80.4	1,710	2.17	1.81	1.93
$CuCs_2(SO_4)_2.6H_2O$	564	78.3	1,720	2.19	1.84	1.07
$CuTl_2(SO_4)_2.6H_2O$	495	81.9	1,670	2.16	1.86	1.97
$Cu(NH_4)_2(SeO_4)_2\,6H_2O$	586	78.4	1,750	2.20	1.84	1.97
$CuK_2(SeO_4)_2.6H_2O$	639	79.3	1,870	2.24	1.86	2.02
$CuRb_2(SeO_4).6H_2O$	630	82.9	1,740	2.21	1.81	1.95
$CuTl_2(SeO_4)_2\,6H_2O$	580	82.9	1,690	2.18	1.86	2.06

$n_\perp$ and $n_\parallel$ denote the effective magnetic moments of the paramagnetic unit when the applied magnetic field is along and perpendicular respectively to the symmetry axis of its *crystalline field* and $\bar{n}$ is the corresponding mean magnetic moment.

V. MAGNETIC BEHAVIOUR OF CUPRIC IONS IN CRYSTALS

Cupric Alkali Halides—As revealed by X-ray studies the paramagnetic units of these crystals are made up of octahedrons of four chlorine and two oxygen atoms with copper at the centre. Two oxygens and two chlorines form a square about the cupric ion ; the other two chlorines lie centrally above and below this square. This octahedron is not a regular one. But the line joining the two chlorines above and below the square is drawn out. As a result the crystalline electric field acting on Cu^{++} ion in the crystal should have approximate tetragonal symmetry like $CuSO_4.5H_2O$. The potential of an electron placed at the point x, y, z is then given by $\phi = D(x^4+y^4+z^4)+A(x^2+y^2-2z^2)$ and the susceptibility along z-axis, *i.e.*, the tetragonal axis should be greater than along directions normal to it. Van Vleck (1932) has shown that the orbital moment is conserved only along the symmetry axis while along other directions it is of high frequency type. Consequently along axes other than the symmetry axis the magnetic moment should have the spin-only value. On referring to Table II we find that $\mu_\perp$ which in this case evidently corresponds to $n_\parallel$, the moment along the symmetry axis of the paramagnetic unit, varies from 1.91 to 1.94 while $\mu_\parallel$ which corresponds to $n_\perp$, the moment along the normal to the symmetry axis, varies from 1.77 to 1.73. Now the magnetic moment for one spin only is $1.73[\mu = 2\sqrt{s(s+1)},\ s=\frac{1}{2}]$. Thus there is fair agreement of the experimental findings with the prediction of the theory.

In case of $CuSO_4.5H_2O$ it was found that $n_\parallel$ was equal to 2.13 and $n_\perp = 1.80$. The distance between the Cu^{++} ion and the oxygen atoms centrally above or below the square 2.4 A. U. and is smaller than the distance (Cu − Cl_{II}) 2.93 A. U. in potassium halide. One naturally expects that n_{II} for $CuSO_4.5H_2O$ should be smaller than n_{II} for potassium cupric halide, symmetry of the crystalline electric field being the same. But reverse is the case as is found in Table II. This is not difficult to understand, for going through various interatomic distances in these two crystals one finds that the symmetry axis of the paramagnetic unit in $CuCl_2.2RbCl_2$ $2H_2O$ is not so symmetrical as that of the paramagnetic unit in $CuSO_4.5H_2O$. So the orbital contribution along this axis is more than for that of the halides. This also explains why the mean moment in alkali halides is nearer the spin-only value than in the case of $CuSO_4.5H_2O$.

Tutton Salts As shown in Table II these salts behave similarly as $CuSO_4$ $5H_2O$. One can therefore say that the disposition of oxygen atoms about Cu^{++} ion in the paramagnetic unit is almost the same and their symmetry axes enjoy the same degree of symmetry as that of $CuSO_4.5H_2O$.

One direct consequence of such magnetic behaviour is that all the three copper halides should follow simple Curie Law more closely than $CuSO_4.5H_2O$ and the Tutton Salts.

$Cu(CH_3COO)_2.H_2O$—Only the space group and the number of molecules in the unit cell is available from X-ray data for this crystal, so it is not possible to evaluate the relative orientations of the paramagnetic units and thence to calculate $n_{\parallel}$ and $n_{\perp}$. Even then the mean moment of the unit is much lower than the spin-only value. This is also very much smaller than those of the other cupric salts. Cupric bromide ($CuBr_2$) has almost the same susceptibility as this salt.

This low value of the effective magnetic moment of this crystal can be due to (*i*) concentrations of the magnetic particles being very large, exchange interactions between the neighbouring moments may be appreciable, destroying magnetism, (*ii*) splitting of the ground state assymmetric electric field due to its neighbours might take place in such a manner that there might be a non-magnetic level somewhere at about 300 cm^{-1}, so that as we come down to room temperature the number of electrons in this level increases and so the moment decreases.

The first point can be decided by diminishing the concentrations of Cu^{++} ions in this salt, *i.e.*, by diluting it with some isomorphous diamagnetic salt and studying the magnetic moment. $\bar{n}$ should reach the value of other cupric salts when it is sufficiently diluted.

For the second point measurements on temperature variation of the magnetic moment, specially at high temperature, is required. Magnetic moment should increase with the increase of temperature and should reach the spin-only value at a temperature at which the non-magnetic level is completely depopulated of electrons.

Whatever may be the cause of this low magnetic moment one point stands out clearly that since the magnetic moment does not agree with the value calculated theoretically for the Cu^{++} ion there should be a complicated temperature variation, *i.e.*, the crystal should not follow simple Curie Law like the other cupric salts. This salt has a moment almost equal to cupric bromide, so its temperature variation may be expected to be similar. μ should decrease rapidly with the fall of temperature as is found in case of cupric bromide (Stoner, Magnetism and Matter, page 482).

The work was carried out at the laboratories of the Indian Association for the Cultivation of Science and the author wishes to express his thanks to its Committee of Management for affording all facilities. The author also expresses his thanks to Prof. K. Banerjee, D.Sc., F.N.I., for his keen interest in the work and valuable advice. Thanks are also due to Mr. R K. Sen, M Sc., for his valuable discussions.

BIRLA COLLEGE,
PILANI,
JAIPUR STATE.

REFERENCES

Angus, W. R. (1932), *Proc. Roy Soc.*, **136A**, 569.

Chrobak, L. (1934), *Z. Kristallogr.*, **88A**, 35.

Jahn, H. A. (1937), *Proc. Roy. Soc.*, **164A**, 117.

Jahn, H. A. and Teller, E. (1937), *Proc. Roy. Soc.*, **161A**, 220.

Hendricks, S. B. and Dickinson, R G (1927), *J. Amer. Chem. Soc.*, **49**, 2149.

Hofmann (1931), *Z Kristallogr.*, **78A**, 279

Krishnan, K. S. and Banerjee, S. (1934), *Phil. Trans.*, **234A**, 265.

Krishnan, K. S. and Mookherji, A. (1936), *Phys. Rev.*, **50**, 860.

" " " (1937), *Phil. Trans.*, **237A**, 135

" " " I (1938), *Phys. Rev.*, **54**, 533.

" " " II (1938), *Phys. Rev.*, **54**, 841.

Krishnan, K. S. and Mookherjee A and Bose A. (1938), *Phil. Trans.*, **238A**, 125.

Van Vleck, J. H. (1932), " The Theory of Electric and Magnetic Suceptibilities."

ON THE PRODUCTION OF MESOTRONS BY NEUTRAL PARTICLES

By P. S. GILL* and MELA RAM

ABSTRACT. Schein, Jess and Wollan type of experiment to study the production of mesotrons by non-ionizing radiation was tried at a height of 16,800 ft at Bara Lacha (22.5°N) in British Lahaul. The production of mesotrons by non-ionizing cosmic rays does not become noticeable at these heights in intermediate latitudes as it does around the latitude of Chicago. The Mesotron producing layer in the atmosphere is at greater height in the equatorial regions.

It is now well known that the penetrating component of cosmic rays at sea level consists mainly of mesotrons and that these particles are secondaries produced by the soft component of cosmic radiation in upper layers of atmosphere. The mode of production of mesotrons has been a subject of interest for the past few years. It was thought that the progeneters of mesotrons were the non-ionizing soft cosmic rays. Rossi (1933) and Hsiung (1934) tried experiments at sea level and Shonka (1939) at an altitude of 14,200 feet. These experimenters got no definite evidence of their production, which would mean that between sea level and 14,200 ft. no detectable part of the mesotrons is being produced as secondaries from neutral cosmic radiation. This led Schein and Wilson (1939) to try Rossi-Hsiung type of experiment at still higher altitudes by taking their apparatus in an aeroplane up to 25,000 ft. Further heights were reached by Schein, Jesse and Wollan (1940) by means of baloon flights. The experiment of Schein and his collaborators showed that at higher altitudes the non-ionizing cosmic radiation produced mesotrons in a 2-cn lead block and that the production of mesotrons begins to be noticeable near about an altitude where the pressure is 40 cm of Hg.

All these experiments were tried at magnetic latitudes greater than 38° where the latitude knee occurs in the Intensity *vs* Latitude curve at sea level. One of us (1939) has shown that the temperature co-efficient of the intensity of cosmic rays is a function of latitude, the equatorial regions having a smaller temperature co-efficient. Blackett (1938) predicted this on the hypothesis that the mesotrons which constitute the penetrating cosmic rays are produced in the upper atmosphere by less penetrating radiation and that they show spontaneous disintegration. When the atmosphere expands at the higher temperature, the elevation at which the mesotron is produced is greater and there is a higher probability of spontaneous disintegration resulting in a lower intensity at sea level. At a latitude of about 38°, the altitude at which the mesotrons are created is a maximum of about 25 kilometers. At lower latitudes, *i.e.*, the latitude of Lahore (22° N) the maximum altitude of the layer of atmosphere where the mesotrons are created should be much higher. If at latitudes higher than 38° the production of mesotrons by neutral particles becomes noticeable at 16,000 ft. above sea level, their production will not be detectable at the same elevations around intermediate latitudes. With this in view an experiment similar to that of Schein, Jesse and Wollan was planned and tried at a height of 16,800 ft. by the side of a hill above Bara Lacha pass, in British Lahaul (22.5° N).

---

* Fellow of the Indian Physical Society.

Four G-M counter tubes were placed in a verticle line as shown in fig. 1, Counters 1, 2 and 3, constitute one coincidence set, while counters 2, 3 and 4 make the other coincidence set. Any cosmic ray particle passing through either set must penetrate at least 8 cm. of lead, therefore the coincidences in both the sets are caused by penetrating particles. The lower set should ordinarily give slightly less counts, about one per cent less than the upper set due to the absorption of the incident mesotron in the last 2-cm block of lead. If mesotrons are produced in the first 2-cm lead block by non-ionizing radiation, the lower set of counters should count more coincidences than the upper one. To reduce the effect of softer horizontal air shower particles, a shield of 2 cm of lead is placed on the sides of counter 3.

Vertical line up of the counters

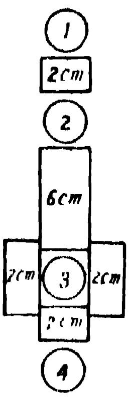

FIG. 1

Counters used are of self-quenching type. Each has a length of 6 inches and a diameter of 1 inch. All the G-M tubes had nearly the same plateau. At Zing Zing Bar (13,800 ft.) both the coincidence sets were tested for their efficiency. It was found that their efficiencies were practically the same. In one hour the upper set gave 176 counts and the lower set gave 177 counts.

RESULTS

TABLE I

Place	Total Time	A No. of counts in the upper set	B No. of counts in the lower set	A/B
Zing Zing Bar (13,800 ft.).	3 hours	282 ± 17	253 ± 16	1.12 ± ·02
Bara Lacha (16,800 ft.).	5 hours	547 ± 23	494 ± 21	1.11 ± ·02

The results at two different elevations are presented in Table I. The ratio of the number of counts in the upper set to the number of counts in the lower set at both the places show that in these latitudes the production of mesotrons from neutral cosmic radiation does not become noticeable at the same altitudes at which it appears to take place at the latitude of Chicago. It would mean that the creation of mesotrons by non-ionizing cosmic radiation in these latitudes should become noticeable at still higher elevations, as would be inferred from temperature co-efficient of the intensity of cosmic rays. The fact that the production of mesotrons by neutral particles at 22° magnetic North does not take place at the same elevation at which it does at 52° magnetic North, would indicate that in the production of mesotrons there is a latitude effect in the sense that at lower latitudes the mesotron producing layer is at greater heights.

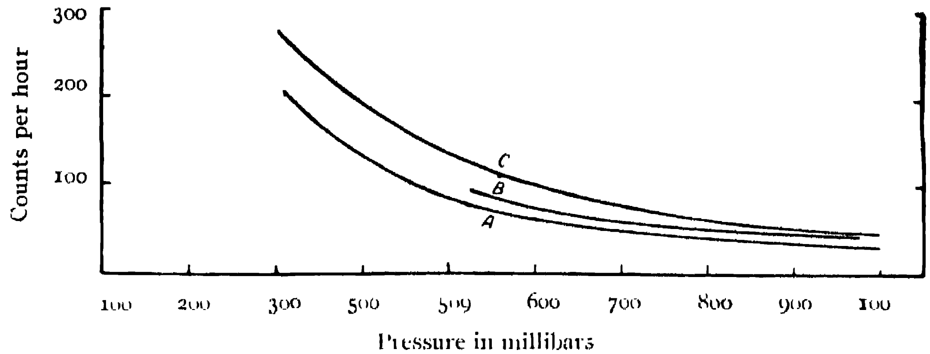

FIG. 2

Curve A—Vertical mesotron intensity at 5.3° N (Bheta, Aiya, Holeko and Saxena)
Curve B—Vertical mesotron intensity at 22.5° N (Gill and Melaram)
Curve C—Vertical mesotron intensity at 52 5° N (Schein, Jene and Wollan)

The data presented in this paper can be compared with that of Schein, Jesse and Wollan (1940) as well as with that recently published by Bhabha and his collaborators (1945). In fig. 2, curve B represents our results giving the intensity of mesotrons penetrating 8 cm. of lead at 22° N; curve A gives the data of Bhabha and his co-workers at 3.3° N and curve C shows the results of Schein, Jesse and Wollan at 52.5° N. Our results confirm the conclusion drawn by Bhabha and his co-workers that the latitude effect of the penetrating component of cosmic radiation shows a very small increase up to an elevation of 16,800 ft. The accuracy of our data is better than that of others due to the longer time of observation at each elevation.

This work has been made possible by a grant from the University of the Panjab for which we are thankful to the University authorities. National Carbon Company (India), Limited, helped us by making a special set of high tension batteries which gave us very good service. Our thanks are due to our colleagues, B.S. Puri and S. P. Malhotra who accompanied us to the hills and helped us. We express our thanks to S. D. Chatterji for filling the Geiger-Muller tubes used in this experiment.

PHYSICS LABORATORIES, FORMAN CHRISTIAN COLLEGE,
LAHORE

REFERENCES

Bhabha, Aiya, Hoteko, Saxena, 1945, *Current Science*, **14**, 98.

Blackett, 1938, *Phys Rev.*, **54**, 973

Gill, 1939, *Phys. Rev.*, **55**, 1151

Hsiung, 1934, *Phys. Rev.*, **46**, 653.

Rossi, 1933, *Zeits. f. Physik*, **82**, 151,

Schein, Jesse and Wollan, (1940), *Phys. Rev.*, **57**, 847

Schein and Wilson, 1939, *Rev. Mod Phys.*, **11**, 292.

Shonka, 1939, *Phys. Rev.*, **55**, 24.

A NEW PULSE GENERATOR CIRCUIT

By B. M. BANERJEE*

(Plate IV)

ABSTRACT. A new pulse generator circuit is described. It delivers a synchronizing pulse, a short time before the main pulse, at a separate terminal for synchronization of the time-base of the oscillograph, with which it is intended to be used. The pulses are approximately triangular in shape. The efficiency of synchronization attained in this work is believed not to have been reached before.

The pulse repetition frequency, the time separation between the synchronizing pulse and the main pulse, the main pulse duration and amplitude are all easily adjustable over a wide range. The circuit can also be used as a two pulse oscillator with slight modifications.

The potentialities and convenience of such a circuit as a tool for development of G.M tube circuits, as a primary pulse source for ionospheric radio-sounding apparatus, as a pulse generator for stimulating muscles and nerves for physiological experiments is also discussed.

INTRODUCTION

The pulses given by a Geiger Muller tube usually pass through certain circuits (amplifying, scaling and recording) before their presence are indicated and their number recorded. As the pulses come at irregular intervals, and are of very short duration, they cannot be well visualised or photographed from a cathoderay oscillograph record because the intensity obtainable from a single trace is very small (Stever, 1942, Dasgupta, 1942). The performance testing of Geiger Muller tube circuits become difficult and one has to rely solely on very indirect methods for estimating the performance. Fault finding becomes still more difficult and circuit development that may be suggested from a visual inspection on the oscillograph screen, of the pulse and its effects, as it goes through different stages and operates on the various circuit elements—is now out of the question. A pulse generator (Manning and Young, 1942) capable of producing short duration pulses in a regular sequence, so that successive traces on the oscillograph screen may be superimposed by proper synchronization with the time-base, is therefore supremely important as a tool for circuit testing and development. Such a pulse generator has many other uses, in various other branches of science, besides the one outlined above.

While developing such a pulse generator—an electron tube circuit—it was observed that for obtaining good photographs of the very sharp pulses that the circuit was delivering, long exposures will be required on the usual types of oscillograph. For prolonged exposures it is necessaiy that the pattern does not move about the screen because of imperfect synchronization with the time-base of the oscillograph. A forced synchronization of the oscillograph time-base with the pulse generator is therefore clearly necessary. A synchronizing pulse must therefore be fed to the synchronizing terminal of the oscillograph time-base. To trip the time-base effectively, it must have the proper polarity. Further, in order that the pulse pattern may come on a convenient position, the synchronizing pulse should also be properly timed with respect to the main pulse.

---

* Fellow of the Indian Physical Society.

The usual method of generation of the saw-tooth wave required for an oscillograph time-base, consists in charging a condenser at a constant rate (by a constant current device like a pentode) and of periodically discharging it very rapidly by means of a trigger circuit, thyratron, etc. Forced synchronization of these time-bases is achieved by initiating the condenser discharge at the proper moment by the synchronizing pulse. If the main pulse (the pulse that is to be observed) is used for synchronization, and if synchronization is actually achieved, the one which is synchronizing cannot be examined properly, because it occurs when the time-base condenser is discharging, during the flyback—the high speed return stroke—of the oscillograph light spot. Pulse patterns will appear on the forward stroke if the time-base operates at a frequency that is a submultiple of the pulse frequency. If the ratio of pulse frequency to time-base frequency be n, then there will be (n-1) pulses visible on the screen, the nth tripping the time-base and falling on the return stroke.

However the locking of the time-base in this type of operation is not and cannot be sufficiently positive because the synchronizing voltage must be kept smaller than a certain limiting value, as otherwise instead of the nth pulse tripping the time-base every time, the (n-1)th one will be sometimes tripping it, depending upon the relative wavering* of the time-base and pulse generator frequencies. If the synchronizing voltage is increased still more, the time-base will be tripped generally by the (n-1)th pulse and both the nth and (n-2)th will be tripping it sometimes. As regards steadiness of pattern nothing is achieved by increasing the synchronizing voltage beyond this limiting value. With this type of operation, maximum steadiness is usually attained by making the time-base frequency just lower than half the pulse repetition frequency, in which condition maximum synchronising voltage can be used. We then get only one pulse pattern on the screen, about half-way in the forward stroke. Every second pulse is superimposed upon the one before and we thus get only half the brightness that is available if every one is superimposed upon the other. The phenomenon that the pulse may start, in an electrical, mechanical or physiological system, can be studied only in the later half of the forward stroke, and thus half of the screen space or observation period remain unexploited.

This difficulty can be avoided if a separated synchronizing pulse be fed to the oscillograph time-base just before the main pulse.† Two pulses separated by a time-interval may be generated from a single pulse if that pulse be first taken direct and then through a delay network. The difficulties of design, and the complication of construction, of a suitable delay network, that will not itself deform the pulse shape and that will readily introduce the different order of time-delays that may be necessary, will be easily understood by one who had the occasion for doing it.

---

* The unsteadiness of the time base and the pulse generator is due to main voltage fluctuations, spontaneous fluctuations in the values of certain circuit components—*e.g.*, a resistance, a tube characteristic, etc They are always present, as otherwise forced synchronisation would have been unnecessary,

† Marshall and Talbot (1940) describe^8 a circuit in which a separate pulse is generated from a primary pulse, after a desired time interval.

The circuit devised by the author produces two pulses separated by a time-interval. These pulses are quite separate from each other and are obtained from different terminals. Their characteristics—amplitude, duration and shape—may be independently controlled. The time-separation between the two pulses may also be adjusted over a wide range. The same applies to the repetition frequency.

Positive synchronization of a very high order has been achieved—to the extent that the time-base controls may be varied at will to produce a wide range of spot velocities, without in any way affecting the synchronism. Such a powerful synchronization can be achieved only if the synchronizing pulse is separate, single and sharp.

The production of separate and sharp synchronizing pulses allows one to use a single-stroke time-base in place of the continuously running ones. With a single-stroke time-base the synchronizing problem does not arise at all.

The complete diagram of the circuit is given in Fig. 1. The circuit con-

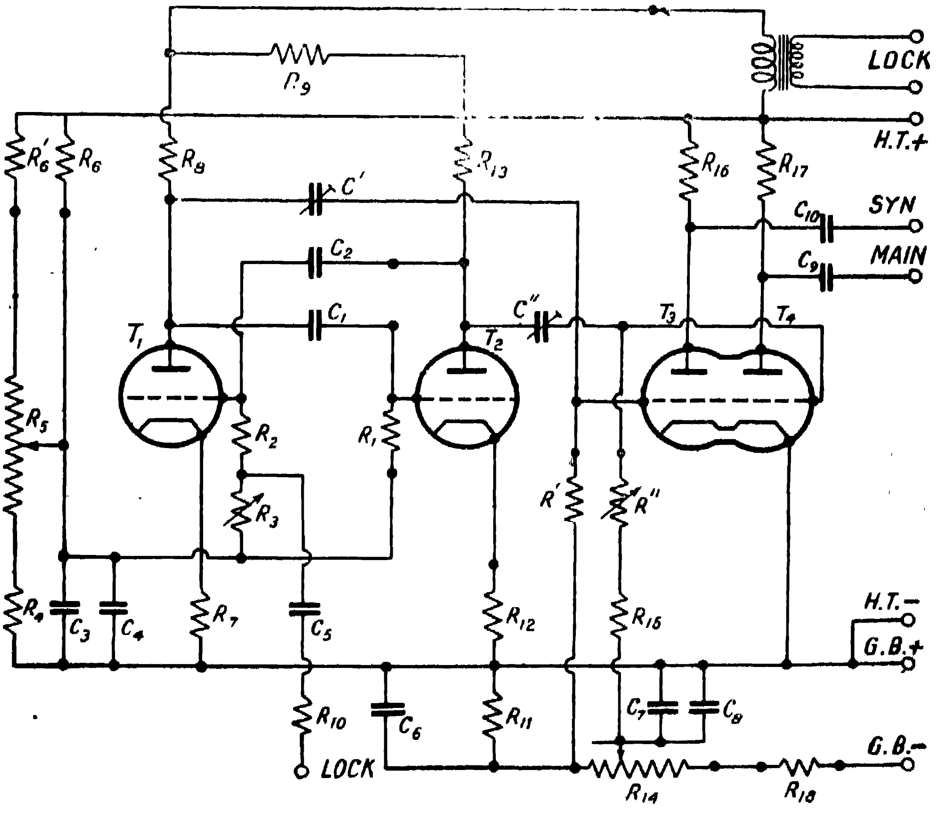

FIG. 1

sists of three parts : an unsymmetrical multivibrator, two pulse generating networks and two pulse amplifiers biased beyond cut off.

RESISTANCES

R_1 = 1 Meg ; $R_2 = R_6 = R_{10}$ = ½ Meg ; R_3 = ½ Meg volume control ; $R_4 = R_{15}$ = 10,000 Ohms; R_5 = 100,000 Ohms volume control ; R_6' = ¼ Meg ; $R_7 = R_{12}$ = 500 Ohms ; $R_8 = R_{13}$ = 2500 Ohms ; R_9 = 100 Ohms ; R_{11} = 50,000 Ohms ; R_{14} = 50,000 volume control ; $R_{16} = R_{27}$ = 1000 Ohms ; R_{18} = 100,000 Ohms.

R' = variable in steps from 10 Meg ; 1 Meg ; 100,000 Ohms ; 20,000 Ohms R'' = 2 Meg volume control.

CAPACITIES

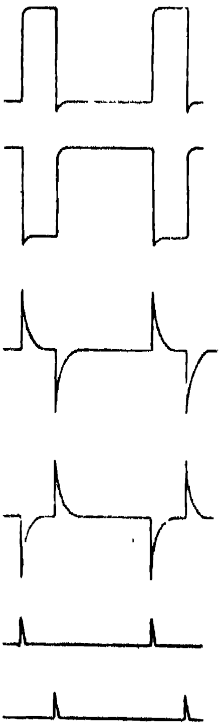

FIG. 2

C_1 = 1 μf to 20 μμf. variable in steps

C_2 = ,, ,, ,, ,,

C' ; C'' see text

$C_3 = C_5 = C_6 = C_7$ = 0·1 μf non-inductive paper condenser.

$C_9 = C_{10}$ = ·01 μf, 600 Volt non-inductive paper condenser.

$C_4 = C_8$ = 10 μf, 450 Volt electrolytic condenser.

Locking Transformer—step-down ratios 1 : 1 ; 1 : 2 ; 1 : 3 ; 1 : 4, secondary inductance—½ Henry.

High tension voltage may have a value lying between 100 to 250 volts for satisfactory operation.

Grid bias voltage should lie between 40-70 volts. About half this amount is sufficient if R_{18} is short circuited.

The wave forms of the anode voltages of the two tubes in the multivibrator (Puckle) is of the well-known shape shown in the Fig. 2.

The pulses that are generated by the pulse generator net-work *CR* and applied to the amplifier tubes T_3 and T_4, are also shown. The mode of operation of the pulse generator net-work is simple. Suppose that the potential applied to the input terminals suddenly change by an amount ΔE. A current i begins to flow through the resistance, controlled by the equation,

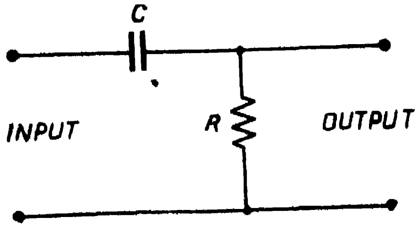

FIG. 3

OSCILLOGRAPH RECORDS

All Photographs taken from Cossor double beam oscillograph Model 339A.
Ten seconds exposure on all photographs.

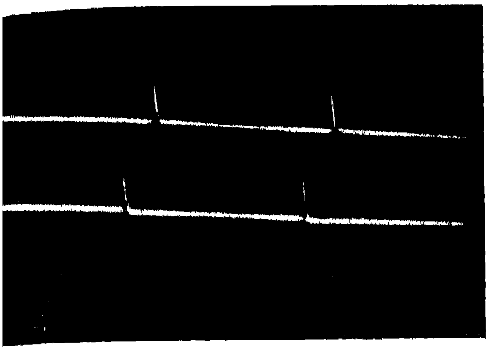

1 The pulse pair as photographed from the lograph screen. Repetition frequency= 10,000 , synchronized self running time-base.

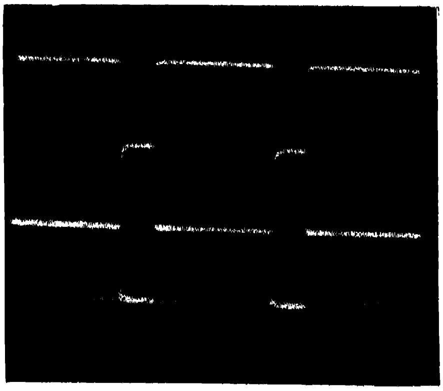

Fig. 2. Anode voltage wave forms of the two tubes in the Multivibrator of the pulse generator. Repetition frequency 1,000 c.p.s. ; synchronized, self running time-base.

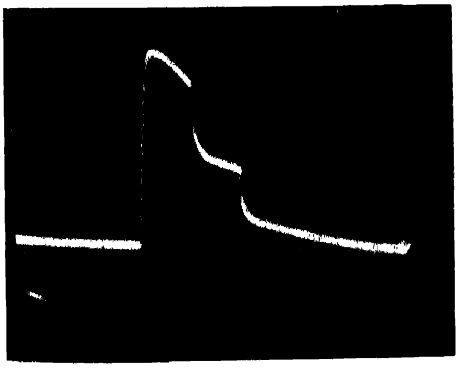

3. Anode voltage waveform of a hard valve M tube pulse recording circuit. Repetition frecy = 10 c.p.s ; self running time-base.

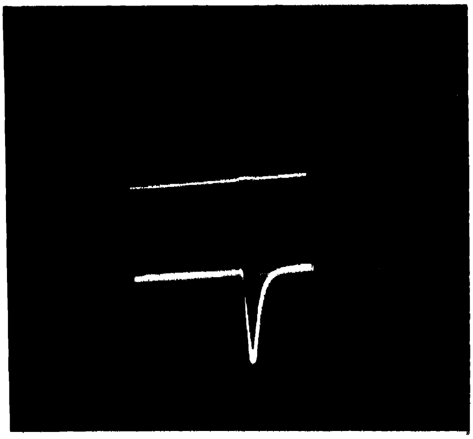

Fig. 4. A two microsecond pulse repeated 70,000 times per second. Single stroke time-base. The time interval from the beginning of the sweep to the start of the pulse corresponds to 6 microseconds.

$$\Delta E = \frac{\int i\,dt}{C} + iR$$

The solution of this equation is

$$i = i_0\, e^{-\frac{t}{CR}} = \frac{\Delta E}{R} \,.\, e^{-\frac{t}{CR}}$$

whence, output voltage

$$iR = \Delta E \,.\, e^{-\frac{t}{CR}}$$

It is thus seen that for every sharp change in voltage across the input terminals, the pulse generator network produces across its output terminals, a voltage which dies off exponentially and which has a peak magnitude equal to the sudden voltage change. The rate of fall is determined by the time constant CR and may be made as rapid as desired by reducing C and R.

The pulse amplifiers are high μ triodes biased beyond the cut off. Only the tips of the positive pulses get through these amplifiers. As a result they are approximately triangular in shape. Their amplitude, and to some extent the shape, is controlled by varying the bias on the amplifiers. The duration is controlled by varying C and R.

The output pulse from T_3 forms the synchronizing pulse while that from T_4 the main pulse.

The repetition frequency of the multivibrator, and so that of the output pulses, is controlled continuously by varying the grid supply voltage. This is taken from the 100,000 Ω volume control potentiometer connected in the reverse way. The taper in this volume control therefore acts in the reverse direction. Such a method of connection is convenient in the sense that, the frequency changes far more gradually than when it is connected in the normal way. As a result, the adjustment for obtaining a steady picture on the oscillograph screen has become much more easy. This control provides a frequency range ratio of about three.†

The repetition frequency is changed in steps by changing the condenser C_1*.

The relative pulse separation over any range is fixed, *i.e.*, the ratio of the time interval between the synchronizing pulse and the main pulse, to the pulse period, is the same and do not vary with the setting of the repetition frequency control potentiometer. If desired the relative pulse separation may be changed by altering C_2 and R_2. The ratio approximates to $C_2/C_1 + C_2$.

The amplitude (and also shape) of the main pulse is controlled by the 50,000 Ω bias control potentiometer. It adjusts the negative bias on the main pulse amplifier T_4, so as to pass a greater or smaller part of the positive tip of the pulse, that is applied to its grid by the pulse generating network. No such continuous control has been provided for the synchronizing pulse in the circuit described. But if desired such a control can easily be fitted.

---

*To some extent also C_2.

†If desired, the frequency range ratio may be increased by using a resistor of lower value for R°_6.

The sharpness of the main pulse is controlled by R″, a 2 megohm vol. control potentiometer connected as a variable resistance. It adjusts the time constant C″ R″ of the main pulse generating network continuously. No corresponding control has been fitted for the synchronising pulse, but R′ can be changed easily if desired, in steps. C′ and C″ are trimmer condensers and their capacities may be changed over the range of 5-30μμf at will. They are kept adjusted to about the maximum capacity.

The 500Ω cathode resistors are for improving the frequency stability and increasing the output voltage. 7A4 triodes are used in the multivibrator and 6N7 in the amplifiers because they proved more than adequate for the author's requirements. Anybody trying to produce pulses of extraordinarily short duration will find 6AG7 television amplifier pentodes better suited than the 7A4 and 6N7 tubes. The 500Ω degeneration resistances may be omitted while anode coupling resistances should be reduced to 1000Ω or less.

A terminal is brought out for injecting a locking voltage for stabilization of the repetition frequency. Locking with a constant frequency source of known value is desirable for accurate measurements in connection with scaling circuits. A transformer for introducing the locking voltage in series with the H. T. is also provided and is also used for the same purpose.

PERFORMANCE

The performance figures are given below. They are by no means ultimate,* and may be extended in both directions by suitable choice of circuit components.

Pulse repetition frequency†	...	Two to 200,000 cycles/second
Pulse separation	...	1/4 second to 2μ second
Pulse duration (Main pulse)	...	100 μ second to 1μ second
(Syn. pulse)	...	500 μ second to 1μ second‡

The generator produces *negative pulses* of 12 volts peak amplitude. This amplitude is sufficient for triggering the single-stroke time base of the Cossor double beam oscillograph (Model 339A) throughout the whole frequency range.

USES

This pulse generator, in conjunction with an oscillograph and an attenuator, may be used for testing, fault-finding and development of pulse amplifying circuits. Linear amplifiers, scaling circuits, recording circuits, etc. may be directly tested and their general performance and shortcomings immediately gauged from the picture that will be obtained continuously on the oscillograph screen. Such a system of testing will show the effect of manipulation of the different controls in the circuit, indicate the presence of A. C. ripple, noise pick-up, microphony, show the net result of frequency, phase and harmonic distortions in modifying the pulse shape, and measure amplification directly on the pulses themselves. Although the response of certain circuits, like linear amplifiers, to pulses of arbitrary shape, may be guessed from an elaborate measurement of the frequency, phase and harmonic distortions, certain other circuits, containing tubes biased beyond cut off, or tubes in which the current or voltage output abruptly begins or saturates, do not lend themselves to even such types of elaborate measurements. But these types of circuits are frequently used in connection with pulses. The pulse generator-attenuator-oscillograph method is the only really satisfactory method of testing the performance of such types of circuits.

---

* The practical limits coincide with the limits of effective resistance coupled amplification.

† If desired the amplitude could be increased to 60 volts peak by using 5000 ohm resistances for R_{16} and R_{17} in place of the 1000 ohm resistances.

‡ A generator designed particularly for low repetition frequencies should preferably omit R_7 and R_{12}, use 50,000 resistors for R_8 and R_{13}, besides using 3 Meg resistors for R_1 and R_2. C′ and C″ must also be increased in value.

As a source of primary pulses for ionospheric or other types of radio sounding apparatus. (Colwell, 1936, Piddington, 1939, Millington and Falloon, 1935), this circuit may represent a revolutionary improvement over the older techniques. Previous workers used mainly some types of thyratron pulse generators. For synchronization of the pulse with the base, they used to synchronize both with the A. C. power supply frequency. The consequences of operating the pulse generator at the fixed unvariable power frequency were a great handicap in low height measurements. (Colwell, 1936, Watson, Watt, etc. 1937). The whole sweep on the oscillograph screen represented quite a long interval of time, some 16 to 20 milliseconds. As a result the dispersion obtainable was very small, not better than 0·1 millisecond, which corresponds to a height of 15 kms. Complicated circuits producing a high velocity sweep at the desired part, were used by Colwell (1936), Haworth (1941) for obtaining better dispersion. Better resolution also demands the production of a short duration pulse, the limit so far reached being 4 μ secs. (Colwell, 1937). A serious and unavoidable defect even with this type of complicated apparatus comes in because of the low repetition frequency, which leads to the reduction of the brilliancy of the trace when the sweep velocity is increased to improve dispersion. The repetition frequency can not be made much greater than the commonly used 50 or 60 c.p.s. as multiple reflections representing long time delays may then come over at the beginning of the second trace producing a confusion with the short delay reflections.

Long delay echoes may be distinguished if the repetition frequency is continuously adjustable, as then a ten per cent shift in the repetition frequency will produce a 10% shift in the position of all the reflected pulses. Long delay "echoes" will thus shift much more than the short delay ones (over the oscillograph screen), and they may thus be distinguished. Synchronization with the power frequency do not allow for such a side experiment.

The pulse generator described in this paper, with its continuously adju-table repetition frequency, its shorter pulse duration, its sharp synchronizing pulse holding the oscillograph time base in synchronism even for considerable variations in the repetition frequency, is a simple solution of all the radio sounding problems associated with ionospheric apparatus. It is therefore expected that it will find wide use in this field.

As a source of pulses for stimulating muscles and nerves for physiological experiments, the circuit probably presents certain advantages.

The circuit may be easily converted into a two pulse oscillator of far greater potentialities than that described by Getting (1937). The only modification is the interconnection of the two output terminals. Getting's circuit uses thyratron relaxation oscillators, tuned and synchronized to the same frequency, but slightly out of step with each other. At each flash of the thyratron a pulse is generated. The two thyratron oscillators that are slightly out of step with each other, produce two pulses separated by a small time-interval. The performance figures claimed for the circuit are, contrasted with my figures

		Getting's circuit.	Author's circuit.
Repetition frequency	=	6,000	2,00,000 c.p.s. max.
Pulse separation	=	20	2 μ sec. min.
Pulse duration	=	5	1 μ sec. min.

The author's performance figures are thus found to greatly exceed that of Getting's. Besides, it will be easily appreciated that the author's circuit permits of quicker and easier adjustments when pulses of different repetition frequency, separation and duration are required.

ACKNOWLEDGEMENTS

The author wishes to express his gratitude to Prof. M. N. Saha, D.Sc., F.R.S., for his keen interest and helpful discussions. He is further indebted to Prof. S. K. Mitra, D.Sc., for permission to use some of the apparatus of the Ghose Laboratory of Physics.

Palit Laboratory of Physics,
University of Calcutta.

REFERENCES

Colwell, Friend and Hall, 1936, R.S I., **7**, 420.
Colwell and Friend, 1937, *P.I.R.E.*, **26**, 1531.
Dasgupta, 1942, *Trans. Nat Inst. Sci. Ind.*, **2**, 121
Getting, 1937, *R.S.I.*, **8**, 412.
Haworth, 1941, *R.S.I*, **12**, 478.
Manning and Young, 1942, *R.S.I.*, **13**, 234.
Marshall and Talbot, 1940, *R.S I* , **11**, 287
Millington and Fallon, 1935, *Marconi Rev.*, **57**.
Piddington, 1939, *P.I.R E.*, **27**, 753.
Puckle, 1943, Time bases, Chapman and Hall.
Stever, 1942. *P. R.*, **61**, 38.
Watson Watt, Wilkins and Bowen, 1937, *Proc. Roy. Soc.*, A, 161, 181.

ELECTRICAL PROPERTIES OF INDIAN MICA: II. THE EFFECT OF VARYING RELATIVE HUMIDITY

By P. C. MAHANTI,* M. K. MUKHERJEE AND P. B. ROY.

ABSTRACT. In continuation of the previous work, the effect of varying relative humidity on the permittivity, power factor and power loss of three typical qualities of Bengal ruby and Madras green mica has been studied The results are in conformity with those obtained by previous workers in the line

INTRODUCTION

In a previous communication (Datta, Sen Gupta and Mahanti, 1942) the results of power factor measurements on different kinds of mica available in different parts of India were reported. In the present paper a comparative study of the effect of varying relative humidity on permittivity, power factor and dielectric loss factor of three typical qualities of Bengal ruby and Madras green micas has been made.

The same technique as has been described previously was employed in preparing the test condenser, which was kept under suitable pressure for about twenty-four hours before being put to use for capacitance and power factor measurements at a desired value of humidity. The measurements have been done by the method of substitution, using the same standard air condenser and the same Schering bridge. It is however of interest to describe the method which has been used in the present investigation to control the relative humidity (hereafter stated very often as humidity) of the experimental chamber in which the test condenser was housed.

METHOD OF CONTROLLING HUMIDITY

Various methods have been used in the past by different investigators to control the humidity of an enclosed space. It is found that a saturated aqueous solution in contact with a definite solid phase, such as $CaCl_2$, $2H_2O$; $CoCl_2$, $6H_2O$; $CaSO_4$, $5H_2O$, etc. maintains constant humidity at a definite temperature within an enclosed space surrounding it. Hence by selecting a proper salt, it is possible to secure almost any desired value of humidity at a given temperature. It is evident that this method is convenient when any definite value of humidity is desired within an enclosed space for a particular purpose. But when it is required to vary the humidity over a wide range of values at a given temperature and maintain it constant at each such value, this method becomes tedious in as much as one has to use different salts for obtaining different values of humidity. Moreover, the fact that the value of humidity set up by a particular salt depends upon the temperature at which the solution is kept presents further difficulties. Another method utilises the fact that sulphuric acid at different concentrations exerts different vapour tensions. It is thus possible to set up conveniently any desired value of humidity in the chamber by varying simply the concentration of the acid. But the corrosive effect of the acid prevents its use in our case. Very recently a very simple and convenient method (Grover and Nicol, 1940) of controlling the humidity within a comparatively small enclosed space has been found by using solutions of glycerine in water at different dilutions. This method possesses many advantages over the previous ones. A solution of glycerine in water is non-corrosive and can be easily standardised by measuring its refractive index. It is easily recovered or re-concentrated, if desired, by boiling or simply by exposing it to warm and dry atmosphere. The most important and useful point is however the fact that the relative vapour pressure of glycerine solution is substantially independent of temperature over the range 0° – 70°C. Hence if a solution is standardised at a given temperature it can be used to give a definite value of humidity without appreciable error even if the temperature undergoes any change at any subsequent period.

---

* Fellow of the Indian Physical Society.

In the present investigation we have used, therefore, glycerine solutions of different concentrations for obtaining different values of humidity as desired. The refractive index of each solution was measured with the help of an Abbe refractometer. A curve showing the variation of humidity with refractive index is given in Fig. 1. In actual practice a vacuum desicator, with its glass stopper replaced by a tight-fitting velvet cork, was conveniently used as the experimental chamber in which the desired value of humidity was set up by placing inside it a basin containing the glycerine solution of proper concentration. In order to check the value of humidity thus set up, an Edney paper hygrometer was also placed inside the chamber. The agreement was found very satisfactory in each

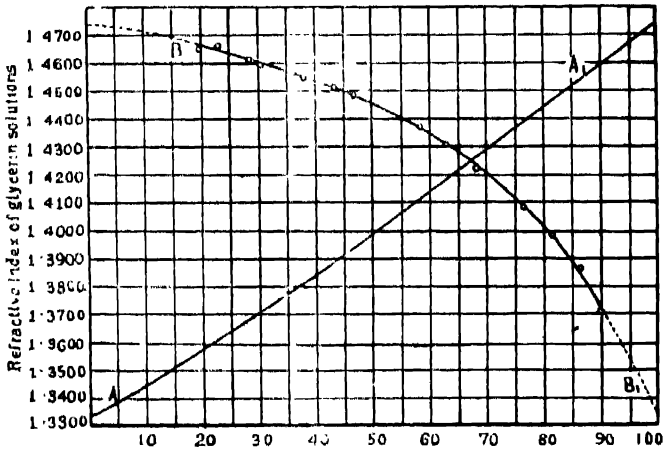

$A - A_1$ = Percentage glycerin by weight
$B - B_1$ = Percentage relative humidity

FIG. 1

case. It was noticed further that it took about 2 hours to attain a steady value of humidity within the chamber.

EXPERIMENTAL

It has been noted already that capacitance and power factor measurements in the present investigation were carried out by the method of substitution, using a standard air condenser and a Schering bridge operating at 220 volts a.c. at one kilocycles per second as described in the previous communication (*loc. cit.*). The test condenser was connected to the bridge by means of two short lengths of V.I.R. copper wire which passed through the velvet cork at the mouth of the chamber and were kept fixed in position throughout subsequent measurements. Before making our final measurements on the test condensers, it was thought of importance, firstly, to determine with definiteness the capacitance of the leads as well as the power factor of their insulation including that of the velvet cork and their variation, if any, with humidity, and secondly, to ascertain whether the time of conditioning a test condenser at any desired value of humidity has any effect on its capacitance and power factor values. In the latter case it was found that conditioning the test condenser for about two hours at any value of humidity not exceeding 80% was sufficient to arrive at a steady value of its capacitance or of its power factor. But above 80% humidity, the time of conditioning increased considerably. Hence in making measurements on the different test condensers, bridge readings at a desired value of humidity were taken at an interval of two hours until they were steady within the limits of experimental error. All measurements were done at a constant temperature of 36°C. With each test condenser observations were made firstly, with increasing humidity to a maximum value of 95%, and then with decreasing values. At each value the two sets of bridge readings were found to agree within allowable limits and their mean was taken to compute as follows the capacity and power factor of the test condenser, after making due allowance for the effects of leads, etc.

It is easily seen that when the bridge is balanced, firstly, with the bridge standard condenser alone in the third arm and then with the test condenser connected across it, we have

firstly, $$\frac{C}{C_s} = \frac{R_2}{R_1} \qquad \ldots \quad (1)$$

and $$\phi - \phi_s = \phi_2 - \phi_1 \qquad \ldots \quad (2)$$

and secondly, $$\frac{C}{C'_s + C_T} = \frac{R_2}{R_1} \qquad \ldots \quad (3)$$

and $$\phi - \phi'_T = \phi'_2 - \phi_1 \qquad \ldots \quad (4)$$

where C and ϕ = capacity and power factor of the standard air condenser in the fourth arm of the bridge respectively;

C_s and C'_s = capacity of the bridge standard condenser in the third arm before and after substitution of the test condenser respectively ;

C_T = capacity of the test condenser ;

ϕ_s = power factor of the bridge standard condenser ;

ϕ'_t = effective diluted power factor of the test condenser ;

R_2/R_1 = ratio of resistances in ratio arms of the bridge ;

$\phi_2-\phi_1$ and $\phi'_2-\phi_1$ = difference of power factor of the balancing arms of the bridge (*i.e.*, power factor dial reading) before and after substitution, respectively.

In actual practice, R_2/R_1 was kept fixed at unity and the standard air condenser at a suitable value under the two conditions of balance. Hence C and ϕ were maintained also constant. From equations (1) and (3), we have

$$C_T = C_s - C'_s \qquad \ldots \quad (5)$$

and from equations (2) and (4)

$$\phi'_T - \phi_s = \phi_2 - \phi'_2 \qquad \ldots \quad (6)$$

Assuming however that ϕ_s is negligible in comparison to ϕ'_T, we get

$$\phi'_T = \phi_2 - \phi'_2 \qquad \ldots \quad (7)$$

It is evident from equations (5) and (7) that the capacity and the effective diluted power factor of the test condenser can be obtained directly from the capacity and power factor dial readings of the bridge before and after substitution. The true power factor of the test condenser is then obtained from the relation

$$\phi_T = \frac{C_s}{C_T} . \phi'_T \qquad \ldots \quad (8)$$

while the permittivity, ϵ, of the test sample is computed from the relation,

$$\epsilon = \frac{113 C_T\, t}{C} \qquad \ldots \quad (9)$$

where C_T is the capacity of the test condenser in micro-micro-farads, t is the thickness of the sample in cm. and S is the area of the electrodes in contact with the sample in sq. cms.

Knowing the values of permittivity (ϵ) and power factor (ϕ_T) of a particular sample at a constant temperature and at a given value of humidity, the dielectric loss factor (ϵ'') can be determined from the the well known relation given by

$$\epsilon'' = \epsilon \tan \delta$$

where δ is the loss angle. Single $\delta + \phi = \pi/2$, we have $\tan \delta = \cos \phi$, when δ is small and ϕ is the phase angle. Hence we may write also

$$\begin{aligned} \epsilon'' &= \epsilon \cos \phi \\ &= \epsilon \phi_T \qquad \ldots \quad (10) \end{aligned}$$

In other words, the dielectric loss factor of a sample is given by the product of its permittivity and power factor.

Tables I and II contain the data of permittivity, power factor and power loss measured at varying relative humidity for Bengal ruby and Madras green mica respectively. In each table column 1 gives the quality and column 2 the designation adopted by the Geological Survey of India of each mica sample. In Figs. 2 to 7, the variations of permittivity or dielectric constant, power factor and power loss of the different qualities of mica with varying relative humidity are shown graphically.

TABLE I

Bengal Ruby Mica

Quality	Designation & colour.	Relative Humidity (%).	Thickness (cm.)	Contract area of electrodes (sq. cm.)	Capacity ($\mu\mu F$).	Permittivity.	Power factor %	Power loss
ar	B.C. 7—Ruby red	20	0·01	2·280	131·8	6·53	0·0116	0.0758
		41	0·01	2·280	131·8	6·53	0·0116	0·0759
		60	0·01	2·280	131·9	6·54	0·0123	0·0802
		80	0·01	2·280	132·2	6·55	0·0148	0·0970
		95	0·01	2·280	133·7	6·63	0·0318	0·2110
Stained	D.—Red	20	0·012	2·204	114·8	7·07	0·0134	0·0944
		41	0·012	2·204	114·8	7·07	0·1344	0·0944
		60	0·012	2·204	115·0	7·08	0·0141	0·0996
		80	0·012	2·204	115·3	7·09	0·0192	0·1362
		95	0·012	2·204	117·0	7·20	0·0415	0·2982
Stained & slightly spotted	A.—Red	20	0·012	2·010	95·5	6·52	0·0256	0·1671
		41	0·012	2·010	96·5	6·52	0·0256	0·1671
		60	0·012	2·010	97·0	6·56	0·0272	0·1784
		80	0·012	2·010	97·4	6·59	0·0357	0·2354
		95	0·012	2·010	98·6	6·67	0·0625	0·4166

TABLE II

Madras Green Mica

Quality	Designation & colour.	Relative Humidity (%)	Thickness (cm.)	Contact area of electrodes (sq. cm.)	Capacity. ($\mu\mu$ F.)	Permittivity.	Power factor. %	Power loss.
Clear	M.C.—green	20	0·01	2·520	141·5	6·35	0·0192	0·1221
		41	0·01	2·520	141·6	6·35	0·0198	0·1256
		60	0·01	2·520	142·4	6·39	0·0209	0·1335
		80	0·01	2·520	143·2	6·42	0·0232	0·1488
		95	0·01	2·520	144·0	6·46	0·0362	0·2337
Stained	C—Green	20	0·013	1·370	64·4	6·80	0·0199	0·1355
		41	0·013	1·370	64·4	6·80	0·0199	0·1355
		60	0·013	1·370	64·4	6·80	0·0212	0·1477
		80	0·013	1·370	65·0	6·86	0·0236	0·1623
		95	0·013	1·370	65·0	6·92	0·0365	0·2526
Stained & spotted.	A—Green	20	0·018	2·323	80·5	7·05	0·0298	0·2098
		41	0·018	2·323	80·5	7·05	0·0298	0·2098
		60	0·018	2·323	80·5	7·05	0·0308	0·2167
		80	0·018	2·323	80·9	7·08	0·0327	0·2318
		95	0·088	2·323	81·5	7·14	0·0640	0·4670

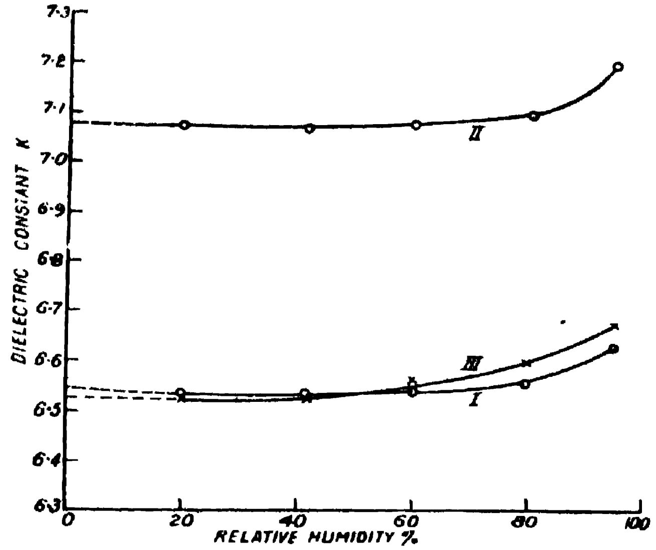

Bengal Ruby Mica

I—Clear, II—Stained, III—Stained and slightly spotted.

FIG. 2

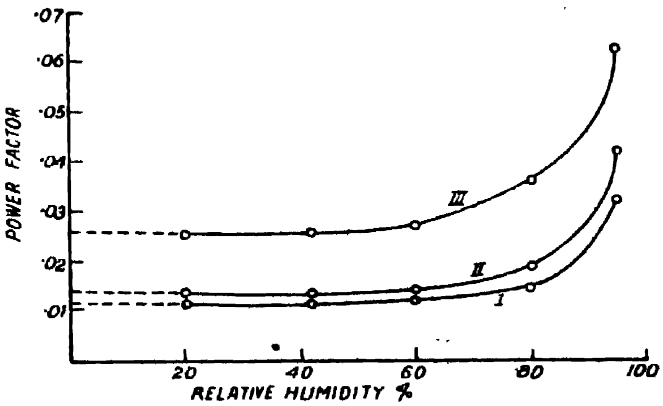

Bengal Ruby Mica

I—Clear, II—Stained, III—Stained and slightly spotted.

FIG. 3

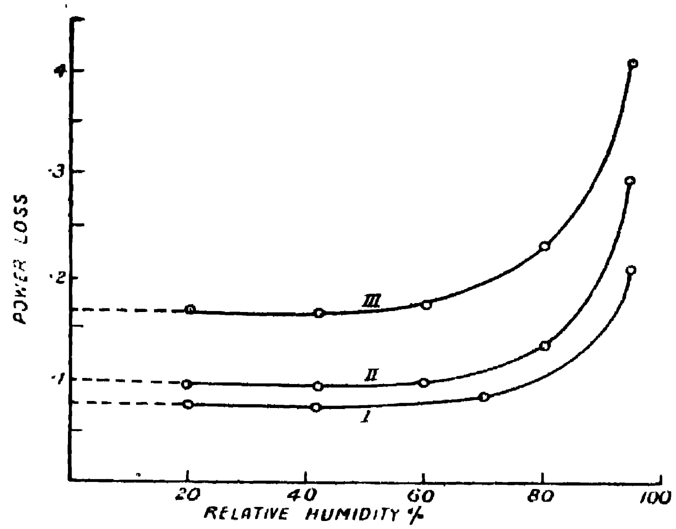

Bengal Ruby Mica

I—Clear, II—Stained, III—Stained and slightly spotted

FIG. 4

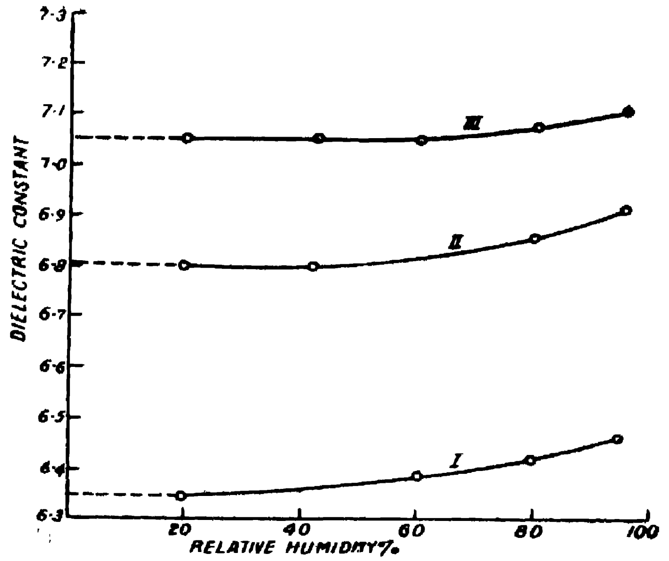

Madras Green Mica

I—Clear, II—Stained, III—Stained and slightly spotted.

FIG. 5

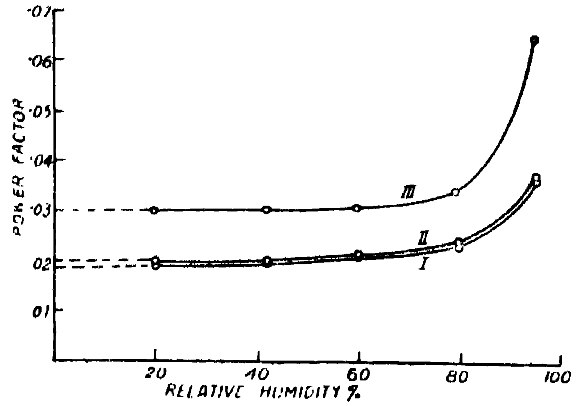

Madras Green Mica
I—Clear, II—Stained, III—Stained and slightly spotted.
FIG. 6

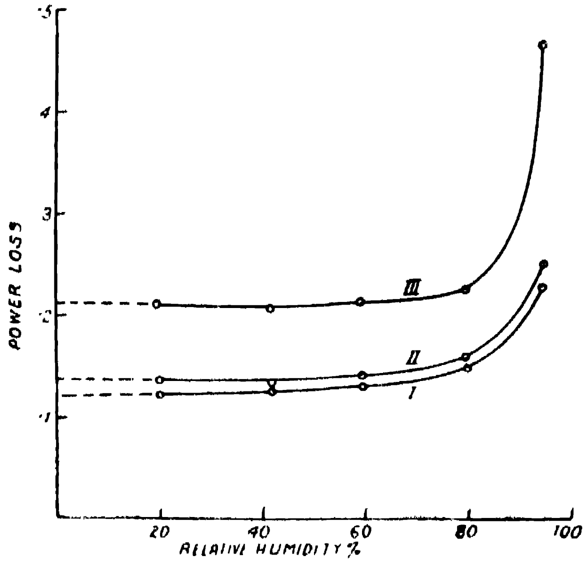

Madras Green Mica
I—Clear, II—Stained, III—Stained and slightly spotted.
FIG. 7

DISCUSSIONS

It is evident from the data in Tables I and II as well as from the graphs (Figs. 2—7) that humidity has an appreciable effect on the permittivity, power factor and power loss of each quality of mica tested, and that the nature of their variation is practically the same in all cases. It is found that the values of permittivity, power factor and power loss remain practically constant up to 40% relative humidity and then increase slowly, the rate of increase increasing with varying humidity and being most marked above a humidity value of 80%. It may be of interest to note here that many investigations in this direction were carried out, notably in England, Germany and Italy, before the present world war. Dannatt and Goodall (1931) were of opinion that changes in the power factor of mica due to variation in the atmospheric humidity were too small to be of any importance from most points of view. But they were contradicted by Hartshorn and Rushton (1931) who found a considerable variation of the power factor of mica with increasing values of relative humidity. In fact they measured the power factor of a particular sample of ruby mica at a frequency of 800 cycles per second and at a temperature of 20° C, and found it to change very appreciably when the relative humidity was varied from 8% to 50%. More recently, they (Hartshorn and Rushton, 1936) have studied also the variation of power loss in typical samples of clear ruby mica with moisture content and have confirmed their earlier opinion. Schwarz (1936) in Germany also observed considerable variation in the power factor of mica with varying relative humidity. He found the value of power factor to decrease from 0·02% under the normal atmospheric humidity to 0·017% when kept under vacuum and to increase to 0·04% at a relative humidity of 90%, the time of conditioning the sample in each case being 24 hours. Tabaracci (1930) in Italy also observed that the loss angle of mica was a function of humidity. Our results are therefore in perfect agreement with the views of the above workers. It may however be noted here that as the capacity and the power factor dial readings of the bridge were practically the same at any value of relative humidity, whether this value was obtained with increasing or with decreasing humidity in the experimental chamber, one is led to infer that the variation observed in the electrical behaviour of mica is very likely due to surface absorption of moisture and is not a case of adsorption or any change in its chemical and capillary structures.

One finds further that the stained and spotted quality of each type of mica has, as one would expect, the largest value not only of power factor but also of power loss. On the otherhand, all the different qualities may be said to have practicaliy the same value of permittivity in view of the fact that the average permittivity of muscovite mica of any type and quality is about 7 (Dye and Hartshorn, 1924; Dannatt and Goodall, 1931) while the individual values obtained from measurements on different samples even of the same quality and geographical origin lie within the limits of 5·83 to 9·64 (Lewis, Hall and Caldwell, 1931). It may however be mentioned here that we have used only one sample of each quality for our measurements since the main object of our present investigation was to study the effect of varying relative humidity on the electrical properties of Indian mica.

In conclusion, the authors acknowledge gratefully their thanks to Prof. P. N. Ghosh, for his kind interest and encouragement during the investigation and to Dr. W. D. West of the Geological Survey of

India for kindly supplying the clear qualities of mica samples used in our measurements.

MEASUREMENT AND STANDARDISATION LABORATORY,
DEPARTMENT OF APPLIED PHYSICS,
CALCUTTA UNIVERSITY.

REFERENCES

Dannatt and Goodall (1931), *J.I.E.E.*, **69**, 490.
Datta, Sen Gupta and Mahanti (1942), *Indian Jour. Phys.*, **17**, 79
Dye and Hartshorn (1924), *Proc. Phys. Soc.*, **37**, 42.
Grover and Nicol (1940), *Jour. Soc. Chem. Industries*, **59**, 175.
Hartshorn and Rushton, (1931), *J.I.E.E.*, **69**, 1034 (1939), *E.R.A.*, *Report, Ref.* L/T 60 24.
Lewis, Hall and Caldwell (1931), *B.S.J.R.*, **7**, 403
Schwarz (1936), *E.T.Z.*, **57**, 7
Tabaracci (1939), *Electrotechnica*, **26**, 649.

ON THE CRYSTAL STRUCTURE OF PHTHALIMIDE. PART I.—DETERMINATION OF THE SPACE-GROUP

By S. N. BAGCHI and M. A. KASEM

(Plate V)

ABSTRACT. Single crystals of phthalimide were studied goniometrically and with X-rays. Goniometric data assign it to the monoclinic holodedral class in agreement with Groth.

The axial ratios, obtained from X-ray studies, are $a:b:c = 2.98:1:0.4946$. Phthalmide is found to belong to space group C^5_{2h}—$P2_1/n$.

According to Groth (1906) phthalimide crystallises in the monoclinic holohedral class with axial ratios $a : b : c = 1.4913 : 1 : 0.4967$ and $\beta = 91°18\frac{2}{3}'$.

The X-ray data of this substance is completely lacking. The present paper deals with the determination of the axial lengths and the space-group of phthalimide.

PREPARATION OF THE CRYSTAL

It is very difficult to get perfect single crystals of phthalimide. Several attempts were made to crystallise it from a solution of alcohol, alcohol and acetic acid, acetic acid and ethyl acetate. None of the solvents had been found to be highly satisfactory. However, amongst the solvents tried, ethyl acetate was found to be the best medium for crystallisation. After repeated and careful crystallisations, only a few perfect single crystals were obtained.

The crystals were all needle-shaped. They were studied with the help of the Czapski Theodolite two-circle goniometer. The observed angles between the various faces were found to agree with those reported by Groth (*loc. cit.*).

MEASUREMENT OF AXIAL LENGTHS

Hadding-Siegbahn type of x-ray tube with copper anticathode was used. Rotation photographs were taken with a cylindrical camera.

(*i*) Rotation about *c*-axis:

The *c*-axis being the long axis of the crystal itself can be easily set by making the prism faces vertical. The photograph is shown in Plate V Fig. 1 and the mean axial length measured from the different layer lines given by Cu K_α and Cu K_β is found to be $c = 3.765$ Å.

(*ii*) Rotation about *b*-axis :

The *b* (010) face does not develop in the crystal. The *b*-axis becomes vertical when the reflections from the prism faces lie in the vertical plane and the bisector between *m* (110) and *m'* ($\bar{1}10$) becomes vertical.

The mean axial length, $b = 7.611$ Å, is found from the rotation photograph (Fig. 2).

(*iii*) Rotation about *a*-axis :

Both *b* (010) and *c* ($00\bar{1}$) faces being absent, *a*-axis was fixed by setting *q* (011) and q' (011) faces vertically.

The rotation photograph (Fig. 3) gives the mean value $a = 22.70$ Å.

Thus the axial ratios, given by the x-ray studies of the crystal are found to be

$$a : b : c = 2.98 : 1 : 0.4946.$$

Comparing the results with those given by Groth (*loc. cit.*) it is found that the length of the *a*-axis is twice the value assumed by Groth.

In order to determine correctly the space-lattice and the space-group the reflecting spots must be identified and indexed unambiguously.

DETERMINATION OF THE SPACE-LATTICE

Oscillation photograph :

The crystal was set with the *c*-axis vertical. The oscillation started with the incident beam normal to a (100) face, *i.e.*, parallel to the reciprocal a-vector -a*-axis. The ocillation ranging from 0° – 180° was covered in ten successive stages, each oscillating within the range of 18°.

The theoretical Bragg angle of reflection of diffracted planes which alone can appear in the oscillation picture as judged from the reciprocal lattice are compared with those obtained from the direct measurement of the photograph. Thus every spot in the photograph is accounted for and given the proper index. The theoretical angles are calculated from the equation

$$\operatorname{Sin}\theta = \frac{\lambda}{\sin\beta}\sqrt{\left[\left(\frac{h}{a}\right)^2 + \left(\frac{k\sin\beta}{b}\right)^2 + \left(\frac{l}{c}\right)^2 - \frac{2\,hl}{ac}\cos\beta\right]}$$

where θ is the Bragg angle of reflection of the plane (*hkl*).
a, *b*, *c* are the axial lengths already determined
β is the axial angle determined from goniometric studies.

A perusal of the indices of the planes reflected in the central layer line showed that no special conditions guide the reflection of (*hko*) planes.

Since there is no restriction in the appearance of (*hko*) reflections, there cannot be also any systematic absent spectra in the general (*hkl*) reflections. Hence, being superfluous, higher layer lines of the *c*-axis oscillation photographs were not analysed.

The unit cell of phthalimide, therefore, belongs to the simple monoclinic lattice.

DETERMINATION OF THE SPACE-GROUP

Weissenberg photographs :

One of the axes being too long, the angles of reflection of (*oko*) planes lie very close to that for (*lko*). Hence in order to decide unambiguously the nature

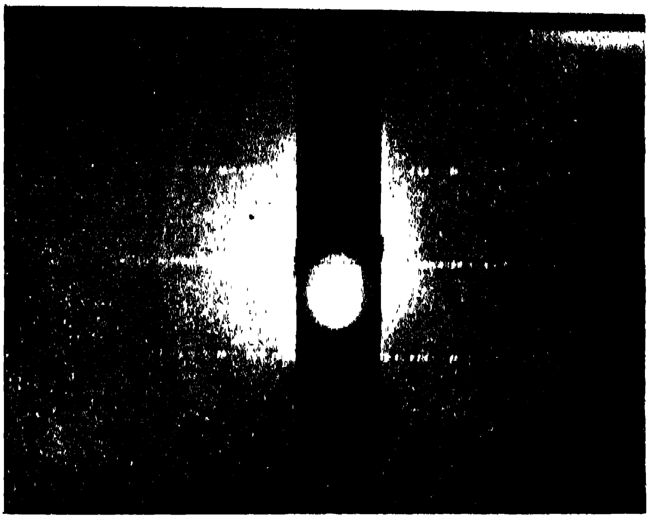

Fig. 1
Rotation photograph
about *c*-axis

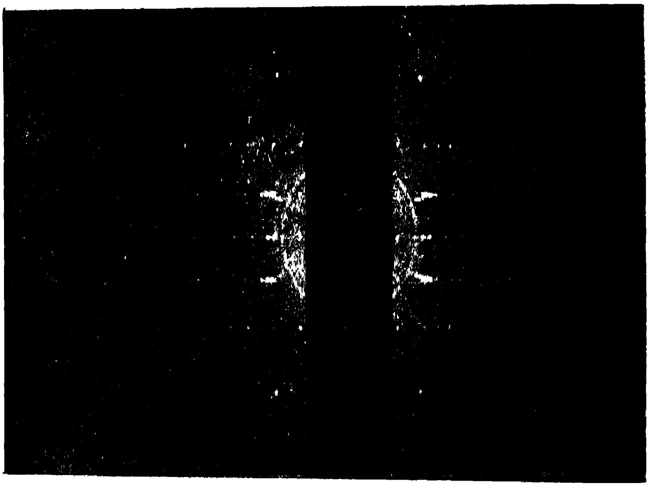

Fig. 2
Rotation photograph
about *b*-axis.

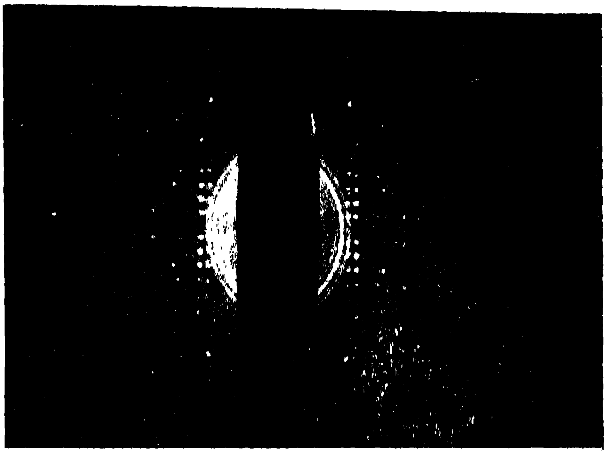

Fig. 3
Rotation photograph
about *a*-axis.

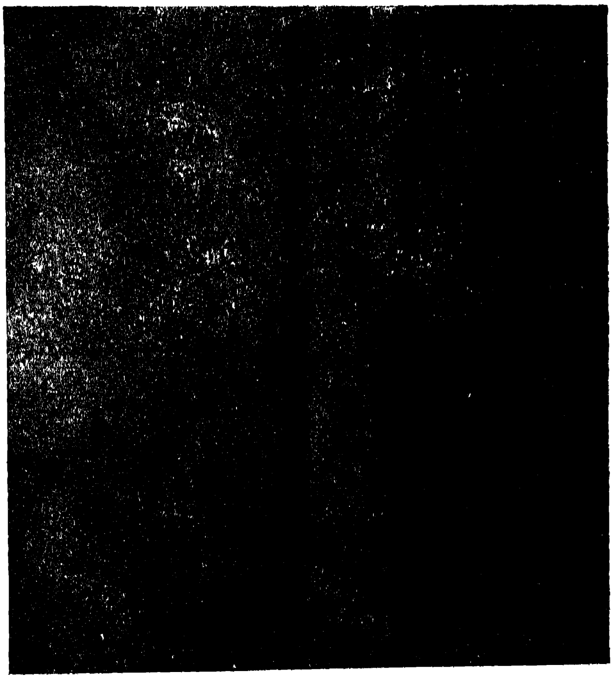

Fig. 4
Rotation photograph
about *c*-axis.

of (*oko*) reflections, Weissenberg photograph of the central layer line around *c*-axis of the crystal was taken (Fig. 4).

All the spots were correctly indexed. It was found that no systematic absent spectra occur in the reflection of (*hko*) planes, as already indicated by oscillation photographs, but (*hoo*) and (*oko*) reflections occur only when *h* and *k* are even.

Since the crystal belongs to the monoclinic hololedral class, halving of (*oko*) indicates a two fold screw axis along *b* while halving of (*hoo*) indicates a glide-plane of symmetry normal to the *b*-axis and having a glide of $a/2$ or $(a+c)/2$.

To choose between these two alternatives we have to study the nature of (*hol*) reflections.

For this purpose a Weissenberg photograph of the central layer line around *b*-axis of the crystal was taken. This also gives us directly the angle β between *a*-and *c*-axes.

β was found to agree satisfactorily with the value reported by Groth.

Indices of all the spots showed that not only the odd orders of (*hoo*) and (*ool*) are absent but also all reflections from (*hol*) where $(h+l)$ is odd, are absent. This means that the glide is $(a+c)/2$ and not $a/2$.

As all the necessary and requisite conditions of finding out the correct space-group of a monoclinic lattice (*cf.* Astbury and Yardley) have been determined, the nature of (*o k l*) reflections were not studied.

To sum up, it is found that (*i*) *b*-axis is a two-fold screw axis, since odd orders of (*o k o*) reflections are absent and (*ii*) the plane normal to the *b*-axis, *i.e.*, (010) plane is a glide plane of symmetry with a glide of $(a+c)/2$, since all reflections from (*hol*) where $(h+l)$ is odd are absent.

On comparing these criteria with those given by Astbury and Yardley (*loc. cit.*) the space-group is found to be $C_{2h}^5 - P2_1/n$

NUMBER OF MOLECULES IN THE UNIT CELL

The number of molecules per unit cell, *n*, is given by the relation

$$\rho = n.\ M.\ m/V$$

where ρ = density of the phthalimide crystal.

n = the number of molecules of phthalimide $C_6H_4(CO)_2NH$ per unit cell.

m = wt. of H atom $= 1.649 \times 10^{-24}$ gm.

M = molecular weight of phthalimide = 147.

V = volume of the unit cell

$= abc \text{ Sin } \beta$

$= 22.7 \times 7.611 \times 3.765 \times \text{Sin } 91^\circ 18\frac{2}{3}' \times 10^{-24}$ c.c.

$= 6.504 \times 10^{-22}$ c.c.

The density was determined by the flotation method from a solution of zinc sulphate. It was found to be 1.452

Hence the number of molecules, *n*, per unit cell

$$\rho V/Mm = 3.896 \approx 4.0.$$

SUMMARY

The axial lengths *a*, *b* and *c* were found out from the three rotation photographs. The length of the *a*-axis is found to be twice that assumed by Groth.

The axial ratios are $a : b : c = 2.98 : 1 : 0.4946$.

Oscillation photographs around *c*-axis showed the general nature of (*hko*) and (*hkl*) reflections indicating the presence of the simple lattice.

Zero-layer-line Weissenberg photographs around *b* and *c*-axes were taken. The *b*-axis photograph gave β angle agreeing fairly well with that found optically, *viz.*, $91°18\frac{2}{3}'$.

All reflections from (*hol*) planes where $(h+l)$ is odd are absent.

From *c*-axis photograph it was found that all odd orders of (*oko*) reflections are absent.

Hence *b*-axis is a two-fold screw axis and (*ac*)-plane is a glide plane of symmetry with a glide $(a+c)/2$, and the space-group is $C_{2h}^{5} - P2_1/n$

$$a = 22.700 \text{ Å}$$
$$b = 7.611 \text{ Å}$$
$$c = 3.765 \text{ Å}$$
$$\beta = 91° \ 18\tfrac{2}{3}'$$
$$n = 4.$$

Our best thanks are due to Prof. S. N. Bose for his guidance and continued interest in this work. One of the authors (S. N. B.) wishes to record his thanks to the Imperial Council of Agricultural Research, India, for financial help and to Prof. J. N. Mukherjee for making it possible for him to work at Dacca.

X-RAY LABORATORY,
DACCA UNIVERSITY.

REFERENCES

Astbury and Yardley, 1934, *Phil. Trans. Roy Soc. Ind.*, **224A**, 221.
Groth, 1906, *Chem. Krist.*, **4**, 712.

THE THEORY OF THE 180° MAGNETIC FOCUSSING TYPE OF BETA RAY SPECTROMETER*

By AJIT KUMAR SAHA

ABSTRACT. A rigorous mathematical theory of the 180° magnetic focussing type of β-ray spectrometer has been worked out. An expression for the transmission factor of this instrument as a function of the magnetic field and the electron-momentum has been obtained. The transmission factor of the spectrometer of Lawson and Tyler has been completely calculated numerically in order to compare this theory with an earlier approximate theory developed by Lawson and Tyler.

§1. The 180° magnetic focussing type of β-ray spectrometer with variable field has become today, like the ionisation chamber, the Geiger Müller counter and the cloud chamber, an indispensable instrument in nuclear physics laboratories. It has found extensive application in the study of the shape of the continuous β-ray spectrum and the determination of the position and the intensity of the conversion electron groups. On account of the great importance of this apparatus it is necessary to have its complete mathematical theory. The only existing theory appears to be that due to Lawson and Tyler (1940). They have, in course of developing their theory, been forced to resort to many approximations and have employed graphical methods even at the initial stages of the theory. Consequently their mathematical working is rather obscure at many points. The following is an alternative treatment of this problem, being essentially a continuation of a method developed by the writer [Saha (1944)]† in connection with his theory of the screen cathode β-ray spectrometer. Almost the same notations, as used in the previous paper, have been employed here throughout. In this theory the method is strictly geometrical, and the analysis may be continued up to the final stages without employing any simplifying approximations. The permissible approximations come out automatically in course of the analysis and these have been clearly indicated in the final calculations of the so-called transmission factor function of this instrument. Again it must be pointed out, that only one graphical integration has to be carried out in this analysis and even that at the final stages, whereas Lawson and Tyler had to carry out more than one graphical integrations. Thus this method turns out, for practical purposes, to be simpler than that of Lawson and Tyler. Finally the method has been used to calculate the transmission factor function for the Lawson-Tyler β-ray spectrometer in order to compare our theory with that of Lawson and Tyler.

---

* Communicated by Prof. M. N. Saha, F.R.S., F.N.I.

† This Paper will be referred to here after as Paper I.

§2. MOTION OF THE ELECTRONS IN A MAGNETIC FIELD H

In fig. 1 O represents the centre of the rectangular plate over which the radioactive sample under investigation is spread. With this point as origin, let us take two axes of co-ordinates $O\xi$ and $O\eta$ as shown in the figure. $O\xi$ is perpendicular to the shorter edge of the sample plate and the positive direction of ξ points away from the reader. $O\eta$ is perpendicular to the longer edge of the sample plate and the positive direction of η points to the right side of the figure, *i.e.*, away from the slit S_1. Let S be a point (ξ, η) on the sample plate. At S we construct a right handed frame of reference as shown in the figure. SZ and SY are respectively parallel to $O\xi$ and $O\eta$. SX is normal to the plane of the sample plate and positive direction of x is upwards from the plate. The magnetic field points to the negative direction of Z axis. Let us suppose that an electron leaves the point S in the direction SA. Let θ be the zenith angle and ϕ the azimuth of SA, *i.e.*, let $\theta = \angle$ ASZ and $\phi = \angle$ XSB, where SB is the projection of SA on the $z=0$ plane. Instead of taking p to be the electron momentum, as has been done in paper I, we shall take

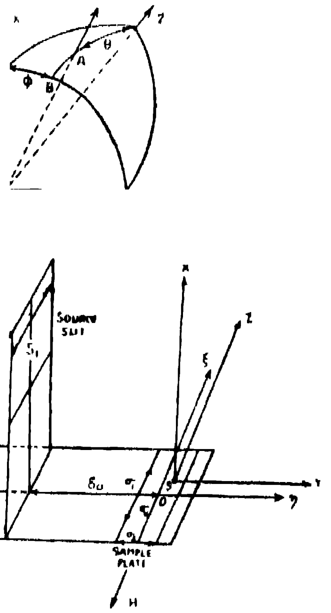

FIG. 1

$$p \qquad \times \text{ electron momentum.} \qquad (2.1)$$

Let H be the magnetic field applied. As pointed out in paper I the electron trajectory has the shape of a helix whose axis is parallel to the magnetic field and whose projection on the $z=0$ plane is a circle. If the quantities D, ρ, L be defined by

$$D = \frac{2p}{H}, \quad \rho = \frac{D}{2} \sin\theta, \quad L = \pi D \cos\theta, \qquad \dots \quad (2.1)$$

then the electron trajectory is given by

$$(x-\rho\sin\phi)^2+(y+\rho\cos\phi)^2=\rho^2, \qquad \text{.. (2.2a)}$$

$$z=\frac{L\psi}{\pi}. \qquad \text{... (2.2b)}$$

Equation (2.2a) represents the projection of the helix on the plane $z=0$. It is a circle of radius ρ, with its centre at N (fig. 2) whose co-ordinates are

$$x_N=\rho\sin\phi, \quad y_N=-\rho\cos\phi \qquad \text{... (2.3)}$$

ψ is an angle which has been called in paper I by the name pitch angle. If E be the projection of any point on the electron trajectory on the $z=0$ plane then the corresponding ψ is the $\angle$ EFS. The significance of the length L, the pitch of the helix has been explained in paper I. For convenience we shall call:

(*a*) the circle (2.2a) as the circle P.

(*b*) the locus of centres of the circles of P for the same D and θ but different ϕ as the circle Q.

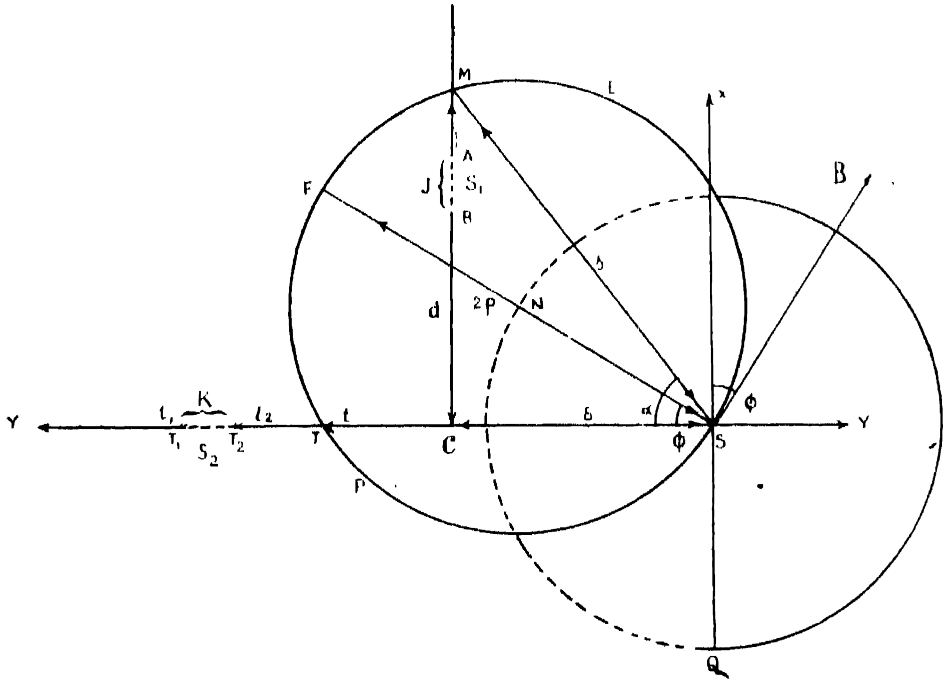

FIG. 2

Before proceeding any further, we shall explain certain symbols which we shall have to use very frequently hereafter. Consider the section of the spectrometer by the plane $z=0$. Let this plane cut the source slit S_1 at points A, B and the counter slit S_2 at points T_1, T_2. Let AB cut ST_1T_2 at C. Let the circle P cut the line AB at a point M and the line OC at a point T.

Let the symbols α, s, δ, t, d be defined as follows

$$\alpha = \angle\, \mathrm{MSC}, \quad s = \mathrm{MS}, \quad \delta = \mathrm{CS}, \quad t = \mathrm{TS}, \quad d = \mathrm{MC}.$$

Then

$$\frac{\sin\alpha}{d} = \frac{\cos\alpha}{\delta} = \frac{t}{s} \qquad \ldots \quad (2.4)$$

If δ_0 denotes the perpendicular distance of the centre O of the sample plate from the plane of S_1 then

$$\delta = \delta_0 + \eta \qquad \ldots \quad (2.5)$$

It is easy to prove that if Φ = the azimuth of an electron (ρ) for which the circle (2.2a) passes through a point M(α) on S_1, then

$$\Phi = \alpha + \sin^{-1}\left(\frac{s}{D\sin\theta}\right) - \frac{\pi}{2} \qquad \ldots \quad (2.6)$$

The distance t for this electron is given by

$$t = 2\rho\cos\Phi = \delta + \sin\alpha\sqrt{D^2\sin^2\theta - s^2} \qquad \ldots \quad (2.7)$$

The z-displacement of the electron when it reaches the counter slit is given by $z = Z$, where

$$Z = \frac{L}{\pi}\left(\frac{\pi}{2} + \Phi\right) = D\cos\theta\left[\alpha + \sin^{-1}\left(\frac{s}{D\sin\theta}\right)\right] \qquad \ldots \quad (2.8)$$

The portion of the line AB extending from A to B will be called by the name J. By K we shall understand the portion of the line SY′ extending from T_1 to T_2. Let $z = \lambda_+, -\lambda_-$ and $y = -l_1, -l_2$ be the boundaries of the slit S_2. If $2C_1$ denotes the length of the longer edge of S_2 then

$$\lambda_+ = C_1 - \xi, \ \lambda_- = C_1 + \xi. \qquad \ldots \quad (2.9a)$$

If $2C_2$ denotes the length of the shorter edge of S_2 and l_0 be the distance of the centre of the sample plate from the centre of counter slit then

$$l_1 = l_0 + \eta + C_2, \quad l_2 = l_0 + \eta - C_2 \qquad \ldots \quad (2.9b)$$

The condition that an electron will be admitted by the counter slit S_2 and be counted are as follows :—

(a) The circle P should cut both the lines J and K ... (2.10a)

(b) (1) $0 < Z < \lambda_+$ for electrons with θ in $0 < \theta < (\pi/2)$ ... (2.10b)

(2) $\lambda_- > Z < 0$ for electrons with θ in $+(\pi/2) < \theta < \pi$ ... (2.10c)

As pointed out in paper I electrons with θ in $2\pi > \theta > \pi$ or ϕ in $3\pi/2 > \phi > \pi/2$ will be cut off by the source plate. We have therefore the following restrictions on ϕ and θ, *viz.*

$$\left.\begin{array}{ll} (a) & \phi \text{ can lie only in the interval } \frac{\pi}{2} > \phi > -\frac{\pi}{2} \\ (b) & \text{and } \theta \text{ within } \pi > \theta > 0 \end{array}\right\} \qquad \ldots \quad (2.11)$$

§3. RESTRICTIONS ON ϕ IN ORDER THAT AN ELECTRON (ρ) MAY PASS THROUGH S_1

The angle α can vary only between the limits α_A, α_B (these being the α's corresponding to the points A and B respectively), for $\alpha_A > \alpha > \alpha_B$ is the only open portion on S_1. Thus Φ can vary only between the limits $\Phi_A > \Phi > \Phi_B$ (Φ_A, Φ_B being the Φ's corresponding to electrons ρ whose M coincide with the points A and B respectively). Let us now examine how Φ for any particular α varies with 2ρ. The Φ v.s. 2ρ plot for any particular α [fig. 4(*a*)] starts at ($2\rho = s_\alpha$, $\Phi = \alpha$) and falls uniformly as we increase 2ρ. Again $\Phi(\alpha) = 0$ at

$$2\rho = s_\alpha \sec \alpha \tag{3.1}$$

Thus for $s < 2\rho < s \sec \alpha$, we have $\Phi_\alpha > 0$ and for $2\rho > s \sec \alpha$ we have $\Phi_\alpha < 0$. Further more as $2\rho \rightarrow \infty$, $\Phi(\alpha) \rightarrow \alpha - \pi/2$ asymptotically. Suppose that at $\rho = \rho_{AB}$ $\Phi_A = -\Phi_B$. ρ_{AB} will be given by

$$2\rho_{AB} = \frac{s_A\, s_B}{\delta} \tag{3.2}$$

Let us now examine the following cases in some detail.

Case I : $s_A < s_B \sec \alpha_B$ (figures 3).

(1) $s_B < 2\rho < s_A$:—The circles P and the line J will cut at points between D $[\alpha = \alpha_D = \cos^{-1}(\delta/2\rho)]$ and B $(\alpha = \alpha_B)$ provided $\Phi_D (= \alpha_D) > \phi > \Phi_B$. *i.e.* provided N is on the arc $N_D N_B$ [fig. 3(*a*)] of the circle Q. Both Φ_D and Φ_B are

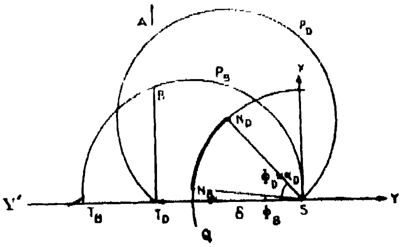

FIG. 3(*a*)

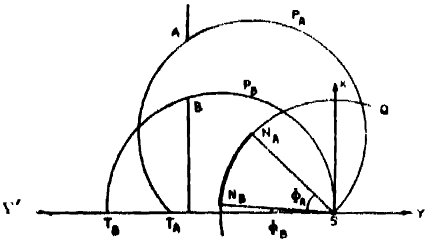

FIG. 3(*b*)

> 0 and therefore the arc $N_B N_B$ is above SY′ so that according to (2.7) $t_B > t > t_D$.

(2) $s_A < 2\rho < s_B \sec \alpha_B$:—The circles P and the line J will cut provided $\Phi_A > \phi > \Phi_B$, *i.e.*, provided N is on the arc $N_A N_B$ [fig. 3(*b*)] of the circle Q. Φ_A and Φ_B are both > 0, so that the arc $N_A N_B$ [fig. 3(*b*)] is above SY′. Hence $t_B > t > t_A$.

(3) $s_B \sec \alpha_B < 2\rho < 2\rho_{AB}$:—$\Phi_A > 0$, $\Phi_B < 0$ and $\Phi_A > -\Phi_B$. The circles P and the line J will cut if $\Phi_A > \phi > \Phi_B$, *i.e.*, provided N is on the arc $N_A N_B$. The position of the centres N_A, N_B of the circles P_A and P_B relative to the line SY′ is as shown in fig. 3(*c*). Let N_C be the centre of the circle P_C for an electron ρ whose $\Phi = 0$. The α of the point where P_C cuts J is given by

$$\alpha_C = \cos^{-1}(\delta/2\rho) \quad \ldots \tag{3.3}$$

Evidently then $t_C > t > t_A$. We must note an important fact here. If the centres N_{E_1}, N_{E_2} of two circles P_{E_1} and P_{E_2} are so placed on the arc N_AN_B, one above, and the other below SY′, that arc $N_CN_{E_1}$ = arc $N_CN_{E_2}$, then since $\Phi_{E_1} = -\Phi_{E_2}$, we find that the circles P_{E_1} and P_{E_2} will intersect each other at a point T_E which lies on the line SY′. Thus $t_{E_1} = t_{E_2}$ [fig. 3(c)].

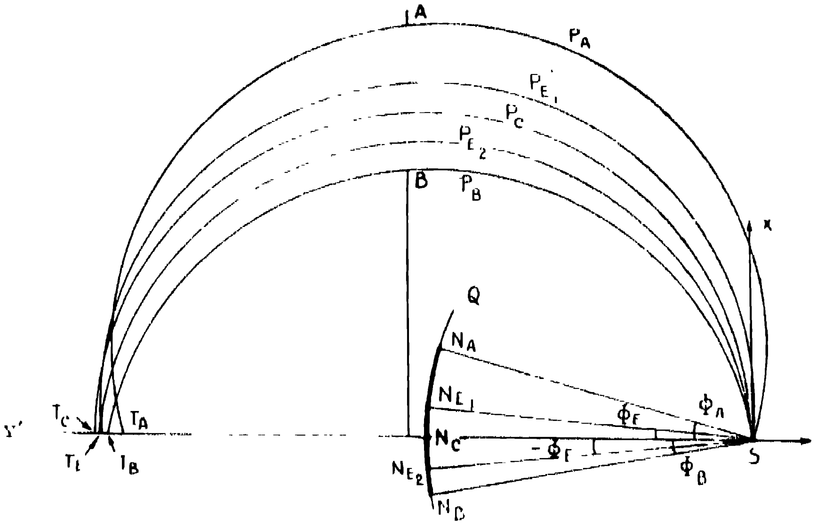

FIG. 3(c)

(4) $2\rho_M < 2\rho < s_A \sec \alpha_A$:—$\Phi_A > 0$, $\Phi_B < 0$, and $\Phi_A < -\Phi_B$. In this case also N must lie on the arc N_AN_B if the circles P are to cut the line J [fig. 3(d)]. But since now $\Phi_A < -\Phi_B$ we shall have $t_C > t > t_B$ [fig. 3(d)]. The rest of the discussion in (3) hold here also.

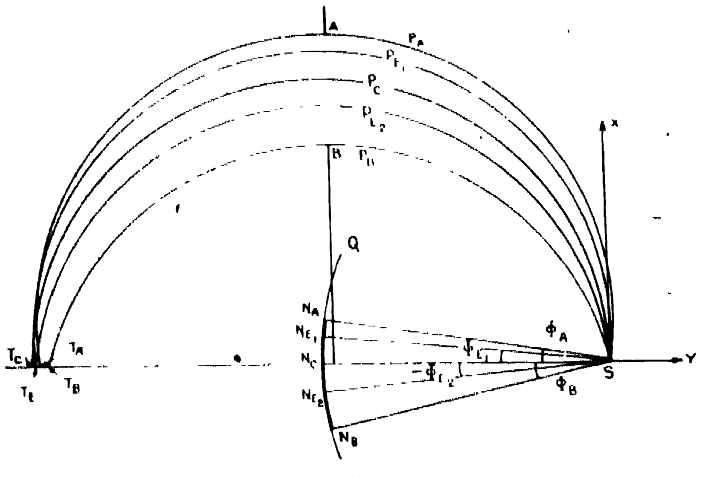

FIG. 3(d)

(5) $s_A \sec \alpha_A < 2\rho < \infty$:—Φ_A and Φ_B are both < 0, and $-\Phi_B > -\Phi_A$. Again

N must lie on the arc N_AN_B if the circles P are to cut the line J. The arc N_AN_B lie wholly below SY′ as shown in fig. 3*e* so that $t_A > t > t_B$.

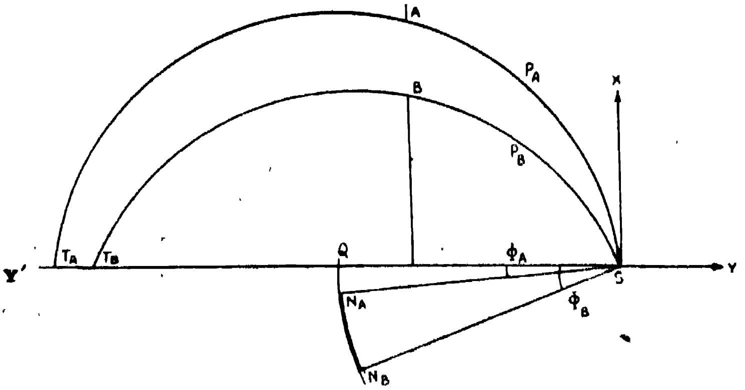

FIG. 3(*e*)

Case II : $s_A > s_B \sec \alpha_B$. This case needs no separate discussion. The conclusions are only trivially different from those of case I.

§4 FURTHER RESTRICTIONS ON ϕ INTRODUCED BY THE COUNTER SLIT S_2

Let us plot t against 2ρ for different α's and consider in detail the curves thus obtained. These are shown in fig. 4(*b*). From (2.7) it is clear that for any definite value of α : (*a*) t does not exist for $2\rho < t$, (*b*) at $2\rho = s_a$, $t = \delta$, (*c*) $dt/d(2\rho) = 1$ at $2\rho = s \sec \alpha$, (*d*) t increases uniformly as 2ρ is increased and (*e*) as $2\rho \rightarrow \infty$, $t \rightarrow$ asymptotically to the value $t = \delta + 2\rho \sin \alpha$, which represents the straight line RM_3 [fig. 4(*b*)] passing through ($2\rho = 0$ and $t = \delta$) and inclined to the 2ρ axis at an angle $\tan^{-1}(\sin \alpha)$. Thus for any particular point M on the line J with the source angle $\alpha (\alpha' > \alpha > \alpha_B)$, the t v.s. 2ρ curve starts at $M_1(2\rho = s_a, t = \delta)$, rises uniformly, touches a line B_2A_2 passing through ($t = 0$, $2\rho = 0$) and inclined to 2ρ axis an angle of $\pi/4$ at a point M_2 ($2\rho = s_a \sec \alpha = t$) and finally approaches asymptotically the line RM_3. The curves corresponding to points A, B on the line J are the curves $A_1A_2A_3$, $B_1B_2B_3$ respectively of the figures. Evidently these curves intersect at N ($2\rho = 2\rho_{AB}$, $t = t_{AB}$). Consider the curves B_1 B_2 A_2 A_3 and B_1 A_1 N B_3. Clearly for any particular value of 2ρ the ordinate of the corresponding point on the former curve gives the maximum possible value of t for the circles P interesting the line J, and that of the corresponding point on the latter curve gives the minimum possible value of t. We may call therefore these curves by the name the t_{max} and the t_{min} curves respectively. In is easy to see that the t_{max} curves coincides (*a*) with . or $s_B < 2\rho < s_B \sec \alpha_B$, (*b*) with the line B_2A_2 (whose equation is $t = 2\rho$) for s_B s $\alpha_B < 2\rho < s_A \sec \alpha_A$ and (*c*) with t_A for $s_A \sec \alpha_A < 2\rho$. Also the t_{min} curve coincides with (*a*) the line B_1A_1 which is parallel to the 2ρ axis and is placed at a distance δ from it for $s_B < 2\rho < s_A$, (*b*) with t_A for $s_A < 2\rho < 2\rho_{AB}$, and

(c) with t_B for $2\rho_{AB} < 2\rho$. In passing, we note that in the regions $s_B < 2\rho < s_B$ sec α_B and s_A sec $\alpha_A < 2\rho$, the t_α curves do not cut each other. But in the region s_B sec $\alpha_B < 2\rho < s_A$ sec α_A each t_α curve cuts any other t_α curve once.

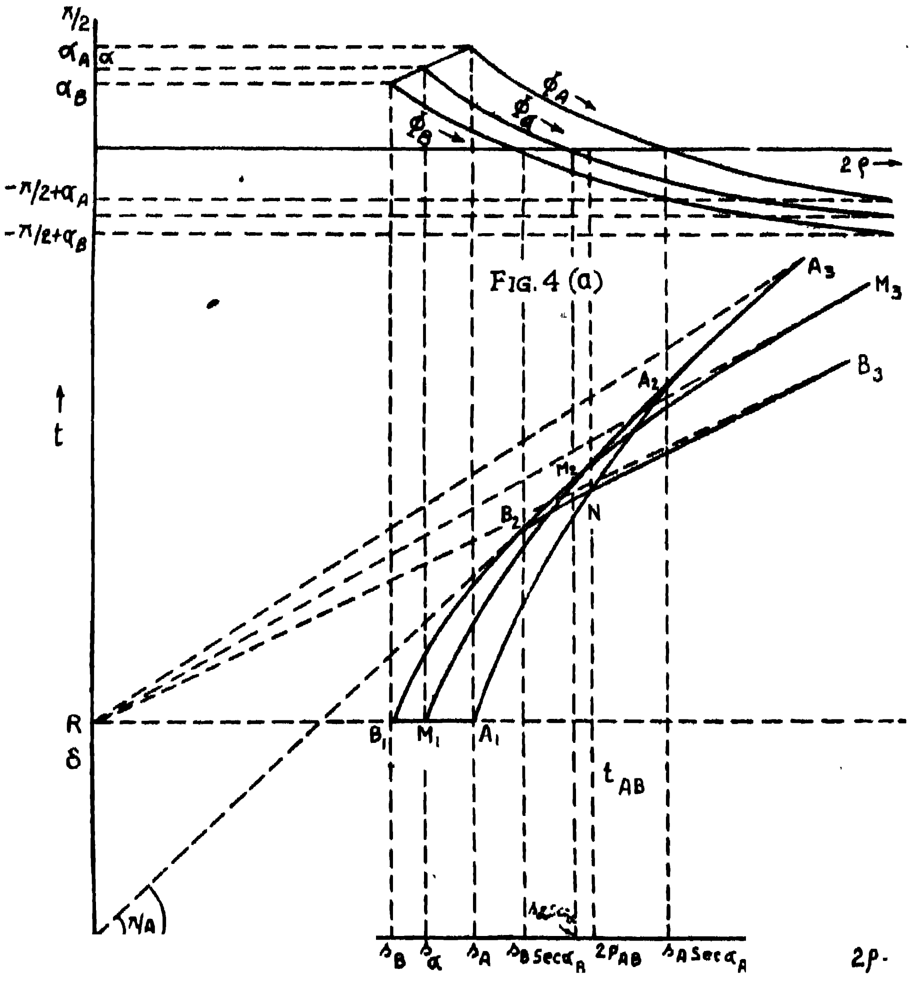

FIG. 4 (b)

Now let us draw two lines L_1 and L_2 parallel to and at distances l_1, l_2 respectively from the 2ρ axis. Let these lines cut the t_{max} curve at the points P_1 and P_2 respectively and the t_{min} curve at the points Q_1 and Q_2 respectively (figs. 5). Let the abscissae corresponding to these points be $2R_i$, $2R_s'$, $2R_i'$, $2R_s$ respectively. Then conditions (2.10a) show that the first condition that must be satisfied by ρ in order that the circles P may cut both the lines J and K is

$$2R_i \overset{*}{<} 2\rho < 2R_s \qquad \ldots \quad (4.1)$$

For each point S on the source plate these values R_i and R_s are constants and it is our purpose to determine them. Suppose that a line L parallel to and at a distance l from the 2ρ axis cuts the t_{max} curve at $2\rho = 2R_{II}$ and the t_{min} curve at $2R_{III}$. It is clear that

$$
\left.
\begin{array}{l}
(a)\ \text{if } l < \delta \text{ then } R_{l\mathrm{I}} \text{ does not exist,} \\
(b)\ \text{if } \delta < l < s_B \sec \alpha_B, \text{ then } R_{l\mathrm{I}} \text{ is given by} \\
\qquad 4R_{l\mathrm{I}}^2 = \left(\dfrac{l-\delta}{\sin \alpha_B} \right)^2 + s_B^2, \\
(c)\ \text{if } s_B \sec \alpha_B < l < s_A \sec \alpha_A \text{ then } R_{l\mathrm{I}} \text{ is given by} \\
\qquad 2R_{l\mathrm{I}} = l, \\
(d)\ \text{if } s_A \sec \alpha_A < l \text{ then } R_{l\mathrm{I}} \text{ is given by} \\
\qquad 4R^2_{l\mathrm{I}} = \left(\dfrac{l-\delta}{\sin \alpha_A} \right)^2 + s_A^2.
\end{array}
\right\} \quad \dots \quad (4.2a)
$$

Again we note that

(*a*) if $l < \delta$ then $R_{l\mathrm{II}}$ does not exist,

(*b*) if $\delta = l$ then $R_{l\mathrm{II}}$ may have all values between s_B and s_A,

$$
\left.
\begin{array}{l}
(c)\ \text{if } \delta < l < t_{AB} \text{ then } R_{l\mathrm{II}} \text{ is given by} \\
\qquad 4R^2_{l\mathrm{II}} = \left(\dfrac{l-\delta}{\sin \alpha_A} \right)^2 + s_A^2, \\
(d)\ \text{if } t_{AB} < l \text{ then } R_{l\mathrm{II}} \text{ is determined by} \\
\qquad 4R^2_{l\mathrm{II}} = \left(\dfrac{l-\delta}{\sin \alpha_B} \right)^2 + s_B^2.
\end{array}
\right\} \quad \dots \quad (4.2b)
$$

The quantity t_{AB} occurring above is the ordinate of the point N [fig. 4(*b*)] where the t_B and the t_A curves intersect. It is evidently given by

$$t_{AB} = \delta + \frac{d_A d_B}{\delta} \quad \dots \quad (4.3)$$

Thus the quantities

$$R_t = R_{l_2\mathrm{I}}, \quad R_s' = R_{l_2\mathrm{II}}, \quad R_t' = R_{l_1\mathrm{I}}, \quad R_s = R_{l_1\mathrm{II}}, \quad \dots \quad (4.4)$$

may be determined by the use of the appropriate formula given above.

We are now in a position after all these foregoing discussions to examine in detail the restrictions that should be imposed on φ in order that a circle P may intersect the lines J and K, the radius of the circle P being such that the condition (4.1) is satisfied. We have two distinct cases to consider.

Case I : It may happen that $R_t' > R_s'$ [fig. 5(*a*)].

(A) Let $2R_t < 2\rho < 2R_s'$. Let the abscissa of the point U_1 be 2ρ. Through U_1 draw the ordinate and let it cut $t_{\max}$ at V_1 and L_2 at W_1. Then

(A—1) :—if $t_{\max}=t_B$, there will be only one t_a curve through W_1 and the azimuth of the circle P passing through this point α on the line J and having $t=l_2$ is

$$\Phi_{l_2}=\cos^{-1}(l_2/2\rho). \qquad \ldots \quad (4.5)$$

The circles P will cut both J and K if

$$\Phi_{l_2} > \phi > \Phi_B. \qquad \ldots \quad (4.6)$$

(A—2) :—If $t_{\max}=2\rho$ then there will be two t_a curves through W_1 and the azimuths of the circles P passing through these points α on the line J are $\pm\Phi_{l_2}$. The circles P will cut both J and K if

$$\Phi_{l_2} > \phi > -\Phi_{l_2}, \qquad \ldots \quad (4.7)$$

provided both the t_A and t_B curves are below the line L_2. If however, one of these curves say t_A fall above this line, then $\Phi_A < \Phi_{l_2}$ and consequently ϕ should lie between

$$\Phi_A > \phi > \Phi_{l_2}. \qquad \ldots \quad (4.8)$$

Similarly if t_B falls above L_2, ϕ should lie between

$$\Phi_{l_2} > \phi > \Phi_B. \qquad \ldots \quad (4.9)$$

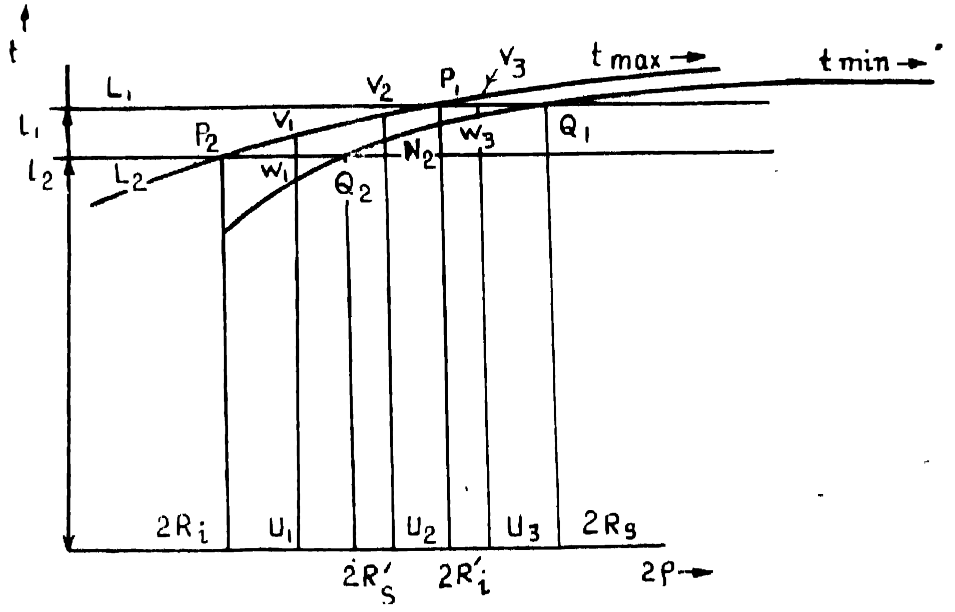

FIG. 5 (a)

(A—3) :—If $t_{\max}=t_A$, then again there will be one t_a curve through W_1 and the corsesponding azimuth is $-\Phi_{l_2}$. The circles P cut both the lines J and K if

$$\Phi_A > \phi > -\Phi_{l_2}. \qquad (4.10)$$

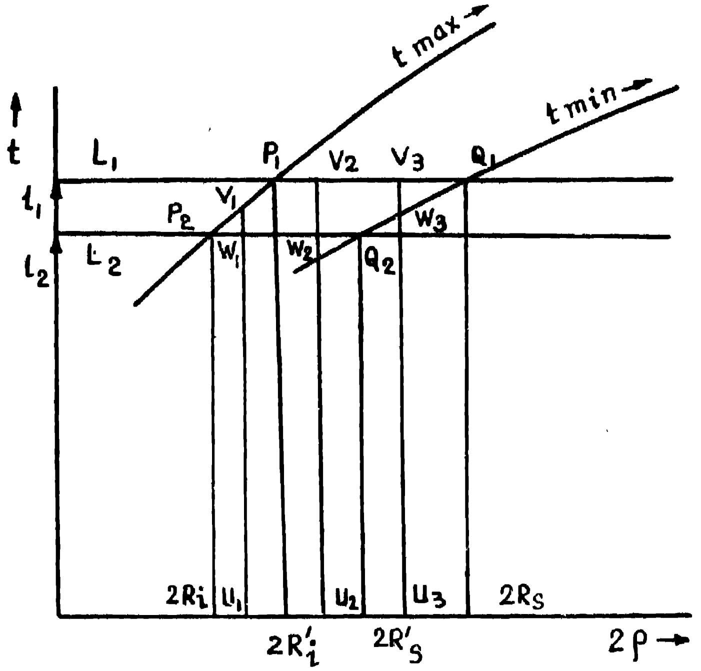

FIG. 5(*b*)

(B) Let $2R_s' < 2p < 2R_i'$. Let the abscissa of the point U_2 [fig. 5(*a*)] be $2p$. Through U_2 draw the ordinate to cut t_{max} at V_2 and t_{min} at W_2. Then it can be easily seen by an examination of figs. 5*a*, 5*b* that no matter what t_{max} or t_{min} curves are, the circles P will cut both J and K if

$$\Phi_A > \phi > \Phi_B. \tag{4.11}$$

(C) Let $2R_i' < 2p < 2R_s$. Let the abscissa of the point U_3 [fig. 5(*a*)] be $2p$. Through U_3 let us draw the ordinate to cut the line L_1 at V_3 and the t_{min} curve at W_3. Then if t_{max} curve is either the curve t_A or the curve t_B we find that there is only one t_a curve through V_3 and the azimuth of the circle P passing through this point (α) on the line J and having $t=l_1$ is $\pm\Phi l_1$ according as $t_{max}=t_B$ or t_A, the angle Φl_1 being defined by

$$\Phi l_1 = \cos^{-1}(l_1/2p). \tag{4.12}$$

On the other hand if $t_{max}=2p$, then there are two t_a curves through W_3 and the azimuths of the two circles P passing through these two points on the line J but meeting at the same point $t=l_1$ on the line K are $\pm\Phi l_1$. Thus the circles P will cut both J and K in the case

(C–1) $t_{max}=t_B$ and $t_{min}=t_A$, if $\Phi l_1 > \phi > \Phi_B$, ... (4.13)

(C–2) $t_{max}=2p$ and $t_{min}=t_A$, if ϕ lies on either of the intervals

$$\Phi_A > \phi > \Phi l_1 \quad \text{or} \quad -\Phi l_1 > \phi > \Phi_B, \qquad \ldots \tag{4.14}$$

provided t_B lies below L_1. If however t_B lies above L_1, then the proper limits are

$$\Phi_A > \phi > \Phi_{l_1} \qquad \ldots \quad (4.15)$$

(C − 3) $t_{max} = 2p$ and $t_{min} = t_B$, if ϕ lies on either of intervals

$$\Phi_A > \phi > \Phi_{l_1}, \quad \text{or} \quad -\Phi_{l_1} > \phi > \Phi_B, \qquad \ldots \quad (4.16)$$

provided t_A lies below L_1. If however t_A lies above L_1, then the proper limits are

$$-\Phi_{l_1} > \phi > \Phi_B \qquad \ldots \quad (4.17)$$

(C − 4) $t_{max} = t_A$ and $t_{min} = t_B$, if $-\Phi_{l_1} > \phi > \Phi_B$. ... (4.18)

Case II : Again it may happen that $R_t' < R_s$ [fig. 5(*b*)].

(A) If $2R_t < 2p < 2R_s'$ then the discussion is the same as that of (I.A).

(B) Let $2R_t' < 2p < 2R_s'$ Let the abscissa of the point U_2 be $2p$. Draw the ordinate through U_2 to cut the lines L_1 and L_2 at V_2 and W_2 respectively. Then as in case I, if t_{max} is either t_B or t_A then only one t_a curve passes through V_2 and another through W_2 and the azimuths of the circles P passing through the corresponding points on the line J and meeting the line K at $t = l_1$ and $t = l_2$ are

$$\Phi_{l_1}, \Phi_{l_2} \text{ respectively if } t_{max} = t_B,$$

or

$$-\Phi_{l_1} - \Phi_{l_2} \text{ respectively if } t_{max} = t_A.$$

On the other hand if $t_{max} = 2p$, then two t_a curves pass through V_2 and another pair through W_2. Thus azimuths of the two circles belonging to the family P which meet the line K at $t = l_1$ are $\pm\Phi_{l_1}$ and those of the two circles P meeting the line K at $t = l_2$ are $\pm\Phi_{l_2}$. Thus circle P will cut both J and K in the case when

(B − 1) $t_{max} = t_B$, if ϕ lies on $\Phi_{l_2} > \phi > \Phi_{l_1}$. ... (4.19)

(B − 2) $t_{max} = 2p$, $t_{min} = t_A$, if ϕ lies on either

$$\Phi_{l_2} > \phi > \Phi_{l_1} \quad \text{or} \quad -\Phi_{l_1} > \phi > -\Phi_{l_2} \qquad (4.20)$$

provided t_B lies below L_2. If t_B lies above L_1 then the interval on which ϕ should lie is

$$\Phi_{l_2} > \phi > \Phi_{l_1}. \qquad \ldots \quad (4.21)$$

Again if t_B lies between L_1 and L_2, then the intervals are

$$\Phi_{l_2} > \phi > \Phi_{l_1} \quad \text{or} \quad -\Phi_{l_1} > \phi > \Phi_B. \qquad \ldots \quad (4.22)$$

(B − 3) $t_{max} = 2p$, $t_{min} = t_B$, if ϕ lies on either

$$\Phi_{l_2} > \phi > \Phi_{l_1} \quad \text{or} \quad -\Phi_{l_1} > \phi > -\Phi_{l_2} \qquad \ldots \quad (4.23)$$

provided t_A lies below L_2. If t_A lies above L_2 then the proper interval is

$$-\Phi_{l_1} > \phi > -\Phi_{l_2}. \qquad \ldots \quad (4.24)$$

Again if t_A lies between L_1 and L_2, then the intervals are

$$\Phi_A > \phi > \Phi l_1 \quad \text{or} \quad -\Phi l_1 > \phi > -\Phi l_2. \tag{4.25}$$

(B−4) $t_{\max} = t_A$, if ϕ lies on $-\Phi l_1 > \phi > \Phi l_2$. (4.26)

(C) If $2R_s' < 2\rho < 2R_t$, then the discussion is the same as that of (I-C).

This discussion, given in this section, is too abstract and tedious, and one may lose the general trend of the method in the maze of mathematical formulae appearing above. So we propose, before proceeding any further, to take up the concrete case of the Lawson-Tyler β-ray spectrometer, and illustrate the use of our method. For this instrument we have

$$2\delta_0 = 24 \text{ cm}, \qquad \sigma_1 = 2C_1 = 1.6 \text{ cm}, \qquad \sigma_2 = 2C_2 = .3 \text{ cm},$$

$$d_A = 13.89 \text{ cm}, \qquad d_B = 10.11 \text{ cm}.$$

Let us take $\eta = +.15$ cm. Then the values of the corresponding quantities δ, l_2, l_1, etc. appear in the following Table.

TABLE I

η	δ	$l_2 = 2R_t$	$l_1 = 2R_t'$	α_B	α_A	s_B	s_A	$s_B \sec \alpha_B$	$s_A \sec \alpha_A$	l_{AB}	$2R_s'$	$2R_s$	$2R_{Al_2}$	$2R_{Al_1}$
.15 cm	12.15 cm	24 cm	24.3 cm.	.6940 rad.	.8525 rad	15.81 cm	18.48 cm	20.68 cm	28.05 cm.	23.71 cm	24.35 cm.	24.71 cm	24.27 cm	24.53 cm.

Since $s_B \sec \alpha_B < l_2 < l_1 < s_A \sec \alpha_A$, it is clear that for the region we are interested in, $t_{\max} = 2\rho$. Consequently $2R_t$, $2R_t'$ are given by formula (4.2a) [case (c)], being therefore respectively l_2 and l_1. Again since $l_{AB} < l_2 < l_1$, $2R_s'$, $2R_s$ are respectively given by formula (4.2b) [case (d)]. Evidently, $2R_t' < 2R_s'$ and therefore we have to discuss a figure like fig. 5(b). Let t_A curve cut the lines L_1, L_2 respectively at the points $2\rho = 2R_{Al_1}$ and $2R_{Al_2}$ respectively. These are determined by

$$(2R_{Al_1})^2 = (l_1 - \delta/\sin\alpha_A)^2 + s_A^2, \quad (2R_{Al_2})^2 = (l_2 - \delta/\sin\alpha_A)^2 + s_A^2.$$

The actual numerical values of these quantities are given in Table I. We shall have later occasion to calculate $T_1(\rho, \eta)$, the total length of domain over which the azimuth ϕ should lie in order that the circles P may cut both the lines J and K. In what follows we shall obtain expressions for $T_1(\rho, .15)$. Thus for

(*a*) $2R_t < 2\rho < 2R_{Al_2}$, the azimuth should lie between $\Phi l_2 < \phi < -\Phi l_2$ [*cf.* II.A above, *i.e.*, formula (4.7)]. Thus $T_1(\rho, .15) = 2\Phi l_2$.

(*b*) $2R_{Al_2} < 2\rho < 2R_t'$, the range on which the azimuth should lie is $\Phi_A > \phi > -\Phi l_2$ [*cf.* formula (4.8)]. Thus $T_1(\rho, .15) = \Phi_A + \Phi l_2$.

(*c*) $2R_t' < 2\rho < 2R_s'$, the intervals are $\Phi_A > \phi > \Phi l_1$ and $-\Phi l_1 > \phi > -\Phi l_2$ [*cf.* formula (4.26)]. Thus $T_1(\rho, .15) = \Phi_A + \Phi l_2 - 2\Phi l_1$.

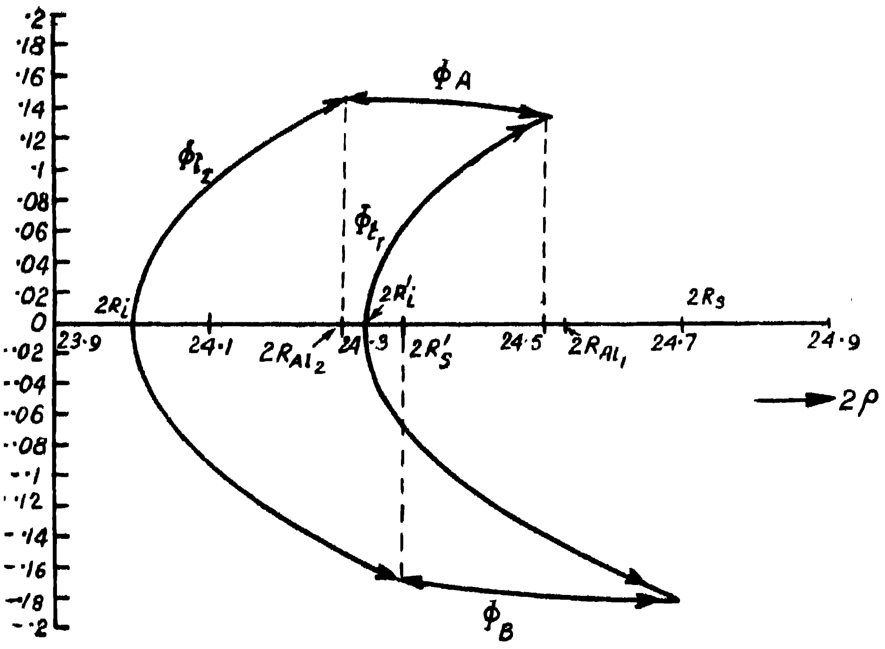

FIG. 6(a)

(d) $2R_s' < 2\rho < 2R_{Al_1}$, the intervals are $\Phi_A > \varphi > \Phi_{l_1}$, $-\Phi_{l_1} > \varphi > \Phi_B$ [*cf.* formula (4.17)]. Thus $T_1(\rho, .15) = \Phi_A - \Phi_B + 2\Phi_{l_1}$.

(e) $2R_{Al_1} < 2\rho < 2R_s$, the range is $-\Phi_{l_1} > \varphi > \Phi_B$ [*cf.* formula (4.18)]. Thus $T_1(\rho, .15) = -\Phi_{l_1} - \Phi_B$.

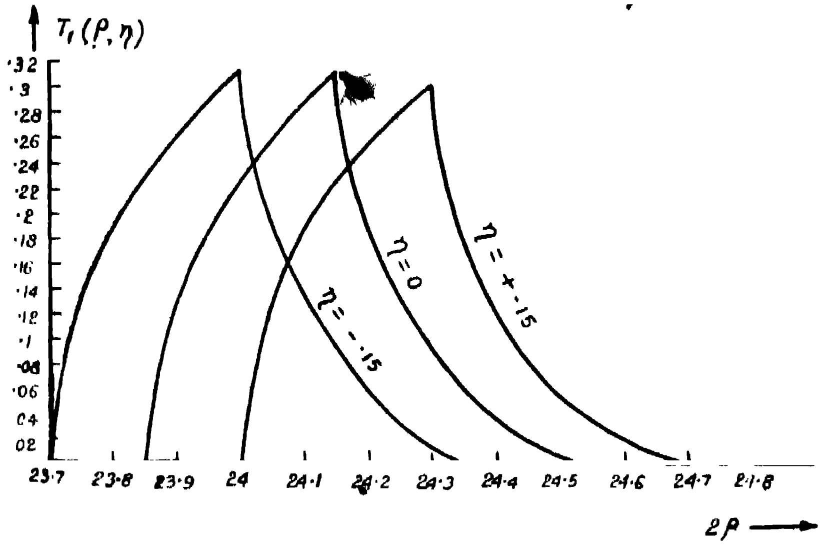

FIG. 6(b)

This discussion should be followed with the help of fig. 6(*a*). The function $T_1(\rho, .15)$ has been plotted against 2ρ in fig. 6(*b*). We may carry out the whole procedure given above, for $\eta = 0$ cm, and $-.15$ cm with necessary modifications. The corresponding curves $T_1(\rho, \eta)$ are shown in fig. 6(*b*). It is clear that forms of these curves do not depend much on η. In fact, the $T_1(\rho, \eta)$ curves for different values of η may be obtained by shifting $T_1(\rho, 0)$ curve by an amount η. Thus we may take in future

$$T_1(D, \eta) = T_1(D - \eta, \eta = 0). \qquad \ldots \quad (4.27)$$

This completes the discussion of the restrictions necessary on the azimuth of an electron in order that it may pass through the counter slit. These restrictions are introduced by the finite extensions perpendicular to the magnetic axis of the slits S_1 and S_2. The extensions of these slits parallel to the z-axis, *i.e.*, to the magnatic field introduces certain restrictions on θ and D so that conditions (2.10) are satisfied. These restrictions will be calculated in what follows.

§5. RESTRICTIONS THAT MUST BE IMPOSED ON θ

We note that the z-displacement of the point where an electron cuts the counter slit S_2 is never less than the z-displacement of the point where this electron cuts the source slit. So it is enough to calculate what restrictions are necessary on the parameters θ and D in order that an electron may pass through the counter slit. We shall confine our attention first to the positive portion of S_2 where $0 < \theta < \pi/2$.

As pointed out already in §2, the z-displacement of an electron when it reaches the slit S_2 is Z, where Z is given by (2.8). Clearly Z will exist only if 2ρ, *i.e.*, $D \sin\theta < s$. Thus if $D > s$ and θ_1 is defined by

$$\sin\theta_1 = s/D, \qquad \ldots \quad (5.1)$$

then Z exists if $\theta < \theta_1$. Evidently

$$Z[\theta_1(\alpha)] = (\alpha + \frac{\pi}{2})\sqrt{D^2 - s^2}\ . \qquad \ldots \quad (5.2)$$

Now $\theta_1(\alpha_A) > \theta_1(\alpha) > \theta_1(\alpha_B)$ for $\alpha_A > \alpha > \alpha_B$. For $\theta > \theta_1(\alpha_A)$ it is clear that $Z(\theta, \alpha_A) > Z(\theta, \alpha) > Z(\theta, \alpha_B)$. The discussion of the $Z(\theta, \alpha)$ curves for $\theta < \theta_1(\alpha_A)$ is difficult but is fortunately unnecessary as we shall see presently we shall have almost always to discuss θ's which are $> \theta_1(\alpha_A)$.

It is clear that a $Z(\theta)$ curve for any particular α and D starts from a maximum at $\theta = \theta_1(\alpha)$, then falls uniformly as we increase θ and reaches the zero value at $\theta = \pi/2$. [*cf.* fig. 7(*a*)].

We have seen already that in order that conditions (2.10) may be satisfied we must have condition (4.1) satisfied. If the angles θ_i, θ_i', θ_s', θ_s be defined by

$$\sin\theta_i = \frac{2R_i}{D}, \quad \sin\theta_i' = \frac{2R_i'}{D}, \quad \sin\theta_s' = \frac{2R_s'}{D}, \quad \sin\theta_s = \frac{2R_s}{D}, \ldots \quad (5.3)$$

then

$$
\begin{aligned}
&(a)\ \text{if } D > 2R_i, &&\text{we have } 2\rho \gtrless 2R_i &&\text{according as } \theta \gtrless \theta_i\,,\\
&(b)\ \text{if } D > 2R_i', &&\text{we have } 2\rho \gtrless 2R_i' &&\text{according as } \theta \gtrless \theta_i',\\
&(c)\ \text{if } D > 2R_s' &&\text{we have } 2\rho \gtrless 2R_s' &&\text{according as } \theta \gtrless \theta_s',\\
&(d)\ \text{if } D > 2R_s &&\text{we have } 2\rho \lessgtr 2R_s &&\text{according as } \theta \gtrless \theta_s\,.
\end{aligned}
\tag{5.4}
$$

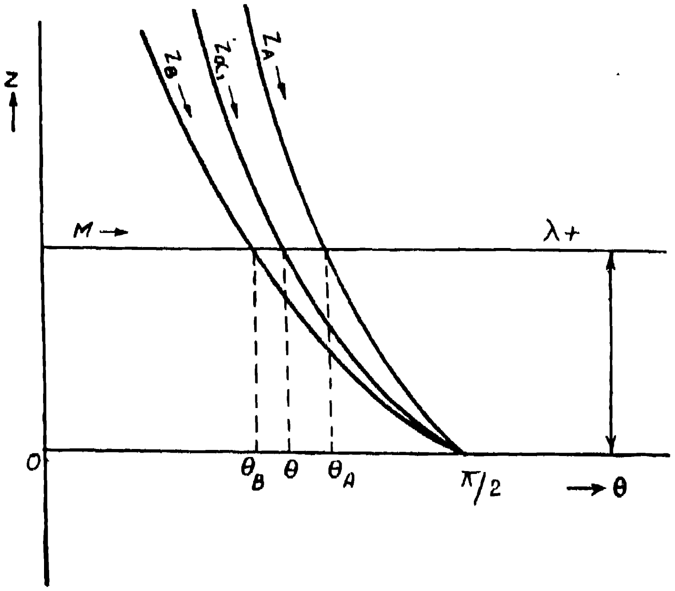

FIG. 7(a)

In fig. 7(b) we have plotted the angles $\theta_1(\alpha)$, θ_i, θ_s, as functions of D. $\theta_1(\alpha_B)$, $\theta_1(\alpha_A)$ v.s. D curves start respectively at $[D=s_B,\ \theta_1(\alpha_B)=\pi/2]$, $[D=s_A,$

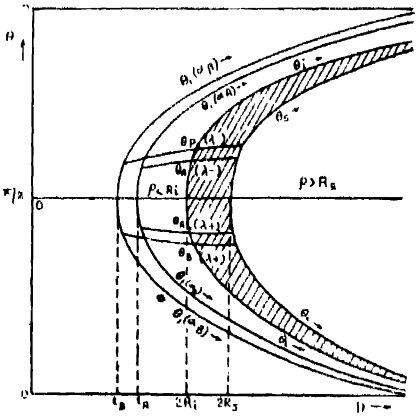

FIG. 7(b)

$\theta_1(\alpha_A) = \pi/2$] and falls uniformly as D is increased. The θ_i, θ_i', θ_s', θ_s curves also start from the maximum value $\pi/2$ at $D = 2R_i$, $2R_i$, $2R_s'$, $2R_s$ respectively and fall uniformly as D is increased. Again since in almost all cases $2R_i > s_A$ we must have $\theta_s > \theta_i > \theta_1(\alpha_A) > \theta_1(\alpha_B)$ for $D > 2R_i$. From the figure it is clear that the condition (4.1) is satisfied only when the point (D, θ) lies on the shaded area bounded by $\theta = \pi/2$ line, $\theta = \theta_i$ and $\theta = \theta_s$ curves.

We shall now calculate for what θ will the curves $Z(\theta)$ for any particular D and α, cut the line M which is parallel to and at a distance λ_+ from the θ-axis [fig. 7(*b*)]. Let us suppose that the two $Z(\theta)$ curves correspondig to $\alpha = \alpha_A$ and $\alpha = \alpha_B$ cut the line M respectively at $\theta = \theta_A$ and $\theta = \theta_B$. To determine these angles we must solve the transcendental equations

$$\left.\begin{aligned} D \sin\theta \;\left[\sin \frac{\lambda_+ \sec\theta_A}{D} - \alpha_A\right] &= s_A \\ D \sin\theta_B \;\left[\sin \frac{\lambda_- \sec\theta_B}{D} - \alpha_B\right] &= s_B \end{aligned}\right\} \quad \cdots \quad (5.5)$$

These equations cannot be solved exactly but numerical solutions by the application of the method of *Regula Falsi* (mentioned in paper I), may be obtained. Let us plot the angles θ_A and θ_B against D as shown in fig. 7(*b*). It is clear that since $\theta_B < \theta_A$ the $\theta_B(D)$ curve lies below the $\theta_A(D)$ curve. If the point (D, θ) lies below ths $\theta_B(D)$ curve then evidently $Z(D, \theta, \alpha)$ for all slit angles $\alpha_A > \alpha > \alpha_B$ will be $> \lambda_+$. Thus in order that condition (2.10b) be satisfied, it is essential that the electron must have its point (D, θ) in fig. 7(*b*) between $\theta = \pi/2$ line and the $\theta_B(D)$ curve. Conditions (2.10b) and (4.1) will be simultaneously satisfied if and only if an electron has its point (D, θ) within the area [marked off by thick lined boundaries in fig 7(*b*)] surrounded by $\theta = \pi/2$ line and the θ_i, θ_B and θ_s curves. The $\theta_B(D)$ curve cuts the θ_s curve at $D = D_{sB}$ where D_{sB} is given by

$$D_{sB}^2 = \frac{\lambda_+^2}{[\alpha_B + \sin^{-1}(s_B/2R_s)]^2} + (2R_s)^2. \quad (5.6)$$

It is immediately clear that if $D < 2R_i$ or $D > D_{sB}$ then no electron can pass through the positive portion of S_2.

Let us examine the curves in fig. 7(*b*) again in detail. For $\pi/2 > \theta > \theta_A$ we have $Z(\theta, \alpha)$ for all slit angles $\alpha_A > \alpha > \alpha_B$ will be $< \lambda_+$ and so if the azimuth of an electron (D, θ) lie within proper limits discussed in §3 and §4, all these electrons will be admitted by S_2. But difficulties arise for $\theta_A > \theta > \theta_B$. Let α_1 be the slit angle, corresponding to which $Z(\theta, D, \alpha_1)$ for any particular θ in $\theta_A > \theta > \theta_B$ is λ_+. Then $Z(\theta, D, \alpha) \gtrless \lambda_+$ according as $\alpha_A > \alpha > \alpha_1$ or $\alpha_1 > \alpha > \alpha_B$. Thus in order that condition (2,10b) be satisfied we must have $\alpha_1 > \alpha > \alpha_B$. α_1 is given by

$$2\alpha_1 = \frac{\lambda_+}{D\cos\theta} - \sin^{-1}\left[\frac{2\delta}{D\sin\theta} - \sin\left(\frac{\lambda_+}{D\cos\theta}\right)\right] \quad (5.7a)$$

Thus Φ_{α_1} = the azimuth of the electron (D, θ) for which the circle P passes through the point $M(\alpha=\alpha_1)$ in the line J, is given by

$$\Phi_{\alpha_1}=\frac{\lambda_+}{D\cos\theta} \qquad \ldots \quad (5.7b)$$

Thus if an electron (D, θ) has to pass through the counter slit, its azimuth ϕ should not lie in $\Phi_A > \phi > \Phi_{\alpha_1}$, but must lie in $\Phi_{\alpha_1} > \phi > \Phi_E$. This must be borne in mind in applying the results of §3 and §4 to electrons (D, θ) for θ in $\theta_A > \theta > \theta_B$.

The discussion for the negative position of the slit S_1, where $\pi/2 < \theta < \pi$, follows closely what has given above. The corresponding conclusions may be immediately drawn by an examination of the upper half of the fig. 7(*b*).

§6. TRANSMISSION FACTOR OF THE SPECTROMETER

We may now proceed to calculate the number of electrons entering the counter space in a magnetic field H. Let $n(p)$ be the distribution function in p, *i.e.*, $n(p)\,dp$ is the number of electrons emitted per second from one unit area of the sample plate per unit solid angle, having their momenta in the range p, $p+dp$. Then the number of electrons entering the counter space is evidently

$$N(H)=\int n(p)\,dp\int d\eta\int d\xi\int \sin\theta d\theta\int d\phi. \qquad (6.1)$$

Let

$$\left.\begin{aligned} &T_1(p, \eta)=\int d\phi, \quad T_2(D, \xi, \eta)=\int T_1 \sin\theta d\theta, \\ &T_3(D, \eta)=\int T_2 d\xi,\ T(\mathrm{D})=\int T_3 d\eta \end{aligned}\right\} \qquad (6.2)$$

The limits of the integrals T_1, T_2 have already been discussed in §3, §4 and §5. We shall now numerically compute these integrals for the concrete case of the Lawson-Tyler β-ray spectrometer. The functions $T_1(p, \eta)$ have already been calculated in §4 for three different values of η, *viz.*, $\eta=-.15$, o, +.15 cm. [*cf.* fig. 6(*b*)].

To calculate $T_2(D, \xi, \eta)$ we proceed as follows. Taking $\eta=0$ cm., we first plot the θ_A, θ_B v.s. D curves for three different values of ξ, *viz.*, o cm., .4 cm., and .8 cm. Since θ is very nearly $\pi/2$ we may use the following approximation instead of using the method of *Regula Falsi*. Taking

$$\epsilon=\pi/2-\theta, \qquad \ldots \quad (6.3)$$

where ϵ is understood to be small, we get

$$\epsilon_A=\frac{\lambda}{D[\alpha_A+\sin^{-1}(s_A/D)]},\ \epsilon_B=\frac{\lambda}{D[\alpha_B+\sin^{-1}(s_B/D)]}. \qquad \ldots \quad (6.4)$$

In fig. 7 (*c*). ϵ_A, ϵ_B have been plotted for the following values

$\lambda_+=.8$ cm., .4 cm., o cm., $\lambda_-=.8$ cm., 1.2 cm., 1.6 cm.

It is quite evident that $\epsilon_B(D)$ are more or less constants. Values of ϵ for which the electron (D, ϵ) enters the counter is so small that $\sin\theta = \cos\epsilon \simeq 1$ and so ρ does not change appreciably as we change ϵ between the limits of the integral T_2. This means that the quantity T_1 in the integral T_2 may be taken constant and so taken out of the integration sign. Thus

$$T_2 = T_1[\epsilon_B(\lambda_+) + \epsilon_B(\lambda_-)]. \qquad \ldots \quad (6.5a)$$

It is also evident from the [fig. 7(c)] that

$$\epsilon_B(\lambda_+) + \epsilon_B(\lambda_-) = .047 \text{ cm}. \qquad \ldots \quad (6.5b)$$

for all the three different values of ξ fixed upon. We have neglected the correction on the azimuth limits due to length of the counter slit parallel to the magnetic field, which, as mentioned at the end of §5, should be applied to those electrons D whose ϵ lie between ϵ_A and ϵ_B. This correction is, in fact, quite small. If we take the two other values of η, we find that the quantity (6.5a) above does not change perceptibly. Thus

$$T_3(D, \eta) = 1.6 \times .047 \times T_1(D, \eta). \qquad \ldots \quad (6.6)$$

It has already been shown in §4 that the function $T_1(D, \eta)$ for different values of η may be obtained by shifting $T_1(D, \eta=0)$ curve by an amount η. Thus we may employ the approximation (4.28) without introducing much error. As mentioned in §5, the proper superior limit to D for any particular point (ξ, η) on the sample plate is D_{sB}. But since the θ_s curve falls extremely steeply for θ near $\pi/2$ [c.f. fig. 7(c)], D_{sB} is practically equal to $2R_s$. Thus it is clear that D must lie in $2R_i\ (\eta=-.15) < D < 2R_s\ (\eta=+.15)$ if the electron D has to enter the counter space. If $2R_i\ (\eta=-.15) = 2R_1$, and $2R_s\ (\eta=+.15) = 2R_2$, we have

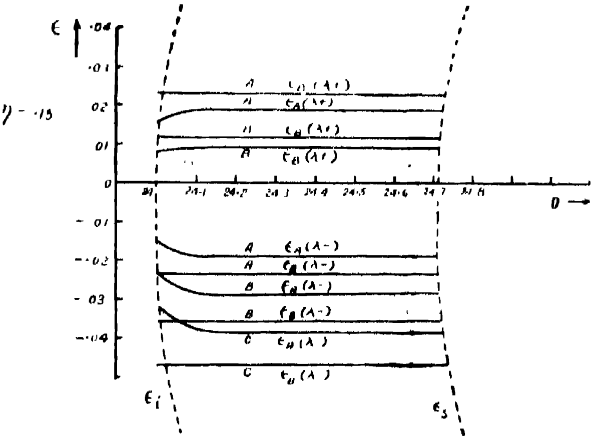

The curves A, B, C correspond respectively to $\xi = 0, .4, .8$ cm.

FIG. 7(c)

$$2R_1 = D_1 = 23.7 \text{ cm.}, \qquad 2R_2 = D_2 = 24.71 \text{ cm.} \qquad \ldots \quad (6.9)$$

For $2R_1 < D < 2R_i\ (\eta = +.15)$ we have to calculate the area under the $T_1(D,$

$\eta=0$) curve between $2R_1(\eta=0)$ and $D+.15$ cm. in order to find $T(D)$, whereas for $2R_1(\eta=-.15) < D < 2R_2$ we have to find the area under the $T_1(D, \eta=0)$ curve

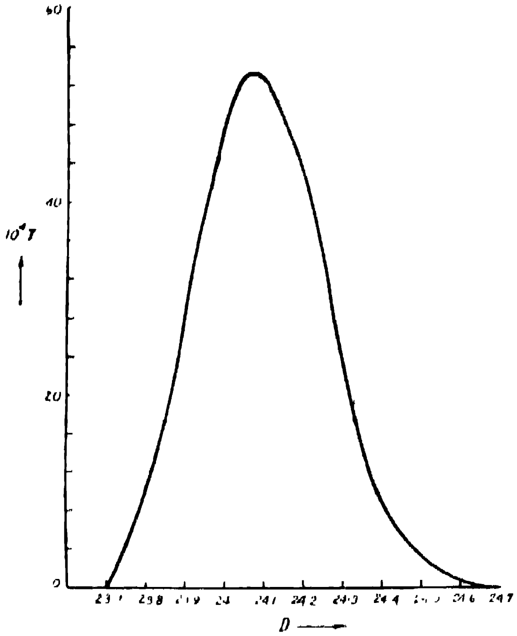

FIG. 8

between $D-.15$ cm and $2R_1(\eta=0)$. For D in $2R_1(\eta=+.15) < D < 2R_2$ $(\eta=-.15)$ we have however to calculate the area under the $T_1(D, \eta=0)$ curve between $D-.15$ cm and $D+.15$ cm. In this way, the $T(R)$ curve has been constructed [*cf.* fig. 8]. This function may be called the transmission factor function of the spectrometer. Our curve may be compared with the one deduced by Lawson and Tyler. We have finally

$$N(H)=\int_{p_1(H)}^{p_2(H)} n(p)T(p/H)dp. \tag{6.10}$$

where $$p_1(H)=D_1H/2, \quad p_2(H)=D_2H/2. \tag{6.11}$$

Equation (6.10) is an integral equation which must be solved in order that the momentum spectrum may be deduced from the experimental $N(H)$ curve.

§7. SOLUTION OF THE INTEGRAL EQUATION (6.10) OF THE SPECTROMETER

To complete the task of this paper we have now to show how the integral equation (6.10) may be solved. Lawson and Tyler have given an extremely elegent way of doing this Their method involves practically no labour. The best that we can do, therefore, is to transcribe their method in our notation. This is done in what follows. Since the range (p_1, p_2) is quite small we may develope $n(p)$ about some point in this range by Taylor's theorem. We have thus

$$n(p)=n(P)+\lambda(p-P)+\mu(p-P)^2+\text{ etc.} \qquad \dots \quad (7.1)$$

Substituting this in equation (6.10) we get

$$n(P)=\frac{N(H)}{HK}-\frac{\lambda H}{2K}\int(D-D_3)T(D)dD-\frac{\mu H^2}{4K}\int(D-D_3)^2T(D)dD-\text{etc.}$$

where
$$K=\tfrac{1}{2}\int_{D_1}^{D_2}T(D)dD, \qquad \dots \quad (7.2a)$$

and
$$D_3=\frac{2P}{H}\,. \qquad \dots \quad (7.2b)$$

Now let D_3 be chosen in such a way that

$$\int_{D_1}^{D_2}(D-D_3)T(D)dD=0. \qquad \dots \quad (7.3)$$

This equation may be solved graphically and the solution D_3 is evidently a constant of the spectrometer, like the quantities D_1 and D_2. For the transmission factor function, which we have calculated, we obtain $D_3=24.1036$ cm., whereas Lawson and Tyler obtain $D_3=24.1264$ cm. We have finally

$$n(P)=\frac{N(H)}{HK}-\frac{\mu}{K}\left(\frac{H}{2}\right)^2\int_{D_1}^{D_2}(D-D_3)^2T(D)dD-\text{etc.} \qquad \dots \quad (7.4)$$

If μ is small, as is in general the case, the correction term in above may be neglected, and

$$n(P)=\frac{N(H)}{HK}. \qquad \dots \quad (7.5)$$

This method fails when the maximum momentum of the electrons fall within the limits p_1 and p_2. Let H_1 be defined by

$$p_2(H_1)=\frac{D_2H_1}{2}=p_{\max}. \qquad \dots \quad (7.6a)$$

Corresponding P is given by

$$P(H_1)=P_1=\frac{D_3H_1}{2}=\frac{D_3}{D_2}\,p_{\max}. \qquad \dots \quad (7.6b)$$

Thus for fields $H < H_1$, the Lawson Tyler method will be applicable on account of the fact that $p_{\max} > p_2(H)$. Consequently the momentum spectrum may be built up by the application of formula (7.5) up to $p \leq P_1$. On the other hand for $H > H_1$, since $p_2(H) > p_{\max}$ the formula (7.5) is not applicable. According to Lawson-Tyler's calculations

$$D_3/2=12.0632\text{ cm},\ D_2/2=12.3\text{ cm},$$

so that
$$\frac{D_2-D_3}{D_2}\simeq .018.$$

Thus the length of the tail of momentum spectrum ($P_1 < p < p_{\max}$) over which the Lawson-Tyler method is inapplicable is about 1.8% of $p_{\max}$. Over this tail the integral equation (6.10) takes the form

$$N(H) = \int_{p_1(H)}^{p_{\max}} n(p)T(p/H)dp. \qquad \dots \quad (7.7)$$

Let

$$D_{\max} = \frac{2\, p_{\max}}{H}. \qquad \dots \quad (7.8)$$

Then the Lawson-Tyler's formula (7.4) may be made applicable over this tail also, if we give to the symbols P, D_3, K new meanings. Thus D_3 is to be determined as the solution of the equation

$$\int_{D_1}^{D_{\max}} (D - D_3)T(D)dD = 0. \qquad \dots \quad (7.9)$$

This equation may be solved graphically for different values of $D_{\max}$ and D_3 v.s. $D_{\max}$ curve may be plotted. P will be connected to D_3 by the old formula (7·2b). K will now have the meaning

$$K = \int_{D_1}^{D_{\max}} T(D)dD. \qquad \dots \quad (7.10)$$

To conclude, we make some remarks about the maximum momentum $p_{\max}$ This is determined from the upper limit of the $N(H)$ curve by

$$p_{\max} = \frac{D_1 H_{\max}}{2}. \qquad \dots \quad (7.11)$$

It is however very difficult to determine $H_{\max}$ for generally, unless the source strength is very great, the $N(H)$ curve approaches zero very gradually. Thus the observed end point $H'_{\max}$ is in general different from the true end point $H_{\max}$. In fact $H'_{\max}$ corresponds to that momentum p_1 for which the integral

$$\int_{p_1(H'_{\max})}^{p_{\max}} n(p)T(D)dp.$$

is indistinguishable from zero. Thus in order to determine $p_{\max}$ more accurately it is necessary to increase $n(p)$ by increasing the source strength, or to increase the transmission factor, If we gradually increase the source strength the observed end point $H'_{\max}$ will gradually increase until after some definite critical source strength, $H'_{\max}$ will remain stationary at some value, which we may take as the true end point. The end point may however be determined much more accurately and conveniently with a screen cathode β-ray spectrometer (Paper I) on account of the fact that the transmission factor of this spectrometer is of a much higher order of magnitude.

We have now to show how the positions and the intensities of the homogeneous groups of the conversion electrons may be determined. To do this we must remember that the transmission factor function $T(D)$ may also be interpreted as proportional to the $N(H)$ curve of a group of electrons of a single momentum. Thus if the momentum of any homogeneous group of electrons be p and the intensity of this group be I, *i.e.* if I such electrons be emitted per second per unit solid angle, per square cm. of the sample plate, then the $N(H)$ curve of these electrons will be given by

$$N(H) = IT(p/H).$$

Let H_1, H_2, H_3 be defined by

$$H_1 = \frac{2p}{D_1}, \quad H_2 = \frac{2p}{D_2}, \quad H_3 = \frac{2p}{D_4}$$

where D_1, D_2 have the same meaning as before and D_4 is the abscissa corresponding to which $T(D)$ has the maximum value. Then the $N(H)$ curve starts from zero at $H = H_1$ rises to a maximum at $H = H_3$ and then falls to zero at $H = H_2$. Thus if we can find accurately H_3 and $N(H_3)$, then it is possible to determine p and I. Evidently it is necessary to distinguish with great precision the $N(H)$ curve due to the β-rays with continuous spectrum from that due to the conversion electrons, and this can quite easily be done in practice.

An $M-F$ β-ray spectrometer with variable field is under construction in this laboratory. It is being planned by Mr. S. Das, M.Sc., in collaboration with the writer to study the β-radiations emitted from Co^{60} supplied to us by the courtesey of the M.I.T. cyclotron laboratory. The writer wishes to express his thanks to Prof. M. N. Saha, D.Sc., F.R.S. for his kind interest in the progress of this work. He thanks also Mr. S. Das, M.Sc. for his kind assistance in carrying out the numerical calculations of this paper.

PALIT LABORATORY OF PHYSICS,
UNIVERSITY OF CALCUTTA.

REFERENCES

Lawson, J. L. and Tyler, A. W. (1940), *Rev. Sci. Inst.*, **11**, 6.
Saha, A. K. (1944), *Proc. Nat. Inst. Sci, India*, **10**, 355.

13

CAPTURE OF ELECTRONS BY POSITIVE IONS WHILE PASSING THROUGH GASES

By M. N. SAHA* and D. BASU

ABSTRACT. This work extends that of Brinkman and Kramers on the capture of electrons by positive ions while passing through gases. Detailed mathematical working is reported, and it is shown that contrary to the opinion of Brinkman and Kramers, the probability of capture of an electron by the α-particle in the $2p$-orbit from the H-atom becomes much larger than that for the capture in the $1s$-orbit when the velocity falls below $2\,(2\pi e^2)/h$. For small velocities, the ratio goes on increasing.

An α-particle passing through a gaseous medium as in a cloud chamber produces a track consisting of ions formed round electrons liberated from the surrounding gas. It was noticed by Henderson (1923) and Rutherford (1930) that towards the end of the track the phenomenon was more complex. They found that when the velocity had slowed down to a value comparable to $2c\alpha$ ($c\alpha$ = the velocity of the outer electron in the normal level of the H-atom in the molecules of the gas through which the α-ray passes) the α-particle might capture an electron and be converted to He$^+$, this might again lose its electron on collision with matter. The phenomenon of alternate loss and capture may occur a large number of times, but ultimately when the particles have sufficiently slowed down, most of them would permanently acquire an electron and be He.$^+$ As He$^+$ further passes through the gas, it may capture an electron and become neutral helium. As it has a velocity of the order of 10^7 to 10^8 cm. sec.$^{-1}$ it may again lose an electron by collision with matter. This process of alternate loss and capture may continue for some more distance till the velocity slows down sufficiently and ultimately we get neutral helium atoms.

This phenomenon occurs at the last cm. of the path of the α-particle so that the experimental technique for its observation is rather difficult. The work of Rutherford and Henderson was continued on by Jacobsen (1930) who calculated the capture and loss cross-section from his own experimental works in which the motion of α-particles in air and hydrogen was studied; and he tried to compare his results with the theoretical conclusions of the authors mentioned below.

The theoretical study of this phenomenon was started by Fowler (1924), Thomas (1927), Oppenheimer (1928) and Brinkman and Kramers (1930). Fowler and Thomas used entirely classical conceptions and they need not be further considered. The work of Oppenheimer (1928) has been criticised by Brinkman and Kramers (1930) as one not free from objection. The latter authors have carried out by two alternative methods the calculations for finding out the capture cross-section. They assume that the atom of the gas through which the α-particles pass are hydrogen-like and the electrons move in 1*s*-orbits, the capture also is assumed to take place in 1*s*-orbits. The results of their calculations are compared with the experimental data of Rutherford and Henderson and of Jacobsen, and on certain assumptions, they are found to be in good agreement. Brinkman and Kramers (1930) have not, however, calculated the general case when the electrons may be moving in any kind of orbit in the atoms composing the gaseous medium and can be captured in any orbit by the α-particles. The restrictions are evidently for the purpose of simplifying the calculations. The laboratory medium mostly consists of nitrogen, oxygen and hydrogen molecules; though it may be possible to represent the motion of their outermost electrons by proper ψ-functions, the calculations with such ψ-functions may be extremely difficult, if not altogether impracticable to carry out. But if we stick to the approximation of Brinkman and Kramers as far as the traversed gaseous molecules are concerned, it is surely feasible to calculate the capture of electrons in orbits higher than 1*s* by α-particles. Brinkman and Kramers have not carried out this calculation because as they remarked correctly that such cross-sections are likely to be small compared with that of capture in 1*s* orbit. They have, however, given an expression for capture cross-section from 1*s*-orbit to *ns* and *vice versa*.

---

* Fellow of the Indian Physical Society.

The question of capture of electrons to higher *p*, *d* and *f* orbits by the α-particle, however, acquires a new importance in view of the recent suggestion (Saha, 1942) that helium lines occurring in the solar atmosphere may originate in this way : The problem of occurrence of helium lines in the sun has been for long a challenge to astro-physicists. It is well-known that none of the He-lines are found in the Fraunhofer absorption spectrum of the sun. This is as expected because at the temperature prevailing in the sun, He can exist only in normal state and as we know the absorption lines of normal helium are in the region λ584A to λ500A, we cannot expect to observe them. The visible lines of He are all due to the excited states and the lowest of these states has 1*s* 2*s* $^3S_1$ an excitation potential of nearly 20.55 volts, which is not possible to have in an atmosphere having a temperature of 6000-7000°K. But when we turn to the spectrum of the chromosphere, we find that the visible lines of neutral helium are extremely strong, even the well-known line of ionised helium λ4686A is found to occur in it. This is rather an unexpected phenomenon, because this line has on excitation potential of nearly 75.25 volts, while the ordinary excitation in the chromosphere is 0 to 14 volts. There are certain other anomalous features in the occurrence of these lines. Evershed first noticed that the intensity of the He-lines appears to vanish near the limb and they are prominent only at some distance. This phenomenon has been more systematically studied by Perepelkin and Melnikov (1935) and Pannekoek and Minnaert (1928); the results obtained by the first mentioned authors on the variation of intensity of well-known D_3-line of helium is given in fig (1). It is seen that the line tends to vanish at the limb and attains its maximum intensity at a height of 2500 km. and beyond that it tends to vanish, though it can be traced up to 7500 km. The ionised line λ4686 occurs in the lower chromosphere up to a height of 2000 km. only. These facts are rather in sharp contradiction to the ionisation theories as we move up in the solar atmosphere.

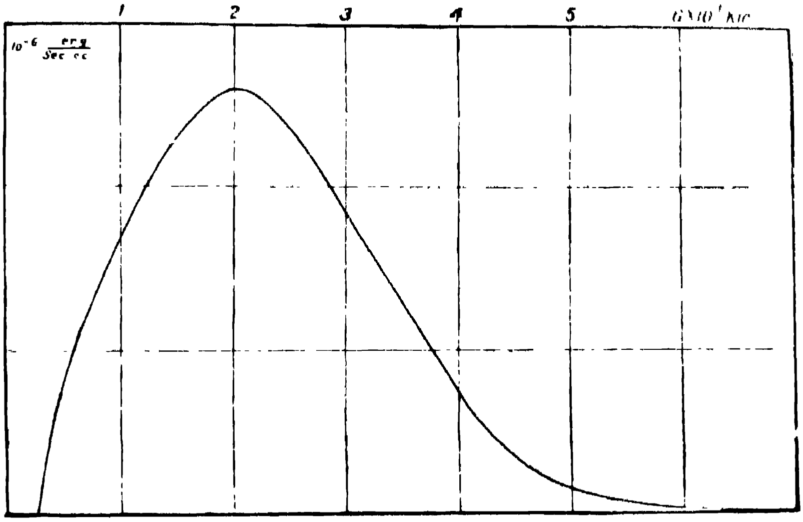

FIG. 1

Emission of 1cc. of Helium chromosphere in D_3-line in ergs per second and solid angle 4π

This phenomenon will probably receive a ready explanation if, as already suggested (Saha, 1942), it is assumed that the helium is not an ordinary constituent of the solar atmosphere; it is taken that due to some nuclear process, α-particles are being constantly generated throughout the solar body and some of them quite near the limb. We need not specify the particular nuclear reaction responsible for the generation of the α-particles as we can make our choice from a host of laboratory experiments. It is well-known that α-particles spontaneously emitted in radioactive disintegration have velocities of the order 6cα to 10cα (energy 4MV to 10MV).

It is clear that when such α-particles pass through the solar atmosphere, they will, during the first part of the motion, go on ionizing the solar gases (ionisation by collision), and losing energy; when they have sufficiently slowed down, they will begin to capture electrons in different orbits 1*s*, 2*p*, 3*d*, *ms*, *mp*, and *md*. When the electron is captured in any orbit higher than 1*s*, we have an excited He^+-atom which will emit a characteristic spectral line and revert back to a lower state. Most of these lines lie in the extreme ultra-violet, and the only one of He^+-line available for observation is λ 4686, $\nu = 4R\left[\frac{1}{3^2} - \frac{1}{4^2}\right]$. The capture takes place in any one of the 4*f*, 4*d* or 4*p*, 4*s* orbit and the line is emitted when the electron jumps back to any one of the 3*d*, *p*, *s* orbits. All other lines of He^+ are outside the limit of experimental observation. This discussion brings out the necessity of calculating the cross-sections for the capture of electrons in orbits higher than 1*s*. This has been attempted in the following sections. We have supposed that the solar gas through which the α-particles pass is entirely composed of hydrogen atoms. This very nearly represents the current idea according to which hydrogen forms more than 90% of the solar atmosphere.

When we turn to the next problem of occurrence of He-lines in the solar chromosphere the mathematical difficulties considerably increase. We cannot represent the field of He^{+} as even approximately coulombian and hence we must resort to very complicated calculations which have been used by Hylleras (1933, 1937) for finding out the He-terms and their transition probabilities. This has not yet been done, but if time permits it will form the subject of a discussion in another paper.

The procedure which we have followed in the calculation of capture of electron from 1*s*- to 2*p*-orbit is similar to the second method as adopted by Brinkman and Kramers in their parallel calculation of 1*s*- to 1*s*-capture. One must bear in mind that the method holds good only when (1) the gaseous molecules of the medium can be regarded as stationary during and after collision and when (2) the velocity of the α-particle is large compared to $c\alpha$.

Obviously these limitations put severe restrictions to the application of the results of the following calculation to solar phenomena. The first limitation means that the molecules or atoms must be very heavy compared to the α-particle; this is far from being the case with hydrogen atoms. The second one has been noted by all workers, but no alternative method has been put forward. It has been suggested that calculations of the Born approximation to second order may be carried out, but in view of past experience the suggestion does not appear very promising.

In spite of these limitations, we have proceeded with the calculations. In view of the fact that we have followed closely the method of Brinkman and Kramers, it is found useful to rewrite the essential steps of the above authors in the first part of this paper. That will be of help to appreciate the extension we have made of their method.

We suppose that the charged particle (α-particle here) having the mass M and the charge $Z'e$ moves past the atom K which has the mass M*q* and the effective charge Ze (without the electron). The type of collision that we propose to study here is the following one: Initially we have an electron moving in the field of the atom, but after collision the same electron is captured by the α-particle in any one of its orbits. The reaction may be schematically represented as follows:

$$\begin{array}{ccccccc}
\mathrm{K} & + & \mathrm{He}^{++} & = & \mathrm{K}' & + & \mathrm{He}^{+} \\
(\mathrm{M}q+m,\ Ze) & & (\mathrm{M},\ 2e) & & (\mathrm{M}q.\ Ze) & & (\mathrm{M}+m,\ 2e) \\
e & & \longrightarrow & & & & e
\end{array}$$

To simplify calculation it is further assumed that M*q* is so heavy that its nucleus remains at rest before and after collision.

Let K, α and *e* represent respectively the atom, the α-particle and the electron which in the beginning of the process belongs to K, and at the end is captured by the α-particle. We further choose the direction of motion of the α-particle as the axis of X, the perpendicular from the centre of the atom to the direction of

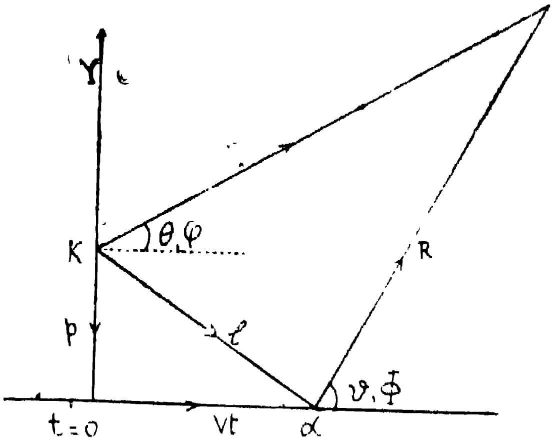

FIG. 2

motion as the Y-axis and Z is perpendicular to both. The quantities that will frequently occur are

p, collision parameter.
R, radius vector from α-particle to electron.
r, radius vector from the centre of the atom to electron.

Let us suppose that the α-particle is moving with velocity V, and in time $t=0$, it is at the origin of the co-ordinate system. Then we have at any instant of time

$$\mathbf{R} = \mathbf{r} - \mathbf{p} - \mathbf{V}\mathbf{t} \tag{1}$$

The total cross-section for such type of collision is

$$Q = \int_0^\infty 2\pi p \, b'^2 dp \tag{2}$$

where b according to the perturbation theory is given by

$$\frac{h}{2\pi i} \frac{db}{dt} = \int \psi_i \frac{2e^2}{R} \psi_f \, d\tau \tag{3}$$

Now ψ_i is the wave function of the electron as attached to the atom in the initial state, while ψ_f is the wave function of the same as attached to the α-particle in the final state. It is easy to see that ψ_f consists of two parts:

$$\psi_f = \psi_{f,\,orb} \times \psi_{f,\,tr}$$

where $\psi_{f,\,orb}$ is the ordinary ψ-function due to the orbital motion of the captured electron round the α-particle and $\psi_{f,\,tr}$ is due to the translation motion of the electron which it shares because of its being attached to the moving α-particle.

$$\psi_{f,\,tr} = exp\left\{ -\frac{2\pi i}{h} . \tfrac{1}{2} m V^2 t + \frac{2\pi i m}{h} (\mathbf{V}\mathbf{r}) \right\}$$

§ 1

For the case of 1s to 1s-capture, we have the ψ-functions:—

$$\psi_{i,\,1s} = \frac{1}{\sqrt{\pi a_z^3}}\, exp\left\{-\frac{r}{a_z} - 2\pi i\nu_0 t\right\} \tag{4a}$$

$$\psi_{f,\,1s} = \frac{1}{\sqrt{\pi a_{\rm He}^3}}\, exp\left\{-\frac{R}{a_{\rm He}} - 2\pi i\nu t + \frac{2\pi i}{h}\, m(\mathbf{V}.\mathbf{r}) - \frac{2\pi i}{h}\,\frac{m\mathrm{V}^2 t}{2}\right\} \tag{4b}$$

where $h\nu_0$ = energy of the electron attached to the atom in the 1s-orbit,

$h\nu$ = energy of the same attached to α-particle in the 1s-orbit.

$a_z = a/z$, $a_{\rm He} = a/z'$, where a is the Bohr-radius $= \frac{h^2}{4\pi^2 e^2 m}$, z = charge on atom and z' = charge on α-particle = 2; z' is retained for the sake of uniformity of notation.

Substitution of (4) in (3) gives us :

$$\frac{h}{2\pi i}\frac{db}{dt} = \frac{2e^2}{\pi(a_z a_{\rm He})^{3/2}}\, exp\{2\pi i\beta t\}.\int exp\left\{-\frac{r}{a_z} - 2\pi i(\sigma,\,\mathbf{r}) - \frac{R}{a_{\rm He}}\right\} d\tau_r . d\tau_R \tag{5}$$

where $\beta = \nu - \nu_0 + \frac{m\mathrm{V}^2}{2h}$, and $\sigma = \frac{m\mathbf{V}}{h}$ (6)

To evaluate (5), use has been made of the following Fourier-integral

$$\frac{1}{R}\, exp\left\{-\frac{R}{a}\right\} = 4\pi a^2 \int \frac{exp\{2\pi i(\mathbf{R}.\mathbf{q})\}}{1 + 4\pi^2 a^2 q^2} \tag{7}$$

where $\mathbf{q}$ is any arbitrary vector having the dimension of 1/Length.

We have

$$(\mathbf{q}.\,\mathbf{R}) = -q_x\mathrm{V}t - q_y p + (\mathbf{q}.\mathbf{r}), \tag{8}$$

then we may rewrite (5) as

$$\frac{h}{2\pi i}\frac{db}{dt} = \frac{8e^2}{(a_z a_{\rm He})^{3/2}}\, exp\left\{2\pi i\mathrm{V}\left(\frac{\beta}{\mathrm{V}} - q_x\right)t\right\}$$

$$\times \int \frac{exp\{-r/a_z + 2\pi i(\mathbf{q} - \sigma,\,\mathbf{r}) - 2\pi i q_y p\}}{(1/a_{\rm He}^2) + 4\pi^2 q^2} . r^2 dr \sin\theta\, d\theta d\phi d\mathbf{q} \tag{9}$$

Integration with respect to 't' gives us the well-known δ-function of Dirac (*vide*, Dirac, Quantum Mechanics (1935), p. 72),

$$\frac{h}{2\pi i}\, b = \frac{8e^2}{(a_z a_{\rm He})^{3/2}}\,\frac{1}{\mathrm{V}} \int \frac{\delta\{\beta/\mathrm{V} - q_x\} exp\{-r/a_z + 2\pi i(q - \sigma)r\cos\theta - 2\pi i p.q_y\}}{(1/a_{\rm He}^2) + 4\pi^2 q^2}$$

$$\times\, r^2 dr \sin\theta d\theta d\phi . d\mathbf{q} \tag{10}$$

The integration with respect to q_τ follows from the properties of the δ-function

$$\frac{h}{2\pi i}\,b=\frac{8e^2}{(a_z^3\,a_{He}^3)^{1/2}}\,\frac{1}{V}\left\{\int\frac{exp\{-r/a_z+2\pi i(q-\sigma)r\cos\theta-2\pi i q_\nu p\}}{(1/a_{He}^2)+4\pi^2q^2}\right.$$

$$\left.\times r^2dr\sin\theta\;d\theta d\phi.dq_\nu dq_z\right\}_{q_x=\beta/V} \qquad (11)$$

Integrating with respect to θ, ϕ, r, we have

$$\frac{h}{2\pi i}\,b=\frac{64\pi e^2}{(a_z^5\,a_{He}^2)^{1/2}}\,\frac{1}{V}\left\{\int\frac{exp\{-2\pi i q_\nu.p\}dq_\nu\,dq_z}{[(1/a_z^2)+4\pi^2(q-\sigma)^2]^2[(1/a_{He}^2)+4\pi^2q^2]}\right\}_{q_x=\beta/V}. \qquad (12)$$

From the energy-principle, the two factors in the denominator are equal (*vide* appendix 1). Hence

$$\frac{h}{2\pi i}\,b=\frac{64\pi e^2}{(a_z^5\,a_{He}^3)^{1/2}}\,\frac{1}{V}\cdot\int\frac{exp\{-2\pi i q_\nu p\}\,dq_\nu\,dq_z}{[(1/a_{He}^2)+4\pi^2\{(\beta^2/V^2)+q_\nu^2+q_z^2\}]^3}. \qquad (13)$$

$$=\frac{64\pi e^2}{(a_z^5\,a_{He}^3)^{1/2}}\,\frac{1}{V}\,\frac{3}{16}\int\frac{exp\{-iyp\}}{(g^2+y^2)^{5/2}} \qquad (14)$$

where

$$y=2\pi q_\nu,\qquad g^2=\frac{1}{a_{He}^2}+\frac{4\pi^2\beta^2}{V^2}$$

or

$$|b| = \frac{2^3.\pi e^2}{(a_z^5\,a_{He}^3)^{1/2}}\cdot\frac{1}{hV}\left(\frac{1}{a_{He}^2}+\frac{4\pi^2\beta^2}{V^2}\right)^{-2}x^2K_2(x),\qquad x=pg \qquad (15)$$

where

$$K_\nu(x)=\tfrac{1}{2}\pi i\,exp\frac{\pi\nu i}{2}\,H_\nu^1(exp\{i\pi/2\}x),$$

H_ν^1 being the Hankel function of the first kind (Copson, 1933). Substituting this value of $|b|$ in (2), we have

$$Q=\frac{2^7.\pi^3e^4}{(a_z^5.a_{He}^3)^{1/2}}\cdot\frac{1}{h^2V^2}\left(\frac{1}{a_{He}^2}+\frac{4\pi^2\beta^2}{V^2}\right)^{-5}\int x^5|K_2(x)|^2dx$$

$$=\frac{2^{12}\pi^3}{5(a_z^5.a_{He}^3)}\cdot\frac{e^4}{h^2V^2}\left(\frac{1}{a_{He}^2}+\frac{4\pi^2\beta^2}{V^2}\right)^{-5}\text{(*vide* appendix 3).} \qquad (16)$$

Replacing the value of β, and after some calculation, we have

$$Q=\frac{2^{12}\pi^3e^4}{5(a_z^5\,a_{He}^3)}\,\frac{e^4}{h^2V^2}\left[\frac{1}{2a_{He}^2}+\frac{1}{a_z^2}+\pi^2\sigma^2+\frac{\left(\frac{1}{2a_{He}^2}-\frac{1}{a_z^2}\right)^2}{16\pi^2\sigma^2}\right]^{-5} \qquad (17)$$

Putting $V=c\alpha s$ we obtain after some reduction

$$Q=\frac{2^{20}\pi a^2z^5z'^3}{5}s^8.[\{s^2+(z+z')^2\}\{s^2+(z-z')^2\}]^{-5} \qquad (18)$$

This is the formula given by Brinkman and Kramers for capture from 1s to 1s-orbits .

§ 2. CAPTURE IN THE $2p$-ORBIT

Let us now proceed with the calculation of the cross-section for the capture of the electron from $1s$ to $2p$-orbits. The ψ-function for the initial $1s$-orbit is the same as before. The ψ-function for the $2p$-orbit is now triple, corresponding to the magnetic quantum numbers $m=0,\ \pm 1$. We have

$$\psi_{t,\,2p}=\frac{1}{4\sqrt{\pi a_{\text{He}}^{2}}}\cdot\frac{\text{R}}{a_{\text{He}}}\,exp\left\{-\frac{\text{R}}{2a_{\text{He}}}-2\pi i\nu t-\frac{2\pi i}{h}\cdot\frac{m\text{V}^{2}t}{2}+\frac{2\pi i m}{h}(\mathbf{V}.\mathbf{r})\right\}\begin{Bmatrix}\dfrac{\cos\vartheta}{\sqrt{2}}\\[2ex] \dfrac{\sin\vartheta\,exp\{\pm i\phi\}}{2}\end{Bmatrix}\qquad\ldots\quad(19)$$

The upper one is for $m=0$, the lower for $m=\pm 1$.

Here ϑ, Φ denote the polar angles of the electron with reference to the α-particle as origin. But in shifting the origin to the nucleus K which, in our approximation, is at rest, the new angles θ and ϕ are connected with ϑ, and ϕ in the following way

$$\text{R}\cos\vartheta=(r\cos\theta-\text{V}t),\qquad \text{R}\sin\vartheta\,exp\{\pm i\Phi\}=(r\sin\theta\,exp\{\pm i\phi\}-p)\qquad(20)$$

The Fourier-integral here takes the form

$$\frac{1}{\text{R}}\,exp\{-\text{R}/2a_{\text{He}}\}=2\pi a_{\text{He}}^{2}\,.\int\frac{exp\{i\pi(\mathbf{q}.\mathbf{R})\}d\mathbf{q}}{1+4\pi^{2}a_{\text{He}}^{2}\,q^{2}}\qquad(21)$$

We obtain as before

$$\frac{h}{2\pi i}\frac{db}{dt}=\frac{e^{2}}{4\sqrt{a_{z}^{3}a_{\text{He}}^{5}}}\,exp\left\{2\pi i\text{V}\left(\frac{\beta}{\text{V}}-\frac{q_{x}}{2}\right)t\right\}$$

$$\int\frac{exp\left\{-\dfrac{r}{a}+2\pi i\left(\dfrac{q_{x}}{2}-\sigma\right)r\cos\theta-\pi i p q_{y}\right\}}{\left\{\dfrac{1}{4a_{\text{He}}^{2}}+\pi^{2}(q_{x}^{2}+q_{y}^{2}+q_{z}^{2})\right\}}\times$$

$$exp\,\{\pi i\,r\sin\theta(q_{x}.\cos\phi+q_{z}.\sin\phi)\}d\mathbf{r}.d\mathbf{q}\begin{cases}(r\cos\theta-\text{V}t)/\sqrt{2}\\ (r\sin\theta\,exp\{\pm i\phi\}-p)/2.\end{cases}\qquad(22)$$

Integrating with respect to t, with the aid of Dirac's delta-functions, we have

$$\frac{h}{2\pi i}\,b_{m=0}=\frac{e^{2}}{4\sqrt{2a_{z}^{3}a_{\text{He}}^{5}}}\,\frac{1}{\text{V}}\int\ldots d\mathbf{r}d\mathbf{q}F(r,\,q_{x},\,q_{y},\,q_{z})$$

$$\left\{r\cos\theta.\delta\left(\frac{q_{x}}{2}-\frac{\beta}{\text{V}}\right)+\frac{1}{2\pi i}.\delta'\left(\frac{q_{x}}{2}-\frac{\beta}{\text{V}}\right)\right\}\qquad(23)$$

where

$$F(r,\,q_{x}q_{y}q_{z})=\frac{exp\left\{-\dfrac{r}{a_{z}}+2\pi i\left(\dfrac{q_{x}}{2}-\sigma\right).r\cos\theta-\pi i p q_{y}+\pi i r\sin\theta(q_{y}\cos\phi+q_{z}\sin\phi)\right\}}{\dfrac{1}{4a_{\text{He}}^{2}}+\pi^{2}(q_{x}^{2}+q_{y}^{2}+q_{z}^{2})}\qquad\ldots\quad(24)$$

Integrating with respect to q_x, we have

$$\frac{h}{2\pi i}.b_{m=0} = \frac{e^2}{2\sqrt{2a_z^3 . a_{\text{He}}^5}} . \frac{1}{V}\int \ldots \Big[F(r, q_x/2=\beta/V, q_y, q_z)\, r \cos\theta . d\mathbf{r}$$

$$- \frac{1}{2\pi i} . F'(r, q_x/2=\beta/V, q_y, q_z)\, d\mathbf{r}\Big] dq_y\, dq_z . \qquad (25)$$

Here F' denotes differentiation of F with respect to $q_x/2$, and the substitution of β/V for $q_x/2$. On simplification

$$b_{m=0} = \frac{4\pi^2 e^2 \beta/V}{hV\sqrt{2a_z^3 a_{\text{He}}^5}} . \int \frac{exp\left\{-\frac{r}{a_z} + 2\pi i\left(\frac{\beta}{V} - \sigma\right) r\cos\theta - \pi i p q_y\, ic\cos(\phi - \chi)\right\}}{\left[\frac{1}{4a_{\text{He}}^2} + 4\pi^2\frac{\beta^2}{V^2} + \pi^2(q_y^2 + q_z^2)\right]}$$

$$\times r^2 dr \sin\theta\, d\theta\, d\phi\, dq_y\, dq_z \qquad (26)$$

where

$$c = \pi r \sin\theta\sqrt{q_y^2 + q_z^2} = k\sin\theta.$$

$$\chi = \tan^{-1}(q_z/q_y).$$

Similarly

$$b_{m=\pm 1} = \frac{i\pi e^2}{2\sqrt{a_z^3 a_{\text{He}}^5}} . \frac{1}{hV}\int \frac{exp\left\{-\frac{r}{a_z} + 2\pi i\left(\frac{\beta}{V} - \sigma\right) r\cos\theta - \pi i p q_y\right\}}{\ldots \left\{\frac{1}{4a_{\text{He}}^2} + 4\pi^2\frac{\beta^2}{V^2} + \pi^2(q_y^2 + q_z^2)\right\}} dq_y\, dq_z$$

$$+ exp\{ic\cos(\phi - \chi)\} . \{r\sin\theta . exp(\pm i\phi) - p\}\, r^2 dr \sin\theta\, d\theta\, d\phi \qquad (27)$$

The integration of (26 & 27) with respect to ϕ, gives us

$$b_{m=0} = \frac{8\pi^3 e^2\beta/V}{hV\sqrt{2a_z^3 a_{\text{He}}^5}} . \int \frac{exp\left\{-\frac{r}{a_z} + 2\pi i\left(\frac{\beta}{V} - \sigma\right) r\cos\theta - \pi i p q_y\right\}}{\left[\frac{1}{4a_{\text{He}}^2} + 4\pi^2\frac{\beta^2}{V^2} + \pi^2(q_y^2 + q_z^2)\right]^2}$$

$$J_0(k\sin\theta) . r^2 dr \sin\theta d\theta dq_y dq_z \qquad (28)$$

and

$$b_{m=+1} = \frac{i\pi^2}{\sqrt{a_z^3 a_{\text{He}}^5}} \frac{e^2}{hV}\int \frac{exp\left\{-\frac{r}{a_z} - 2\pi i\left(\frac{\beta}{V} - \sigma\right) r\cos\theta - \pi i p q_y\right\}}{\left\{\frac{1}{4a_{\text{He}}^2} + 4\pi^2\frac{\beta^2}{V^2} + \pi^2(q_y^2 + q_z^2)\right\}}$$

$$\times r^2 dr \sin\theta\, d\theta\, dq_y dq_z . \{r\sin\theta\, i J_1(k\sin\theta) exp(+\chi) - p J_0(k\sin\theta)\} \qquad (29)$$

A similar integration with respect to θ gives us

$$b_{m=0} = \frac{16\pi^3 e^2\beta/V}{hV\sqrt{2a_z^3 a_{\text{He}}^5}} . \int \frac{exp\left\{-\frac{r}{a_z} - \pi i p q_y\right\}\sin nr}{\left[\frac{1}{4a_{\text{He}}^2} + 4\pi^2\frac{\beta^2}{V^2} + \pi^2(q_y^2 + q_z^2)\right]^2} . \frac{r}{n} dr . dq_y . dq_z \qquad (30)$$

and

$$b_{m=1} = \frac{2i\pi^2 e^2}{hV} \int \frac{exp\left\{-\frac{r}{a_z}\right\}\left(\frac{\sin nr}{nr} - \cos nr\right)\frac{im}{n^2}\, exp\{-\pi i p q_y\}}{\left\{\frac{1}{4a_{He}^2} + 4\pi^2\frac{\beta^2}{V^2} + \pi^2(q_y^2 + q_z^2)\right\}} r^2\, dr\, dq_y\, dq_z \quad (31)$$

where

$$n = \sqrt{l^2 + m^2}, \quad l = 2\pi\left(\frac{\beta}{V} - \sigma\right), \quad m = \pi\sqrt{q_y^2 + q_z^2}. \quad (32)$$

Integrating with respect to r, we have

$$b_{m=0} = \frac{32\pi^3 e^2 \beta/V}{hV\sqrt{2a_z^5 a_{He}^5}}$$

$$\times \int \frac{exp\{-\pi i p q_y\}dq_y\, dq_z}{\left\{\frac{1}{4a_{He}^2} + 4\pi^2\frac{\beta^2}{V^2} + \pi^2(q_y^2 + q_z^2)\right\}^2 \left\{\frac{1}{a_z^2} + 4\pi^2\left(\frac{\beta}{V} - \sigma\right)^2 + \pi^2(q_y^2 + q_z^2)\right\}^2} \quad (33)$$

$$b_{m=1} = \frac{4i\pi^2}{\sqrt{a_z^5 a_{He}^5}} \cdot \frac{e^2}{hV} \int \frac{exp\{-\pi i p q_y\}dq_y dq_z}{\left\{\frac{1}{4a_{He}^2} + 4\pi^2\frac{\beta^2}{V^2} + \pi^2(q_y^2 + q_z^2)\right\}}$$

$$\times \left\{ \frac{4im\, exp\{i\chi\}}{\left[\frac{1}{a_z^2} + 4\pi^2\left(\frac{\beta}{V} - \sigma\right)^2 + \dots\right]^3} - \frac{p}{\left[\frac{1}{a_z^2} + \dots\right]} \right\} \quad (34)$$

It is easy to deduce from the law of conservation of energy that the two factors in the denominator are equal; *i.e.*,

$$\left\{\frac{1}{4a_{He}^2} + \frac{4\pi^2\beta^2}{V^2} + \pi^2(q_y^2 + q_z^2)\right\} = \left\{\frac{1}{a_z^2} + 4\pi^2\left(\frac{\beta}{V} - \sigma\right)^2 + \pi^2(q_y^2 + q_z^2)\right\} \quad (35)$$

Making use of this relation, and integrating with respect to q_y and q_z, we have

$$\left.\begin{aligned} b_{m=0} &= \frac{2\pi}{3} \cdot \frac{2\pi\beta/V}{(2a_z^5\, a_{He}^5)^{\frac{1}{2}}} \cdot \frac{e^2}{hV} g^{-6}\, x^3 K_3(x) \\ b_{m=1} &= -\frac{i}{3} \cdot \frac{\pi}{(a_z^5\, a_{He}^5)^{\frac{1}{2}}} \cdot \frac{e^2}{hV} \cdot g^{-5} x^3 K_2(x) \end{aligned}\right\} \quad (36)$$

where

$$g^2 = \left(\frac{1}{4a_{He}^2} + 4\pi^2\frac{\beta^2}{V^2}\right), \qquad x = pg.$$

Substituting the above values in expression (2) we obtain

$$\left.\begin{aligned} Q_{m=0} &= \frac{2^2 . \pi^3}{3^2} \cdot \frac{(2\pi\beta/V)^2}{a_z^5\, a_{He}^5} \cdot \frac{e^4}{h^2V^2} \cdot g^{-14} \int_0^\infty x^7 dx \{K_3(x)\}^2 \\ Q_{m=1} &= \frac{2\pi^3}{3^2 a_z^5\, a_{He}^5} \cdot \frac{e^4}{h^2V^2} \cdot g^{-12} \int_0^\infty x^7 dx \{K_2(x)\}^2 \end{aligned}\right\} \quad (37)$$

The general method to work out this type of integrals has been given in appendix 3. We have finally

$$\left.\begin{aligned} Q_{m=0} &= \frac{2^9}{7}\cdot\frac{\pi^3(2\pi\beta/V)^2}{a_z^5\, a_{He}^5}\cdot\frac{e^4}{h^2V^2}\left[\frac{1}{4a_{He}^2}+4\pi^2\frac{\beta^2}{V^2}\right]^{-7} \\ Q_{m=1} &= \frac{2^7}{3\cdot 7}\cdot\frac{\pi^3}{a_z^5\, a_{He}^5}\cdot\frac{e^4}{h^2V^2}\left[\frac{1}{4a_{He}^2}+4\pi^2\frac{\beta^2}{V^2}\right]^{-6} \end{aligned}\right\} \tag{38}$$

Reducing still further, we have finally

$$Q_{m=0} = \frac{2^{19}}{7}\cdot\frac{\pi a^2 . z^5 z'^5 . s^{10} . [s^2+z^2-(z'^2/4)]^2}{[\{s^2+(z+z'/2)^2\}\{s^2+(z-z'/2)^2\}]^7} \tag{39}$$

$$Q_{m=1} = \frac{2^{17}}{3\cdot 7}\cdot\frac{\pi a^2 . z^5 z'^5 . s^{10}}{[\{s^2+(z+z'/2)^2\}\{s^2+(z-z'/2)^2\}]^6} \tag{40}$$

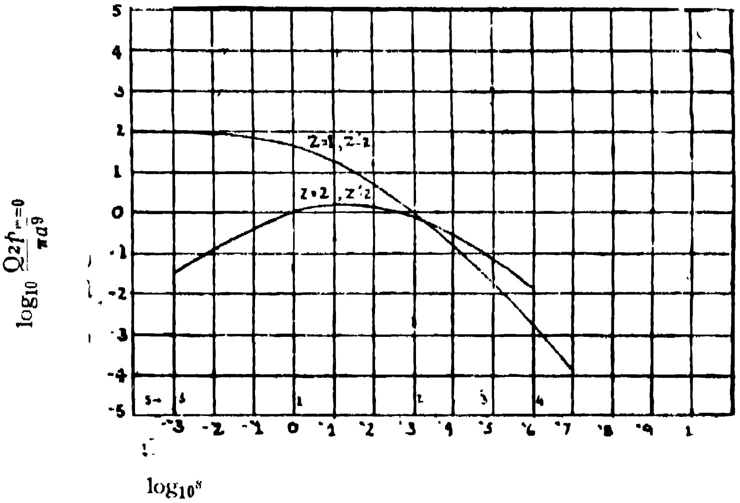

FIG. 3

DISCUSSION

Let us first compare the relative values of the different cross-section. We have for $z'=2$ and $z=1$.

$$\frac{Q_{2p_{m=\pm 1}}}{Q_{2p_{m=0}}} = \frac{s^2+2^2}{6s^2} \simeq \frac{1}{6} \quad \text{when } s \text{ is large,}$$

$$\sim \frac{2}{3s^2} \quad \text{when } s \text{ is small.}$$

This shows that the probability of capture is much larger from 1s to $(2p)_{m=0}$ than from 1s to $(2p)_{m=\pm 1}$, except when $s \ll 1$.

Let us next compare $Q_{2p_{m=0}}$ to Q_{1s}. We have from (39) and (40).

$$\frac{Q_{2p_{m=0}}}{Q_{1s}} = \frac{10}{7}\,\frac{(s^2+9)^5(s^2+1)^5}{s^8(s^2+4)^7} \quad \text{for the case} \quad z'=2 \text{ and } z=1.$$

$Q_{2p_{m=0}}/Q_{1s}$ =	58.53	21.00	9.77	5.23	3.09	1.30	0.60	0.24
For s =	1.0	1.25	1.5	1.75	2.0	2.5	3.0	4.0

We thus obtain that for $z=1$ and $z'=2$, the capture cross-section $Q_{2p_{m=0}}$, though small compared to Q_{1s}, when $s>4$, is no longer so when s continues to fall.

At $V=2$, *i.e.*, when the α-particle has twice the velocity which the captured electron would have in its orbit, the ratio is nearly three times and at lower velocities it assumes a far higher value. Though there is some doubt whether these calculations can apply when s becomes small, it appears that the probability of capture in excited states increases rapidly with diminishing s, *i.e.*, towards the end of its path the charged particle would mostly be capturing the electron in the higher orbits. This is quite contrary to the view of Brinkman and Kramers that the capture probability in the higher orbits is negligible compared to that in the $1s$-orbit.

We have not yet been able to finish our calculation for capture in ns or higher nd or nf orbits. These will be taken up in a later paper.

APPENDIX 1

To prove

$$\frac{1}{a_z^2} + 4\pi^2\left\{\frac{\beta}{V} - \sigma\right\}^2 = \frac{1}{a_{ne}^2} + 4\pi^2\,\frac{\beta^2}{V^2}$$

we have

$$\beta = \nu - \nu_0 + \frac{mV^2}{2h}$$

where

$$\nu = -\frac{h}{8\pi^2 m a_{ne}^2}$$

$$\nu_0 = -\frac{h}{8\pi^2 m a_i^2}.$$

On substitution

$$\frac{\beta}{V} = \frac{1}{8\pi^2\sigma}\left(\frac{1}{a_i^2} - \frac{1}{a_e^2}\right) + \frac{\sigma}{2}$$

where as usual

$$\sigma = \frac{mV}{h}$$

or

$$\frac{1}{a_i^2} - \frac{1}{a_{no}^2} = \left(\frac{\beta}{V} - \frac{\sigma}{2}\right)8\pi^2\sigma = 4\pi^2\left\{\frac{\beta^2}{V^2} - \left(\frac{\beta}{V} - \sigma\right)^2\right\}$$

Hence follows the result.

APPENDIX 2

The integral

$$I_1 = \int_0^\pi e^{iu\cos\theta} J_0(k\sin\theta)\sin\theta\, d\theta$$

we have on putting the standard form of J_0,

$$I_1 = \sum \frac{(-1)^m (\tfrac{1}{2}k)^{2m}}{(m!)^2} \int_0^\pi e^{iB\cos\theta} (\sin\theta)^{2m+1} d\theta$$

$$= \frac{(-1)^m (\tfrac{1}{2}k)^{2m}}{(m!)^2} \frac{\Gamma(m+\tfrac{1}{2})\,\Gamma(\tfrac{1}{2})}{(\tfrac{1}{2}B)^{m+\frac{1}{2}}} J_{m+\frac{1}{2}}(B)$$

$$= \sum \frac{\Gamma(\tfrac{1}{2})\sqrt{2}}{m!} k^{2m} \left(\frac{d}{2BdB}\right)^m \left\{B^{-\frac{1}{2}} J_{\frac{1}{2}}(B)\right\}$$

$$= 2\sum \frac{1}{m!} \left(k^2 \frac{d}{2BdB}\right)^m \left\{\frac{\sin B}{B}\right\}$$

$$= 2\frac{\sin\sqrt{B^2+k^2}}{\sqrt{B^2+k^2}}.$$

The integral $\qquad I_3 = \int_0^\pi e^{iB\cos\theta} J_1(k\sin\theta)\sin^2\theta\, d\theta$

Let us take the integral $I_2 = \int_0^\pi e^{iB\cos\theta} J_0(k\sin\theta)\sin\theta\cos\theta\, d\theta$ and integrate the above by parts ; we have

$$I_2 = \frac{1}{k}\Big[e^{iB\cos\theta}\sin\theta\, J_1(k\sin\theta)\Big]_0^\pi + \frac{iB}{k}\int_0^\pi e^{iB\cos\theta} J_0(k\sin\theta)\sin^2\theta\, d\theta$$

The first term vanishes and it can be easily shown that

$$I_2 = -\frac{1}{i}\frac{dI_1}{dB},$$

so we have

$$I_3 = -\frac{k}{B}\frac{dI_1}{dB} = \frac{2k}{B^2+k^2}\left\{\frac{\sin\sqrt{B^2+k^2}}{\sqrt{B^2+k^2}} - \cos\sqrt{B^2+k^2}\right\}$$

APPENDIX 3

The evaluation of the integrals of the general type $\int_0^\infty x^m \{K_\nu(x)\}^2 dx$ is due to Dr. F. C. Auluck of the Delhi University to whom we express our thanks.

$$I_m = \int_0^\infty x^m dx \{K_\nu(x)\}^2 = \int_0^\infty x^m dx \int_0^\infty\int_0^\infty e^{-x(\cosh t + \cosh t')} \cos\nu t \cos\nu t'\, dt\, dt'.$$

Further the integral on the right hand side is the coefficient of $(-1)^m (a^m/m!)$ in the integral

$$I = \int_0^\infty\int_0^\infty\int_0^\infty e^{-x(a+\cosh t+\cosh t')} \cos\nu t \cos\nu t'\, dt\, dt'\, dx$$

$$=\int_0^\infty\int_0^\infty \frac{\cos \nu t \cos \nu t'}{a+\cosh t+\cosh t'}\,dt\,dt' \quad \text{(on integration with respect to } x\text{)}$$

$$=\tfrac{1}{2}\int_0^\infty\int_0^\infty \frac{\cosh \nu(t+t')+\cosh \nu(t-t')}{a+2\cosh (t+t')/2\cosh (t-t')/2}\,dt\,dt'$$

If we put

$$t+t'=2x$$

$$t-t'=2y$$

we get

$$I=\iint \frac{\cosh 2\nu x+\cosh 2\nu y}{a+2\cosh x\cosh y}\,dx\,dy$$

$$=\int_{x=0}^{\infty}\int_{y=0}^{x} \frac{\cosh 2\nu x}{a+2\cosh x\cosh y}\,dx\,dy+2\int_{y=0}^{\infty}\int_{x=0}^{\infty} \frac{\cosh 2\nu y}{a+2\cosh x\cosh y}\,dx\,dy$$

$$=2\int_{x=0}^{\infty}\int_{y=0}^{\infty} \frac{\cosh 2\nu x\,dx\,dy}{a+2\cosh x\cosh y}$$

$$=2\int_{x=0}^{\infty} \frac{\cosh 2\nu x}{\sqrt{4\cosh^2 x-a^2}}\cos^{-1}\frac{2\cosh x+a\cosh y}{a+2\cosh x\cosh y}\,dx\,\Bigg|_{y=0}^{\infty}$$

assuming $a<2$.

$$=\int_0^\infty \frac{\cosh 2\nu x}{\sqrt{4\cosh^2 x-a^2}}\cos^{-1}\frac{a}{2\cosh x}\,dx$$

Expanding $\dfrac{1}{\sqrt{4\cosh^2 x-a^2}}$ and $\cos^{-1}\dfrac{a}{2\cosh x}$ in series

$$I=\int_0^\infty \frac{\cosh 2\nu x}{\cosh x}\Bigg[\frac{\pi}{2}-\frac{a}{2\cosh x}+\frac{\pi}{2}\frac{1}{2!}\frac{a^2}{(2\cosh x)^2}-\frac{2^2}{3!}\frac{a^3}{(2\cosh x)^3}$$

$$+\frac{\pi}{2}\frac{1^2.3^2}{4!}\frac{a^4}{(2\cosh x)^4}-\frac{2^2.4^2}{5!}\frac{a^5}{(2\cosh x)^5}$$

$$+\frac{\pi}{2}\frac{1^2.3^2.5^2}{6!}\frac{a^6}{(2\cosh x)^6}-\frac{2^2.4^2.6^2}{7!}\frac{a^7}{(2\cosh x)^7}\cdots\Bigg]dx$$

Hence for $m\geq 4$

$$I_m=\int_0^\infty x^m dx\iint e^{-x(\cosh t+\cosh t')}\cosh \nu t\cosh \nu t'\,dt\,dt'$$

$$=\frac{2^2.4^2.6^2.\ldots(m-1)^2}{2^m}\int_0^\infty \frac{\cosh 2\nu x}{\cosh^{m+1} x}\,dx \quad \text{if } m \text{ is odd}$$

$$=\frac{\pi}{2}\cdot\frac{1^2.3^2.5^2.\ldots(m-1)^2}{2^m}\int_0^\infty \frac{\cosh 2\nu x}{\cosh^{m+1} x}\,dx \quad \text{if } m \text{ is even}$$

The cases that concern us are for $\nu = 2$ and $\nu = 3$. For $\nu = 2$, the expression under the integral may be written as

$$\int_0^\infty \frac{\cosh 4x}{\cosh^{m+1} x} = \frac{(m+1)(m+3)}{m(m-2)} \int_0^\infty \operatorname{sech}^{m-3} x \, dx$$

From which follows

$${}^2I_4 = \frac{315}{256}\pi^2, \qquad {}^2I_5 = \frac{2^5}{5}$$

$${}^2I_6 = \frac{3^3 \cdot 175}{2^{11}}\pi^2, \qquad {}^2I_7 = \frac{3 \cdot 2^6}{7}$$

Similarly for $\nu = 3$

$${}^3I_7 = \frac{2^7 \cdot 3}{7} .$$

ACKNOWLEDGEMENTS

One of us (D. Basu) has been receiving a scholarship from the Radio Research Committee of the Council of Scientific and Industrial Research, Government of India, and wishes to express his grateful thanks for the financial assistance.

PALIT LABORATORY (PHYSICS),
CALCUTTA UNIVERSITY.

REFERENCES

Brinkman, H. C. and Kramers, 1930, *Proc. Amst.*, **33**, 973.
Fowler, R. H., 1924, *Phil Mag.*, **47**, 257.
Henderson, G. H., 1923, *Proc. Roy. Soc.*, **102**, 496.
Hylleraas, E. A., 1937, *Zs. f. Phys.*, **106**, 395.
Jacobsen, J. C., 1930, *Phil. Mag.*, **10**, 401.
Oppenheimer, J. R., 1928, *Phys. Rev.*, **31**, 349.
Pannekoek and Minnaert, 1928, *Proc. Amst.*, **31**, 104.
Perepelkin, E. J. and Melnikov, O. A., 1935, *Pulkovo Bulletin*, **14**, 1.
Rutherford E., 1924, *Phil. Mag.*, **47**, 277.
Saha, M. N., 1942, *Proc. Nat. Inst. Sc.*, **8**, 99.
Thomas, L. H., 1927, *Proc. Roy. Soc.*, **114**, 561.

NOTE ON THE EMISSION BANDS OF THE SILVER IODIDE MOLECULE

By C. RAMA SASTRY and K. R. RAO*

ABSTRACT. The silver iodide bands are obtained in emission using a high frequency oscillatory electrodeless discharge, through the vapour contained in a quartz tube The complete band system is obtained. The stronger bands form the progression $(0, v'')$. The intensity distribution of these bands in emission is compared with that in absorption and fluorescence.

INTRODUCTION

The band spectra of the halides of silver were first investigated by Frank and Kuhn (1927) in absorption and fluorescence. The complete vibrational analysis of the bands was due to Brice (1930 and 1931) who photographed the bands in absorption at temperatures higher than those obtained by Frank and Kuhn. Characteristic bands of the three molecules AgCl, AgBr and AgI are found in the vicinity of the resonance line of the silver atom at about λ3300. In addition to these main systems, absorption bands were reported in the further ultra-violet for AgCl at λ 2300 by Jenkins and Rochester (1937) and for AgI at λ 2250 by Metropolis (1939), having the respective common ground states.

In emission, only in AgCl was the main system reported (mention has been made by Brice of emission bands in AgBr also) by Brice who used a high voltage discharge in hydrogen at reduced pressure between silver electrodes containing the fused salt. The purpose of the present note is to describe the results of experiments performed to excite the bands of silver iodide in emission which do not appear to have been hitherto done, and particularly to record the differences in the intensity distribution among the bands as excited by the various methods, *i.e.*, fluorescence, absorption and emission.

EXPERIMENTAL

Two different sources of excitation are used in this investigation. One is the ordinary uncondensed discharge from a quarter K.W. transformer giving 20,000 volts in the secondary and the other is a specially constructed low power high frequency oscillatory discharge between external electrodes. The silver iodide is heated to about 700° C in quartz discharge tube provided with sealed-in quartz end-on windows. The bands were found to be better developed in the high frequency discharge. Hilger medium quartz spectrograph was employed giving exposures of one to two hours.

---

* Fellow of the Indian Physical Society.

RESULTS

The bands obtained on our plates are diffuse and isotope effects are not resolved but approximate measurements could be made and the band system definitely identified with that of AgI as obtained by Frank and Kuhn, and by Brice under different conditions. The following table contains the wavenumbers of all the bands (AgI ^{107}) given by Brice (1930). Columns 2 and 3 give the band heads obtained by Frank and Kuhn in flourescence and absorption at about 800° C. Column four contains bands measured by Brice in absorption at temperature higher than 800° C. The last column gives the intensities of the bands as octained in emission, in the present work. It would be seen that the system is excited only partially in absorption and in fluorescence while it appears completely in emission. The distribution of intensity among the bands in emission is similar to that in fluorescence, the stronger bands forming the progression (o, v″). In absorption, on the other hand, as might be expected from the differences in the temperature of the vapour, Frank and Kuhn obtained only the bands involving the lower quantum numbers while Brice could measure only those having higher vibrational quantum numbers. When represented on a diagonal array the intensities in emission gave a wide Condon parabola with only one arm strongly developed, which appears to be a general characteristic of bands of several iodide molecules.

TABLE

v′, v″	Frank and Kuhn		Brice Absor.	Authors Int.	v′, v″	Frank and Kuhn		Brice Abs.	Authors. Int.
	Fluor.	Absor.				Fluor.	Absor.		
4 0	—	31565	—	-	1·8	—	-	29654	
3·0	—	31480	—	—	2·9	—	-	29565	—
2·0	—	31380	—	2	1·9	—	-	29455	0
1·0		31270	—	1	2·10	—		29368	2
0·0	31148	31153	—	4	3·11	—	-	29270	2
1 1	—	31067	—	1	2·11	—		29171	2
0·1	30943	30917	-	4	3·12			29076	0
1·2	—	30863	-	1	2·12	—	—	28976	0
0·2	30739	30744	—	4	3·13	- -	- -	28881	0
0 3	30535	30539		3	2·13	-	—	28781	1
0·4	30334	30339	—	3	3·14			28688	0
1·5	—	30260	—	2	3·15	—	-	28404	-
0·5	30132	30137	30136	0	4·16		- -	28388	—
1·6	—	30056	30053	3	3·16	-	—	28303	-
0·6	29931	—	—	—	1·17	-	-	28194	- -
1 7		29856	29853	- -	3·17		-	28109	—
2·8	—		29765	—	—	—	-		

ANDHRA UNIVERSITY, GUNTUR.

REFERENCES

Brice, 1930, *Phys. Rev.* **35**, 960, 1931, *Ibid.*, **38**, 658.
Frank and Kuhn, 1927, *Zeits. f. Physik.*, **43**, 164.
Jenkins and Rochester, 1937, *Phys. Rev.*, **52**, 1141.
Metropolis, 1939, *Ibid.*, **55**, 636.

15

ON THE THEORY OF DIFFUSION PUMP

By KAMALESH RAY and NANDA DULAL SENGUPTA

ABSTRACT. Attempt has been made, in this paper for an explanation of the successful functioning of the diffusion pump and experiments have been carried out in support of the theory. It has been observed that the partial pressure of the vapour of the pump filling in the vacuum chamber is much less than the vapour pressure of the fillings, which directly shows that the ultimate vacuum is independent of the vapour pressure of the filling. The ultimate vacuum, however, depends upon the degree of backstreaming at the jet, chiefly due to the imperfection of jet design. Further experiments have been done, which demonstrates the independence of partial pressure of air in vacuum chamber on the nature of pump filling The explanation of the working of multi-nozzle pump is suggested to be due to the gradual freeing of the oil in successive compartments from air contamination and also due to the more perfect stream-line flow of vapour in the upper jet

INTRODUCTION

The stage of perfection which the technique of diffusion pump has attained after thirty years of its invention by Gaede (1916) can give us today a vacuum which is well beyond the present measuring technique. The maximum vacuum which has been produced by Hickman (1940) passed the range of the ionization gauge and is claimed to be in the region of 10^{-10} mm. of mercury.

Despite the great advances in the technique of production of high vacuum by diffusion pumps, the mechanism of pumping is not yet understood very clearly, and a good deal of controversies remain on the basic question on the physical mechanism of the pumping process and the ultimate vacuum attainable by a diffusion pump. The choice of pump fluid attracted the attention of various workers in high vacuum technique, and mercury was recognised to be the ideal fluid for a long time until of late petroleum distillate oils (Apiezon types) and more recently synthetic oils (phthalates) have come to be used as suitable pump fluids.

The major question has been the dependence of the ultimate vacuum on the vapour pressure of the pump fluids. Some have held that the ultimate vacuum produced by a diffusion pump depends upon the vapour pressure of the fluid at the room temperature. For instance, Hickman reported that a mercury diffusion pump cannot get a vacuum better than the vapour pressure of mercury, without a trap. " It has been assumed since 1915 that the lowest pressure that can be attained by a vapour pump should correspond with the vapour pressure of the working fluid in the coldest part of the high vacuum side of the system. With mercury on a summer day, and in absence of a special cooling trap, this proves to be about 5×10^{-3} mm., agreeing well with theory."

On the other hand Gaede showed that even water can be used as a diffusion pump fluid. He was able to reduce the pressure from atmosphere down to 15 mm. of mercury by the use of a water diffusion pump, without the help of any backing pump. Backed by a water jet pump a three-stage water diffusion pump could produce X-ray vacuum. Further, we have the following quotation due to Langmuir (1916). " Maurice Leblanc showed that it is possible to get a vacuum of the order of 1 mm. of mercury in the condenser of a steam engine by using a steam injector." The vapour pressures of water at room temperatures of 10°, 20° and 30°C are 9.2, 17.5 and 31.8 mm. respectively.

If it is accepted that mercury diffusion pump cannot produce a vacuum better than the vapour pressure of mercury at room temperature (1.6×10^{-3} mm. at 20° C), one is confronted with the question as to how a mercury diffusion pump is successfully employed in laboratories to generate X-rays without any cold trap. Langmuir ovserved that there is no lower limit to which the pressure may be reduced by the diffusion pumps.

Discussing the question of ultimate vacuum attainable by a diffusion pump Newman (1925) expressed the view that not only the vapour pressure of mercury itself, but also the partial pressure of air contaminated with the mercury vapour jet was of primary importance. " Although the mercury vapour pressure may be a thousand times greater than the air pressure, the latter is continuously exhausted, due to the fact that diffusion of the gas depends solely on the ratio of the *partial* pressures of the gas, and not the *total* pressure of the vapour and gas. When the partial pressures are equal, diffusion ceases, but, as long as the stream of vapour is free from air, diffusion will not cease until the receiver is also free from air, and, as it is quite easy to produce a stream of air free vapour, the highest vacuum can be attained by this method ; in fact, a perfect vacuum should, *theoretically*, be attained." The italics are given by the author himself in the book.

Speed of Suction

If we examine the formulae used for the diffusion pump we find that they give only the speed of suction in relation to diffusion aperture, tube resistance, etc.

According to Gaede's formula, the speed of suction is given by

$$\frac{dv}{dt} = \frac{1}{l} \frac{\pi r^3}{2\eta_1} e^{-\frac{rP_1}{1520 d\eta_2}} \qquad \dots \quad (1)$$

where r = radius of the vacuum connecting line, or the diffusion aperture.

l = length of the line.

P_1 = vapour pressure of pump fluid at the jet.

η_1 = ' friction ' of gas (air) against the connecting line.

η_2 = ' friction ' of the vapour against the tube.

d = constant of gas diffusion.

The equation suggests that, when other conditions are the same, the speed of pumping is higher for the lower vapour pressure (P_1) of the fluid. The pumping action, according to this formula is continuous and asymptotic, and does not set any abrupt limit to it.

The formula, however, is complicated due to the factor containing the gaseous frictions and has not such a handy form as to admit of practical applica-cation. The more practical form now generally used is derived from the consideration of diffusion of gas through an aperture. If n_1 and n_2 be the number of molecules of a gas per unit volume on the two sides of the aperture, p_1 and p_2 their respective pressures, P_1 and P_2 their respective densities ($P_2 = n_1 m$ and $P_2 = n_2 m$), m the mass of each molecule, c the average velocity, the mass μ which passes through per unit area of the aperture per second is equal to the difference in masses which cross it both ways.

Thus,
$$\mu = \tfrac{1}{4} n_1 mc - \tfrac{1}{4} n_2 mc$$

$$= \tfrac{1}{4} c (P_1 - P_2)$$

Since
$$P = \frac{M}{RT} \quad \text{and} \quad c = \sqrt{\frac{8RT}{\pi M}}$$

We have
$$\mu = \tfrac{1}{4} \sqrt{\frac{8RT}{\pi M}} \cdot \frac{M}{RT} p_1 - p_2$$

$$= (p_1 - p_2) \sqrt{\frac{M}{2\pi RT}} \qquad (2)$$

If we assume $p_2 = 0$ that is to say that the gas at p_1 is diffusing into a space with perfect vacuum we have

$$\mu = p_1 \sqrt{\frac{M}{2\pi RT}} \qquad \ldots \quad (3)$$

But the mass of gas has its volume v under a pressure p_1 given by

$$v = \frac{\mu}{P_1} \quad \text{and} \quad P_1 = \frac{M}{RT} p_1$$

So that
$$\mu = v P_1 = p_1 \sqrt{\frac{M}{2\pi RT}}$$

$$v = \sqrt{\frac{RT}{2\pi M}} \qquad \ldots \quad (4)$$

Taking $R = 8.3 \times 10^7$, T = room temp. 300 K, and M = 29 for air we have the volume of escape of air by diffusion

= 11.7 litres per second per unit aperture

For a diffusion aperture A the rate of escape may be given by

= 11.7A litres per second ... (5)

For a diffusion pump, the diffusion aperture is taken for the annular aperture ('neck') round the vapour jet, through which the air is 'sucked.' The practical pumping speed, however, usually about 1/2 or 1/3 of the calculated speed, and the factor is sometimes known as the Ho coefficient (Ho, 1932).

Pumping Action

The essential point in this equation (4 or 5) also is the fact that it does not set any limit to the pumping action, and that it does not take into account the vapour pressure of the pump fluid.

We need a more critical analysis of this formula to justify its applicability, for a major objection might arise on the question that it has been assumed that the air is diffusing freely into a vacuum through the aperture, whereas we know that the space below the diffusion aperture contains copious vapour of the fluid and other gases (*e.g.* air) and we have set $p_2 = 0$ in equation (2) to get (3).

As a matter of fact we shall see that these are just the criteria for a perfect diffusion pump. In order that air may be 'sucked out' we shall have to provide a space with vacuum or lower pressure so that the air from the receiver may diffuse out. The vapour jet, if well designed, gives a stream of vapour all in the forward direction so that it has no component in the direction of the aperture. The 'pressure' of the jet is therefore 'zero' *in the direction* of the aperture, and hence it justifies putting $p_2 = 0$. Physically, the jet makes all the molecules (of vapour, air contamination, etc., from the jet) move away from the aperture so that diffusion takes place one way only, and whatever air molecules diffuse down into the vapour stream are caught and knocked on forward down to the backing pump.

Ultimate Vacuum

If all the vapour particles of the jet stream move in perfect stream line away from the diffusion aperture, air from the receiver would escape freely as indicated in equation (5). This would theoretically lead to any vacuum provided that sufficient time is allowed. But it is not possible to have a perfect jet (one not giving rise to turbulence), so that there is always a small fraction of vapour, mixed up with air, diffusing back through the neck of the pump.

The back-escape occurs not only due to the imperfection of the jet design, but also due to the pressure condition and condensation of the vapour below the jet. This is why a low vapour-pressure fluid would be preferable in order to avoid the accumulation of pressure and creation of turbulence in the body of the pump.

Taking back-diffusion into consideration the mass rate of escape through the neck would be given by

$$\eta = \tfrac{1}{4} n_1 mc - \tfrac{1}{4}(n_2 mc + n_v m_v c_v)$$

where n_1 = number of molecules of air per unit volume of the air above the neck (or receiver).

n_t = the same for back-escaped air, and those with subscript v are those for back-diffused vapour.

We can omit the terms for the vapour as the vapour molecules can be removed by cold or charcoal traps. It is the back-escaped air which affects the vacuum really. Thus, considering the air on either side of the neck we find that the pumping action ceases when the partial densities or pressure of the gas equalise on either side (assuming uniform temperature at the neck). The amount of the back-escaped air depends upon several factors and does not necessarily equal the partial pressure of the oil vapour at the jet. In fact the pressure of the oil vapour would affect the vacuum. As the initial amount of air contamination, *i.e.*, partial pressure of vapour of the jet is difficult to measure, the difference is demonstrated indirectly. The vapour, for instance, does not manifest fully in the back diffusion. In an experiment with a mercury diffusion pump (Table II) the partial pressure of mercury vapour in the receiver was $4{\cdot}8 \times 10^{-4}$mm. when the full (saturation) pressure for mercury at the room temperature would be 2×10^{-3}mm. Thus, in the dynamic condition, *i.e.*, when the pump is on, the receiver has not the full pressure of the jet vapour.

EXPERIMENT ON THE PUMPING MECHANISM AND ULTIMATE VACUUM

Fig. 1 shows the interior of an orthodox type of an oil diffusion pump which was constructed in this laboratory, and side tubes were attached to the nozzles to study the pressure distribution inside the pump body. Table I and Fig. 2 show the result on the pressure distribution at different parts of the diffusion pump. It shows up the partial pressure of air (or CO_2, etc., all of which would behave as

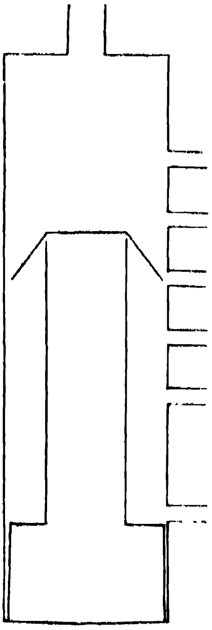

FIG. 1

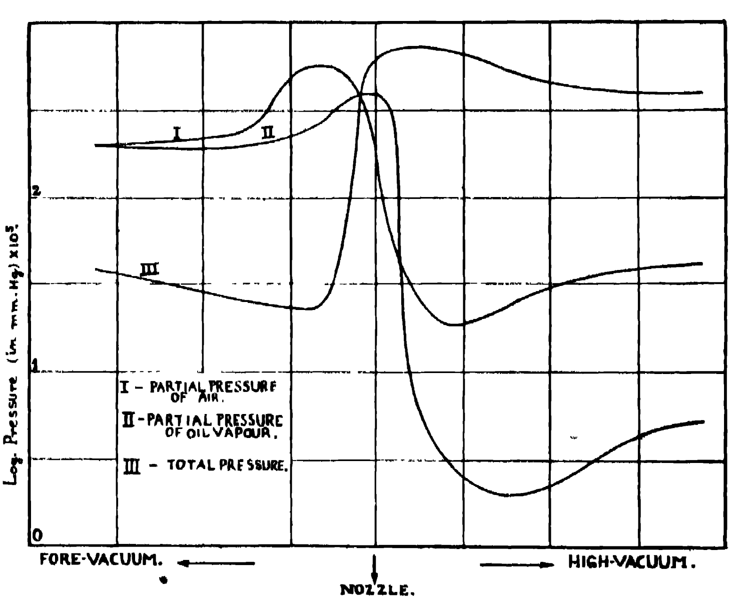

FIG. 2

'gas' to obey Boyle's law to appear in the compression column of the McLeod gauge), total pressure including vapour, and the vapour pressure by their difference. The Pirani gauge, calibrated across a liquid air trap, would record the vapour also when the trap is removed during the measurement of the total pressure.

TABLE I

Distribution of Pressure (mm. Hg.) *inside a Single Stage Oil Diffusion Pump*

Positions of tappings relative to vapour jet	Pressure measured by		Partial pressure of oil vapour (Difference of Cols 2 & 3)	Ratio of vapour pressure to air pressure = col. 4/col. 2
	McLeod Gauge (Partial pressure of air).	Pirani Gauge (Total pressure)		
1	2	3	4	5
1. 7.0 inch above jet	5.0×10^{-5}	4.0×10^{-4}	3.5×10^{-4}	7
2. 3.0 inch above jet	2.0×10^{-5}	2.6×10^{-4}	2.4×10^{-4}	12
3. 1.5 inch above jet	3.0×10^{-5}	2.3×10^{-4}	2.0×10^{-4}	6.6
4. At the jet	4.0×10^{-3}	6.0×10^{-3}	2.0×10^{-3}	0.5
5. 1.5 inch below jet	2.5×10^{-3}	8.6×10^{-3}	$.5\times10^{-3}$	2.2
6. 3.0 inch below jet	2.0×10^{-3}	5.0×10^{-3}	3.0×10^{-3}	1.5
7. 6.5 inch below jet, at backing pump nozzle	2.0×10^{-3}	4.0×10^{-3}	2.0×10^{-3}	1.0

TABLE II

Vacuum Produced by a Three-Stage Mercury-Diffusion Pump
(in mm. Hg.)

Measured by		Partial pressure of Hg differ-ence of 1&2	Vap. pressure of Hg at room temp 26°C	Ratio of back diffusion of Hg. vap	Ratio of total pressure to Sat. Vap. pressure of Hg.
McLeod Gauge	Pirani Gauge				
1	2	3	4	5	6
2×10^{-4}	5×10^{-4}	4.8×10^{-4}	2×10^{-3}	0.16	0.167

Table I gives the pressure distribution inside a diffusion pump and shows the compression effect below the jet. The maximum pressure occurs at and just below the jet. Column 4 shows that the back diffusion of the vapour differs according to the vacuum condition and remains below the saturation pressure (as it cannot go above it). This point is more clearly shown in Column 5 of Table II in the case of mercury.

Table II shows that a mercury diffusion pump can reduce the pressure, even without a trap, lower than the vapour pressure of mercury at room temperature. Both the partial pressure of air and the back-diffused vapour go far below the saturated vapour pressure of mercury.

INDEPENDENCE OF ULTIMATE VACUUM WITH VAPOUR PRESSURES OF FLUIDS

That the evacuation of air is almost independent of the vapour pressure has been demonstrated by the use of different fluids in a diffusion pump (Ray and Sengupta, 1945). Five kinds of pump fillings were tried, namely, Apiezon oil B, Capella oil D (Caltex Co), Petroleum jelley (white) and solid paraffin, and all of them gave the same minimum pressure (Table III) with certain adjustments, chiefly heat input and jacket cooling.

TABLE III

Effect of Pump Fluids on the Production of Vacuum by a Single Stage Diffusion Pump

(Pressure in $\mu = 10^{-3}$ mm. Hg.)

Pump filling	Vacuum conditions		Relative heat input (Tentative estimate)	REMARKS
	Partial pressure of air	Partial pressure of fluid vapour*		
1. Apiezon Oil	0.03	0.10	1	
2 Capella D (Caltex)	0.03	0.17	1.5	
3. Mobil B	0.03	0.97	1.5	–
4 Petroleum Jelly (White)	0.03	0.67	2	Water circulation is to be low enough to maintain fluidity and adequate boiling.
5. Solid Paraffin	0.03	0.57	2.5 to 3	Do.

*This is however not the true vapour pressure of the fluid under static saturation condition, as the pressure is measured under constant pumping condition.

The Fractionating Pump

The advantage of Hickman's self-fractionating pump was also investigated in the light of the picture we put forward. The fractionating pump with three compartments gave a good performance not as regards as the suction of air but regarding the back escape of the fluid used, solid paraffin was tried in this pump and the back-escaped vapour pressure was found to be 0.36μ as compared with 0.6μ with a single stage diffusion pump of the otherwise same design. The partial pressure of air however remained the same at °0 3μ in both cases The phenomenon can be explained by the idea of forward stream line flow of vapour, which is facilitated by the successive vapour jets, making the upper jets more and more stream-line. The total pressure in the vacuum chamber could thus be much reduced by the use of a multi-jet pump without the help of a special trap.

DISCUSSION

The foregoing experiments suggest that it is necessary to define the 'vacuum' in distinct terms of the 'partials', *viz.*, 'partial pressure of the air left in the chamber' and the partial of the back-escaped vapour of the pump fluid

The results of the experiments shows that air pressure can be pumped down much below the vapour pressure of the fluid and the partial pressure of the escaped vapour is also much less than the saturated vopour pressure under the room temperature. The success of the diffusion pump depends largely on the jet design to give a stream line flow directed away from the diffusion aperture.

ACKNOWLEDGEMENTS

Our thanks are due to Prof. M. N. Saha, D.Sc., F.R.S., for his keen interest and kind encouragement in the work. We also acknowledge our thanks to the authorities of B.S I.R. for the stipend awarded to one of us and for kindly permitting the work to be published.

PALIT LABORATORY OF PHYSICS
UNIVERSITY OF CALCUTTA.

REFERENCES

Gaede, W., 1916, *Ann. D. Physik*, **46**, 357.
Hickman, K. C. D., 1940, *Journal of Applied Physics*, **11**, 303.
Ho, T. L., 1932, *Rev. Sci Inst.*, **3**, 133
Langmuir, I., 1916, *Phys. Rev.* **8**, 48.
Newman, 1925, The Production and measurement of low pressure, 52.
Ray, K., and Sengupta, N. D., 1943, *Nature*, **155**, 727.
Ray, K. and Sengupta, N. D., 1945, *Science and Culture* **10**, 500.

THE SCATTERING OF FAST ELECTRONS BY ATOMS

By K. C. KAR

ABSTRACT. The wave statistical theory of scattering of fast electron by atomic nucleus is developed by taking into account the effect of relativity and spin-orbit interaction. The correction term due to the spin-orbit interaction is derived from entirely statistical consideration and is in exact agreement with Mott's second correction obtained from Dirac's theory. However, Mott's first correction which is independent of the atomic number is not derived by the present method. It is suggested that this correction is due to the spin-spin interaction between the incident electron and the nucleus.

The problem of the scattering of fast electrons by atoms has been treated theoretically by Mott (1929) using Dirac's equations. Accordingly Mott's formula is valid for electron spin $\pm(h/4\pi)$ and it takes account of the effect of relativity. The relative intensity of scattering at an angle between θ and $\theta+d\theta$ and per unit solid angle is according to Mott

$$I=\left(\frac{ze^2}{2m_0v^2}\right)^2\left(1-\frac{v^2}{c^2}\right)\left(\operatorname{cosec}^4\tfrac{1}{2}\theta-\frac{v^2}{c^2}\operatorname{cosec}^2\tfrac{1}{2}\theta+\pi\frac{v}{c}\cdot\frac{2\pi ze^2}{hc}\frac{\cos^2\frac{1}{2}\theta}{\sin^3\frac{1}{2}\theta}\right.$$
$$\left.+\text{higher terms}\right)\qquad(1)$$

It is evident that the second factor $1-(v^2/c^2)$ gives a general correction for relativity. In the last factor, the first term, *viz.*, $\operatorname{cosec}^4\frac{1}{2}\theta$ gives the Rutherford value of intensity while the second and third terms, *viz.*, $-(v^2/c^2)\operatorname{cosec}^2\frac{1}{2}\theta$ and $\pi\frac{v}{c}\frac{2\pi zc^2}{hc}\frac{\cos^2\frac{1}{2}\theta}{\sin^3\frac{1}{2}\theta}$ give the two corrections for spin-relativity. These two corrections will be hereafter called the *first* and *second spin* corrections of Mott. Of the two corrections, the second is appreciable only for heavy elements, *i.e.*, for high value of z, whereas the first is independent of z.

It should be noted that in deriving the above formula Mott has taken the interaction potential to be $-(ze^2/r)$ due to the nuclear charge $+zc$ of the atom. In other words, the repulsive potential of the orbital electrons for the incident electron is completely neglected. This may be justified only when the incident velocity is very high and the interaction is very close.

In the present paper I propose to develop the wave-statistical theory of the above problem.

It is well-known in wave-statistics (Kar and Mukherjee, 1934) that on taking into account the effect of relativity and spin, the wave equations are

$$\Delta\chi+\frac{4\pi^2}{h^2c^2}\left[(E-V)^2-E_0{}^2-\frac{V^2}{2(l+1)}\right]\chi=0,\quad +\text{spin}\qquad\ldots\quad(2.1)$$

and

$$\Delta\chi+\frac{4\pi^2}{h^2c^2}\left[(E-V)^2-E_0{}^2-\frac{V^2}{2l}\right]\chi=0,\quad -\text{spin}\qquad\ldots\quad(2.2)$$

where for positive spin $l_{\min}=0$ while for negative spin $l_{\min}=1$. It is evident that the term $-\frac{V^2}{2(l+1)}$ or $-\frac{V^2}{2l}$ in the above equations represents the spin-orbit interaction potential for positive or negative spin. On neglecting it one gets the usual Schrödinger's relativistic wave equation which does not give the correct eigen-value of energy for fine-structure. On the other hand, it has been already shown (Kar and Mukherjee, 1934) that the wave-statistical equations (2.1) and (2.2) do give the correct eigen-energy. Therefore, in developing the theory of the present problem, we should use these fundamental equations. Now, we take for l, the minimum value for both the spin. Thus the two equations (2.1) and (2.2) become identical and we have

$$\Delta\chi+\frac{4\pi^2}{h^2c^2}\left[(E-V)^2-E_0{}^2-\left(\frac{V^2}{2}\right)_{\text{spin}}\right]\chi=0 \qquad \ldots \quad (2.3)$$

the last term being written $(V^2/2)_{\text{spin}}$ in order to distinguish it from the other terms not connected with spin but involving V.

Outside the potential field the spin-orbit interaction evidently vanishes and so (2.3) becomes

$$\Delta\chi_0+\frac{4\pi^2}{h^2c^2}\left[E^2-E_0{}^2\right]\chi_0=0 \qquad \ldots \quad (2.4)$$

On proceeding in the usual way (Kar, Ghosh and Mukherjee, 1937) we have for the differential equation satisfied by the first order scattering function $(\lambda_1\chi_1)$

$$\Delta(\lambda_1\chi_1)+k^2(\lambda_1\chi_1)=\frac{4\pi^2}{h^2c^2}\chi_0\left[2EV-V^2+\left(\frac{V^2}{2}\right)_{\text{spin}}\right] \qquad \ldots \quad (2.5)$$

$$k^2=\frac{4\pi^2}{h^2c^2}\left[E^2-E_0{}^2\right] \qquad \ldots \quad (2.6)$$

Of the three perturbation terms on the righthand side of Eq. (2.5), the first is evidently the most important, the other two give only higher order corrections. On solving (2.5) as before (Kar, 1937) with only the first perturbation term we have for the scattering function

$$\lambda_1\chi_1=-\frac{2\pi^2E}{h^2c^2k^2}\operatorname{cosec}^2\tfrac{1}{2}\theta A\,\frac{e^{ikr}}{r}\,F(r_0) \qquad \ldots \quad (3)$$

where A is the amplitude of the incident wave and

$$F(r_0)=k'\int_{r_0}^{\infty}V(r)\sin k'r\;r\,dr \qquad \ldots \quad (3.1)$$

in which

$$k'=2k\sin\tfrac{1}{2}\theta \qquad \ldots \quad (3.2)$$

and r_0 the critical approach. Now, because the interaction potential $V(r)=-(ze^2/r)$, we have from (3.1)

$$F(r_0)=-ze^2\cos k'r_0.$$

On substituting the above value of $F(r_0)$ in (3) and also remembering that $E = E_0/(1-\beta^2)^{\frac{1}{2}}$, we have from (3) after simplification

$$\lambda_1\chi_1 = + \frac{ze^2}{2m_0v^2}(1-\beta^2)^{\frac{1}{2}}\operatorname{cosec}^2 \tfrac{1}{2}\theta\, A\, \frac{e^{ikr}}{r} \cos k'r_0 \qquad \dots \quad (3.3)$$

On solving (2.5) with only the second perturbation term on the righthand side, we have for the scattering function [*vide* (3)]

$$\lambda_1\chi_1 = + \frac{\pi^2}{h^2c^2k^2}\operatorname{cosec}^2 \tfrac{1}{2}\theta\, A\, \frac{e^{ikr}}{r} F(r_0) \qquad \dots \quad (4)$$

where

$$F(r_0) = k'\int_{r_0}^{r} V^2 \sin k'r\, dr \qquad \dots \quad (4.1)$$

On substituting for V and integrating we get from (4.1)

$$F(r_0) = k'z^2e^4\left(\frac{\pi}{2} - k'r_0\right) \qquad \dots \quad (4.2)$$

On combining (4) and (4.2) and after simplification we get

$$\lambda_1\lambda_1 = \frac{(\pi - 2k'r_0)}{2m_0v^2}\cdot\frac{v}{c}\cdot\frac{\pi z^2e^4}{hc}(1-\beta)^{\frac{1}{2}}\operatorname{cosec} \tfrac{1}{2}\theta A \frac{e^{ikr}}{r} \qquad \dots \quad (4.3)$$

It may be easily seen that the last spin perturbation term in (2.5) will give for the scattering function, $-\frac{1}{2}$ the value given in (4.3). However, because it is the case of a spin-orbit perturbation there may arise two cases. The scattered electron may have the same or the opposite spin-direction as the incident. Of course, in assigning the spin direction one should not give much importance to the geometry. It should be rather looked at from the statistical point of view. Now, in order to take account of the two events mentioned above we have to multiply the scattering function by a spin-factor (δ), which may be evaluated in the following way.

If there is no change in the direction of spin due to scattering the spin factor should evidently be unity. The same result may also be obtained for $l = \frac{1}{2}$, $m = \frac{1}{2}$, if we take the spin factor as the product

$$\delta = P_{+\frac{1}{2}}^{-\frac{1}{2}}(\theta)\, P_{-\frac{1}{2}}^{+\frac{1}{2}}(\theta)\, e^{-i\frac{1}{2}\phi} e^{+i\frac{1}{2}\phi} \qquad \dots \quad (5)$$

where the Legendre functions (*vide* Appendix)

$$\left.\begin{aligned} P_{+\frac{1}{2}}^{-\frac{1}{2}}(\theta) &= \text{const.}\ (\sin\theta)^{\frac{1}{2}} \\ P_{\frac{1}{2}}^{+\frac{1}{2}}(\theta) &= \text{const.}\ (\sin\theta)^{-\frac{1}{2}} \end{aligned}\right\} \qquad \dots \quad (5.1)$$

It should be noted that the possible values of l and m taken in (5) are symmetrical and form a complete group.

Now, of the three spin functions, namely,

$$P^{-\frac{1}{2}}_{+\frac{1}{2}}(\theta)e^{-\frac{1}{2}i\phi},\ P^{+\frac{1}{2}}_{-\frac{1}{2}}(\theta)e^{+\frac{1}{2}i\phi},\ P^{+\frac{1}{2}}_{+\frac{1}{2}}(\theta)e^{+i\frac{1}{2}\phi} \qquad \ldots \quad (5.2)$$

the product of any two gives the corresponding spin factor. Again, because the scattering has axial symmetry, the spin factor must be taken independent of ϕ. From the above considerations, we find for the spin-factor

$$\delta = P^{+\frac{1}{2}}_{+\frac{1}{2}}(\theta)P^{-\frac{1}{2}}_{+\frac{1}{2}}(\theta)e^{+\frac{1}{2}i\phi}e^{-\frac{1}{2}i\phi} \qquad \ldots \quad (5.3)$$

where (vide Appendix)

$$P^{+\frac{1}{2}}_{+\frac{1}{2}}(\theta) = \text{const.}\ \frac{\cos\theta}{(\sin\theta)^{\frac{1}{2}}} \qquad \ldots \quad (5.4)$$

and $P^{-\frac{1}{2}}_{+\frac{1}{2}}(\theta)$ is given in (5.1). Now, to the observer of scattering the spin factor in (5.3) should be obtained by putting $\pi-\theta$ for θ. Thus, on substituting for the Legendre functions we have from (5.3)

$$\delta = -\cos\theta \qquad \ldots \quad (5.5)$$

The spin-factor in (5) is not changed by putting $\pi-\theta$ for θ. Hence, we have for the total spin factor

$$\delta = 1-\cos\theta \qquad \ldots \quad (5.6)$$

Therefore, we have for the scattering function due to the spin-orbit perturbation

$$(\lambda_1\lambda_1)_{\text{spin}} = -\frac{\pi-2k'r_0}{2m_0v^2}\cdot\frac{v}{c}\cdot\frac{\pi z^2e^4}{hc}(1-\beta^2)^{\frac{1}{2}}\operatorname{cosec}\tfrac{1}{2}\theta.\ \frac{1-\cos\theta}{2}\ A\ \frac{e^{ikr}}{r} \qquad \ldots \quad (6)$$

On adding the scattering functions in (3.3), (4.3) and (6) we have for its total value

$$\lambda_1\lambda_1 = \frac{ze^2}{2m_0v^2}(1-\beta^2)^{\frac{1}{2}}\ A\ \frac{e^{ikr}}{r}\left\{\operatorname{cosec}^2\tfrac{1}{2}\theta\cos k'r_0 + (\pi-2k'r_0)\frac{v}{c}.\ \frac{\pi ze^2}{hc}\operatorname{cosec}\tfrac{1}{2}\theta\cos^2\tfrac{1}{2}\theta\right\} \qquad \ldots \quad (7)$$

Let B be the amplitude of the incident wave with opposite spin. The scattering function corresponding to it is obtained from (7) by simply putting B for A. Thus remembering that the total intensity of the incident wave is (A^2+B^2) we have for the relative intensity of scattering

$$I = \left(\frac{ze^2}{2m_0v^2}\right)^2(1-\beta^2)\left\{\operatorname{cosec}^4\tfrac{1}{2}\theta\cos^2k'r_0 + (\pi-2k'r_0)\frac{v}{c}.\ \frac{2\pi ze^2}{hc}\cos k'r_0 \times\frac{\cos^2\frac{1}{2}\theta}{\sin^3\frac{1}{2}\theta}\right\} \qquad \ldots \quad (8)$$

The second term in (8) gives the spin-orbit correction for the relative intensity of scattering. If the critical approach is neglected, it reduces to the second correction of Mott [*vide* Eq. (1)]. We do not get Mott's first correction by considering the spin-orbit interaction. It appears that Mott's first correction which is independent of z, might be due to the spin-spin interaction between the incident electron and the nucleus

Critical Approach

Let us next find the corrected critical approach (r_0) appearing in the formula for the intensity (8). Using the well-known boundary conditions at $r=r_0$, *viz.*,

$$\left.\begin{aligned} \frac{d\chi_0}{dr}+\frac{d(\lambda_1\chi_1)}{dr}&=0 \\ \chi_0+\lambda_1\chi_1&=0 \end{aligned}\right\}_{r=r_0} \qquad \ldots \quad (9)$$

we have as before (Kar, 1937)

$$r_0=\rho\,\frac{ze^2}{m_0v^2}(1-\beta^2)^{\frac{1}{2}}(\operatorname{cosec}\tfrac{1}{2}\theta-1) \qquad \ldots \quad (9.1)$$

when we take only the scattering function (3.3), without the spin-orbit correction. The difference between (9.1) and the previous value of r_0 is the additional relativistic factor $(1-\beta^2)^{\frac{1}{2}}$ in (9.1). It is evident that the above value of the critical approach is only approximate, and it should be corrected for the spin-orbit interaction. This correction for the V^2-perturbation and the spin-orbit interaction may be evaluated in the following way. The total scattering function for the V^2-perturbation and the spin-orbit interaction may be taken in the form [*vide* Eqs. (4) and (6)]

$$\lambda_1\chi_1=\frac{\pi^2}{h^2c^2k^2}\operatorname{cosec}^2\tfrac{1}{2}\theta\cos^2\tfrac{1}{2}\theta\,A\,\frac{e^{ikr}}{r}F(r_0) \qquad \ldots \quad (10)$$

where $F(r_0)$ is given in (4.1). Now, on using the second boundary condition in (9) and proceeding in the usual manner (Kar, 1937) we get

$$r_0=-\frac{\pi^2}{h^2c^2k^2}\operatorname{cosec}^2\tfrac{1}{2}\theta\cos^2\tfrac{1}{2}\theta\,e^{2ikr_0\sin^2\frac{1}{2}\theta}F(r_0) \qquad \ldots \quad (11)$$

On remembering that r_0 cannot be negative, the above may be written in the form

$$r_0=\frac{\pi^2}{h^2c^2h^2}\operatorname{cosec}^2\tfrac{1}{2}\theta\cos^2\tfrac{1}{2}\theta\,e^{2ikr_0\sin\frac{1}{2}\theta-2ikr_0\sin^2\frac{1}{2}\theta}G(r_0) \qquad \ldots \quad (11.1)$$

Or, transforming as before with the help of the first boundary condition in (9), we get

$$r_0=\rho.\frac{ze^2}{m_0v^2}(1-\beta)^{\frac{1}{2}}(\operatorname{cosec}\tfrac{1}{2}\theta-1)\frac{2\pi ze^2}{hc}.\frac{v}{c}\cos^2\tfrac{1}{2}\theta\sin\tfrac{1}{2}\theta\,I \qquad \ldots \quad (11.2)$$

where

$$I=\cos k'r_0\left(\frac{\pi}{2}-k'r_0\right)+\sin k'r_0(C-\log(k'r_0)) \qquad \ldots \quad (11.2)$$

C being Euler constant.

On adding we get from (9.1) and (11.2)

$$r_0=\rho.\ \frac{ze^2}{m_0v^2}\ (1-\beta^2)^{\frac{1}{2}}(\operatorname{cosec}\tfrac{1}{2}\theta-1)\left(1+\frac{2\pi ze^2}{hc}\cdot\frac{v}{c}\cos^2\tfrac{1}{2}\theta\sin\tfrac{1}{2}\theta\right) \qquad (11.4)$$

being the corrected critical approach. It is obvious that (11.4) reduces to (9.1) when z is small. Thus, to a first approximation, one may use the uncorrected critical approach given in (9.1).

APPENDIX

The general value of the Legendre function $P_l^m(\mu)$ is (Hobson, 1931)

$$P_l^m(\mu)=\frac{1}{\Gamma(1-m)}\left(\frac{1+\mu}{1-\mu}\right)^{\frac{1}{2}m} F(-l,\ l+1\ ;\ 1-m\ ;\ \tfrac{1}{2}(1-\mu)) \qquad \dots\ (12)$$

where $\mu(=\cos\theta)$ is restricted to be real and l, m are real but unrestricted. F in (12) is the well-known hypergeometric function. Let us now consider some special cases.

Case I :—Put $l=+\frac{1}{2}$, $m=-\frac{1}{2}$ We have from (12)

$$P_{\frac{1}{2}}^{-\frac{1}{2}}(\mu)=\frac{1}{\Gamma(\frac{3}{2})}\left(\tan\frac{\theta}{2}\right)^{\frac{1}{2}}F(-\tfrac{1}{2},\ \tfrac{3}{2}\ ;\ \tfrac{3}{2}\ ;\ \tfrac{1}{2}(1-\mu))$$

$$=\frac{\sqrt{2}}{\Gamma(\frac{1}{2})}\ (\sin\theta)^{\frac{1}{2}} \qquad \dots\ (12.1)$$

Case II :—Put $l=-\frac{1}{2}$, $m=+\frac{1}{2}$. We have from (12)

$$P_{-\frac{1}{2}}^{\frac{1}{2}}(\mu)=\frac{1}{\Gamma(\frac{1}{2})}\left(\cot\frac{\theta}{2}\right)^{\frac{1}{2}}F(\tfrac{1}{2},\ \tfrac{1}{2}\ ;\ \tfrac{1}{2}\ ,\ \tfrac{1}{2}(1-\mu))$$

$$=\frac{\sqrt{2}}{\Gamma(\frac{1}{2})}\ (\sin\theta)^{-\frac{1}{2}} \qquad \dots\ (12.2)$$

Case III :—Put $l=+\frac{1}{2}$, $m=+\frac{1}{2}$. We have from (12)

$$P_{\frac{1}{2}}^{\frac{1}{2}}(\mu)=\frac{1}{\Gamma(\frac{1}{2})}\left(\cot\frac{\theta}{2}\right)^{\frac{1}{2}}F(-\tfrac{1}{2},\ \tfrac{3}{2}\ ;\ \tfrac{1}{2}\ ,\ \tfrac{1}{2}(1-\mu)) \qquad \dots\ (12.3)$$

Now, it may be easily proved from the definition of hypergeometric function that

$$F(-n,\ \beta+1\ ;\ \beta\ ;\ -z)=F(-n,\ \beta\ ;\ \beta\ ;\ -z)+\frac{nz}{\beta}F(-n+1,\ \beta\ ;\ \beta\ ;\ -z) \qquad (12.4)$$

Thus from (12.3)

$$P_{\frac{1}{2}}^{\frac{1}{2}}(\mu)=\frac{\left(\cot\frac{\theta}{2}\right)^{\frac{1}{2}}}{\Gamma(\frac{1}{2})}\ \{F(-\tfrac{1}{2},\ \tfrac{1}{2}\ ;\ \tfrac{1}{2}\ ;\ \tfrac{1}{2}(1-\mu))-\tfrac{1}{2}(1-\mu)F(+\tfrac{1}{2},\ \tfrac{1}{2}\ ;\ \tfrac{1}{2}\ ;\ \tfrac{1}{2}(1-\mu))\}$$

$$=\frac{\sqrt{2}}{\Gamma(\frac{1}{2})}\ \frac{\cos\theta}{(\sin\theta)^{\frac{1}{2}}} \qquad \dots\ (12.5)$$

The above results may also be obtained from an alternative general formula given by Hobson (*l.c.*), *viz*,

$$P_l^m(\mu) = 2^m \cos\frac{l+m}{2}\pi \frac{\Gamma\left(\frac{l+m-1}{2}+1\right)}{\Gamma\left(\frac{l-m}{2}+1\right)\Gamma(\frac{1}{2})}(1-\mu^2)^{\frac{1}{2}m} F\left(\frac{l+m+1}{2}, \frac{m-l}{2}; \tfrac{1}{2}; \mu^2\right)$$

$$+ 2^{m+1} \sin\frac{l+m}{2}\pi \frac{\Gamma\left(\frac{l+m}{2}+1\right)}{\Gamma\left(\frac{l-m-1}{2}+1\right)\Gamma(\frac{1}{2})} \mu(1-\mu^2)^{\frac{1}{2}m} F\left(\frac{l+m+2}{2}, \frac{m-l+1}{2}; \tfrac{3}{2}; \mu^2\right)$$

where l and m are unrestricted. ... (13)

18, RAMKANTO BOSE STREET,
CALCUTTA.

REFERENCES

Hobson, E. W., 1931, Theory of Spherical and Ellipsoidal Harmonics (Cambridge)

Kar, K. C., 1937, *Phil. Mag.*, **24**, 971.

Kar, K. C., Ghosh, M. and Mukherjee, K. K., 1937, *Phil. Mag.*, **24**, 964.

Kar, K. C., and Mukherjee, K. K., 1934, *Phil. Mag.*, **17**, 995

Mott, N. F., 1929, *Proc. Roy. Soc.*, **124**, 425

MEASUREMENT OF HIGH ROTATIONAL SPEED*

By SUDHANSU DATTA MAJUMDAR

(Plate VI)

ABSTRACT. The method is an application of the stroboscopic principle Intermittent light of very regular frequency is produced by allowing the light reflected from a mirror attached to one prong of an electrically maintained tuning fork to pass through a narrow slit. This light is then reflected from a slightly tilted mirror fixed to the rotating turbine of the centrifuge; as a result, a circle of bright dots appears on a screen placed at a suitable distance The number of these dots is equal to the denominator of the ratio of the frequency of rotation to that of vibration. To obtain the numerator the slit is moved a little away from the zero-position of vibration of the image of the light source. Each dot splits up into two which again coincide. The displacement of the slit from the zero position necessary to get this coincidence is measured, and from this the numerator is calculated The method is capable of a very high degree of accuracy

After the invention of the ultra-centrifuge by Svedberg it became necessary to measure rotational speeds ranging from 500 to 3,000 rev. per sec. Various methods have been suggested from time to time by different workers in the line. Of these a brief account is given below for convenience of comparison. In simplicity, accuracy and range of applicability, however, the stroboscopic method described here seems to have superseded all the others so far adopted for measuring high rotational speed.

(1) The method usually adopted in the earlier work was to view the rotor or turbine of the centrifuge stroboscopically through perforations near the periphery of a rotating disc. The speed of rotation of the disc was maintained at a constant value which was either known or determined by some suitable means. The chief source of inaccuracy in this experiment is that it is almost impossible to keep the speed of rotation of the disc sufficiently uniform for any accurate measurements. Another disadvantage is that with such a stroboscope we can measure only speeds which are integral multiples of the speed of the disc and it is also difficult to know which one of the integral multiples we are measuring.

2. "Recently a more convenient method has been developed by Svedberg, Björnstähl and McFarlane. A portion of the rotor shaft was magnetized lamellarily (by surrounding it with a piece of the same kind of steel during the process of magnetization) and a two-pole stator of a total resistance of 240 ohms and wound with 0.10 mm copper wire was mounted in the centrifuge casing so as to surround this portion of the rotor. When the centrifuge is running an A. C. current of the same frequency as the speed of the rotor is generated" (quoted from "The Ultra-centrifuge" by Svedberg and Pedersen). This current is then amplified and its frequency determined by producing Lissajous figures in the cathode ray oscillograph. The method is accurate and is capable

---

* Communicated by Prof. S. N. Bose, Khaira Professor of Physics, Calcutta University.

of measuring any speed, its only drawback being that the experimental arrangements involved in its use are rather too complicated.

3. Another stroboscopic method due to Harvey (1934) is to illuminate the turbine by means of a neon lamp fed by an intermittent electric current. The interrupted electrical contacts are made by pressing a carbon brush of rectangular section against the rim of a metallic toothed-wheel clamped between two bakelite discs of the same outer diameter. The wheel is made to rotate at a constant speed by means of a synchronous motor. This method is subject to all the disadvantages of the first method.

4. A fourth method due to Snoddy and Beams (1937) is to induce an A. C. current in a coil by fixing a small magnet to the rotor or turbine of the centrifuge. The coil is connected across an A. C. bridge consisting of 4 fixed non-inductive resistances, but in series with one of these is included a variable capacity and a variable inductance which enable the bridge to be balanced at the induced frequency. Though this method is simple the accuracy of the electrical measurements cannot be very high.

For other papers on speed measurement see (1) Pickels (1938) and (2) Bjornstähl (1939).

EXPERIMENTAL ARRANGEMENT

The method is a simple application of the stroboscopic principle. Light from a straight filament lamp was brought to a focus at a distance of about a meter and a half after reflection from a plane mirror attached to one prong of an electrically driven tuning fork of known frequency which was 256 in the

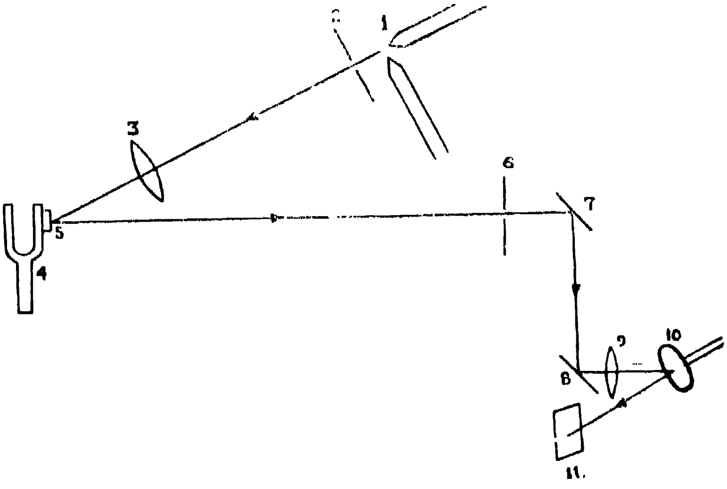

Fig. 1

1. Carbon arc. 2. Narrow horizontal slit. 3. Condensing lens. 4 Electrically maintained tuning fork. 5 Plane mirror attached to a prong of the fork. 6 horizontal slit for producing intermittence of light 7. Movable plane mirror. 8. Fixed plane mirror. 9. Condensing lens, 10. Tilted mirror fixed to the turbine or rotor of the centrifuge, 11. Ground glass screen.

experiment performed (see Fig. 1.) The filament was horizontal and the plane of vibration of the fork vertical so that with the vibration of the fork the image of the filament vibrated transversely. A narrow horizontal slit was then placed so as to coincide exactly with the filament image when the fork did not vibrate. As the fork was then set into vibration the slit allowed light to pass through it only intermittently with a frequency double that of the fork, *i.e.*, 2 × 256 = 512 in the present case. A condensing lens was then placed after the slit. Owing to the approximate parallelism of light coming through it this lens condensed the light into a small bright spot on a screen placed at the proper distance. Now a plane mirror was attached to the rotor of the centrifuge such that its normal made a very small angle of a few degrees with the axis of rotation. This mirror was placed after the lens and the light coming through the lens was first reflected from this mirror and then brought to a focus on the screen. With this arrangement when the fork was at rest and the mirror was made to rotate, the spot of light on the screen moved, giving rise to a bright circular ring of small width. This was due to the inclination of the normal to the mirror to its axis of rotation. When, however, the fork was vibrating and at the same time the mirror was made to rotate with slowly accelerated speed, this circular ring broke up into a number of bright dots slowly moving round the circle. This phenomenon was a result of the intermittent nature of light falling on the mirror, and occurred only when the frequency of rotation bore any simple ratio to the frequency of vibration of the fork. For example, when the frequency of rotation was any even integral multiple of 256 only one dot appeared, and when it was any odd integral multiple of 256 the number of dots was two.

THEORY

Let n be the frequency of the fork and $n \times p/q$ the frequency of rotation to be measured, where p/q is a fraction in its lowest terms. The frequency of intermittence is therefore $2n$ and that of rotation can be written equal to $2n \times p/2q$. If p is odd then p and $2q$ are also relatively prime and therefore $2q$ equidistant dots will appear on the circle. If p is even (equal to $2m$, say) then $p/2q = m/q$ and therefore q equidistant dots will appear, where q must be an odd number in this case. So the number of dots gives us complete information about the denominator of the fraction p/q. These remarks are valid if the slit is placed exactly at the zero-position of vibration of the filament image. To determine the numerator of p/q the slit is to be placed a little away from the zero-position, *i.e.*, at a position whose distance from the zero-position measured in phase angle is θ, say. For this eccentric position of the slit the interval between two consecutive flashes will no longer be $1/2n$ but alternately $\frac{1}{2n} - \frac{2\theta}{2\pi}.\frac{1}{n}$ and $\frac{1}{2n} + \frac{2\theta}{2\pi}.\frac{1}{n}$. The 1st, 3rd, 5th,...... flashes, *i.e.*, the flashes of odd order will, however, give rise to a system of q equidistant dots, and the 2nd, 4th, 6th...... flashes, *i.e.*, the flashes of even order will give rise to a different system of q equidistant dots on the circle. The two systems may or may not coincide. The angular distance between the two systems is $2\pi n.\frac{p}{q}\left(\frac{1}{2n}-\frac{2\theta}{2\pi}.\frac{1}{n}\right)$. This is equivalent to $2\pi n.\frac{p}{q}\left(\frac{1}{2n}-\frac{2\theta}{2\pi}.\frac{1}{n}\right)-2\pi\frac{k}{q}$ where k is any integer. If p is odd it is equivalent to $2\pi.\frac{1}{2q}-\frac{2p\theta}{q}$ and when p is even it is equivalent to $-\frac{2p\theta}{q}$ Therefore if the no. of dots is odd (for zero-position of the slit), then each dot will split up into two dots separated by an angular distance $-2p\theta/q$ as soon as the slit is displaced from its zero-position through a small phase-angle θ. If the no. of dots is even no such splitting up of the dots will take place, only the symmetry in the distribution of the dots round the circle will be lost.

The condition of coincidence of the two systems is

$$p\left(\frac{1}{2}-\frac{\theta}{\pi}\right)-k=0 \quad \text{or} \quad p\theta=\pi.\frac{p-2k}{2}$$

If p is odd then this gives

$$p\theta=\ldots\ldots\ldots-\frac{3\pi}{2},\ -\frac{\pi}{2},\ +\frac{\pi}{2},+\frac{3\pi}{2},\ldots\ldots\ldots$$

If p is even then

$$p\theta=\ldots\ldots\ldots-2\pi,\ -\pi,\ 0,\ +\pi,\ +2\pi,\ldots\ldots\ldots$$

It may not be out of place here to answer a question which naturally presents itself. If the frequency ratio be 1/7.001 instead of exactly 1/7 will there be 7001 dots on the circle? The answer will be in the negative. Owing to the failure of the persistence of vision such a large number of dots are never found to appear on the circle. Instead of 7001 dots there will be only 7 dots on the circle rotating with a frequency from which the exact ratio 1/7.001 can be calculated out.

Difficulties in measuring high speed.—The method described above is quite suitable for speeds below 400 r.p.s. A difficulty arising out of the duration of the flashes, however, creeps in as one tries to measure higher and higher speeds. Let a be the width of the filament image focussed on the slit and b the width of the slit and let $w=a+b$. Now if L be the amplitude of vibration of the filament image, then the duration of a flash is $T=\frac{w}{2\pi L}.\frac{1}{n}$ sec. If T is not sufficiently small then for high speeds each dot will be elongated so as to cover a considerable part of the circumference of the circle on which the dots appear. The value of T can be diminished either by decreasing w or by increasing L. As there is a practical limit to the extent to which w can be decreased the only other alternative is to diminish T by increasing L. This has been easily accomplished by attaching two plane mirrors one to each prong of the fork such that they are parallel and their reflecting surfaces face each other. Light from the lamp is now multiply reflected from these two mirrors before coming to a

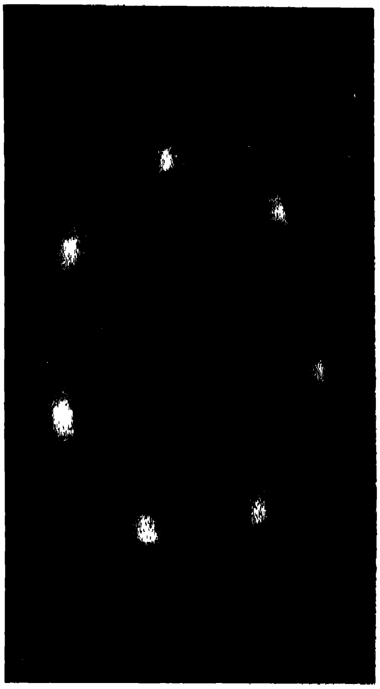

Fig. 2

Photograph showing 7 dots at a speed of 256 × 43/7 = 1572·57 r.p.s.

focus on the slit. If there are r reflections the amplitude of vibration (for a single reflection) is magnified r times. In the actual experiment 8 reflections were taken which gave an amplitude equal to 20 cm. The value of a was 4 mm.

$$\therefore \quad T = \frac{\cdot 4}{2\pi \times 20} \cdot \frac{1}{n} = \frac{1}{300} \cdot \frac{1}{n} \quad \text{sec. approx.}$$

Therefore for a rotational speed equal to $10n$ (=2560 r.p.s) each dot will cover an arc subtending an angle 360° × 1/30. So at the stated speed we will be able to distinguish dots on the circle if their number does not exceed 30. But it should be noted that as one tries to shorten the duration of flashes in this way the intensity of light falls off considerably. This difficulty has been removed by taking instead of an ordinary straight filament lamp a carbon arc as the light source with a water-cooled slit placed very close to it.

PRACTICAL DETERMINATION OF THE NUMERATOR OF p/q

To determine p one is to move the slit away from the zero-position of vibration of the filament image and measure the phase angle θ through which it is moved to get the next coincidence of dots in pairs. If the number of dots is even $p = \pi/2\theta$ and if it is odd $p = \pi/\theta$. Instead of doing this, however, it is more convenient to count the total no. of coincidences that occur as one moves the slit through a fixed phase angle $\pi/4$. From this number N the numerator p can be easily found out. For example, if the no. of dots be odd (for zero-position of the slit) and if there is a coincidence at the position $\pi/4$ of the slit then p is equal to 4 times the no of coincidences observed as the slit is moved from the zero position to the final position, in other words $p = 4N$ in this case. It is easy to see how p and N are related to each other in other cases. A difficulty, however, arises as one moves the slit away from the zero position. For if the displacement of the slit is fairly large, the light passing through it will no longer fall on the mirror attached to the rotor. This difficulty has been removed by using two parallel mirrors (Fig. 1) with their reflecting surfaces facing each other, one rigidly fixed to the slit and moving with it and the other kept fixed just in front of the mirror attached to the rotor. Both the mirrors are inclined approximately at 45° to the direction of the incident light which after passing through the slit is now successively reflected from the two parallel mirrors and therefore continues to fall on the mirror attached to the rotor inspite of the motion of the slit. The condensing lens may be placed somewhere between the fixed mirror and the rotor.

DISCUSSION

The advantage of this method is its striking simplicity and the remarkably high degree of accuracy attained by it if proper precautions are taken. A difference of 1/100 cycle per sec. is easy to detect by this method. Great precautions are, however, necessary in order to attain this high order of accuracy. For example, the fork must be of carefully tempered steel and should be maintained preferably by using thermionic valves so that the process of maintenance itself may not affect the vibration of the fork. Finally, the fork should be calibrated by comparison with a standard gravity pendulum at a definite temperature and the necessary temperature corrections applied to the frequency of the fork. Another advantage which is usually lacking in stroboscopic methods is that this method enables one to measure speeds which are not merely integral multiples of the frequency of intermittence but also almost any fractional speed. To measure any fractional speed the only thing required is to devise a suitable means of rapidly counting a large number of dots. The difficulty of counting arises out of the rotation of the dots which are not found to be steady even for a fraction of a second. A method of counting may be to compare the bright dots with a number of opaque dots distributed over the same circle. If, during rotation, the bright dots are at times completely extinguished we can be sure that the no. of bright dots is equal to that of the opaque dots.

The photograph given here (Plate VI) shows 7 dots at a speed of

$$256 \times \frac{44}{7} = 1609.1 \text{ r.p.s.}$$

I am grateful to Prof. M. N. Saha for his kind interest in the work, and to Prof. S. N. Bose for kindly going through the paper. Thanks are also due to the authorities of the B. S. I. R under whose grant-in-aid the work has been carried out for their kind permission to publish this paper.

Palit Laboratory of Physics
University College of Science,
Calcutta

REFERENCES

Björnstahl, 1939, *Rev. Sci. Instruments*, **10**, 258-260.
Harvey, 1934, *Biol Bull.*, **66**, 48-54.
Pickels, 1938, *Rev. Sci. Instruments*, **9**, 354-358
Snoddy and Beams, 1937, *Science*, **85**, 273-274
Svedberg and Pedersen, 1940. The Ultra-centrifuge (Oxford).

WAVE-TREATMENT OF PROPAGATION OF ELECTRO-MAGNETIC WAVES IN THE IONOSPHERE

BY M. N. SAHA* AND B. K. BANERJEA

ABSTRACT. Wave-equations for the propagation of e m. waves through the ionosphere have been obtained by the use of a new mathematical method involving the use of dyadic analysis introduced by Gibbs Expressions for steady current conductivity of the ionosphere have been obtained by this method and the results are concordant with those of Chapman; an extra term for the conductivity, which is more prominent in the F_2-layer has been obtained.

It has been shown that the wave is split up into three waves, as in Zeeman effect, one of which is ordinary, the other two extraordinary, in accordance with observations by Toshniwal, and Harang.

1 INTRODUCTION

The subject of propagation of electromagnetic waves in the ionosphere appears to be at the present time in a rather confused state. Appleton (1932), in his pioneering work, used what is now commonly known the ray treatment, *i.e.*, starting from Maxwell's equations, he obtained a value of the refractive index of the e.m. waves in terms of the electron concentration, the earth's magnetic field and the damping coefficient of electrons. He further postulated that the wave gets reflected when the refractive index vanishes. From the two values of refractive index it was deduced that the wave splits up into two, one ordinary and the other extraordinary and the sense of polarisation of each wave was determined. The condition of reflection of the extraordinary wave is, however, satisfied, at two distinct levels given by the condition $p_0^2=p^2\pm pp_h$. It appears to have been assumed that only one of these waves, corresponding to the negative sign existed. Toshniwal (1935) and Harang (1936) have however, obtained at times reflections corresponding to the conditions $p_0^2=p^2+pp_h$, so that it is legitimate to think that the wave really gets split into three components on entry into the ionosphere, one of which fails usually to get reflected owing to heavy absorption. Further, we have to explain the pheuomena of M-reflections, which prove that the wave does not get completely reflected even when $\mu=0$, but may leak through the ion-layer in considerable intensity, and get reflected from a higher layer.

The wave treatment was first attempted by Hartree (1929, 1931) in three important papers. The papers of Hartree are extremely difficult to follow on account of the difficult notations used and some unnecessary complications introduced. He used throughout the notation of dyadics, introduced by Gibbs.

---

* Fellow of the Indian Physical Society.

This notation, though much convenient for mathematical working is not generally familiar and to make the deductions intelligible the results have to be transcribed to ordinary notations which was not carried out by Hartree. Hartree obtained the displacement of the electron or the ion as **S.E** where S is a tensor, **E** = Electric field. This part is rendered rather complicated because the electron is regarded as bound by a quasi-elastic force. From the expression for S, he obtained an expression for σ called the scattering tensor. The underlying physical idea is borrowed from a paper by Darwin (1925), who has shown that almost all optical phenomena, *e.g.* reflection and refraction can be explained in terms of scattering by elementary constituents of the medium. Hartree has shown from the equivalence of two different processes that the equation of propagation of the electromagnetic waves in the ionosphere continues to obey the Maxwellian form. The treatment was also rendered complicated by the introduction of the term β, the Lorentz polarisation term which he took not much far from $1/3$. It has, however, been shown by Darwin (1934) that $\beta = 0$, and this considerably simplifies Hartree's method. The expression for refractive index was obtained by considering the case of normal incidence in a stratified medium where μ is supposed to be constant. He ultimately obtains the same result as Appleton. So far his treatment led to a justification rather than laying the foundations of a rigorous wave treatment. In a later paper he takes the wave equation with a variable μ and tries to solve this equation for a few simple cases but it is obvious none of these assumptions corresponds to reality.

Saha, Rai and Mathur (1937) expressed the displacement of the ions in simpler analytical form, which may be shown identical with those of Hartree in spite of the apparent differences in form. From this displacement they obtained the value of the dielectric tensor for a stratified medium and ultimately obtained the same expression for μ as that of Appleton. The wave treatment was applied in a simple case for the O-wave and the penetrability of the electron barrier for a simple case was deduced.

In the present paper the foundations of a rigorous wave treatment have been laid down and the expressions for refractive index, conductivity and direct current conductivity have been deduced. The solution of the wave-equations has not yet been tried.

2. THE DISPLACEMENT OF THE IONS IN THE IONOSPHERE

The equation of motion of the charged ions referred to any system of axes can be written in the form

$$\frac{d^2\mathbf{r}}{dt^2} + \nu\frac{d\mathbf{r}}{dt} + \frac{e}{m_0 c}\left[\mathbf{H} \times \frac{d\mathbf{r}}{dt}\right] = \frac{e\mathbf{E}}{m_0} \tag{1}$$

where $\mathbf{r}$ = displacement vector of the ions with components (ξ, η, ζ)

m_0 = mass of the ions

ν = collision frequency of the ions

$\mathbf{H}$ = Earth's magnetic field with direction cosines l, m, n.

$\mathbf{E}=\mathbf{E}_0\cos pt$, the electric vector of the incident e.m. wave with direction cosines l', m', n'.

The effect of the magnetic vector and space charge have been omitted as usual. The notation conforms as closely as possible to those used by Appleton (1932) and Saha, Rai and Mathur (1937).

It can be easily verified that the solution of the above equation with $\mathbf{E}=\mathbf{E}_0\cos pt$ is the real part of the solution when we put $\mathbf{E}=\mathbf{E}_0e^{ipt}$; we use $\mathbf{E}$ in this form, because the solution is now easy to obtain. The quantity analogous to static conductivity now comes out to be complex (Stratton, 1939) whose real part gives ordinary conductivity, imaginary part gives the deviation of the refractive index from unity.

Starting with $\mathbf{E}=\mathbf{E}_0e^{ipt}$ and introducing the notations

$$p_0^2=\frac{4\pi Ne^2}{m_0}\ ; \qquad \alpha=i\nu p-p^2\ ; \qquad p_h=\frac{e\mathrm{H}}{m_0c}\ ;$$

$$\beta=ipp_h\ ; \qquad \mathbf{r}=(\xi,\eta,\zeta)e^{ipt}$$

and breaking up the above equation into components we get

$$\begin{aligned}\alpha\xi+ipp_h(m\zeta-n\eta)&=\frac{e}{m_0}\,l'\mathrm{E}_0\\ \alpha\eta+ipp_h(n\xi-l\zeta)&=\frac{e}{m_0}\,m'\mathrm{E}_0\\ \alpha\zeta+ipp_h(l\eta-m\xi)&=\frac{e}{m_0}\,n'\mathrm{E}_0\end{aligned} \qquad \ldots \quad (2)$$

Solving these equations by the usual determinant method, we have

$$\xi=\frac{e\mathrm{E}_0}{m_0}\,[l'(\alpha^2+\beta^2l^2)+m'(\alpha\beta n+\beta^2ml)+n'((\beta^2nl-\beta\alpha m)]/[\alpha(\alpha^2+\beta^2)] \quad \ldots \quad (3)$$

$$\eta=\frac{e\mathrm{E}_0}{m_0}\,[l'(\beta^3ml-\beta\alpha n)+m'(\alpha^2+\beta^2m^2)+n'(\beta^2mn+\beta\alpha l)]/[\alpha(\alpha^2+\beta^2)]$$

$$\zeta=\frac{e\mathrm{E}_0}{m_0}\,[l'(\beta^2nl+\beta\alpha m)+m'(\beta^2mn-\beta\alpha l)+n'(\alpha^2+\beta^2n^2)]/[\alpha(\alpha^2+\beta^2)]$$

Let $\boldsymbol{\sigma}$ denote the complex conductivity. We have

$$\boldsymbol{\sigma}.\mathbf{E}=\text{current}=-\mathrm{N}e\frac{d\mathbf{r}}{dt}=-ip\mathrm{N}e\mathbf{r} \qquad \ldots \quad (4)$$

Substituting the value of $\mathbf{r}$ from (3) we get $\boldsymbol{\sigma}$ in the tensor form

$$\boldsymbol{\sigma}=\frac{-m_0/ip\mathrm{N}e^2}{\alpha(\alpha^2+\beta^2)}\begin{vmatrix}\alpha^2+\beta^2l^2 & \beta^2ml-\beta\alpha n & \beta^2nl+\beta\alpha m\\ \beta^2lm+\beta\alpha n & \alpha^2+\beta^2m^2 & \beta^2mn-\beta\alpha l\\ \beta^2nl-\beta\alpha m & \beta^2mn+\beta\alpha l & \alpha^2+\beta^2n^2\end{vmatrix} \qquad \ldots \quad (5)$$

Let us next find out the principal axes of the tensor ellipsoid by using the Hamilton-Cayley method. The principal components are given by the roots of the equation,

$$\lambda^3 - \Phi_1\lambda^2 + \Phi_2\lambda - \Phi_3 = 0 \qquad \dots \quad (6)$$

where Φ_1 = spur of the tensor, σ, $q = x, y, z$

$\Phi_2 = \Sigma(\sigma_{qq}\sigma_{ss} - \sigma_{qs}\sigma_{sq})$ s, $q = x, y, z$, $s \neq q$

Φ_3 = Determinant of σ.

We obtain from (5)

$$\Phi_1 = 3\alpha^2 + \beta^2;\ \Phi_2 = 3\alpha^2(\alpha^2 + \beta^2);\ \Phi_3 = \alpha^2(\alpha^2 + \beta^2)^2$$

Hence the cubic equation reduces to

$$\lambda^3 - (3\alpha^2 + \beta^2)\lambda^2 + 3\alpha^2(\alpha^2 + \beta^2)\lambda - \alpha^2(\alpha^2 + \beta^2)^2 = 0$$

or

$$[\lambda - (\alpha^2 + \beta^2)]\,[\lambda - (\alpha^2 + i\alpha\beta)]\,[\lambda - (\alpha^2 - i\alpha\beta)] = 0 \qquad \dots \quad (7)$$

If $\nu = 0$, α, $i\alpha\beta$, and β^2 are all real, and the roots are all real, such a dyad has been classified by Gibbs as a tonic dyad.

In general case, for $\nu \neq 0$, we separate the complex conductivity tensor $\boldsymbol{\sigma}$ in (5) into real, and imaginary parts. Then forming the corresponding Hamilton-Cayley equations for the real and the imaginary parts we get the roots for $R_e\boldsymbol{\sigma}$ as

$$\lambda_1 = \frac{Nc^2}{mp}\cdot\frac{\nu}{p^2 + \nu^2};\ \lambda_2 = \frac{Nc^2}{mp}\cdot\frac{\nu + ip_h}{p^2 + (\nu + ip_h)^2};\ \lambda_3 = \frac{Nc^2}{mp}\cdot\frac{\nu - ip_h}{p^2 + (\nu - ip_h)^2} \qquad \dots \quad (8)$$

and for $I_m\boldsymbol{\sigma}$

$$\lambda_1 = \frac{Nc^2}{m}\cdot\frac{1}{p^2 + \nu^2};\ \lambda_2 = \frac{Nc^2}{m}\cdot\frac{1}{p^2 + (\nu + ip_h)^2};\ \lambda_3 = \frac{Nc^2}{m}\cdot\frac{1}{p^2 + (\nu - ip_h)^2} \qquad \dots \quad (9)$$

Dyads of this type, having two complex conjugate roots of the H. C. equation are classified by Gibbs as cyclotonic dyad. All the properties of the ionosphere are of this type.

Let us next find out the orientation of the characteristic principal axis of the tensor σ, to the earth's magnetic field. We consider a vector $\boldsymbol{\rho}$ such that

$$\sigma\rho = \lambda\rho$$

where λ is a proportionality factor. If I_0 be the idem factor

$$\sigma\rho = \lambda I_0\rho \qquad \text{or} \quad (\boldsymbol{\sigma} - \lambda I_0)\rho = 0$$

i.e.

$$\left.\begin{aligned} (\sigma_{11} - \lambda_1)L + \sigma_{12}M + \sigma_{13}N &= 0 \\ \sigma_{21}L + (\sigma_{22} - \lambda_1)M + \sigma_{23}N &= 0 \\ \sigma_{31}L + \sigma_{32}M + (\sigma_{33} - \lambda)N &= 0 \end{aligned}\right\} \qquad \dots \quad (10)$$

where L, M, N are the direction cosines of the principal axis. Substituting $\lambda = \alpha^2 + \beta^2$ and the corresponding values of σ_{11}, σ_{12}, etc., and remembering that

$$L^2 + M^2 + N^2 = 1$$

we get

$$L = \pm l, \quad M = \pm m, \quad N = \pm n \qquad \ldots \quad (11)$$

We thus see that the real characteristic principal axis of the tensor $\boldsymbol{\sigma}$ coincides with the earth's magnetic field. Similarly we can show that the other properties like ordinary conductivity, dielectric constant, etc., have the same characteristic principal axis. The other two axes of the cyclotonic dyad are in a plane perpendicular to this axis, and may be oriented arbitrarily.

Let us next choose a new system of axes with the direction of the earth's magnetic field as the X-axis, Z-axis being in the magnetic meridian and Y axis horizontal perpendicular to the magnetic meridian. Referred to this new coordinate system, let us now express the displacements and the tensor $\boldsymbol{\sigma}$ in the new coordinates, We put $l = 1$, $m = n = 0$ in (5). Then

$$\boldsymbol{\sigma} = \frac{-ipNe^2/m_0}{\alpha(\alpha^2 + \beta^2)} \begin{vmatrix} \alpha^2 + \beta^2 & 0 & 0 \\ 0 & \alpha^2 & -\alpha\beta \\ 0 & \alpha\beta & \alpha^2 \end{vmatrix} \qquad \ldots \quad (12)$$

and from (3)

$$\xi = -\frac{eE}{m_0}\,[l'(\alpha^2+\beta^2)]/[\alpha(\alpha^2+\beta^2)] \qquad \ldots \quad (13)$$

$$\eta = -\frac{eE}{m_0}\,[\alpha^2 m' + \beta\alpha n']/[\alpha(\alpha^2+\beta^2)]$$

$$\zeta = \frac{eE}{m_0}\,[\alpha^2 n' - \beta\alpha n']/[\alpha(\alpha^2+\beta^2)]$$

Let us next form that the real parts of the displacements, which are the true solutions of equation (1) with $E = E_0 \cos pt$. We have, putting $E(l', m', n') = (E_x, E_y, E_z,)$

$$\text{Re}\,\xi = -\frac{eE_x}{m_0(p^2+\nu^2)}\left[\cos pt - \frac{\nu}{p}\sin pt\right] \qquad \ldots \quad (14)$$

$$(\text{Re}\,\eta \pm i\,\text{Re}\,\zeta) = -\frac{e(E_y \pm iE_z)}{m_0[p^2 + (\nu \pm ip_h)^2]}\left\{\cos pt - \frac{\nu \pm ip_h}{p}\sin pt\right\}$$

From the above expressions, we can easily obtain expressions for the steady current electrical conductivity in the ionosphere as obtained by Schuster, Chapman and Pedersen. We have to put $p = 0$

We get

$$\dot{\xi} = -\frac{cE_x}{m_0}\,; \quad \dot{\eta} = \frac{c}{m_0(p_h^2+\nu^2)}[\nu E_y + p_h E_z]; \quad \dot{\zeta} = \frac{c}{m_0(p_h^2+\nu^2)}[\nu E_z - p_h E_y)$$

We have therefore $I_x = Ne\dot{\xi} = \frac{Ne^2}{m\nu} E_x$ and

$$\sigma_x = I_x / E_x = \text{conductivity parallel to the magnetic field} = \frac{Ne^2}{m\nu} \quad \ldots \quad (15)$$

If now $E_z = o$, *i.e.* the e.m.f. is in the horizontal plane perpendicular to the magnetic meridian, we have

$$\sigma_y = \frac{Ne^2}{m_0} \cdot \frac{\nu}{(\nu^2 + p_h^2)} \quad \ldots \quad (16)$$

This is known as the transverse conductivity.

We have an additional current along the Z-axis, *i.e.*, in the meridian plane perpendicular to the lines of force, and the conductivity

$$\sigma_z = -\frac{Ne^2 p_h}{m_0(\nu^2 + p_h^2)} \quad \ldots \quad (17)$$

If $E_z \neq o$, but $E_x = E_y = o$, we have flow of currents both along Y and Z axes.

We observe from these results that even when ν tends to zero as in the F region, we have a conductivity transverse to the magnetic meridian $= \frac{Ne^2}{m_0} \cdot \frac{p_h}{(\nu^2 + p_h^2)}$ and this has a limiting value $\frac{Ne^2}{m_0 p_h}$

We have thus got an extra term for transverse conductivity, viz. $\frac{Ne^2}{m_0} \cdot \frac{p_h}{(\nu^2 + p_h^2)}$ in addition to those already known but we have not yet had time to examine its probable contribution to the theory of L and S terms in geomagnetism.

3 THE FUNDAMENTAL MAXWELLIAN EQUATIONS

The fundamental equations for the propagation of the e.m. waves in the ionosphere are

$$\nabla \times H = \frac{1}{c}\dot{E} + \frac{4\pi}{c} I. \quad \ldots \quad (18)$$

$$\nabla \times E = -\frac{1}{c}\dot{H}.$$

$$\nabla \cdot E = 4\pi \rho$$

$$\nabla \cdot H = o$$

Here 'I' denotes total current, which requires some elucidation. We have $\mathbf{I} = \sigma.\mathbf{E}$, where $\mathbf{E}$ = total field (*i.e.* sum of incident field plus radiation field due to surrounding ions. Also in the ionosphere, it is customary to take $\rho = o$. Thus (18.1) is modified as

$$\nabla \times H = \frac{1}{c}\dot{E} + \frac{4\pi\sigma.\mathbf{E}}{c}.$$

It can now be easily shown, taking curl of curl E, etc., that E satisfies the equation

$$\nabla^2\mathbf{E} - \frac{\ddot{\mathbf{E}}}{c^2} = -\frac{4\pi}{c^2}.\boldsymbol{\sigma}\dot{\mathbf{E}}$$

or

$$\nabla^2\mathbf{E} + \frac{p^2}{c^2}\left(\mathrm{I}_o + \frac{4\pi i\boldsymbol{\sigma}}{p}\right).\mathbf{E} = o \qquad \ldots \quad (19)$$

and similarly H satisfied the the equation

$$\nabla^2\mathbf{H} - \frac{1}{c^2}\ddot{\mathbf{H}} = -\frac{4\pi}{c}\nabla \times (\boldsymbol{\sigma}.\mathbf{E}) \qquad \ldots \quad (20)$$

Now for $\boldsymbol{\sigma}$ we have to substitute in the case of any coordinate system expressions (5), but it will simplify matters if we introduce the principal coordinates defined in (12). We have then

$$\mathrm{I}_o + \frac{4\pi i\boldsymbol{\sigma}}{p} = \left|\begin{array}{ccc} 1 + \frac{p_o^2}{\alpha} & o & o \\ o & 1 + \frac{p_o^2\alpha}{\alpha^2 + \beta^2} & -\frac{p_o^2\beta}{\alpha^2 + \beta^2} \\ o & + \frac{p_o^2\beta}{\alpha^2 + \beta^2} & 1 + \frac{p_o^2\alpha}{\alpha^2 + \beta^2} \end{array}\right| \qquad \ldots \quad (21)$$

The equations (10) can then be split up into three equations

$$\nabla^2 E_x + \frac{p^2}{c^2}\left(1 - \frac{p_o^2}{p^2 - i\nu p}\right)E_x = o \qquad \ldots \quad (22)$$

$$\nabla^2 E_y + \frac{p^2}{c^2}(bE_y - cE_z) = o$$

$$\nabla^2 E_z + \frac{p^2}{c^2} pE_y + bE_z) = o$$

where

$$b = 1 + \frac{p_o^2\alpha}{\alpha^2 + \beta^2}, \qquad c = \frac{p_o^2\beta}{\alpha^2 + \beta^2}$$

The last two equations had better be written in the form

$$\nabla^2(E_y \pm iE_z) + \frac{p^2}{c^2}\left\{1 - \frac{p_o^2}{p^2 - i\nu p \mp pp_h}.\right\}(E_y \pm iE_z) = o \qquad \ldots \quad (28)$$

From these equations, we see clearly that on entrance into the ionosphere, the three components E_x, $E_y + iE_z$, $E_y - iE_z$ travel with different velocities, depending on p_o^2, ν, and p_h. If these quantities are slowly varying, we can talk of refractive index. The E_x-component (electric displacement parallel to the magnetic field) has the complex refractive index

$$\mu_o = 1 - \frac{p_o^2}{p^2 - ip\nu}$$

and the $E_y + iE_z$, $E_y - iE_z$ components have the refractive indices

$$\mu_e = 1 - \frac{p_0^2}{p^2 - i\nu p \mp p p_h}$$

The analogy with Zeemann-effect is obvious ; $(E_y + iE_z)$ denote anticlockwise circular polarisation and $(E_y - iE_z)$ denote clockwise circular polarisation. If we neglect ν and put $\mu_0 = 0$ we get Appleton's conditions for the reflexion of the o-wave, $p_0^2 = p^2$, and if we put $\mu_e = 0$, we get the two conditions for the reflexion of the two extraordinary waves $p_0^2 = p^2 \mp p p_h$, which have different sense of polarisation.

The complete solution of the equations (21), however, are rather difficult, for we are using a coordinate system which, except at the magnetic equator, and at the magnetic poles, cannot be linked to the local coordinates in a simple manner.

At the magnetic equator, the X and Y axes are horizontal and Z-axis is vertical. In a vertical propagation of the e.m. wave, $E_z = 0$, and we have only E_x and E_y definite. The reflected wave will therefore have its o-component polarized parallel to the magnetic field, the X-component polarized parallel to the Y-axis, *i.e.*, perpendicular to the magnetic field in a horizontal direction. We have, however, not yet tried to evaluate E_x, E_y in terms of the amplitudes of the wave sent out by the antenna.

For the magnetic pole, the X-axis is vertical, and for a vertical propagation we have $E_x = 0$, and we have only $E_y \pm iE_z$, *i.e.*, two circularly polarized X-waves. We have to obtain the reflexion coefficient from a solution of (21), which will be attempted in a future paper.

ACKNOWLEDGMENT

One of us, B. K. Banerjee, has been the recepient of a Research Scholarship from the Radio Research Committee of the Council of Scientific and Industrial Research, and wishes to express his thanks to the Council for facility to work, and permission to publish this paper.

PALIT LABORATORY OF PHYSICS
CALCUTTA UNIVERSITY.

REFERENCES

Appleton, 1932, *Journ. Inst. Elec. Eng.*, **71**, 646.
Chapman and Bartels, 1940, Geomagnetism, Vol. 1, p. 524
Darwin, 1925, *Trans. Camb. Phil. Soc.*, **28**, 1940.
Darwin, 1934, *P R. S.*, **146**, 17.
Gibbs and Wilson, 1907, Vector Analysis.
Harang, 1936, *Terrestrial Magnetism*, **41**, 143.
Hartree, 1929, *Proc. Camb. Phil. Soc.*, **26**, 97.
Hartree, 1931, *Proc. Camb. Phil. Soc.*, **27**, 143.
Saha, Rai and Mathur, 1937, *Proc., Nat. Inst.*, **4**, 53.
Stratton, 1942, Electromagnetic Theory, p. 326.
Toshniwal, 1935, *Nature*, **135**, 471.

19

HIGH PRESSURE CARBON BANDS AND THEIR RELATION TO THE SWAN SYSTEM

By NAND LAL SINGH

ABSTRACT. In this paper the suggestion that the high pressure carbon bands do not form a new electronic system but belong to the $v'=6$ progression of the Swan system is examined in detail. It is shown that available data on these bands do not prove this suggestion. A complete rotational analysis of the bands is expected to decide the point unequivocally and show whether the bands are instances for the proposed phenomenon of inverse induced predissociation.

The high pressure carbon bands were first discovered by Fowler (1910) in the course of his work on the low pressure or Comet-tail bands in tubes containing carbon monoxide at relatively high pressure (100 mm.). The bands rapidly disappeared when the pressure was reduced and they could not be observed in the spark at atmospheric pressure or at a pressure of half an atmosphere with or without capacity. Fowler had obtained these bands along with the Angstrom bands and the Swan bands, though both the latter were very faint. According to him, these bands are double headed and are degraded towards the violet. He did not get these bands in CO_2, petroleum, benzene, CN, or CO mixed with air. These bands were also observed in Borelly's Comet in 1903 and in the Comet of 1910a. The conditions of production of these bands were further investigated by Merton and Johnson (1923). They obtained these bands with greater intensity in condensed discharges in capillary tubes fitted with carbon electrodes. The tubes contained carbon monoxide at pressures of 5 mm. and more. The authors have given a reproduction of these bands photographed under low dispersion. They observed that the Swan bands and the high pressure bands were both present in the light coming from the capillary part of the discharge tube, but the high pressure carbon bands were isolated in the bluish jets where the two ends of the capillary merged into the wider parts of the tube. It was further observed that the introduction of a little CO_2 made the bands disappear which appeared again only after a short while in which time presumably the CO_2 was reduced to monoxide by the carbon electrodes.

Johnson and Asundi (1929) photographed the system in the first order of a 21 ft. grating with a view to doing the rotational analysis of these bands and thereby deciding about their emitter. The discharge tube in their experiment was 60 to 70 cm. long having a bore of about 15 to 20 mm. One of the electrodes at least was made of carbon. The tube was filled with carbon monoxide at a pressure of 20-40 mm. The high pressure carbon bands were strongly developed on passing a condensed discharge from a ¼ K. Watt, 15,000 volt transformer. Further observations indicated that impurities such as hydrogen, carbon-dioxide, water vapour inhibited the formation of these high pressure carbon bands and the tube always attained its best condition after running for about an hour and removing meanwhile any little hydrogen through the palladium regulator attached to the discharge tube. The light filling the wide bore of the discharge tube gave an appearance of dense pale blue puffs of smoke which was rich in high pressure carbon bands. These pale blue puffs were threaded with a green narrow ribbon which showed only the Swan system. By the proper selection of plates and careful search on them the authors were able to record six more bands which along with the previously recorded bands formed one v'' progression ($v'=0$). They represented the bands by the formula

$$\nu = 29212 - (1627v'' - 11.7v''^2) \quad \ldots \quad (1)$$

Table (I) contains the list of bands observed together with their visually estimated intensity and the v'' numbering as proposed by them. The (O−C) values are given in the last column.

TABLE I

v''	Intensity	λ air I.A.	ν vac.	O−C
0	1	3419	29241	+29
1	1	3619.5	27620	−23
2	1	confused	—	—
3	2	4093	24426	−10
4	7	4368.8	22833	− 8
5	15	4680.2	21361	− 8
6	1	V faint	—	—
7	5	5434.9	18394	− 2
8	10	5899 3	16946	+ 2
9	8	6442.3	15518	+ 1
10	6	7083 2	14114	+ 2
11	4	7852.5	12731	0

The close agreement between the coefficients of v'' of this equation and those of v'' in the equation representing the origins of the Swan bands led them to conclude for the first time that the final state of both these systems is the same, the accepted equation for the Swan system representing the origins being

$$\nu = 19379.20 + (1773.42v' - 19.35v'^2) - (1620.28v'' - 11.67v''^2).$$

Thus the two band systems were shown to be due to a common emitter. This emitter is now accepted to be the C_2 molecule on various and sound grounds both theoretical and experimental. The common final level in these two band systems was considered to be the normal state of the C_2 molecule. This has been confirmed lately by absorption experiments (Klemenc and others, 1934). The small difference between the coefficient of v'' in the two equations is well accounted for by the fact that in the equation for the high pressure carbon bands the data on heads have been used while in that for the Swan bands those on the origins are used. The apparent double character of the high pressure bands as seen under low dispersion is due to the condensations which constitute the P and R branches. The high pressure carbon bands then form a band system which consists of only one v'' progression. Numerous examples are, however, known of band systems having only one progression. Even in the same molecule, as for example in CO, we have the Herzberg-Asundi bands and 3—A bands involving different electronic states but having only one progression.

Fox and Herzberg (1937) and later Herzberg (1939) discussing the processes of dissociation, predissociation, and recombination refer to the C_2 molecule. In a three body recombination the energy of formation may be carried away as excitation energy by one or both of the resulting systems. Thus in discharges in CO under high pressure the two carbon atoms formed by dissociation combine to form C_2 while the energy of formation of C_2 may be directly utilised in exciting it. This energy is identified by Herzberg with the excitation energy of the high pressure carbon bands. The process is according to him one of chemiluminescence and the observation of Johnson and Asundi (1929), that the high pressure carbon bands are completely isolated in the smoky puffs outside the discharge while in the path of the discharge itself the bands are absent, support this view. If this is correct, as it seems likely, the lower limit of dissociation energy of C_2 is accurately determined as 3.6 volts. Herzberg, however, goes one step further and suggests that the high pressure carbon bands do not involve a new electronic level but are extensions of the Swan system and form indeed the $v'=6$ progression. If this view is correct, a serious difficulty arises in visualising the process outlined above. One can understand the excitation of $v'=6$ progression in C_2 on the basis of the availability of energy of 3.6 volts, but it is rather surprising that the excitation should exhibit such great selectivity that practically none of the lower vibrational levels are excited. If it is true that the high pressure carbon bands are really extensions of the Swan system, this great selectivity of excitation can only be reconciled by the introduction of a new phenomenon the so-called inverse induced predissociation. Thus according to Herzberg, the two carbon atoms which form C_2 recombine only when they approach each other on a potential curve from which a radiationless transition into the upper state of the Swan bands is possible under the action of a third particle. Once formed the molecule will not predissociate again except after collision (induced predissociation). No other example of such inverse induced predissociation has, however, so far been observed. The observation that the bands are very strong in the glowing cloud surrounding the main path of the discharge in the experimental tube is taken as evidence of the chemiluminescent nature of exciatation brought about according to this mechanism. Asundi and Pant (1942), however, have found in spectra of gases excited by high frequency discharge only these high pressure carbon bands to the exclusion of all other bands of C_2 including those of the Swan system obviously in the path of direct discharge. Before the concept of inverse induced predissociation is invoked, it becomes, therefore, necessary to investigate in detail the experimental evidence for regarding the high pressure carbon bands as extensions of the Swan system. As far as we are aware, no definite evidence has been adduced to prove that the high pressure carbon bands are extensions of the Swan system. Unless this is proved unequivocally, there is no need for the conception of inverse induced predissociation and the value $D(C_2)=3.6$ volts will have to be regarded only as the lower limit.

One argument in support of the view that the high pressure carbon bands are extensions of the Swan system may be that these bands appear to fit in the (v′ v″) scheme for the Swan bands forming the $v'=6$ progression if the following formula* for the heads is used :

$$\nu_h = 19354.9 + (1765.3\nu' - 16.35\nu'^2 - 9\nu'^3) - (1625.9\nu'' - 10.95\nu''^2) + 1.8\nu'\nu'' \quad \ldots \quad \text{(III)}$$

This evidence is collected in Table 2 in which the wave numbers of the band heads, as recorded by Johnson 1927 for the Swan system and by Johnson and Asundi (*loc. cit.*) for the high pressure system, are given alongside the wave numbers (in italics), calculated from the above equation. The agreement between the observed and calculated values is indeed remarkable. This, however, is mainly brought about by the last term, $1.8v'v''$, in the equation. Thus if the values are calculated ignoring that term, we shall find that the agreement between the observed and the calculated values which is as good as one can expect from an equation representing the heads for bands of low quantum numbers, becomes increasingly worse for higher quantum numbers. These data are collected in Table 3. The theoretical significance of the term $1.8\,v'v''$, is not very clear and in earlier literature this term has been used to bring greater agreement between the observed and the calculated values when band head data were to be expressed by means of a formula. Evidently it serves to take into account the varying distance between the head and the origin of a band and also the irregularities in the vibrational levels brought about by various causes such as perturbations.† It is not possible to separate the contributions of these two effects by this term alone. The fact that the (O−C) values become unusually great for higer quantum numbers in this special case seems to indicate the existence of strong irregularities in the spacings of the vibrational levels. This is further confirmed as we shall see presently when we discuss the data in the light of the equation for the origins of the bands of the system.

Generally the ν_h equation is not found to be truly representing a band system; further in some cases because of ill-defined heads, the measurements may not be very accurate. If, however, it is possible to do fine structure analysis of the bands of the system then the system can be truly represented by ν_0 equation. Fine structure analysis of each band gives ν_0 and we can thus find $(\nu_0 - \nu_h)$ experimentally for each band. This value can also be calculated theoretically by the equation :

---

* 'Report on Band Spectra of Diatomic Molecules' by W. Jevons, pp. 11, 61 and 62.

† The cubic term in v' in eqn. III would apparently indicate perturbations. Such a term, however, is not needed if origins are used, *e.g.*, eqn. II.

$$\nu_0 - \nu_h = \frac{(B' + B'')^2}{4(B' - B'')} \div \frac{(B'_0 - \alpha' v' + B''_0 - \alpha'' v'')^2}{4(B'_0 - \alpha' v' - B_0'' + \alpha'' v'')} \qquad \text{(IV)}$$

where B_0, α, and v, have their usual significance. The variation of ν_h from ν_0, from band to band is of great importance in checking the analysis. It is easy to deduce from the above expression that for the bands degraded towards the red ($B' < B''$) the interval increases with diminishing v' (v'' constant) and also with increasing v'' (v' constant) provided $3B' > B''$ and for the bands degraded towards the violet ($B' > B''$) the interval increases with increasing v' (v'' constant) and also with decreasing v'' (v' constant) provided $B' < 3B''$. The Swan bands and the high pressure bands are degraded towards the violet and so the variation in the interval must increase regularly with increasing v' (v'' constant) and also with diminishing v'' (v' constant). Table 4 gives the intervals. In italics are given the theoretically calculated intervals (Eqn. IV) and in normal type the intervals obtained from the origin equation and the head data given by Johnson (1927) for the Swan bands and Johnson and Asundi (*loc. cit.*) for the high pressure carbon bands. The values for origins and heads are given in Table 5. For such of the bands marked *, ν_0 values directly observed are available and these are exactly the same as those calculated by the equation. ν_0 values for some of the bands of the high pressure carbon system can be determined approximately by the data given by Johnson and Asundi. These are, however, discussed later. The values of ν_0 used in the table are those calculated by Johnson's equation. It is seen from Table 4 that the interval regularly decreases as it should, in going from the (O, O) band to higher v'' values for a fixed v'. The (O – C) values for the intervals (Table 6) also indicate this regularity and are negligibly small up to and including bands with $v' = 4$. Indeed, the average (O – C) of about 3.8 cm^{-1} for the four bands (o, o), (o, 1), (1, 1), and (1, o) for which the origin data of Shea (1927) are available, will practically vanish if Shea's data are used. They are, however, large for bands with $v' = 5$ and are very much more so for the bands of the high pressure system which are regarded as forming the $v' = 6$ progression of the Swan system. It may be further remarked that the bands with $v' = 5$ have very low intensity so that the band head data on them will not have the same accuracy as the rest and high (O – C) values may, in part, be due to this cause.

This discussion indicates either that the high pressure carbon bands cannot be regarded as extensions of the Swan system or that violent perturbation occurs far bands with $v' = 5$ and 6. Since the fine structure analysis of the bands having $v' = 5$ has not been done, it is not possible to decide between these two alternatives. There is also no other electronic level known in C_2 which can bring about this perturbation. Hence it is not possible to prove conclusively by this evidence alone that the high pressure carbon bands are extensions of the Swan system. It should also be mentioned that the two bands with $v'=5$ recorded by Johnson may not be genuine bands at all but chance accumulation of structure lines of bands preceding them in the sequence. Shea (*loc. cit.*) records only one of them *viz.*, (5, 4) band. If, therefore, these two bands are neglected the Swan band system definitely ends with $v'=4$ and hence the high pressure carbon bands have to be regarded as forming an independent system.

The second argument which appears to favour the view that the high pressure carbon bands are extensions of the Swan system is probably the intensity distribution. Thus if the Condon parabola for the Swan system be extended to higher quantum numbers, it appears to pass through bands which are relatively more intense in the high pressure system. It must be remembered, however, that in the first place, the intensities recorded are photographic intensities visually estimated only and are to be regarded as descriptive rather than quantitative. Secondly, all the bands are not recorded under identical conditions of excitation and on one plate. Johnson and Asundi have already drawn attention to the main features of the peculiar intensity distribution in the high pressure carbon band system which has a notable minimum at about the (0, 6) band. Similar oscillating intensity phenomena are observed in certain other band systems (Johnson and Jenkins, 1926). Therefore this evidence from the intensity distribution can at best be used only as a subsidiary evidence.

We shall now discuss the experimental evidence in favour of the view that the high pressure carbon bands form an independent system :—

(*a*) These bands are obtained not only in the smoky puffs outside the path of the discharge as in Johnson and Asundi's experiment (1929) but also in the direct path of the discharge as recorded by Asundi and Pant (1942). This means that chemiluminescence is not the only mode of excitation which will bring up these bands. Asundi and Pant (1942) have observed only the high pressure carbon bands in their experiments on high frequency discharge to the exclusion of all other band systems due to C_2.

(*b*) Although a complete analysis of the rotation structure of the high pressure carbon bands has not been done, the fine structure data recorded by Johnson and Asundi (*loc. cit.*) allow us to extrapolate the origins of the four bands for which the data are recorded. The origins thus extrapolated can at least be regarded as upper limits. This allows us to find out the lower limit of the distance between the head and the origin in these bands. The values thus obtained are given in column 4, Table 7, and can be compared with the values of $(\nu_o - \nu_h)$ given in column 5 calculated as before by equation IV, assuming the high pressure carbon bands as extension of the Swan system. In column 6 are tabulated the values of the doublet separation of the high pressure carbon bands as observed by Fowler (*loc. cit.*). These double heads as already pointed out by Johnson and Asundi represent the P and R heads. The data of Fowler are admittedly inaccurate but it is seen that the values given in column 6 are of comparable magnitude if we keep in view the two limitations, *viz.*, that the data

TABLE II

v' \ v''	0	1	2	3	4	5	6	7	8	9	10	11
0	19355.0 *19354.90*	17740 *17739 95*	16148 *16146.95*									
1	21105 *21102 95*	19490 *19490*	17899 *17899*	16330 *16329*								
2	22812 *22812.9*	21202 *21202*	19612 *19612*	18043 *18044.6*	16498 *16495.9*	14972 *14975*						
3		22870 *22869*	21282 *21282*		18171 *18172.55*	16649 *16650.6*	15149 *15150.6*					
4			22902 *22903*	21343 *21339.4*		18276 *18277.2*	16778 *16778.9*	15391 *15392.4*				
5					21368 *21367.8*			16875 *16875.4*				
6	29241 *29163.7*	27620 *27559.6*	... *25977*	24426 *24416*	22883 *22875.5*	21361 *21361.9*	19571 *19567*	18394 *18394.6*	16946 *16945.7*	15518 *15514.5*	14114 *14107.7*	12731 *12722.6*

In italics are given the calculated values according to equation

$$\nu_a = 19354.9 + (1765.3v' - 16.35v'^2 - .9v'^3) - (1625.9v'' - 10.95v''^2) + 1.8v'v''.$$

In normal type are given the values (correct to 5 figures) observed by Johnson for the Swan bands up to $v' = 5$, and for $v' = 6$ those observed by Johnson and Asundi for the high pressure carbon bands.

TABLE III

v' \ v''	0	1	2	3	4	5	6	7	8	9	10	11
0	19355.0 *19354.9*	17740 *17739.9*	16148 *16146.95*									
1	21105 *21102.65*	19496 *19493.5*	17899 *17895.0*	16330 *16321.4*								
2	•22812 *22812.9*	21202 *21198.4*	19612 *19604.2*	18043 *18032.5*	16468 *16453.9*	14972 *14954*						
3		22876 *22864.0*	21282 *21270.7*		18171 *18148.9*	16649 *16621.5*	15149 *15116*					
4			22902 *22887.8*	21340 *21318.2*		18276 *18239.5*	16778 *16734.5*	15301 *15250.7*				
5					21368 *21332.0*			16878 *16814*				
6	29241 *29163.7*	27620 *27548*	... 25955.4	24426 *24373.6*	22883 *22835.3*	21361 *21307.0*	19871 *19802.2*	18394 *18310.[illegible]*	16946 *16857.3*	15518 *15417.6*	14114 *13999.7*	12731 *12603.8*

In italics are the calculated values after being corrected for the term 1.8 $\nu'\nu''$, *i.e.*, according to equation

$$\nu_h = 19354.9 + (1765.3\nu' - 16.35\nu'^2 - .9\nu'^3) - (1625.9\nu'' - 10.95\nu''^2).$$

In normal type are the values as given in Table II observed by Johnson and Johnson and Asundi.

TABLE IV

v' \ v''	0	1	2	3	4	5	6	7	8	9	10	11
0	18.94 *23.06*	16.0 *20.4*	13.3 *18.25*									
1	23.6 *26.55*	19.3 *23.05*	16.2 *20.36*	13.4 *18.19*								
2	31.8 *31.39*	23.0 *20.64*	18.8 *23.09*	15.3 *20.33*	12.6 *18.13*	13.8 *16.32*						
3		32.5 *31.64*	25.4 *26.74*		16.7 *20.30*	13.8 *18.01*	11.5 *16.24*					
4			42.7 *31.91*	33.5 *20.86*		24.8 *20.25*	21.3 *18.00*	19.4 *16.16*				
5					56.5 *26.99*			42.4 *17.85*				
6	76.8 *135.85*	79.6 *76.63*	*53.08*	107.2 *40.41*	102.0 *32.55*	99.1 *27.12*	87.1 *23.21*	86.5 *20.22*	79.6 *17.55*	76.1 *16.00*	72.0	69.0

Figs. in italics are calculated values.

Figs. in normal type are those obtained from difference of figures in Table V.

TABLE V

v' \ v''	0	1	2	3	4	5	6	7	8	9	10	11
0	19354.96 *19373.9**	17739.7 *17755.7**	16147.5 *16160.8**									
1	21104.3 *21127.9**	19490.4 *19509.7**	17898.7 *17914.9**	16329.9 *16343.3**								
2	22811.5 *22843.3*	21202.1 *21225.1*	19611.4 *19630.2*	18043.4 *18058.7*	16497.9 *16510.5*	14971.9 *14985.7*						
3		22869.3 *22901.8*	21281.5 *21306.9*		18170.5 *18187.2**	16648.5 *16662.3**	15149.3 *15160.8*					
4			22902.2 *22944.9*	21339.8 *21373.3*		18275.5 *18300.3*	16777.5 *16798.8*	15301.2 *15320.6*				
5					21367.9 *21424.4*			16877.5 *16919.9*				
6	29241 *29317.8*	27620 *27699.6*	... *26104.7*	24426 *24533.2*	22883 *22985.0*	21361 *21460.1*	19871 *19958.6*	18394 *18480.5*	16946 *17025.6*	15518 *15594.1*	14114 *14186.0*	12731 *12799.98*

ν_0 calculated by the Johnson equation (in italics) $\nu_0 = 19373.87 + (1773.42v' - 19.35v'^2) - (1629.88v'' - 11.67v''^2)$

ν_k observed by Johnson for the Swan bands and by Johnson and Asundi for the high pressure carbon bands (in normal type).

* Denotes that the value is directly observed.

TABLE VI

O−C Values of Intervals

v' \ v''	0	1	2	3	4	5	6	7	8	9
0	−4.12	−4.14	−4.95							
1	−2.95	−3.78	−4.16	−4.79						
2	+.41	−3.64	−4.29	−5.03	−5.53	−2.52				
3		+.86	−1.34		−3.60	−4.26	−4.74			
4			+10.79	+6.64		+4.55	+3.30	+3.24		
5					+29.51			+24.45		
6	−59.03	+2.97		+66.79	+69.47	+71.98	+64.27	+66.27	+61.72	+60.1

are not accurate and the difference represents the distance between the P and R heads and not that between the P head and the origin which will be the greater.

TABLE VII

v''	ν_h	ν_0 observed	$(\nu_0-\nu_h)$ observed	$(\nu_0-\nu_h)$ calculated by equation IV	Doublet width Fowler (1910)
4	22883	22934	51	32.53	64
5	21361	21410	49	27.12	73
8	16946	16976	30	17.88	55
9	15518	15545	27	16.00	51

This table clearly shows that the moment of inertia of the molecule emitting the high pressure carbon bands is not correctly given if the bands are regarded as extensions of the Swan system.

(*c*) There is yet another experimental evidence which is fully discussed by Johnson and Asundi (*loc. cit.*) and which also favours the view that the high pressure carbon bands are to be regarded as a separate system. This concerns the triplet electronic interval. It should be remembered that the high pressure carbon bands are due to a transition between two triplet II levels, the lower of which is, without doubt, the same as that of the Swan system. If, therefore, the high pressure carbon bands did not involve a new electronic initial level, the triplet width should be the same as that for the Swan bands. It has been observed, however, that the triplet width in high pressure carbon bands is greater than that of the Swan bands. This is in perfect agreement with the view that the initial electronic level of the high pressure carbon bands is not the same as that of the Swan system but lies higher. Since the triplet widths represent the difference between the triplet separations of the initial and the final states, the fact that the triplet width in the high pressure carbon bands is greater than in the Swan bands, is a consequence of the regular diminution in triplet width for the higher excited $^3\Pi$ level of the high pressure carbon bands,

Thus we see that a certain vibrational extrapolation of the Swan bands can include in that system the high pressure carbon bands also. The peculiar intensity distribution may also to a certain extent support the inclusion of the high pressure bands in the Swan system but there are serious difficulties for this view. One is that the $(\nu_0-\nu_h)$ values for the high pressure carbon bands calculated on this assumption do not agree with the values which can be deduced from the observed data. This will then mean that we shall have to assume the existence of a strong perturbation of the $v'=6$ level of the Swan system. Such a perturbation can be brought about by the vibrational terms of another electronic level which possesses the right properties for such a perturbation. No such electronic level has been so far observed in the C_2 molecule. A study of the possible potential curves of the C_2 molecules indicates that the existence of such a perturbing electronic state possessing vibrational levels is not very probable. On the other hand (r_0v_h) values as well as the increased interval between the triplet components of the high pressure carbon bands as compared to the Swan bands indicate that the high pressure carbon bands are to be regarded as an independent system. The controversy can, therefore, only be resolved by more complete data on the rotational structure of the high pressure carbon bands. In view of this and of the fact that the high pressure carbon bands can be excited by methods which are not necessarily chemiluminescent in nature, has to be reserved as to the existence of the phenomenon of inverse induced predissociation which is necessary to explain the great selectivity of the bands, if they are not an independent system but only extensions of the Swan band system.

HINDU UNIVERSITY
BENARES.

REFERENCES

Asundi, R. K , 1929, *Proc. Roy Soc.*, A **124**, 277

Asundi, R. K., and Pant, D. D., 1942, *Current Science*, **10**, 520.

Duffendack, O S., and Fox, G. W., 1927, *Astrophys. Jour.*, **65**, 214

Fowler, A , 1910, *M. N. R. A. S* , **70**, 484

Fox, G. W., and Herzberg, G., 1937, *Proc. Roy. Soc.*, A, **52**, 638.

Gero, L., 1938, *Zeits Phys.*, **109**, 210

Herzberg, G., 1929, *Zeits. Phys* , **52**, 815

Herzberg, G., 1939, *Astrophys Jour.*. **89**, 291

Johnson R. C., and Asundi, R. K., 1929, *Proc, Roy. Soc* , A, **124**, 668.

Johnson R. C., and Asundi, R. K., 1929, *Proc. Roy Soc* , A, **123**, 560.

Johnson, R. C., 1927, *Phil. Trans. Roy. Soc. A.*, **226**, 157.

Johnson, R. C., and Jenkins, 1926, *Phil Mag.*, **2**, 631.

Klemenc, A., Wehsberg, R , and Wagner, G. 1934, *Z. Elektrochem.*, **40**, 488.

Schmidt R., and Gero, L., 1937, *Nature*, **139**, 928.

Merton, T. R., and Johnson, R C., 1923, *Proc. Roy. Soc.*, A, **103**, 386.

Shea, J. D.. 1927, *Phys, Review.*, **30**, 825

20

ON THE HYPER-FINE STRUCTURE AND ANALYSIS OF THE COMPLEX LINE λ 3842.82. $sp^{33}D_3$-$5p.^3P_2$. IN THE FIRST SPARK SPECTRUM OF ARSENIC IN THE ULTRA-VIOLET-REGION

By S. K. MUKERJI

(Plate VII)

ABSTRACT. The hyper-fine structure of the complex line λ3842.82 $sp.^{33}D_3$-$5p^3P_2$, in the first spark spectrum of arsenic in the ultra-violet region has been investigated using a quartz Lummer plate and a water-cooled hollow cathode discharge tube. This line has been observed as a well resolved quartet with a coarse structure, the components degrading in intensity to the violet. These components are at intervals of 298, 278 and 162. The predicted, graphical, resultant and observed patterns are shown diagrammatically and compared. The resultant and observed patterns have shown fairly good agreement. The analysis has been made using the graphical method of Fisher and Goudsmit (1931) and assuming the nuclear spin of arsenic to be 3/2, as previously determined by the author (Mukerji 1937).

INTRODUCTION

The hyper-fine structure of the first spark spectrum of arsenic in the ultra-violet region was first investigated by the author (Mukerji, 1938), using a hollow-cathode discharge tube. In this investigation the fine structure of the complex and incompletely resolved line λ3842.82. $sp^{33}\ D_3$-$5p.\ ^3p_2$. has been studied. In a previous investigation the author (Mukerji, 1938) has already shown, as previously proposed by Tolansky (1932), that the nuclear spin of arsenic is 3/2. Therefore, in this investigation the nuclear spin of arsenic has been assumed to be 3/2 ; and the gross-structure multiplet analysis of AsII lines as made by Rao (1933), and his line classification has been used here. Previous investigators on arsenic (*loc. cit.*) who have studied only the visible region did not use the hollow-cathode discharge tube which is perhaps the best type fo discharge tube that will enable the Stark and Doppler broadening effects to be sufficiently reduced so as to obtain reliable numercial values of the structures.

EXPERIMENTAL

The reason as to why previous workers did not use a hollow-cathode discharge tube appears to be that it is extremely difficult to excite the arsenic lines in such a tube. The first attempt in this case to sputter arsenic lines proved a complete failure, the lines obtained being too weak to be observed at all. But, as has been pointed out in previous papers (7) (1938), an iron hollow-cathode tube of the form designed by Paschen and modified by Schüler, about

7 cm. long and 1 cm. internal diameter, served the purpose of the present investigation. The tube was water-cooled and pure helium was circulated continuously through the tube at a pressure of about one millimeter. The current employed was varied from 300 to 500 milli-amperes at a pressure which was varied from 1000 to 2500 volts at the source. The arsenic used was of the purest quality free from all oxide. This was acheived by heating ordinary arsenic in vacuum and then allowing it to deposit on the sides of the hollow-cathode as a pure oxide-free coating of arsenic. A brilliant spectrum of AsII was then observed. The object was to obtain, as far as possible, oxide-free arsenic and this was simply done by deliberately omitting to heat the usual copper oxide furnace in the circuit, so that an appreciable amount of hydrogen was present in the discharge. The hydrogen then combines with the oxygen of the arsenic oxide coating and reduces the oxidised surface to that of the pure metal which is then easily sputtered. This is how a brilliant arsenic spectrum in the hollow-cathode discharge was for the first time obtained. A certain mineral known as chabazite was used in liquid-air traps as an absorbent in place of the usual charcoal. This mineral was found to be very efficient in absorbing the water-vapour formed in the circuit and it gave the other advantage of not absorbing helium that was used in the circuit in any large proportion. Thus the helium supply to the discharge had not to be renewed too frequently.

The fine structure of the line was examined by using a quartz Lummer plate in conjunction with a Hilger E_2 spectrograph. Ilford Monarch plates, speed 525, were used for this part of the spectrum and the exposure time was varied from four to seven hours. The temperature and pressure variations were negligibly small andwere neglected in calculations. But there were some lines which though fairly strong have only shown unresolved broad structures. Such lines are mainly the complex lines with fairly high J values. The terms split up, as the analysis will show, into a number of fine structure levels giving a large number of fine structure components which can not be resolved by a Lummer plate. The resolution becomes still more difficult when the widths of both the upper and lower terms are of the same order. Also on the shorter wave-length side, in the ultra-violet region, the Doppler width of the lines increases with the frequency as measured in frequency units. Also the Stark broadening and line width due to collision phenomena increase similarly, and consequently the practical separating power, as measured by the smallest frequency distance between two lines that can be separated or resolved, steadily increases with frequency. With a complex group of fine structure components in the ultraviolet no single component can be resolved, and therefore the only measurement possible in such cases is to determine the total width of the pattern. But this also often enables the intervals to be estimated from other well resolved lines involving common terms. The line under investigation has been observed as a well resolved quartet with a coarse and slightly blurred structure. But out of a very large number of photographs taken only a few showed good resolution of the line structure as during the long hours of exposure the temperature and pressure of the air do not always remain constant. Moreover, variations of temperature and pressure displace the fringes considerably, so that only those few plates were measured in which these variations were negligible, and the line structures fairly sharp.

The apparatus used was the same as described by the author in a previous communication (*loc. cit.*) The cathode and the anode of the modified form of Schüler tube employed were both water cooled by continuous flow of cold water throughout the course of the experiment. As described in the previous paper, liquid air cooled traps were used in the circuit to absorb mercury vapour and other impurities. A quartz tube containing copper oxide and two pumps were also included in the circuit. The copper oxide tube was heated when necessary in order to absorb the hydrogen in the system while one of the pumps, usually a hyvac rotary pump, was used to exhaust the whole system to a hard vaccuum. The second pump was a mercury vapour two stage pump which when set in action served to keep the admitted quantity of helium in circulation in the whole system. Exposures were begun only after all impurities were absorbed, which usually took several hours. The fine structures of the lines were examined by means of a quartz Lummer plate in conjunction with a Hilger E_2 quartz spectrograph. The strongest component of each line is taken as the main or null line and the separations of the rest are given in units of cm.$^{-1}$ 10^{-3}.

ANALYSIS

As arsenic does not have an isotope, the structure observed here is of the magnetic type and free from complications due to isotopy. But when the structure is complex and the components are incompletely resolved as in the present case, it is found that the Fisher-Goudsmit method of analysis is particularly valuable A brief description of this method of analysis has already been given by the author in a previous paper :

Analysis of the line,—λ3842.82. $sp^{33}D_3$—$5p.^3P_2$.

This line is a well resolved quartet with a coarse and slightly blurred structure, degraded in intensity and intervals to the violet. The interval factor of the lower term is already known from the analysis of the line λ4371.4 $sp^{33}D_3$-$5p^3D_2$. already reported in a previous paper. Hence the interval factor of the upper term can be obtained. For this purpose we will now make use of the Fisher-Goudsmit diagram and proceed with the analysis. It will be seen, as shown in the diagram, that this line fits into its graph fairly accurately at a ratio of lower to upper interval factors of 100 to 17.5 (approx.), that is, of 81 to 17.5. Hence the interval factor of the upper term is 14. The predicted intervals are 316, 49, 199, 35, 49, 97, 21 and 35. The graphical intervals are 316, 47, 199, 37, 51, 92, 19 and 40. The resultant intervals obtain-

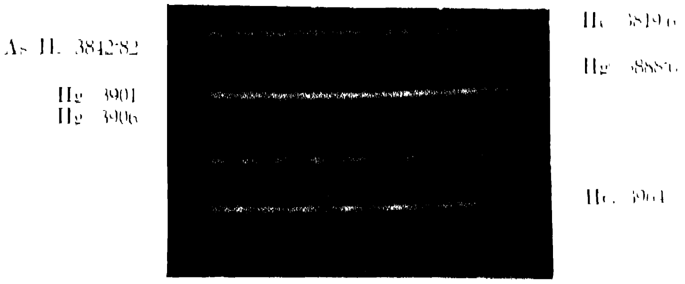

(b)

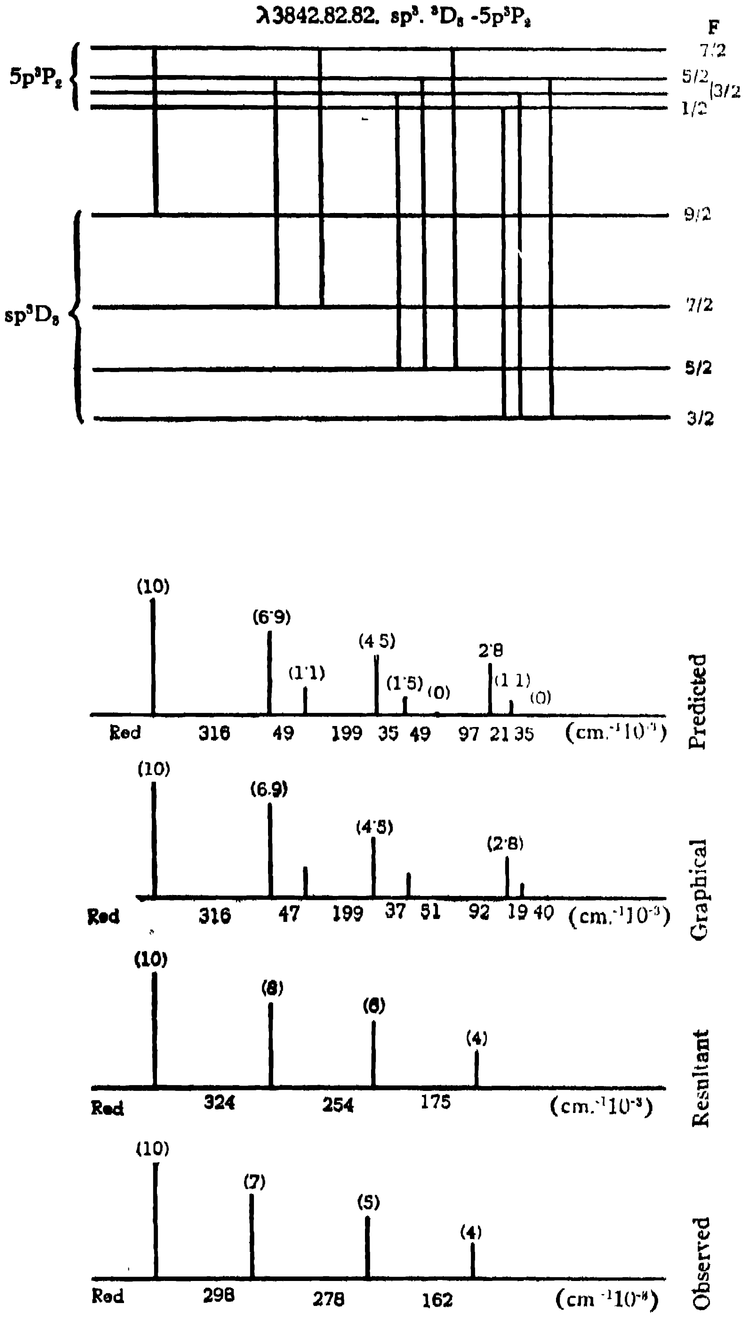

FIG. 1

ed by determining the centres of gravity of the close unresolved groups are 324, 254, 175, and the observed intervals are 298, 278 and 162, which, considering the difficulties of accurate measurement, is a fairly good agreement.

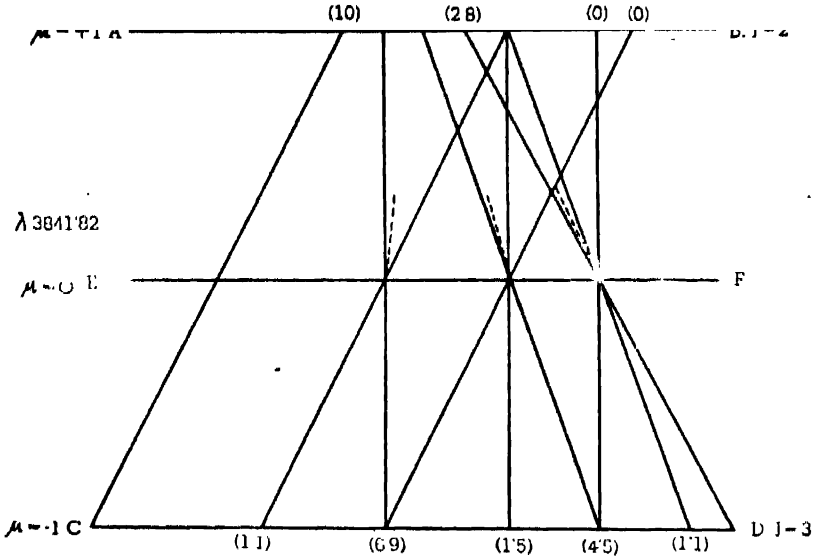

FIG. 2

The predicted, graphical, resultant and observed patterns are shown in Fig. 1. The Fisher Goudsmit diagram is shown in Fig. 2. Plate VII shows the structure of the AsII line λ3842.82 which has become blurred in reproduction. A very narrow photograph could only be taken as the lines are extremely close together at this part of the spectrum.

DEPARTMENT OF PHYSICS,
AGRA COLLEGE

REFERENCES

Fisher and Goudsmit, 1931, *Phys. Rev.*, **37**, 1041.
Mukerji, (1937). *Ind. J. Phys.*, **11**, 123.
Mukerji, 1938 *Ind. J. Phys.*, **12**, 212.
Tolansky, S., (1932) *Proc. Roy. Soc.*, A, 137, 541.
Rao., A. S., 1933, *Ind. J. Phys.*, **7**, 561.

21

SOME NUCLEAR DISINTEGRATIONS

By M. F. SOONAWALA *

ABSTRACT. Endothermy and exothermy of several nuclear disintegrations have been studied. The radioactive nuclei show pronounced exothermy with a release of energy per disintegration ranging from 165 Mev to 236 Mev according to the structure assigned to the nucleus. The potential depth within the nucleus varies from about 4×10^{18} for the stable nuclei to 10^{-20} for the unstable radioactive nuclei.

The following is a study of the endothermy and exothermy of several nuclear disruptions, particularly of the radioactive nuclei, in light of the hypothesis advanced by the writer (Soonawala, 1920, 1942). There can be little doubt that a nucleus is made up of smaller constituents, and the protons and neutrons can be the smallest of these. If the sum of the masses of the constituents is greater than that of the nucleus, energy is required to break up the nucleus and the process is endothermous. This energy is equivalent to the difference of the masses of the nucleus and its constituents. On the other hand, if the nucleus is synthesised from its constituents, a similar amount of energy would be released and the process would be exothermous. Also energy is liberated in the fission of a nucleus of mass greater than the combined masses of its constituents. In the study of atomic nuclei presented before, it was shown that the rare gas nuclei are, in all probability, the constituents of the majority of the nuclei; and to these, the lighter particles such as alpha particles, neutrons and protons are added to make up the remaining nuclei. We may now consider whether the disruption of the various nuclei can be endothermic or exothermic. We shall consider the main groups of elements obtained by the synthesis of the rare gas nuclei, and the result is presented in Table I. One nucleus is selected from each group as representative of it, as the packing fractions and the mass differences would be about the same for the others. When known, the accurate atomic mass is used; else, it is calculated from the packing fractions as obtained from the smooth curve between the packing fractions and the logarithms of the atomic masses. The packing fraction of the nucleus of mass 227 is thus taken to be 5. Δ is expressed as the difference of the masses of the constituents on the one hand and the mass of the resulting nucleus on the other. Therefore, positive values of mass defect, Δ, indicate endothermy and negative values exothermy.

The alternative hypothesis of the constituents being the light particles protons and neutrons can be also examined here. The results are set out in Table II of the syntheses of protons or neutrons taken ten at a time and the masses of the nearest actual nuclei are shown for comparison. We observe that endothermy lasts till the synthesis of about mass 50 and gives way to exothermy at about 60. Again, if we assume a synthesis of the alpha particles to form nuclei, even for a nucleus of such large atomic mass as, say, 228, the disintegration would be endothermic. For, the packing fraction gives the mass of to be 228.114 while 57 × 4.00216 = 228.122. Thus, of the three hypotheses considered for nuclear syntheses, the proton hypothesis shows exothermy setting in too early, the alpha particle hypothesis indicates endothermy even for the heaviest nuclei, while the rare gas nuclei hypothesis shows exothermy to commence decidedly just with the radioactive nuclei.

---

* **Fellow of the Indian Physical Society.**

RADIOACTIVE NUCLEI

Nuclei 206, 207, and 208. The three radioactive series, uranium, actinium and thorium, terminate in the end products of atomic masses 206, 207 and 208, all isotopes of lead, by successive alpha and beta ray changes. Our hypothesis reverses the usually ascribed role of parent and progeny, and these three nuclei are taken to be the parent ones from which the others ensue by further syntheses with alpha or beta particles. The rare gas hypothesis ascribes the structure Kr+X to each of these nuclei. The nucleus 206 can be synthesised as 128+78 or 126+80 or 124+82, the nucleus 207 as 129+78, and the nucleus 208 as 130+78 or 128+80 or 126+82. The sum of the masses of the constituents, the mass of the resulting nuclei, and the mass defects are shown in Table I. The disintegration of these three nuclei is exothermic and the energy given out ranges between 160 Mev and 168 Mev.

The structure ascribes to 206 is shown as follows :

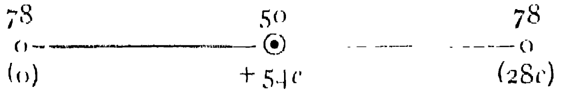

There are the two equal end particles of masses 78 each at a distance 21 from each other, with a central particle of mass 50. An exchange particle of the proper mass and charge keeps moving between the end particles and keeps them tied up with sufficient energy. The central particle passes the exchange particle from side to side. Here we shall follow the procedure adopted previously (Soonawala, 1920, 1942) and the references are to the equations there. We can easily see that formula (16) is also valid for the three particle system used here. For, referring to the end particles as 1 and 2 and the middle one as 0, the wave equation of the system becomes

$$\frac{1}{m_1}\Delta_1^2\psi_T + \frac{1}{m_2}\Delta_2^2.\psi_T + \frac{1}{m_0}\Delta_0^2.\psi_T + \frac{8\pi^2}{h^2}(W_T'' - V)\psi_T = 0,$$

where W_T is the total energy and ψ_T the total wave function. If

$$\psi_T = F(x_0, y_0, z_0).\ \psi(r, \theta, \phi) \text{ and } W_T = W_F + W,$$

then, the equation gets separated into the two equations

$$\frac{m_1+m_2+m_0}{(m_1+m_2)m_0}.\nabla_0^2 F+\frac{8\pi^2 W_1 F}{h^2}=0$$

and
$$\frac{1}{\mu}\left\{\frac{1}{r^2}.\frac{\partial}{\partial r}\left(r^2.\frac{\partial\psi}{\partial r}\right)+\frac{1}{r^2.\sin\theta}.\frac{\partial}{\partial\theta}\left(\sin\theta.\frac{\partial\psi}{\partial\theta}\right)+\frac{1}{r^2\sin^2\theta}.\frac{\partial^2\psi}{\partial\phi^2}\right\}$$
$$+\frac{8\pi^2\mu}{h^2}(W-V)\,\psi=0,$$

where
$$\frac{1}{\mu}=\frac{1}{m_1}+\frac{1}{m_2},$$

with the usual transformations

$$x_2-x_1=r\sin\theta\cos\phi,\quad y_2-y_1=r\sin\theta.\sin\phi,\quad \text{and}\quad z_2-z_1=r.\cos\theta.$$

The moment of inertia of the nucleus (Soonawala, 1942) 206 is $1.007.10^{-46}$, and this is also equal to $2\times 78\times 1.67\times 10^{-24}\times r^2$, from which $2r=1.72.10^{-12}$ cm. We take this to be the range $1/\lambda$, and calculate the mass of the exchange particle from (24). This comes out to be 22.35 times the electronic mass.

To find the potential depth V, we now take $E=+\epsilon$, [eqn.(10)]. With $M=78,\times 1.67\times 10^{-24}$, $\epsilon=2.705.10^{-4}$ erg, $2\pi\sqrt{M\epsilon}/h.\lambda=310$, Eqn.(68) becomes

$$\frac{d^2u}{dx^2}=-\frac{4\pi^2 M\epsilon}{h\lambda}u$$

giving as the solution
$$u=C\cos\left(\frac{2\pi\sqrt{M\epsilon}}{h\lambda}\,x\right)$$

Therefore,
$$u'=C.\frac{2\pi\sqrt{M\epsilon}}{h\lambda}\sin\left(\frac{2\pi\sqrt{M\epsilon}}{h\lambda}\,x\right)$$

and
$$\frac{u'}{u}=\frac{2\pi\sqrt{M\epsilon}}{h\lambda}\tan\left(\frac{2\pi\sqrt{M\epsilon}}{h\lambda}\,x\right).$$

Joining up the two values of u'/u as in (73), at x_0,

$$1-a/2=1-\frac{4\pi^2 M.V}{h^2\lambda}=1-1.03.10^{20}.V=310.\tan(310.x_0).$$

Assuming x_0 to be equal to about 10^{-12} cm, $310.x_0$ is small enough for $\tan(310.x_0)$ to be equal to $310.x_0$. Hence,

$$1-1.03.10^{20}.V=310\times 310\times x_0.$$

The term on the right hand side is so small in comparison with unity that

$$1-1.03.10^{20}.V=0,\ \text{and}\ V=9.7.10^{-21}.$$

We should get closely similar values for the constants of the nuclei 207 and 208.

Nucleus 227.—It is known for certain that krypton is one of the primary products of uranium fission and at least four of its isotopes have been discovered. It is also almost certain that xenon is another such primary particle

(Meitner, 1945). The two particles given out during fission are always of masses similar to those of xenon and krypton. Very probably, Kr^{88} and X^{139} are such primary products, Sr^{88} and Ba^{139} being their end products (Heyn, & others, 1939). The combination of these two nuclei gives a nucleus of mass 227, which would be actinium or an isobare of it. The disruption of this nucleus would be exothermic as seen from Table I. The mass defect is 0.25 unit, which is equal to $3.76.10^{-4}$ erg, or 236 Mev. The potential depth, calculated as for 206 above, is $1.7.10^{-20}$, and the mass of the exchange particle $21.97 \times m_e$. This nucleus is an illustration of the principle noted above that we can have two nuclei of the same atomic mass and number but different in constitution. For, above is shown a two particle structure of 227, while commencing with 207 we can have a six particle structure with five alpha particles added to the nucleus 207. Another example would be to consider radon as a rare gas nucleus and follow up the radioactive series to 226, 230, 234 and 238.

TABLE I

Nucleus and its mass	Masses of constituent nuclei	Mass defect	V	M	2r
Na 21.0035	19.9988+1.00812	+0.0034	...	...	...
Mg 23.9924	19.9988+4.00216	+0.00956	3.8×10^{-18}	29.05	1.37×10^{12}
K 39.975	38.9755+1.00812	+0.00862	...	...	...
Ca 39.974	35.9780+4.00216	+0.00616	...	...	...
Ni 57.942	39.971+17.997	+0.026	...	...	...
Br 80.926	79.926+1.00812	+0.00812	...	...	...
Sr 87.931	83.928+4.00216	−0.0008	...	...	...
Mo 99.915	79.926+19.997	−0.022	3.5×10^{-20}	20.83	1.85×10^{12}
Cd. Sn 119.912	79.926+39.971	−0.015 = 14 Mev.	...	...	...
Cs 132.933	132.930+1.00812	+0.00512	...	...	...
Ba 137.916	133.929+4.00216	+0.01516	3.8×10^{-18}	7.01	5.47×10^{-12}
R. E. I (143.93)	123.93+19.997	−0.003	...	...	...
R. E. II (169.92)	131.93+37.97	−0.02	...	...	...
RaG 206.038	125.932 + 79.926	−0.18 = 167.6 Mev	1×10^{-20}	22.35	1.72×10^{-12}
AcLead 207.038	128.030+77.926	−0.172 = 160.1 Mev	...	...	...
ThLead 208.039	127.936+79.926	−0.177 = 164.8 Mev	...	...	...
Ac 227.114	138.93 + 88.93	−0.25 = 236 Mev	1.7×10^{-20}	21.97	1.75×10^{-12}

M is the mass of the exchange particle expressed in the electronic mass, 9.038×10^{-28} gm, as the unit.

2r is the distance between the end particles in cm.

R. E. I and R. E. II refer to the two rare earth groups.

Nuclei 235 and 239.—These would result from addition of three or four alpha particles to the nucleus 227 with slightly higher energies of fission.

Neutrons are also known to be the product particles of uranium fission; and if they are assumed to be among the primary product particles, then the above constitution of nucleus 227 would be revised to something like $X^{138}+Kr^{87}+2.n.=227$. This is on the assumption that two neutrons are emitted in the fission of 227. The energy of fission is, then, $3.517.10^{-4}$ erg, or 221 Mev. V cannot, of course, be calculated as before. Similar considerations would apply to another nucleus, such as, say, 206.

A few values of the potential depth are shown, and these are necessarily approximate. Even then we can discern a definite trend for the relatively unstable and exothermic nuclei to have systematically smaller values of V, indicating proportionately smaller binding forces between the constituent particles.

TABLE II

n	$10 \times n \times 1{\cdot}008$	Mass of nearest nucleus
1	10.08	10.01
2	20.16	20.00
3	30.24	29.98
4	40.32	39.97
5	50.40	49.95 50.95
6	60.48	59.04 60.04

DEPARTMENT OF PHYSICS,
MAHARAJA'S COLLEGE,
JAIPUR (RAJPUTANA).

REFERENCES

Soonawala, M. F. (1929), *Ind. Jour. Phy.*, **3**, 489

Soonawala, M. F. (1942) (*a*) *Ind. Jour. Phy* **16**, 291 (1942); (*b*) *Ind. Jour. Phy*, 301-302.

Meitner, L., (1945); *Rev. Mod. Phy.*, **17**, 287.

Heyn, F. A., Aten, A. H. W., and Bakker, C. J., (1939); *Nature*, **143**, 516.

TRUE RELATIVE INTENSITY DISTRIBUTION FROM MICROPHOTOGRAMS

By J. N. NANDA

ABSTRACT Harrison's test of self-consistency has been applied to rotating wire gauze screen type calibration method described earlier (*Nanda*, , 1945), for use in spectrophotometry. This device adheres to the test in at least the range of wavelengths 3,000 to 5,000 Å within the sensitiveness of the barrier-layer photo-cell microphotometer. Earlier calibration of various screens from area consideration is found to be correct from comparison with the self consistent inverse square method.

The effect of finite width of the spectrograph and microphotometer slits is considered in detail. In the study of sharp lines, the dispersion of the spectrograph must be such that the half width covers a greater length on the plate than that covered by the monochromatic image of the slit. It is shown that the modified contours on account of finite slit width have less curvature than the true ones, though the areas under the two are equal.

Among the methods of measuring the intensity distribution in microphotometer slit image, it is seen that differentiation of the pattern of a straight edge is most convenient and may also be advantageously used to determine the purity of an image formed by any microscope objective.

The microphotometer deflections depend on the intensity of the blackening on the photograph and the characteristic sensitiveness of the light-measuring device being employed in the microphotometer. As the response of the photographic plate as well as the light-measuring device is not always linear with the intensity of light incident on each, the deflections are not simply proportional to the original intensities which were photographed. Thus even if effect of finite width of slits have been allowed for, the deflections have to be reduced to true relative intensity magnitudes by some calibration device. The usual procedure is to get on the same photographic plate some exposures with proportionally reduced intensities ; and by measuring these for the same setting (tracer light intensity, galvanometer sensitiveness, record to plate ratio) of the microphometer, the deflections for known ratios of intensities can be determined. The set of calibration curves with λ are independent of slit widths, provided the original distribution is uniform or as in practice shows a slow variation warranting the neglect of such effects. From these curves the intensity relative to maximum, corresponding to any observed deflection at any wavelength can be easily determined.

A large number of devices are in vogue for this calibration of photographic plates. A brief description of some of these is given in a paper by Ditchburn (1927). It has been shown by the author (1945) in a recent paper that the simple wire screen type device has the largest sensitiveness and can be considered best for absorption spectrophotometry, for the reasons discussed there. Sawyer and Vincent (1943) have pointed out that any of these calibration devices should be used only after ascertaining their self-consistency. The method of doing this according to Harrison (1920) is to see if the common portion of any two calibration curves obtained by the device for two different initial intensities can be made to coincide by the same proportional sliding of one curve along the intensity axis. Grossman (1943) has found that the inverse square calibration is self-consistent and can serve as a check for any device.

It is attempted to show that the wire gauze screens calibrated from area considerations, give practically the same reduction of intensity as obtained by the calculated inverse square illumination. The inverse square check could be applied only in the visible or the near ultraviolet ($\lambda = 3{,}000$ to $\lambda = 5{,}000$ Å), as the ultraviolet source (the long water-cooled hydrogen discharge tube used in previous work) could neither be regarded as a point source nor could it be conveniently moved about to give inverse square intensity. A ground-glass screen was illuminated by a point-o-lite lamp. The ground glass was focussed on the slit by a suitable lens placed in the middle. Between the lens and the ground glass the short wooden tube capable of rotation in ball bearings was placed in which different wire gauze screens could be fixed. By keeping the distance between the lamp and the ground glass fixed, certain exposures were given with the same time of exposure and different wire screens (labelled 76.5%, 53 5%, 23.0%, etc.); later the wooden tube was kept empty while exposures for the same time were interspersed with the previous ones on the same plate (Ilford process) for different distances of the source from the ground glass. The ratios of successive distance to the first being $\sqrt{1.33} : 1$, $\sqrt{2} : 1$, $\sqrt{3} : 1$, $\sqrt{4} : 1$, exposures of true relative intensities 75%, 50%, 33%, 25%, were obtained. The ground glass is used so that light cone of the same width enters the spectrograph slit whatever the distance of the source, thus not altering the geometry of the spectrograph optics

After developing the plate carefully, sets of microphotometer deflections were observed for different exposures at the same wave lengths. To guard against the effect of photographic grain and any irregularities along the breadth of exposed strips, the microphotometer slit image was kept at its maximum length, *viz.*, 3 mm. The calibration curves were obtained from the two methods under comparison, at different points on the wavelength scale. The curves were found to coincide practically (Fig. 1). In view of no special precautions being taken to eliminate any variations of the light source or to ensure that there is no slight displacement regarding λ for points on the same curve, the maximum variation of 5% (which occurs only in small intensities) in the two sets of curves can be taken to be not much outside the experimental error. Taking the mean values from all the curves the labelled values may be altered to become 76·9%, 56·0% 23·4%.

As regards self consistency any two curves for the calibration device, of the type obtained in figure 1, were tested and it was found that their common portions could (making a proportional shift all along them) slide into each other (fig. 2). The divergences in the slow portions are due to poor accuracy in this region.

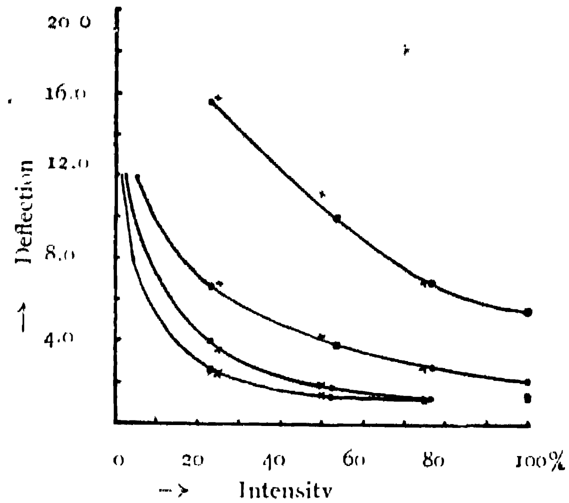

Comparison of wire gauze (o) and inverse square (×) calibration methods Different curves are for different maximum intensities.

FIG. 1

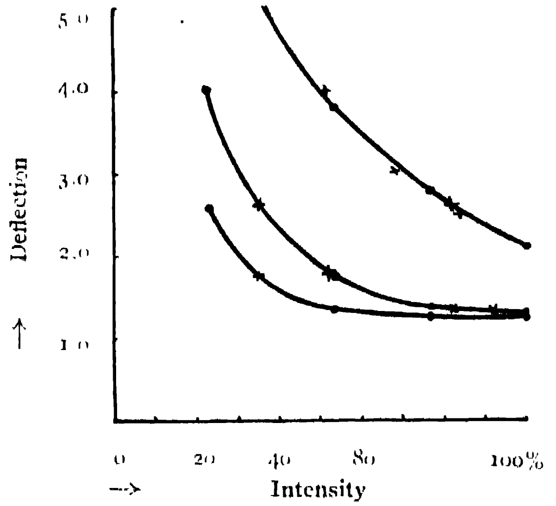

Self consistency of the wire gauze calibration method in the visible region— points marked (×) are obtained by transposition from other curves.

FIG, 2

The microphotogram can be directly converted into intensities using the calibration curves only if there were no modification of the contour, *e.g.*, by the finite width of the spectrograph slit and the microphotometer slit image. Changes brought about by these effects are prominent only for distributions that are quite close as in the case of resonance lines or lines in absorption. Let us first consider the distortion on account of the spectrograph slit.

Following the notation of Van Cittert, in the coherent case to which the method of slit irradiation in actual practice corresponds, the slit image for monochromatic light of frequency ν gives an intensity distribution.

$$(J_{\phi d})_{\nu_0} \propto [Si(\psi_0-\phi)d + Si(\psi_0+\phi)d]^2 \qquad \ldots \quad (1)$$

where the function $Si(\alpha)=\int_0^{a} (\sin\ \alpha/\alpha)d\alpha$ and $\psi_0=\frac{2\pi\nu_0}{c}\ \psi_0'$ where ψ_0' is the half angular width of the slit viewed from the centre of the collimator lens. Similarly ϕ' is the angular distance of any point Q from the point P_0, where the monochromatic light reaches the plate after dispersion in the same spectrograph with infinitesimal slit-width, when viewed from the centre of the camera lens of the spectrograph, d is the aperture of the prism, etc., causing dispersion.

Let the incident light be of a continuous distribution $T/T\nu$ or $T_{\phi,\nu}$ on the plate if photographed through an infinitesimal slit. If as a special case $T_{\phi,\nu}=T$, a constant, in an ideal case any point P will simply have an intensity ordinate T_0 while in actual practice the point P will lie on all parts of curves analogous to $J_{\phi,d}$ with maxima at all points on the photographic plate. Therefore, the resulting intensity at P is just proportional to the integral of the curve $J_{\phi,d}$ with ϕ. The constant of proportionality in $J_{\phi,d}$ can be known if the resulting constant intensity is to be interpreted as T_0. Thus

$$T_0=T_0\int_{-\infty}^{+\infty} J_{\phi,d}\ d\phi, \text{ or} \int_{-\infty}^{+\infty} J_{\phi,d}\ d\phi=1$$

For the distribution given by (1) the constant is $1/\pi'$. Now let $T_{\phi,\nu}$ vary with ν or in the same meaning with ϕ. To find the resultant intensity at P corresponding to ν, we have to write

$$T_{j\nu}=\int_{-\infty}^{+\infty} T_{\phi,\nu}\ J_{\phi,d}\ d\phi \qquad \ldots \quad (2)$$

For integration, ψ_0 occurring in J can be taken as a constant for the narrow lines under discussion. The above integral can give results anywhere near the distribution T only when distribution J is much closer than T. If the original distribution does not extend beyond J of the monochromatic image of the slit, the photographed distribution will only be giving something near the monochromatic image distribution for all T, however the maximum amplitude shall depend on total intensity under the T-distribution.

It is clear that this modification of T-contour is only due to the resolution of the spectrograph, the least resolvable limit further levels out the original distribution, as in simple words the limiting resolvable distance is the size of slit image even if an infinitesimal slit is illuminated by monochromatic light.

Another effect occurs due to a limiting resolvable distance of the photographic emulsion, this levels out $T_{j,\nu}$ still further.

For usual spectrograph slit—width, the observed intensity, neglecting other effects, will be practically similar to the true one excepting for very narrow lines whose half width in terms of ϕ becomes of the order of H_c, the half width for the monochromatic slit image ($H_c = .63\pi$ for optimum results for coherent arrangement). It is thus clear that for studying any line of a given order of sharpness there is a minimum resolution of the spectrograph which must always be maintained. When this consideration has been kept in view, the area of the observed curve which is generally needed for line intensity will be exactly equal to the true one. It will be clear from the accompanying treatment regarding effect of finite width of microphotometer slit image, that the width of a line that is uneffected by these effects is between the points of inflexion rather than between those of half intensity amplitude.

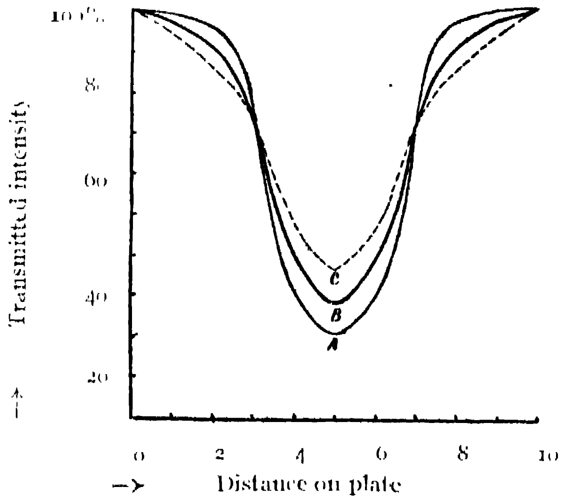

A—$T\nu$ is the actual intensity distribution.
B—$T(j\nu)$ on account of spectrograph slit width.
C—$T(ij\nu)$ on account of finite resolution of the spectrograph and photographic plate as well.
The curves cut at the points of inflexion,
Areas under all the curves are equal.

FIG. 3 (a)

Before proceeding with the microphotometer slit effects it will be instructive to study how successive distributions arise, (Figs. 3). $Tj\nu$ in figure (3*a*) is the modified curve obtained by the changes brought about by finite spectrograph slit in the true curve T^{ν} (e.g., of an absorption line). $T_{j,\nu}$ will be further levelled out slightly on account of limiting resolving power of the prism (i_1) and the photographic emulsion (i_2) to give T (i, j, ν). The T-distribution will now give an F-distribution of the photographic blackening; for simplicity

F has been considered exactly similar to T. This F or T_s-distribution gives the J-distribution of Fig (3*b*) standing for microphotometer beam intensities at different points ; J_s includes the effect of microphotometer slit width while J does not, for the same T-distribution. The J-distribution will further give the recorded curve D of deflections of the microphotometer, and again for simplicity

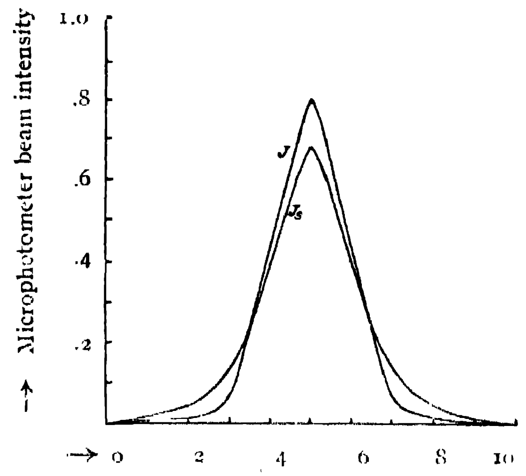

Js—on account of modification of J by the width of the microphotometer slit image. J curves are always narrower than T curves (opposite for emission lines). This necessitates use of calibration device even in the determination of width of spectral lines.

FIG. 3 (*b*)

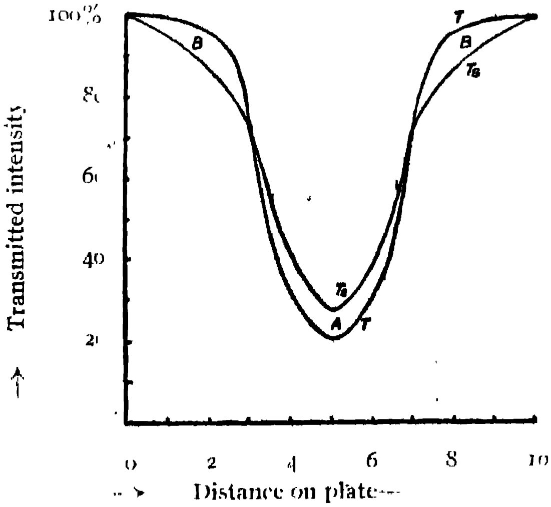

Ts-curve is obtained if Js-curve is directly used without first correcting it to get the J-curve.
Area A is less than the areas B. (opposite for emission lines).

FIG. 3 (*c*)

J and D can be regarded as exactly similar, otherwise these too can be interchanged by an experimental conversion curve (Fig. 4).

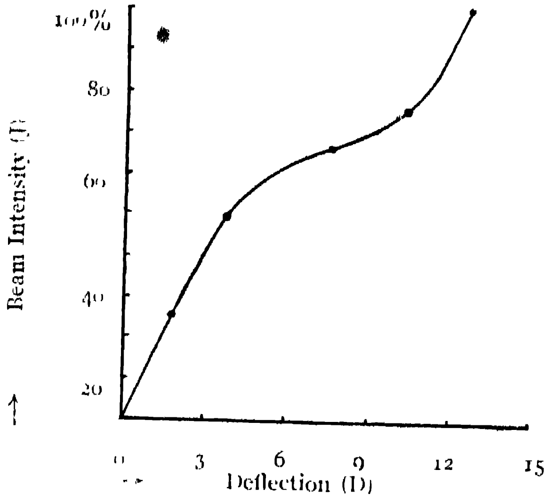

Sensitiveness curves of the light-measuring device in the microphotometer, obtained by inverse square illumination Deflection can be converted into relative beam intensities from such a curve

FIG. 4

The observed calibration curves obtained even from a practically uniform spectral distribution, and expressed as a relation between J and T can be applied to any observed contour, only if all disturbing effects were absent. To get true T-curve, the J(s, r, j, ν,) curve is corrected first to give J(r, j, ν) and by the application of the calibration curve, T (r, j, ν) is obtained, which when corrected for the sundry effects gives T_ν. Ordinarily when corrections are known to be small and not considered we get T (s,...ν) distribution of figure 3(c) and not the T-distribution.

It can be shown that area under the complete curve T^ν is equal to that under $T_{j,\nu}$, and also the same rule holds for the complete curves J. While areas under T(s,...), T or D(s,...), D are only approximately so. Langesth and Walles (1934) have calculated graphically the difference on T curves to be capable of being represented empirically by the formula $\Delta = 16A_0p^2$ where A_0 is the maximum absorption amplitude (here) and p is the ratio of the effective slit-width to line half-width. The Δ in case of absorption lines is opposite in sign to that considered by Langesth and Walles, and so area under the T_s curve will be slightly larger than the true one. The area under T_s, T is practically the same and this fact has been used by Minkowski (1926) in his determination of radiation damping from total absorption rather than from integrated absorption coefficient, in case of sodium D lines. The area under k_ν (the absorption coefficient) curve is not safe to work with especially if T(s,...) falls to less than 20% in the centre as small spurious changes here give large error in k curve. The spurious effects described by Korff (1931), apart from those of slit widths, are due to defective focussing the creep of the image on the emulsion at high exposures, and general scattering of light inside the spectrograph.

To take up the emergence of J_s in place of J, let x or x' stand for the distance along the plate, then at every point $P(x')$, the transparency of the plate is given by $J_{x'}$ corresponding to the blackening $F_{x'}$ at that point. When the point P comes exactly at the centre of the intensity pattern $S(x-x')$ of the slit image, the beam intensity (or deflection) $J_{s,x'}$ is said to correspond to $P(x')$. Evidently $J_{s,x'}$ is the convolution integral of the contour J, and the pattern $S(x-x')$. Thus we have

$$J_{s,x'}=\int_{x'-\beta}^{x'+\beta} J(x)\, S(x-x')\, dx \qquad \dots \quad (3)$$

where 2β is the effective width of the slit image, *i.e.*, $S=0$ for $|x-x'|>\beta$. In the ideal case of an infinitesimally narrow slit, the S function for correct interpretation of results is the δ function *i.e.*, unity at $x=x'$ and zero at all other points. In the finite case, for constant $J(x)=C$, $J_{s,x'}=C\int_{x'-\beta}^{x'+\beta} S(x-x')dx$ and for regarding it as actually the same constant,

$$\int_{x'-\beta}^{x'+\beta} S(x-x')=1 \qquad \dots \quad (4)$$

which gives the correct value of the constant in the S function.

Repeated integration of R.H.S. of equation (3) above by parts gives

$$J_{s,x'}=\Big|J(x)D^{-1}S(x-x')-J'(x)D^{-2}S(x-x')+J''(x)D^{-3}S(x-x')\dots\Big|_{x'-\beta}^{x'+\beta}$$

where negative powers of the operator D stand for the order of repeated integration. Since the function S is much more close than $J(x)$, which is important and as alternate D's have negative and positive symmetry, we can write down

$$J_{s,x'}=\Big[J(x'+\beta)+J(x'-\beta)\Big]\Big|D^{-1}S(x-x')\Big|_{0}^{x'+\beta}-\Big[J'(x'+\beta)-J'(x'-\beta)\Big]\times$$

$$\Big|D^{-2}S(x-x')\Big|_{0}^{x'+\beta}+\Big[J''(x'+\beta)+J''(x'-\beta)\Big]\Big|D^{-3}S(x-x')\Big|_{0}^{x'+\beta}-\quad\dots \quad (5)$$

$$=\Big[J(x')+\frac{\beta^2}{2}J''(x')\Big]2D_1-\beta J''(x')2D_2+J''(x')2D_3 \qquad \dots \quad (6)$$

The meaning of symbols D_1, D_2, etc., is obvious. For any particular S distribution these integrals can be worked out for small β. Two special cases may be considered :—

(*i*) $S(x-x')=$ a constant for 2β about x' and zero everywhere outside this range. From consideration of (4), $S(x-x')=1/2\beta$ and the result is

$$J_{s,x'}=J(x')+\frac{\beta^2}{4}J''(x')+\dots\dots \qquad \dots \quad (7)$$

Effects like those of limited resolving power of the prism or the grating in the spectrograph and that of the photographic emulsion, already referred to, can be treated like this case in the first approximation.

(*ii*) When S has got some Gaussian or such symmetrical distribution within the range 2β of x it may be put as $\sqrt{\frac{a}{\pi}}\, e^{-a(x-x')^2}$ and outside this range as zero. Thus

$$J_{s,x'} = J(x') + \frac{\beta^2}{2} J''(x') \left\{ 1 - \sqrt{a} + \frac{a}{2} \right\} + \ldots\ldots \qquad \ldots \quad (8)$$

Practically similar results are obtained if $S(x-x')$ were any other expression like $Si^2[a(x-x')]$ or $Si_2[b(x-x')]$ where Si has the usual meaning and Si_2 stands for the form $\int_0^{\alpha} \frac{\text{Sin}^2 \alpha}{\alpha^2}\, d\alpha$. Such cases arise whenever slit effects or in other words limited resolving power on account of finite slit widths is considered.

From (7) and (8) it is obvious that for the points of inflexion where $J''(x')=0$ we have $J_{s,x'}=J(x')$. Thus as pointed out earlier the distance between the points of inflexion is independent of slit effects. It is also obvious that neglecting higher order terms than the second, the complete areas (or the areas in the symmetrical halves) $\int J_{s,x'}dx'$ and $\int J(x')dx'$ are equal. Thus the area A in fig. 3 is equal to the areas B. However similar areas are not equal on the blackening or on the deflection curves when these are not proportional to the illuminations. It is also clear from equation (7) as to how the curve $J_{s,x'}$ always faces the concave side of Jx'. For usual graphical calculations in connection with the slit effects, *viz.*, those of Langesth and Walles (*loc. cit.*), only the first term in (5) is kept in view and

$$J_{s\,x'} = \tfrac{1}{2}\left[J(x'+\beta) + J(x'-\beta) \right] \qquad \ldots \quad (9)$$

It must be clearly borne in mind that when a particular line has a distribution closer than that of the photometer slit image the observed distribution will in no way be near the real one but it will tend to correspond to the S distribution. Only in this case the maximum amplitude will be proportional to the area under the original curve. Thus for any photometer slit width $b=2\beta$, line contours only of larger half width than this can be studied. Therefore, b must be small. But one does not gain much by reducing b to less than the value required to give a resolution equal to that of the photographic emulsion. The least distance that can be resolved by a photographic fine grain process emulsion is 12μ according to Mees (1931), and the slit distribution with a given purity of a projected slit width about 10μ can resolve distances up to 10μ according to Plaskett (1934). So b should at least be kept of the order 10μ.

For determination of the purity of the microscope objectives as well as the theoretical resolution of the microphotometer, the determination of effective width of the slit image and the intensity distribution inside, is of interest. The simple procedure followed by Sandström (1933) of regarding the difference between the breadth of a microphotogram of a fine scale division at the foot and at the top as four times the effective breadth of the slit is evidently incorrect. Such a method can be applicable only if the intensity distribution inside the slit image is uniform falling suddenly to zero at the extremities. Even then the difference in breadth is only twice the width of the slit image and not four times. Also the microphotogram must be first corrected for the non-linear response of the barrier layer photo cell employed in the Siegbahn design.

Plaskett has obtained the distribution from the microphotogram of transmission across a narrow opening as a cut on an Abbe test plate. However this is an unnecessarily laborious method. The simple method of a straight edge mentioned also by him may be considered in the following way. In Fig. 5 the intensity distribution (I) inside the slit image is represented as being progressively unscreened by an extended obstacle with a straight edge (E). For any variable point P of plate falling on the x' centre of the slit image when the straight edge is at x, the beam intensity is given by

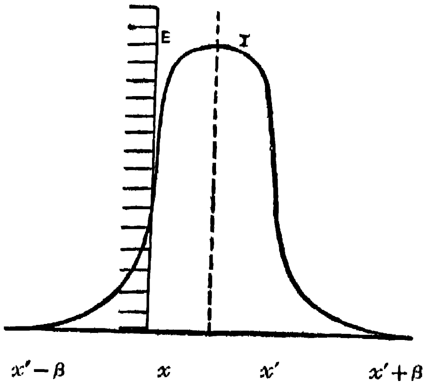

A straight edge traversing the slit image.

FIG. 5

$$J(x') = \int_{x}^{x'+\beta} S(x-x')\,dx \qquad \ldots \quad (10)$$

Differentiating (10) we get $\frac{dJ(x')}{dx'} = S(x-x') - S(\beta) = S(x-x')$

since $S(\beta)=0$. Thus we have simply to get a microphotogram when a straight edge traverses the microphotometer slit and then differentiate, at every point, the J curve computed from the deflection curve. Fig. 6*a* gives such a microphotogram in case of Siegbahn instrument of this laboratory. Fig. 6*b* gives intensity distribution derived from it. From the record to plate ratio the half width is found to be 25μ in this case. Slight structure clearly shown by the curve (also visible through a high power microscope) and the large width must be ascribed to the causes as have been given in connection with methods of slit irradiation by Stockbarger and Burns (1931), namely, coherent illumination of primary slits of about double the size necessary to give single maxima. The double structure was actually removed by readjustment on simply reducing the primary slit width inside the illumination unit of the microphotometer. The half width, at present is about 6μ.

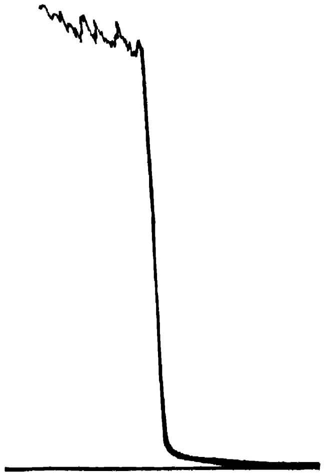

Microphotogram when a straight edge traverses the slit image

FIG. 6 (a)

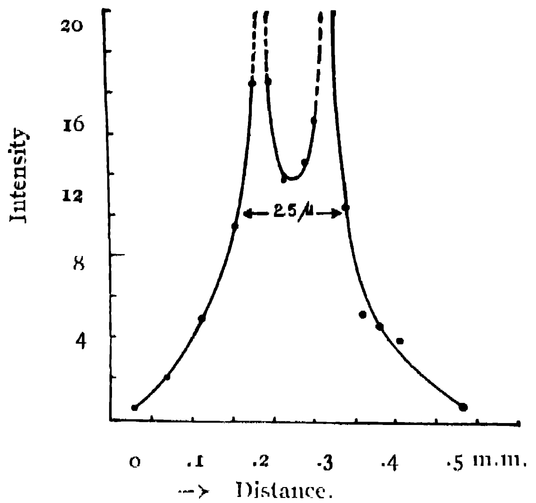

Intensity distribution inside the image of a microphotometer slit Doubling up is due to incorrect setting.

FIG. 6 (b)

CONCLUSION

(1) In absorption spectrophotometry the necessary calibration of individual photographic plates must be carried out by a self-consistent device. The rotating wire gauze screens have been found to give a self-consistent curve within the sensitiveness of the photo-cell arrangement. Inverse square comparison of the transmissions of different screens known from area consideration gave satisfactory results inside the wavelength region studied (process plates and point-o-lite in glass source).

(2) For the given resolution of a spectrograph, lines of certain minimum width alone can be studied. Otherwise the spurious effects cause the calculated transmission in the centre to be very much different from the actual which may lead to totally erroneous k_ν's. The effects of limited resolving power of the dispersing agent in the spectrograph and that of the photographic emulsion can be distinguished from the effects of finite size of the slit images for the spectrograph and the microphotometer. The calibration curves obtained especially from a source of uniform spectral distribution are free from all levelling errors described above. However, the observed contours must be corrected for all the

errors, before the use of the observed calibration curves can be made to give original intensities.

(3) All these errors individually tend to level out the contours, *i.e.*, depressing the convexities and lifting the concavities of the curves, the points of inflexion remaining undisturbed. Nevertheless, the complete areas of the true and the disturbed curves in each step are equal.

(4) Microphtogram of a straight edge gives an easy and accurate method of knowing the intensity distribution inside the slit pattern in a microphotometer assembly. This method may also be applied with advanatage in testing the purity of the image given by a microscope objective.

ACKNOWLEDGMENT

In the end I wish to thank Dr. P. K. Kichlu at whose suggestion this discussion of various problems of spectrophotometry has been attempted. My thanks are also due to Dr. A. M. Mian and Mr B. M. Anand of the Panjab University, Physics Department, for gladly helping me in theory and experiment whenever approached.

Physics Laboratory,
Government College,
Lahore.

REFERENCES

Cittert, (1930), *Zeits. fur Phys.*, **65**, 517.
Ditchburn, (1927), *Proc. Camb. Phil Soc* , **27**, 959.
Grossman, (1943), *J. Opt Soc. Amer* , **33**, 185.
Harrison, (1929), *J. Opt. Soc. Amer* , **18**, 492.
Korff, (1931), *Phys. Rev* , **38**, 473.
Langseth and Walles, (1934), *Nature*, **133**, 210.
Minkowski, (1926), *Zeits. für Phy.*, **36**, 839.
Mees, (1931), *J. Opt. Soc. Amer.*, **21**, 753.
Nanda, (1945), *Ind. J. Phy.*, **19**, 8.
Plaskett, (1934), *Month. Not. Roy. Astr. Soc.*, **96**, 160.
Sandström, (1933), *Zeits. für Phy.*, **84**, 541.
Sawyer and Vincent, (1943), *J. Opt. Soc. Amer.*, **33**, 247
Stockbarger and Burns, (1931), *Phy. Rev.*, **37**, 920.

THE EFFECT OF TRANSVERSE MAGNETIC FIELD ON THE LONGITUDINAL JOULE MAGNETOSTRICTION EFFECT IN NICKEL

By OM PARKASH SHARMA

ABSTRACT. The effect of a transverse magnetic field on the longitudinal Joule magnetostriction effect in nickel, predicted by Williams (1912), has been observed for low values of longitudinal magnetic fields. Williams' (1927) method of combining mechanical and optical magnifications has been used. Since the magnification of the present apparatus ($\sim 10^6$) is insufficient, no quantitative conclusions have been drawn. According to a view of Williams, the effect is possibly caused by the imposition of the transverse field on the specimen, longitudinally magnetised. However, it has been explained on Becker's ideas, assuming that the effect of a transverse field is equivalent to that of tension.

INTRODUCTION

The phenomena of magnetostriction *i.e.* changes in dimensions especially of ferromagnetic substances, when subjected to the action of magnetic fields, have been known since long. In 1912 S. R. Williams (*loc. cit.*), on the basis of his so called Planetesimal theory of magnetism, mentioned the possible occurrence of an additional change in length due to imposing a transverse magnetic field on a longitudinally magnetised rod of a ferromagnetic material. The author has not come across, in the existing literature, any attempt that may have been made to detect this effect. Recently I have observed such an effect of a transverse field on a longitudinally magnetised rod of nickel. The effect of the transverse field comes out to be an increase in the ordinary magnetostrictive contraction.

As the largest magnetostrictive changes are of the order of 10^{-5} cm per unit length of the material, it is necessary to sufficiently magnify them before they can be visually observed or suitably recorded. Out of the various methods employed, the combination of a mechanical and an optical lever has been the most frequently used. In this work also such a combination with a magnification of 4.67×10^5 was used, but since the phenomenon observed under the present conditions involves exceedingly minute changes, the present study can only be said to be of a qualitative nature.

APPARATUS

The apparatus used is shown in diagram. A solenoid (4) wound with enamelled copper wire (S. W. G. 22) on a wooden bobbin, 17 cms long, with an internal diameter of 1 inch and having 2400 turnes in all, rests on a suitable, very rigid brass frame work. This consists of two brass plates, A and B, of which A is permanently fixed at one end of the rod (2), whereas B is capable of sliding along the length of the rod and may be fixed at a desired position.

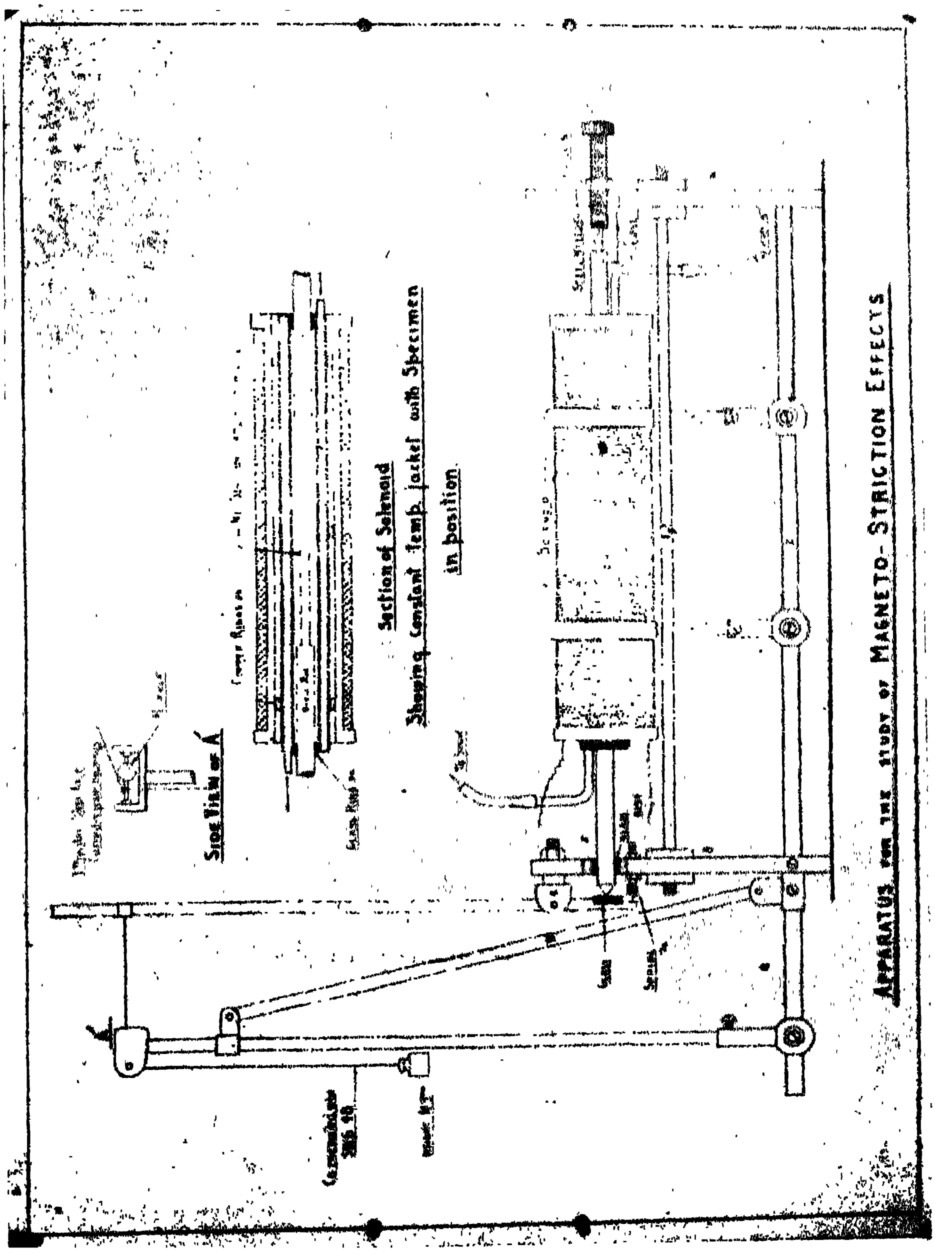
APPARATUS FOR THE STUDY OF MAGNETO-STRICTION EFFECTS
Section of Solenoid Showing Constant temp. Jacket with Specimen in position
Side View of A

DIAGRAM

There are two strong and stout supports (3, 3) similarly held on the rod (2). A double walled copper cylinder (9), through which water can be circulated fits symmetrically well inside the solenoid by three copper rings (9*b*). The nickel rod, (above 90% pure but the purity has not been tested) 9 cms long and .40 cm diameter, has its two ends soldered exactly straight to two extension brass rods each ¼″ in diameter (shown in section diagram), and is axially and centrally placed inside the solenoid, (or the water jacket) care being taken to allow it complete longitudinal freedom of movement. The symmetry of the rod inside the solenoid is achieved by the fact that not only the double walled copper vessel is symmetrically and tightly held inside the solenoid but also that two glass sleeves are fixed as shown (9*a*) of just the internal diameter as to allow the free sliding of the extension brass rods without any sideways movement. The free end of one brass rod has a sharp steel needle soldered to it, the tip of the needle resting in a jewelled screw, whilst the free end of the other brass rod, which is tappered to a point presses against a glass plate fixed on the shorter arm of the mechanical lever (7) with an adjustable lever ratio. On the longer arm of the mechanical lever, and at about a distance of 20 cms from the axis of rotation (6), is slid a small brass sleeve. The axle of the optical lever, having a diameter of 1.00 mm, is prepared from a thin steel needle. A small portion of the axle is filed flat and a small mirror attached to it. The optical lever is then supported in jewelled bearings mounted in a brass yoke (A′).

One end of thin copper wire (S. W. G. 48) is soldered to the brass sleeve (6). The wire is given one turn round the axle of the optical lever (kept at the same level as the brass sleeve) and is kept taut by a 10 gms weight soldered to its other end. Two terminals (not shown in the diagram) are fixed on the brass rods (which form the continuation of the nickel rod) for passing the current through the specimen. The rod is electrically insulated from the other parts of the apparatus by annular glass sleeves. Two other brass rods (1, 1) are used to ensure rigidity of the apparatus and a rod (8) to avoid any yielding of the support of the optical lever. Any changes occuring in the length of the specimen on magnetisation, are observed through the telescope on a scale placed at a distance of one metre from the optical lever.

EXPERIMENTAL PROCEDURE AND RESULTS

Calibration of the solenoid: Let $2b$ be the length of the solenoid (Fig. 1), a its mean radius and O its centre. Taking the axis of the solenoid as axis of X,

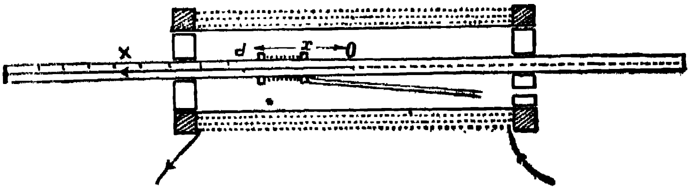

Calibration of the solenoid

FIG. 1

the magnetic field at any point P, where $OP=x$, is given by the expression (Pidduck)

$$H=\frac{2\pi ni}{10}\left[\frac{l+x}{\{a^2+(l+x)^2\}^{\frac{1}{2}}}+\frac{l-x}{\{a^2+(l-x)^2\}^{\frac{1}{2}}}\right]$$

where n = number of turns per cm.

i = current in amps.

H = field in gauss.

The values of the field (H_{cal}) at different points along the axis of the solenoid for $i=1$ amp., as calculated from the above expression are given in Table 1 and

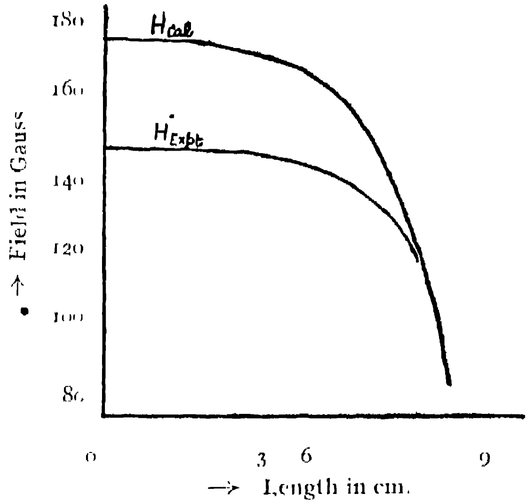

Variation of H with distance from the centre of the solenoid.

FIG. 2

graphically shown in Fig. 2. However, to determine the actual values of the field, a small search coil, 2 cms long. wound on a glass rod, with enamelled copper wire (S. W. G. 38) with 263 turns, was placed along the axis of the solenoid, the search coil being at a particular position. A current of 1 amp* was passed through the solenoidal winding and the field obtained from the inductive throws of the moving coil ballistic galvanometer. The search coil was then shifted in steps of one cm and the field (H_{expt}) obtained at different places along the axis of the solenoid (Tab. 1) and graphically shown in Fig. 2. It is seen from Fig. 2, that the field is sufficiently uniform (within 2%) in the central region occupied by the rod. The experimental value (144 gauss per amp) is, however, lower than the theoretical value (169.6 gauss per amp.).

---

[*] Actually observations were taken with three values of the current, namely, .7, 1.0, and 1.4 amps.

TABLE I

Length in cms. measured from the centre of the solenoid.	0	1	2	3	4	5	6	7	7·7	8.5
H_{cal}	172.1	172.0	171.4	170.1	167.9	163.9	156.0	139.7	119.7	87.9
H_{expt}	145·5	145·5	145·5	142.9	142.9	141.6	137.7	129.7	118.0	...

EXPERIMENTAL PROCEDURE

The specimen rod was demagnetised in a separate solenoid by passing a suitable value of A.C. 50 c.p.s, reducing it slowly to zero and then carefully mounted in the solenoid. Known currents were passed through the solenoid and the corresponding scale deflections were recorded. The changes in the length of the specimen due to temperature variations being quite slow could be very well differentiated from those due to the magnetic field, which are instantaneous. Still, to minimise any temperature effects due to the heating of the solenoid, the current through the solenoidal winding was passed for short intervals. As a further precautionary measure, water was kept circulating through the double walled copper cylinder surrounding the specimen.

A set of readings for the Joule magnetostrictive changes was recorded for low values of the longitudinal magnetising fields and, immediately after each observation, a transverse magnetic field was established by passing an electric current (5 amps) through the specimen itself for a short interval, of the order of a second or so, the resulting scale deflection being recorded (Table II).

TABLE II

Showing the effect of a transverse magnetic field on the longitudinal Joule magnetostriction effect in nickel.

Serial No.	Longitudinal magnetising field†		Readings of the scale					
			No current through the Specimen			5 amps. through the specimen deflection,	Current and field both off (zero reading)	Change in deflection due to current through the specimen
	current (amps)	Field (Gauss)	Zero reading (no field)	Final reading (field on)	Deflection			
1	.20	28.8	214.5	214.6	.1 mm.	.2 mm.	214.5	.1 mm.
2	.295	42.5	221.5	221.7	2 ,,	·4 ,,	22.5	.2 ,,
3	·40	57.6	196.0	196.3	·3 ,,	.6 ,,	196.0	·3 ,,

† The demagnetisation factor has not been taken into account.

REMARKS

With higher longitudinal fields, the transverse field being kept constant, the effect vanishes. Higher transverse fields were tried by increasing the value of the current through the specimen, but it was found that even during the fraction of a second, for which the current was passed, the heating of the specimen was sufficient to shift the zero reading appreciably, and give very discordant observations. However, the effect observed (*i.e.*, a greater contraction when an electric current is passed through the specimen) cannot be attributed to a temperature increase, because an increase in temperature should produce an elongation and not a contraction, which is actually observed.

It may be remarked that the effect, whether longitudinal or transverse will depend upon the specimen. Thus if we have two specimens both of the same size and cut from the same rod, the longitudinal and transverse effects will be different. This is due to the different magnetic history and heat treatments of the specimen. That is why, as Heaps has shown, the observations of two independent observers, using different samples, cannot be compared with each other with any degree of exactness.

DISCUSSION

From the above observations it is evident that qualitatively speaking, the effect of a transverse magnetic field is to double the Joule magnetostrictive contraction for low values of the longitudinal magnetising field but for higher longitudinal fields, there is practically no change observed in the ordinary contraction. Such an effect may be explained on Becker's theory of magnetostriction. Becker has shown that within the region of technical saturation, a nickel wire under the simultaneous action of a sufficiently great longitudinal tension F and a longitudinal field H, would be magnetised with the magnetic vectors making an angle of the average value θ with the axis of the wire, given by,

$$\cos\theta = \frac{I_s}{3\lambda_{0,s} \cdot F} \cdot H \qquad (i)$$

where I_s is the technical saturation intensity of magnetisation and $\lambda_{0,s}$ is the experimental value of the contraction per unit length when saturated. I_s and $\lambda_{0,s}$ being constants for a particular specimen, equation (*i*) can be written as,

$$\cos\theta = \frac{k}{F} . H \qquad \text{where } k = \frac{I_s}{3\lambda_{0,s}}.$$

and under such circumstances, the magnetostriction constants $\lambda_{0,s}$ for an unstretched wire and $\lambda_{F,s}$ for a wire under tension are related as

$$\lambda_{F,s} = 3/2\ \lambda_{0,s} \qquad \ldots \quad (ii)$$

i e. to say the magnetostriction contraction in a stretched wire is 1.5 times that in an unstretched wire.

The effect observed is in close conformity with the above ideas of Becker. When transverse field is applied, radial contraction of the specimen results, with a necessary result of longitudinal extension (Heaps 1915). This longitudinal extension due to the transverse field being sufficiently small, does not affect the original reading appreciably. However, to check this point, the mentioned value of the current was passed through the specimen (longitudinal magnetic field being absent) and it was found that there was no change in the reading, which probably means that the longitudinal extension due to the passage of the current through the specimen (or the accompanying field) is not sufficient (Heaps) as to be detected by the present apparatus. It was found that the change in length due to temperature rise, being slow, appeared nearly after 30 seconds. However the present effect cannot be confused with the temperature effect, as the first one being instantaneous and the other being much slower the two can be very well differentiated. Thus we suppose that the imposition of transverse field is equivalent to applying tension to the specimen. The reverse of this, *i.e.* that when tension is applied to a nickel rod, a transverse magnetism is developed, is clearly evident from equation (*i*), thus showing a reciprocity of magnetic and mechanical effects (Williams), (Mckeehan, 1926).

Considering the rod to be initially magnetised by a magnetic field along OX (Fig. 3), the magnetic vectors point along OX. If such a rod is stretched

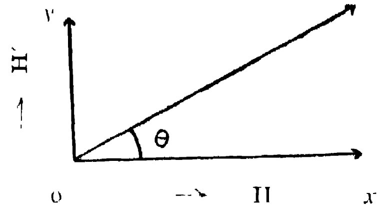

FIG. 3

the magnetic vectors make an angle θ with OX given by eq. (*i*). Instead of stretching, if we apply a transverse field (H') along OY again the magnetic vectors will make an angle $\theta = \tan^{-1}$ OY/OX and therefore a tension should result. Under such conditions equation (*ii*) will be applicable. The results obtained are nearly 33% higher than the theoretical ones, however, the present accuracy does not allow any exact comparison.

The above also explains the null effect in higher longitudinal fields, because as H is increased H' remaining constant, the resulting tension is insufficient and hence there is no effect. However, with higher transverse fields, greater magnification and elimination of heat effects the exact quantitative nature of the phenomenon may be studied.

ACKNOWLEDGMENTS

In the end I wish to express my deep gratitude to Prof. J. B. Seth and Dr. H. R. Sarna for their kind interest and guidance in this work and Mr. Harish Chander, M. Sc. for his help while setting the apparatus. I also thank S. Harbhajan Singh, our laboratory mechanic, for assisting me in constructing certain parts of the apparatus.

PHYSICS LABORATORY,
GOVERNMENT COLLEGE,
LAHORE,

REFERENCES

Bates, Modern Magnetism, p. 305-307.
Heaps, C. W , 1915, *Phys. Rev* , **6**, 34
Mckeehan, L.W., 1926, *Phys. Rev.*, **28**, 158.
Fidduck, Treatise on Electricity, p. 158-159
Williams, S. R., Magnetic Phenomena.
,, ,, 1912, *Phys. Rev.*, **34**, 280.
,, ,, 1927, *Jour Opt. Soc. Amer.*, **14**, 385

The following special publications of the Indian Association for the Cultivation of Science, 210, Bowbazar Street, Calcutta, are available at the prices shown against each of them :—

No.	Subject		Author	Price		
				Rs.	A.	P.
III	Methods in Scientific Research	...	Sir E. J. Russell	0	6	0
IV	The Origin of the Planets	...	Sir James H. Jeans	0	6	0
V	Separation of Isotopes	...	Prof. F. W. Aston	0	6	0
VI	Garnets and their Role in Nature.	...	Sir Lewis L. Fermor	2	8	0
VII	(1) The Royal Botanic Gardens, Kew.	...	Sir Arthur Hill	1	8	0
	(2) Studies in the Germination of Seeds.	...	,,			
VIII	Interatomic Forces	...	Prof. J. E. Lennard-Jones	1	8	0
IX	The Educational Aims and Practices of the California Institute of Technology	...	R. A. Millikan	0	6	0
X.	Active Nitrogen A New Theory	...	Prof. S. K. Mitra	2	8	0

A discount of 25% is allowed to Booksellers and Agents.

RATES OF ADVERTISEMENTS

Third page of cover	... ...	Rs	25, full page
do. do.	... ...	,,	15, half page
do. do.	... ...	,,	8, quarter page
Other pages	... ...	,,	19, full page
do.	... ...	,,	11, half page
do.	... ...	,,	6/8, quarter page

Suitable reductions are allowed for six or more consecutive insertions.

ON THE SPONTANEOUS EMISSION OF NEUTRONS FROM THE URANIUM NUCLEUS

By S. D. CHATTERJEE[*]

ABSTRACT. Using a boron-lined ionisation chamber filled with BF_3, the spontaneous emission of neutrons from the uranium nucleus has been detected. It is suggested that they are produced as a result of the spontaneous fission of uranium and that 3 neutrons are emitted per each such process.

INTRODUCTORY

Soon after the discovery of the induced fission of the uranium nucleus due to neutron bombardment, it was realised that in whatsoever way the ${}_{92}U^{239}$ nucleus divided itself, there must be an excess of neutrons over that contained in normal nuclei of the same atomic number. There seemed to be two possibilities of getting rid of this neutron excess :

(1) by the emission of a β-ray, a neutron may be transformed into a proton, thus reducing the neutron excess by two units.

(2) by the direct liberation of the neutrons taking place either as a part of the fission itself, or as an "evaporation" process from the resulting nuclei which would be formed in an excited state.

The evidence for the first process was obtained from the successive β-transformation of many of the fission products. The direct emission of neutrons during the second process, was sought for and obtained by several experimenters, employing various methods.

Von Halban, Joliot and Kowarski (1939), measured the distribution of neutrons surrounding a neutron-source placed at the centre of a large container filled with a solution of uranyl nitrate. Another set of measurements was made in which a solution of ammonium nitrate of the same strength was used instead of uranyl nitrate. They found a 5% higher intensity in the former case and associated it with the production of secondary neutrons due to the induced fission process in uranium. The average number of neutrons produced per fission was calculated to be 3.5 ± 0.7. Dodé et al (1939) also demonstrated that the neutrons produced during induced fission were fast neutrons.

Further experimental evidence of neutron emission during induced fission was obtained by Anderson, Fermi and Hanstein (1939), and Haenny and Rosenberg (1939).

The experimental investigations on the spontaneous fission of the uranium nucleus, carried out by the author, (Chatterjee, 1944) raised the interesting question whether the process of spontaneous fission of U is likewise accompanied by the emission of neutrons. The following experiment was therefore undertaken to verify the correctness of the above hypothesis and also to determine the half-life period of the corresponding process. A preliminary report of our findings was published in a note in Science and Culture (1944).

---

[*] Fellow of the Indian Physical Society

PRINCIPLE OF THE METHOD OF MEASUREMENT

A proportional counter, lined with a thin layer of boron powder and filled with BF_3 gas is used. Owing to the comparatively high gas-pressure (~ 1 atm), the counter is used as an ionisation chamber, in conjunction with a linear amplifier and a thyratron-operated mechanical recorder. The rate of counting of such an arrangement may be represented by

$$A + B + C,$$

where A represents the number of slow neutron-induced boron disintegrations, the resulting α-particles being counted.

B is the number of recoil nuclei produced by fast neutrons traversing the counter.

C is the number of other particles of high specific ionization passing through the counter.

It is evident that

$$A = VN_B \rho \sigma_B v_B + (N_A \rho / \mu) R_B \sigma_B .$$

$$B = VN \int_{v_2}^{v_1} i(v) \sigma(v)\, dv .$$

$$C = S \int_{v_4}^{v_3} I(v)\, dv$$

where V = volume of the counter.

N = the total number of nuclei per c.c. in the counter.

N_A = Avogrado's number.

N_B = the number of B^{10} nuclei per c.c.

ρ = the density of neutrons per c.c. with energies in the $1/v$ region.

σ_B = the capture cross-section for B^{10} for neutrons of velocity v_B.

R_B = the range of α-particles in boron.

μ = atomic weight of boron (B^{10}).

$i(v)dv$ = the current of fast neutrons of velocity between v and $v \mp dv$.

$\sigma(v)$ = the recoil cross-section of the nuclei of the gas for neutrons of velocity v.

S = the cross-sectional area of the counter.

$I(v)dv$ = the current per cm^2, of particles of high specific ionization, of velocity between v and $v + dv$.

The limits of integration, v_1 is the highest and v_2 the lowest neutron velocity producing measurable recoils, v_3 the the highest and v_4 the lowest velocity of a particle traversing the counter and producing enough ions to be recorded as a count.

It is evident that the counter is essentially a slow neutron detector, because $\sigma_B >> \sigma(v)$. It can also be seen that the factor C is due practically entirely to the radio-active contamination of the inner surface of the counter and that of the boron-layer; since the number of penetrating heavily ionizing particles in the cosmic rays at the sea-level is extremely low. Likewise, the contribution of factor B (due to cosmic ray fast neutrons at sea-level) is negligible. In fact, the back-ground of such a counter is practically solely determined by

(*i*) the radio-active contamination of the internal surface layer of the counter and (*ii*) the presence of slow neutrons in the atmosphere.

Owing to the high-value of the half-life period for the spontaneous fission of the uranium nucleus (as obtained in a separate experiment and described in details in the *Trans. Bose Res. Inst.*, (1945) the expected number of neutrons emitted by one gram of uranium per minute is extremely small in comparison with the back-ground count. The sensitivity of our arrangement has, therefore, been sought to be enhanced by

(1) employing a large quantity of U_3O_8 (corresponding to 1.2 kg. of metallic uranium),

(2) surrounding the U_3O_8-container with a thick paraffin cylinder in order to slow down the neutrons, and

(3) increasing the efficiency of the slow-neutron counter by using an optimum thickness of the boron layer on the inner surface and filling it with BF_3-gas at a pressure of 50 cms. of Hg.

EXPERIMENTAL ARRANGEMENT

The experimental arrangement is shown diagrammatically in Fig. 1. The neutron counter consisted of a brass-tube 5 cms. in diameter and 26 cms. in length. The two open ends were closed with ebonite discs fitted with amber plugs and earth guard rings. In order to prevent the occurrence of any paralysis of the subthreshold counter (Montgomery and Montgomery, 1940), due to an electron back-ground of high intensity, the field-strength in the neighbourhood of the central wire was reduced by replacing it with a thick brass-rod of about

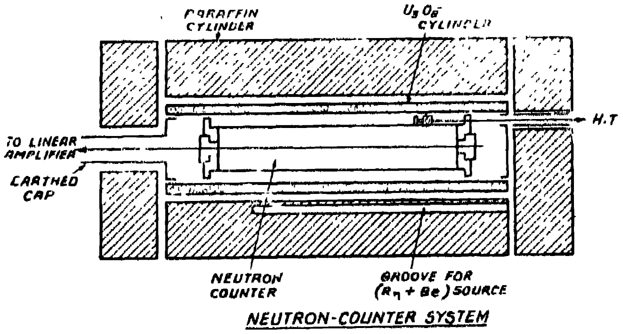

FIG. 1

2 mms. diameter. The inner surface of the outer brass-tube was lined with a thin layer of amorphous boron powder ($\sim$0.1 mm. thick) so that the range of the α-particles produced by the ${}_5B^{10}$ (n, α) ${}_3Li^7$ reaction was somewhat greater than the stopping-power of the layer. The counter tube was filled with BF_3 gas at a pressure of 50 cms. of Hg. The surface of the ebonite end-pieces within the counter was protected from the action of BF_3 gas by a thin layer of paraffin, while only piecein was used for making the counter gas-tight. A potential of +1200 volts was given to the body of the counter, while the inner electrode was connected directly to the grid of the first tube of the proportional amplifier. The counter was operated in the ionisation chamber region. The pulses were recorded by a thyratron operated mechanical counter.

The U_3O_8-container consisted of a hollow double-cylinder made of galvanized iron sheet, whose inner diameter was just large enough to accommodate the neutron-counter tube within it. Thus we had a layer of U_3O_8 of about 1 cm. thick surrounding the counter tube. The metal container was earthed. The U_3O_8 was prepared by igniting uranium-nitrate crystals.

The uranium container was further surrounded by a bigger double-cylinder of galvanised iron sheet containing paraffin of about 6 cms. thickness. The two open ends of the paraffin cover were also closed with paraffin bricks of suitable size.

The necessary measurement comprises of the following steps :

(1) Determination of the back-ground of the counter, when it is surrounded by the paraffin cover.

(2) Determination of the effect of slow neutrons by interposing the uranium container between the neutron-counter and the paraffin cover.

(3) Determination of the effect of fast neutrons, any other penetrating ionising particle or γ-rays emitted by U by keeping the uranium container in situ and removing the paraffin cover.

(4) calibration of the over-all efficiency of the neutron counter under working conditions by means of a weak standard (Rn + Be) source.

The calibration of the detector was performed by a method similar to that adopted by Booth, Dunning and Slack (1939) in their investigation on the delayed neutron emission from Uranium after the removal of the source of irradiation. For this purpose, the U_3O_8 container was replaced by a weak (0.11 mc.) Rn + Be source. In order to maintain the symmetry of the arrangements, as far as practicable, the (Rn + Be) source was contained in a narrow glass tube of about the same length as that of the uranium cylinder and inserted into a narrow groove in the inner surface of the paraffin cover as shown in Fig. 1. Care was taken to start the standardisation measurements about 4 hours after admitting radon gas into the glass tube containing Be, when the calculated rise of RaC from the pure emanation attained the maximum values. The effective number of neutrons per sec. per mc. from the (Rn + Be) source was taken to be 15,000 as recommended by Dunning *et al.*

RESULTS

The experimental results are presented in the following table :—

TABLE I

Expt.	Disposition of the experimental arrangement	Counts per minute	Remarks
A	Counter + paraffin cover	0.83 ± 0.02	Back-ground effect
B	Counter + U_3O_8 cylinder + paraffin cover	2.97 ± 0.04	Counts of slow neutrons per minute = B − A = 2.14
C	Counter + U_3O_8 cylinder	0.85 ± 0.04	Effect of neutrons emitted directly by uranium (without being slowed down by paraffin) C − A = 0.02
D	Counter + (Rn + Be) source (0.11 mc.)	206	* Efficiency of the counter = 1/480

* Determined from the ratio of the actual number of counts recorded by the neutron counter to the number of neutrons emitted by the Rn+Be source when placed in position indicated in Fig. 1.

It will be recognised from a comparative study of (C-A) with (B-A) that uranium emits essentially fast neutrons. When these are slowed down by scattering in the paraffin cover, they produce an effect which is approximately three times the back-ground effect. Incidentally, it is also clear that the γ-ray emitted by U has practically no influence on the number of counts per minute. That the observed increase in the number of counts is really due to the detection of slow neutrons was further verified by covering the counter with a cadmium foil of 0.5 m.m. thickness, when the number of counts per min. practically dropped down to the back-ground level.

Now, since the efficiency of our detector is only 1 in 480, the actual number of neutrons emitted by 1.2 Kg of uranium is 1027 per minute. Assuming, as before, that U^{238}, the most abundant isotope (99.2%) of uranium, undergoes spontaneous fission, and that a single neutron is emitted per fission process, the corresponding half-life period comes out to be 3.8×10^{15} years.

DISCUSSION OF THE RESULT

We have used two different methods to measure the half-life period of the products of the spontaneous fission of the uranium nucleus. The first one described in the Transactions of the Bose Research Institute (1945), is based upon the actual counting of the frequency of fission by measuring the large impulses produced by them in an ionisation chamber or a proportional counter. The second method described in the present paper counts the number of neutrons emitted per given mass of uranium nucleus. Now, in order to calculate the mean half-life of the spontaneously disintegrating nucleus, we have to make some assumption as to which of the three isotopes of U, is undergoing fission.

For the sake of definiteness, we assume that the most abundant of the isotope, *viz.*, U^{238} is undergoing fission. Based on this assumption, it is found that

$$T_{f_1} = 1.3 \times 10^{16} \text{ years by method (1)}$$

and

$$T_{f_2} = 3.8 \times 10^{15} \text{ years by method (2).}$$

We find that there is a discrepancy of the order of 3.4 in the ratio of the values of the mean life of spontaneous fission of U nucleus given by the methods (1) and (2). The second value is based on the assumption that associated with each spontaneous fission only one neutron is emitted. This discrepancy is removed if the assumption is made that on an average about 3.4 neutrons are emitted instead of one. This value is of the same order as that found by Dode' (*loc. cit.*) for the emission of fast neutrons associated with the induced fission of U nucleus. The value found will be independent of any particular assumption as to which particular isotope undergoes fission. It is obvious that the absolute value of T_f will change if it is found that some other isotope of uranium is responsible for the spontaneous fission ; but the ratio of the two T_f, which gives the number of neutrons emitted per nuclear fission is independent of any such particular assumption. More precise experiment is in progress.

The author is indebted to Prof. D. M. Bose, Director, Bose Research Institute, for his keen interest, helpful suggestions and discussion.

PHYSICAL LABORATORY,
BOSE RESEARCH INSTITUTE,
CALCUTTA.

REFERENCES

Anderson, Fermi and Hanstein, 1939, *Phys. Rev.*, **55**, 797.
Booth, Dunning and Slack, 1939, *Phys Rev.*, **55**, 981.
Chatterjee, S. D. and P. B Sarkar, 1944, *Science and Culture*, **9**, 560.
Chatterjee, S. D , 1944, *Science and Culture*, **10**, 263.
Chatterjee, S. D., 1945, *Trans. Bose Research Institute.*
Dode' *et al*, 1939, *Comp. Rend.*, **208**, 995.
Haenny and Rosenberg, 1939, *Comp. Rend.*, **208**, 898.
Montgomery and Montgomery, 1940, *R.S.I.*, **11**, 137.
Szilard and Zinn, 1939, *Phys. Res.*, **55**, 799.
Von Halban, Joliot and Kowarski, 1939, *Nature*, **143**, 680.

X-RAY DIFFRACTION STUDY OF DYED MERCERISED AND INTENSIVELY DELIGNIFIED JUTE FIBRES

BY N. G. BANERJEE, B. S. BASAK AND R. K. SEN

(Plate VIII)

ABSTRACT. Effects of the organic dye-stuffs methylene blue and congo-red on the structure of (1) raw jute fibres, (2) jute fibres subjected to intensive delignification, and (3) jute fibres subjected to incomplete mercerisation have been studied by means of X-rays. In the case of intensive delignification it was found that the cellulose crystallites remain unaffected but their orientations parallel to the fibre axes become deranged considerably. This change does not take place on incomplete delignification. Thus it is concluded that a fraction of the lignin in jute cements the cellulose fibrils to parallelism in a jute fibre and gives strength to it. This part of the lignin is more difficult to remove. The dye-stuffs were found to produce no effect on either the structure or the orientations of the cellulose crystallites whether native or mercerised. No change could even be discerned in the case of the dishevelled crystallite structure of intensively delignified jute.

INTRODUCTION

X-ray diffraction study of cellulose fibres has attracted the attention of a large number of workers over more than a quarter of a century and this has contributed much to our knowledge regarding the crystalline structure of cellulose and its derivatives. The unit cell structure of cellulose proposed by Polanyi (1921) and later by Sponsler and Dore (1926) were orthorhombic. Later on Meyer and Mark (1929) worked out a monoclinic cell with four glucose units ($C_6H_{10}O_5$) per unit cell. A new type of monoclinic cell was later suggested by Sauter (1937). Gross and Clark (1935), however, concluded that a monoclinic cell with $a=8.35$ A, $b=10.3$ A, $c=7.95$ A and $\beta=84°$ is in best agreement with the experimental results. It has also been established that the cellulose fibre is a crystalline aggregate consisting of small crystal areas (crystallites) separated by the amorphous or intercrystalline areas. A crystalline area is built up by the repetition of the unit cell arrangement of the glucose units, mentioned above, in all directions. The cellulose fibres studied by X-rays are ramie, flax, hemp, jute, etc. X-ray diffraction photographs of jute fibres have been taken in recent years in India by Banerjee and Roy (1941) and the work has been followed by Sircar, Rudra and Saha (1944), who are carrying out an extensive X-ray investigation of jute fibres. Banerjee and Roy found that the crystalline structure of jute cellulose is indentical with that of ramie and other varieties of cellulose. They also observed that lignin and fat do not enter into chemical combination with cellulose in jute fibre. It has also been found that the partial delignifications that have been studied in these earlier communications have no effect on the sharpness of the X-ray diffraction spots showing that even the orientations of the crystalline parts of cellulose are unmodified. The effect of complete delignification has been studied by us and the results form a part of the present communication. The effect of dyeing cellulose fibre has not apparently received sufficient attention of the X-ray diffraction workers. The purpose of the present investigation is also to study by the X-ray diffraction method the effect of dyeing raw, delignified and mercerised jute fibres by organic dye-stuffs.

EXPERIMENTAL

X-ray beam from a Hadding tube run at a voltage of about 40 K.V. and a tube current of 5 to 7 milliamps after collimation through a narrow circular slit was allowed to be incident on a bundle of parallel fibres about 1 mm. in diameter in a direction perpendicular to the fibre axis. The camera used was a cylindrical one of diameter 6 cm. The circular slit had a diameter of about .5 mm. and length 5 cm. In a cylindrical camera the diffracted rays in the equatorial plane fall normally on the film and the diffraction spots on the equatorial line are at equal distances from the centre of the camera thus minimising the intensity loss of the large angle spots that occur in a plate camera. This also produces a great increase in the range of observations in the equatorial plane.

Photographs of the following samples were taken :—

1. Untreated jute fibre
2. Untreated jute fibre dyed with methylene blue
3. Untreated jute fibre dyed with congo-red
4. Intensively delignified jute fibre
5. Jute fibre intensively delignified and dyed with methylene blue
6. Jute fibre mercerised with 25 % NaOH solution at a temperature between 25°C and 30°C for half an hour
7. Jute fibre mercerised as above and dyed with methylene blue
8. Jute fibre mercerised as above and dyed with congo-red

From the co-ordinates of the positions of the maxima in the spots on the different photographs their angular co-ordinates ϕ and μ were determined from the relations

$$\phi=\frac{x}{R} \quad \text{and} \quad \tan\mu=\frac{y}{R}$$

where x = half of the horizontal distance in the film between the two symmetrical spots on the same horizontal line at the two sides of the central spot.

y = vertical distance in the film of the spots from the equatorial layer line

R = radius of the camera

The relation $\cos\phi\cos\mu=\cos 2\theta_{n}$, then gives the angle of diffraction. The indices of the planes giving rise to the X-ray diffraction spots were determined by comparing the observed Bragg angles of reflection, with those calculated from the formula,

$$\sin\theta_{n}=\frac{\lambda}{2}\sqrt{\left(\frac{h^2}{a^2}+\frac{l^2}{c^2}-\frac{2hl}{ac}\cos\beta\right)\Big/\sin^2\beta+\frac{k^2}{b^2}}$$

where θ_{n} = Bragg angle of reflection for the plane (hkl) and a, b, c, are the axial lengths along the three axes ; β = angle between a and c axes ; and λ = wave-length of the characteristic radiation used. The values of a, b, c and β were

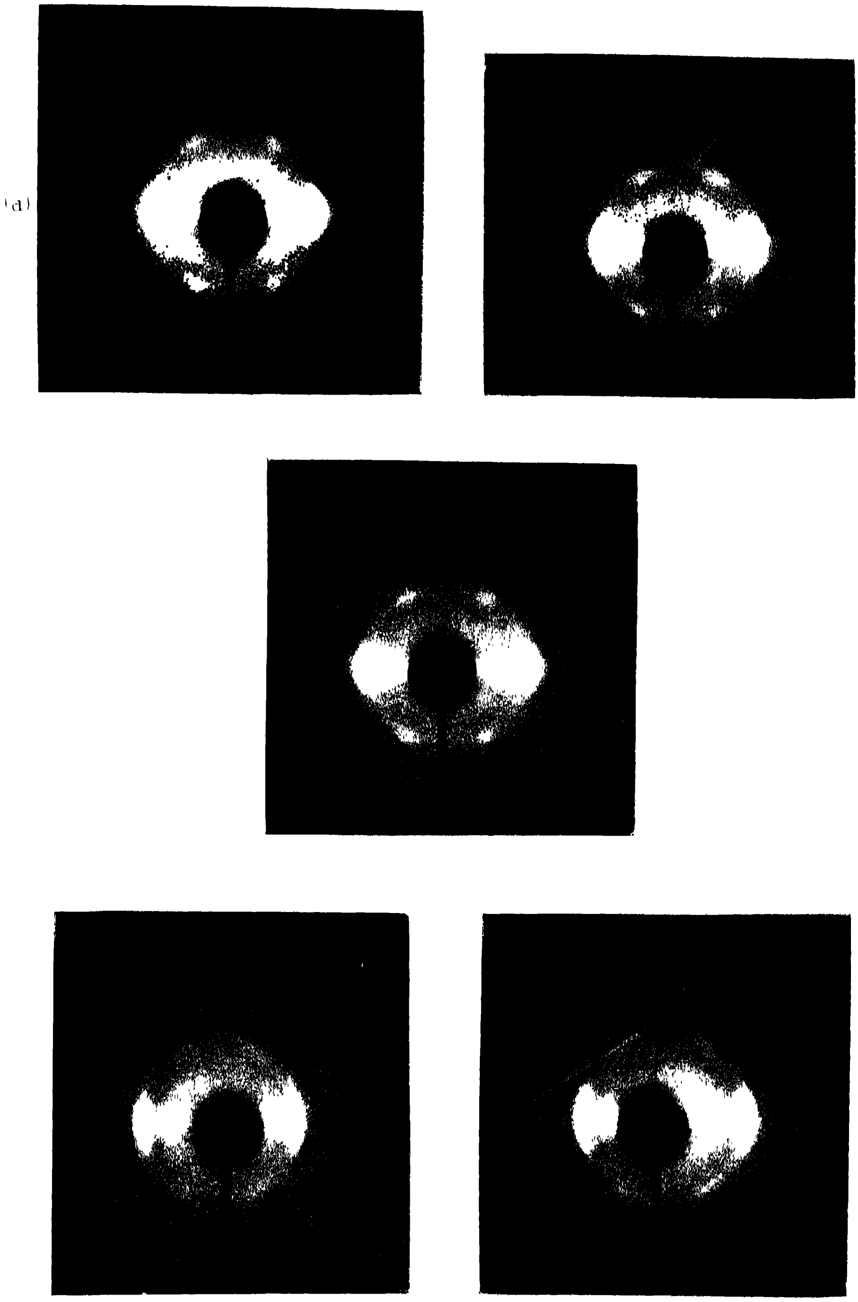

(a) — Raw Jute.

(b) — Raw Jute dyed methylene blue.

(c) -- Raw Jute dyed congo red.

(d) — Raw Jute delignified and dyed blue.

(e) -- Raw Jute delignified.

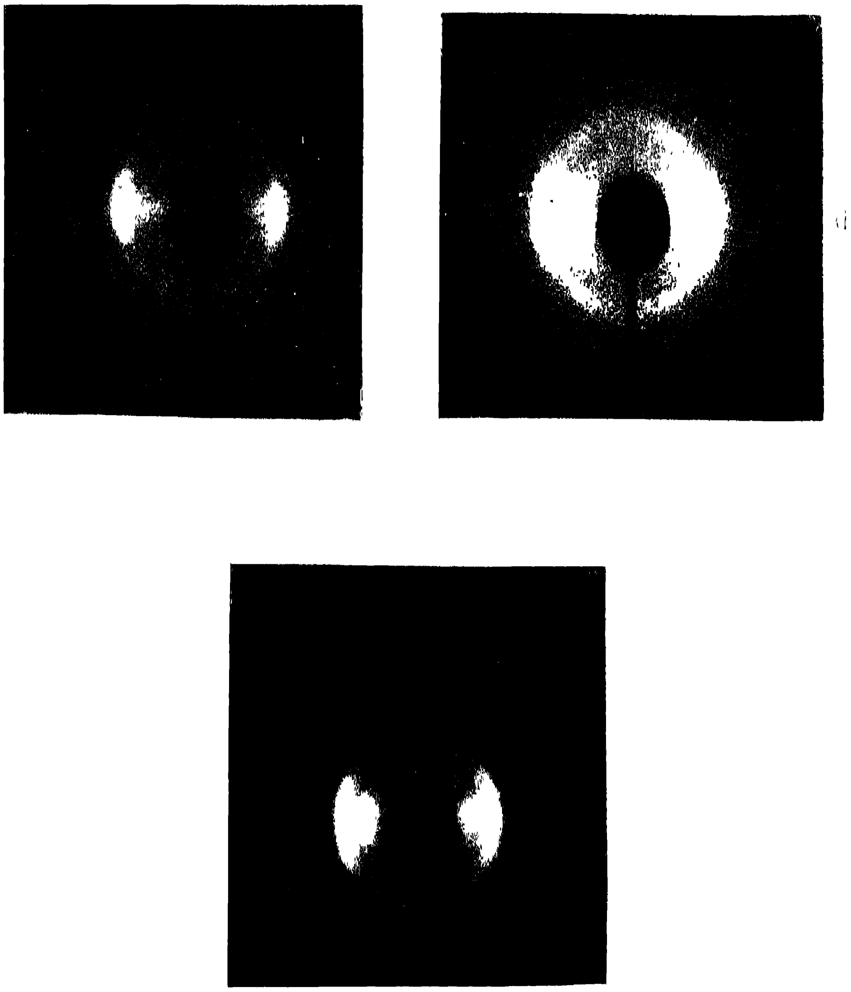

(a) Mercerised Jute

(b) — Raw Jute Mercerised and dyed blue.

(c) — Raw Jute Mercerised and dyed red.

taken to be those given by Meyer and Mark for (1929) the unit cell structure of cellulose. The indexing was facilitated by the knowledge of the order of the layer line to which a spot belongs. For this uniquely determines the index *k* of the planes giving rise to the spots. The Bragg angles of reflection for the different reflecting planes observed in the photographs of the different samples of jute and the calculated Bragg angles for the corresponding planes are given in the following tables.

TABLE I

Indices of the reflection planes	θ_n observed in the present investigation			θ_n Calculated
	Raw jute	Raw jute dyed blue	Raw jute dyed red	
101	7° 39′	7° 35′	7° 39′	7° 18′
101				8° 6′
120	10° 10′	10° 12′	10° 10′	10° 6′
021				10° 18′
002	11° 5′	11° 3′	11° 4′	11° 18′
311	17° 20′	17° 17′	17° 17′	17° 6′
212				17° 0′
032	17° 11′	17° 17′	17° 21′	17° 18′
$0\bar{0}4$	23° 1′	23° 8′	23° 1′	23° 6′

TABLE II

Indices of the reflection planes	θ_n observed in the present investigation		θ_n Calculated
	Delignified jute	Jute delignified and dyed with methylene blue	
101	7° 49′	7° 46′	7° 18′
$\bar{1}01$			8° 6′
120	10° 11′	10° 16′	10° 6′
021			10° 18′
002	11° 22′	11° 18′	11° 18′
032	17° 18′	17° 18′	17° 18′
311	17° 20′	17° 21′	17° 6′
212			17° 0′
004	22° 56′	22° 53′	23° 6′

TABLE III

Indices of the reflection planes	θ_B observed			θ_B Calculated
	Mercerised jute fibre	Jute mercerised and dyed blue	Jute mercerised and dyed red	
$\bar{1}01$ mercerised	5° 55′	5° 58′	5° 48′	6° 3′
101 native	8° 1′	8° 5′	7° 53′	7° 18′
$10\bar{1}$,,				8° 6′
002 mercerised	11° 1′	10° 59′	10° 54′	11° 0′
101 ,,				10° 3′
002 native				11° 18′

EFFECT OF COMPLETE DELIGNIFICATION OF JUTE

From the tables it is observed that the values of θ_B observed for the corresponding diffraction spots in the photographs of raw jute and perfectly delignified jute are within the limits of experimental error, in conformity with the earlier results of comparatively milder delignification. But in the case of completely delignified jute (Plate VIIIA*a*) there is an important difference namely that the spots are no longer as sharp as those of raw jute (Plate VIIIA*a*). They retain their sharpness along the radial directions but extend along the directions of Debye Scherrer rings so as to form arcs. This shows that the crystallites of retain their cellulose δsize but deteriorate as regards their alignment along the fibre axis. A part of the lignin thus helps to keep the cellulose crystallites in regular orientation. This part of the lignin is more difficult to remove while at the same time it does not produce any alteration in the cellulose lattice. From the above results we are led to the conclusion that in jute a bundle of elementary cellulose fibres are cemented together by a small amount of lignin to form a fibre in which the crystallites of cellulose are parallel. This fibre is again imbedded into an excess of lignin which is comparatively easier to remove. The removal of this excess of lignin does not produce appreciable change in the nature of X-ray diffraction spots or the strength of the fibres. The removal of the more resistant part of the lignin, however, produces a dishevelling of the fibres producing an extension of the X-ray spots as well as weakening of fibre strength.

ACTION OF ORGANIC DYESTUFFS ON JUTE FIBRES

X-ray photographs of raw jute fibres dyed with congo-red (Plate VIIIA*b*) as well as with methylene blue (Plate VIIIA*c*) and also delignified jute fibres dyed with methylene blue (Plate VIIIA*e*) have been found to be exactly identical with those of the corresponding undyed fibres as shown by the positions of the maxima (Tables I and II) and diffuseness of the spots. The dyestuffs do not give rise to any powder lines indicating that they enter the fibres in the amorphous state. This shows that not only the dyestuffs do not enter into the fibre crystallites but they are also unable to affect in any way the nature of the cementing of the cellulose fibrils by lignin, far to speak of any chemical combination with cellulose. It is of special interest that in perfectly delignified cellulose also dyeing does not produce any change in the extension of the diffraction spots. So the dyestuffs do not have any cementing action like lignin which would have produced an ordering of the crystallites and consequent shortening of the extensions of the spots.

X-ray photographs of jute fibres mercerised with 25% NaOH solution for half an hour at a temperature lying between 25 -30°C were taken (Plate VIIIB*a*). They showed the superposed patterns of both native and mercerised cellulose indicating that the fibres were partially mercerised. X-ray photographs of these mercerised fibres after dyeing with methylene blue (Plate VIIIB*b*) and with congored (Plate VIIIB*c*) were also taken. The patterns were quite identical with those of the fibres previous to dyeing as seen from the measurements of the positions of the maxima (Table III) as well as from the diffuseness of the spots except for an extension along the direction of the Debye Scherrer rings. This proves that even for mercerised cellulose the dyestuff has neither any effect on the crystalline structure of the mercerised cellulose nor on its aggregation, but a deterioration of alignment of the crystallites of both native and mercerised cellulose along the fibre axis takes place.

The authors have great pleasure in thanking Prof. K. Banerjee for valuable advice during the progress of the work.

INDIAN ASSOCIATION FOR THE CULTIVATION OF SCIENCE,
210, BOW BAZAR STREET, CALCUTTA.

REFERENCES

Banerjee, K. and Ray, A. K., (1941), *Proc. Nat. Inst. Sci.* (India), **7**, 376.

Gross, S. T. and Clark, G. L., (1935), *Z. Krist.*, **A 89**, 357.

Meyer, K. H. and Mark, H., (1929), *Z. Physik. Chem.*, **B 2**, 115.

Polanyi, M., (1921), *Naturwissenschaften*, **9**, 288.

Sauter, E., (1937), *Z. Physik. Chem.*, **B 35**, 83.

Sircar, S. C., Saha, N. N. and Rudra, R. M., (1944), *Proc. Nat. Inst. Sci.* (India), **10**, 325.

Sponsler, O. L. and Dore, W. H., (1926), *Colloid Symposium Monograph*, **4**, 192.

THE EFFECT OF TEMPERATURE ON THE ABSORPTION AND FLUORESCENCE SPECTRA OF IMPURITY CRYSTALS

By S. C. GANGULY

(Plate IX)

ABSTRACT. The absorption and fluorescence spectra of green Anthracene crystal at different temperatures were studied. At -180°C (liquid oxygen temperature) a new absorption band has been observed and at this temperature the fluorescence bands get sharper. As the temperature is lowered below room temperature the absorption bands become more and more intense and fluorescence bands sharper. At temperatures above room temperature the intensity of fluorescence bands diminishes and absorption bands grow weaker and weaker with rise of temperature.

INTRODUCTION

From studies of the absorptions and fluorescence spectra of single crystals of green anthracene the following important results were obtained previously (1944, 1945) by the author :—

(1) The positions and number of fluorescence bands of naphthacene are independent of exciting wavelength as long as the wavelength is not longer than its lowest absorption band.

(2) If the crystal is excited by strong ultra-violet radiations from a Hg. arc (3650, 4047A) in addition to the characteristic bands of naphthacene we get four more fluorescence bands which are due to anthracene.

(3) With the change of frequency of incident radiation we find a change of intensity of the fluorescence bands ; the intensity is greater when the incident light wave is an absoption band of the substance. The change of intensity is practically the same for all the fluorescence bands of the substance.

As the study of absorption and fluorescence spectra at different temperatures is expected to give much valuable information about the nature of the physical process involved in emission of fluorescence spectra and as the study at low temperature has been confined so far on powdered substances (1939) we have undertaken the study of fluorescence and absorption of a single crystal at different temperatures including low temperature.

EXPERIMENTAL

Absorption at low temperature.—A single crystal of Anthracene with slight traces of Naphthancene is taken. It is mounted on a copper plate (with a groove inside) attached at the end of a thin copper rod. The copper plate with the crystal in the groove is now introduced into a long narrow pyrex tube. A

PLATE IX

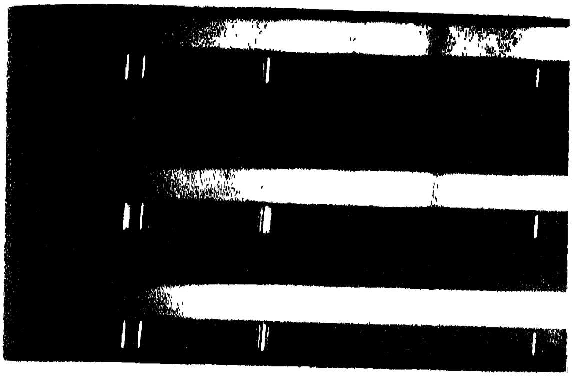

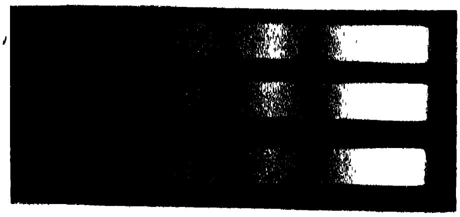

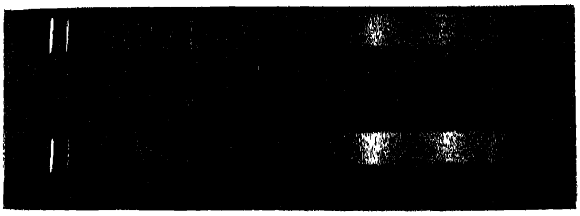

Fig. 3

Fig. 4

Absorption Spectra of Napthacene in Solid solution of Anthracene.

Fig. 1. : (a) at 30 c. (b) at 117 c. (c) at 180 c.

Fig. 2. : (a) at 30 c. (b) at 50 c (c) at 75 c.

Fluorescent Spectra of Napthacene in Solid solution of Anthracene

Fig. 3. : (a) at 30 c. (b) at 180° c.

Fig. 4. : (a) at 30 c. (b) at 50° c. (c) at 75° c.

copper plate just fitting the lower end of the interior of the tube and projected upward has been introduced for conduction. The whole is now immersed into a double walled vacuum flask. White light from a coiled-coil lamp is focussed on the crystal by means of a condensing lens. The transmitted light is received on the slit of the spectrograph. The absorption spectra at 30°C, 0°C, −10°C, −117°C, −180°C is taken. For 0°C, the lower end of the pyrex tube was filled with ice, for −10°C it was filled with ice and salt, for −117°C, it was filled with solidified alcohol, and for −180°C liquid oxygen is taken in a dewar flask. The temperature is recorded by a pentane thermometer. The Fig. (1) of Plate X shows the absorption bands at various temperatures. Time for each exposure is the same and current flowing in the lamp is kept fairly constant. Besides the continuous absorption bands shorter than 405 *m μ*, we find absorption band at 435, 460, 491 *m μ* which are all due to naphthacene.

Absorption at high temperature.—The crystal is mounted on the groove in a thick copper disc. The disc is placed well inside an electric heater both ends of which are open. For uniform heating a hollow copper cylinder both ends of which are open is inserted inside the heater. The heater is held horizontally and adjusted so that light from a coiled coil lamp passes through the crystal. The transmitted light is received on the slit of a Fuess spectrograph. By adjusting the resistance which is connected in series with the heater the current is adjusted. By inserting a thermometer the temperature is recorded. When the temperature becomes steady exposure is started. The current in the lamp is kept fairly constant all through the experiment. Time for each exposure is the same and photographs at different temperatures are taken on the same plate. (Fig. 2).

Fluorescence Spectra at Low Temperature.—The crystal is mounted in the same way as it was mounted for absorption experiment. Light from a mercury arc is condensed on the crystal and between lens and the crystal a filter transmitting 4047 A, 3650 A, is interposed. The fluorescent radiation with the transmitted incident light is received on the slit of the Fuess Spectrograph. The fluorescent spectra at room temperature (30°C) and liquid oxygen temperature (—180°C) are shown in Fig. (3).

Fluorescence Spectra at High Temperature.—The crystal is mounted exactly in the same manner as it was mounted for absorption spectra at high temperature. The ordinary lamp is replaced by a mercury arc lamp and between the mercury arc and the crystal a filter is interposed which transmitted only 3650, 4047 A. Light from the Hg. arc is condensed on the crystal by means of a condenser. The condenser should be placed between the filter and the Hg. arc. By adjusting the resistance which is connected in series with the heater the current is adjusted. By suitable adjustment of resistance we maintained 50°C and 75°C temperature inside the heater. When the temperature becomes steady exposure is given. Photographs are taken on the same plate and time for each exposure is the same (Fig. 4).

RESULT

Besides the continuous absorption bands shorter than 405 $m\mu$ we find absorption bands at 435, 460, 491 $m\mu$ which are all due to naphthacene. From visual observation it is quite evident that with the decrease of temperature, from room temperature the bands get sharpened. At liquid oxygen temperature we observe a new absorption band which is very sharp, on the shorter wave-length side of 491 $m\mu$, its actual wave-length being 486 $m\mu$. On careful inspection of the photograph it will be revealed that there is another absorption band on the shorter wavelength side of this new absorption band. That is due to liquid oxygen. The blank exposure shows the presence of it. As the crystal was surrounded by liquid air it is clear that this is due to liquid air. The temperature was raised from 30°C to 50°C, and hence to 75°C. It is found that the intensity of the absorption bands gradually diminishes with the rise of temperature.

Naphthacene has three fluorescence bands at 408, 533, 574 $m\mu$. From the plate it is evident that as the temperature is lowered below room temperature the bands get sharper and the intensity slightly diminishes, when the temperature is raised above room temperature, the intensity of fluorescence bands also gradually diminishes.

In conclusion, the author desires to express his grateful thanks to Professor K. Banerjee, D.Sc., for his keen interest in the work.

Indian Association for the Cultivation of Science,
210, Bowbazar, Calcutta.

REFERENCES

S. C. Ganguly (1944), *Nature*, **153** 652.
S. C. Ganguly (1945), *J. Chem. Phys*, **13**, 128.
J. T. Randall (1939), *Trans. Faraday Soc.*, **35**, 2.

27

MAGNETIC ANISOTROPY OF MOLYBDENITE AT DIFFERENT TEMPERATURES

By AJIT KUMAR DUTTA

ABSTRACT. The diamagnetic anisotropy and one of the principal susceptibilities of molybdenite crystals have been measured from 700° K down to 80° K. At low temperatures, the anisotropy tends to become independent of the temperature and at high temperatures its variation tends to obey approximately the Curie law. From the nature of the variation of the anisotropy with temperature and the considerations of its structure, the presence of metallic electrons having their motions restricted along the basal plane has been concluded. An attempt has been made to study the behaviour of these electrons in the light of modern theoretical investigations.

INTRODUCTION

Molybdenite crystal belongs to the hexagonal system and occurs in the form of a thin flake parallel to the basal plane. From the consideration of its structure it has been decided (Hultgren, 1932) that the binding between the molybdenum and sulphur atoms in it are essentially of the co-valent type; but the exact nature of the bonds that are formed along the basal plane is difficult to ascertain. The interatomic distances observed along that plane do not support the presence of ionic bindings. Workers on stereo-chemistry however, suggest the presence of bonds of partially metallic character. This view receives further support from its metallic lustre along the cleavage planes, metallic reflection from its surface (0001) (Coblentz and Kahler, 1919-20) and from its appreciable electrical conductivity along this plane. Moreover, molybdenite being a semiconductor the presence of free electrons in it does not appear improbable. The presence of free electrons having their mobility restricted along a plane should cause an enhanced amount of diamagnetism at right angles to that plane.

The magnetic measurements on molybdenite single crystals (1944) showed that whereas its susceptibility along directions in the basal plane, $\chi_\perp$, has the value -44.3×10^{-6} per gram. mol., the suceptibility along the hexagonal axis, $\chi_\parallel$, is about -87.1×10^{-6} per gram. mol. *i.e.*, the anisotropy is about 72 per cent. Thus our above conjecture receives much support from this finding. Now it seems proper to extend these measurements to various other temperatures, both high and low, since it is known that the free-electron-susceptibility is extremely temperature sensitive. The present paper gives an account of these measurements.*

EXPERIMENTAL

Since the difference between the two susceptibilities is easier to measure accurately than either of them separately, measurements have been made of the anisotropy $\chi_\perp - \chi_\parallel$, and of the smaller of the two susceptibilities $\chi_\perp$, at different temperatures.

---

* A preliminary report of these measurements was published in *Nature*, **156**, 240, 1945.

(i) *Measurements of Anisotropy at Low Temperatures :*

Before describing the actual measurements at low temperatures a brief description of the cryostatic arrangement for attaining any desired temperature between room temperature and 80° K will be given. The arrangement is quite similar to that designed in this laboratory by Dr. A. Bose (1940). It is of the gas flow type. The flow chamber of the cryostat is a cylindrical double-walled copper vessel closed at both ends. It is made of thin sheet of copper and is kept inside a cylindrical Dewar vessel. The gas flow chamber contains a large number of thin copper discs perforated by small holes, the planes of the discs being at right angles to the axis of the cylinder. The discs are arranged in such a way that the holes in the consecutive discs are not in a line, so that the flow of the gas is turbulent and hence a thorough interchange of heat between the gas and the cryostat is obtained. The large mass of copper employed ensures a steady temperature, and due to large conductivity of copper there is very little temperature gradient. Through a hole along the axis of the disc is inserted a thin walled copper tube in which is kept the specimen whose properties are being studied. The space between the double walls of the copper chamber is connected to a mercury manometer and constitutes a constant volume air thermometer. Any change in the volume of air in this chamber due to temperature change in the cryostat operates a sensitive relay which controls the pump supplying the cold air flowing through the cryostat. In actual practice, liquid air is sucked at an adjustable rate directly into the cryostat and the desired temperature kept steady within 0.1°C may be obtained.

The measurements of the magnetic anisotropy were made by the usual torsional method. The crystal is suspended inside the copper tube of the cryostat, with its basal plane vertical. The suspension for the crystal consists of two parts. The upper part is a fine quartz fibre, which has been calibrated previously and the lower part is a thick glass fibre, sufficiently stout in comparision with the quartz fibre to be regarded as rigid. The whole length of the quartz fibre is above the cryostat, and is practically at room temperature all the time, so that its torsional constant is independent of the temperature of the cryostat. The whole cryostatic arrangement is placed between the flat pole pieces of a large electro-magnet, so that the crystal remains in the centre of the field. The upper end of the quartz fibre is attached centrally to the pin of a graduated torsion head. The torsion-head is initially adjusted so that when the crystal takes up its natural orientation in the magnetic field, namely with its basal plane along the field, the torsion of the fibre is zero. If the torsion head is now slowly rotated from this position there will come a stage when the equilibrium of the crystal in the field becomes unstable and the crystal suddenly turns. The field strength and the dimensions of the fibre have been so adjusted that α_c, the total angle by which the torsion head has been rotated from its initial position, is always more than 3 or 4 rotations of the torsion head. The anisotropy $\chi_\perp - \chi_\parallel$ per gm. mol. will then be given by the approximate relation :

$$\chi_\perp - \chi_\parallel = \frac{2M}{m} \cdot \frac{C}{H^2} \cdot \left(\alpha_c - \pi/4\right) \qquad \ldots \quad (1)$$

where m and M are the mass and molecular weight of the crystal respectively, H is the field strength and C is the torsional constant of the fibre.

The temperature of the cryostat is measured with a copper constantan thermo-couple, one junction of which is inside the crystal chamber, just below the crystal, and the other is kept at the temperature of melting ice. The thermo-couple is calibrated by keeping the latter junction at the temperature of melting ice and the former junction at four different temperatures covering the range within which the magnetic measurements are to be made.

(*ii*) *Measurements of Anisotropy at high Temperatures*

For the high temperature measurements the crystal is suspended inside a large-sized tube of unglazed porcelain, closely wound on the outside with "nichrome" wire, over which is rolled tightly a thin sheet of asbestos. By sending a steady electric current through the wire, the temperature inside can be maintained at any desired value up to about 800°C. Over the layer of asbestos there are a number of sheets of mica and over which there is an outer jacket for the circulation of cold water. The arrangement of water-circulation is for protecting the pole-pieces of the electromagnet from the influence of the high temperature. The temperature inside the chamber is maintained fairly steady.

The temperature is measured by a copper constantan thermo-couple, one junction of which is introduced inside the heating chamber through its bottom and is kept just below the crystal, while the other junction is at the temperature of the melting ice. The thermo-couple is calibrated as before by keeping the latter junction at 0°C and the former successively at four different steady temperatures covering the range of temperature required for this investigation.

The suspension of the crystal consists of two parts; the upper one is a fine quartz fibre as before which has been kept at the room temperature by means of water circulation; the lower one is now a thin copper wire to the lower end of which is tied rigidly the crystal with its basal plane vertical. The copper wire stands the high temperature better than the stout glass fibre used in low temperature measurements, and the use of cements for attaching the crystal is also thus avoided. The wire does not show any anisotropy. The method of measurements are the same as in the case of low temperature.

(*iii*) *Measurement of* $\chi_\perp$

In view of the small value of $\chi_\perp$, and its sensitiveness to small traces of impurities which are usually present in natural crystal of molydenite, and the uncertain temperature variation of the disturbing effect of the impurities, much accuracy on the measurements of $\chi_{\perp}$ cannot be claimed. The measurements of $\chi_{\perp}$ were made by the quartz torsion balance deviced by Dr. A. Bose for his measurements on paramagnetic crystals. It consists of quartz fibre stretched horizontally between a graduated torsion-head and a metal chuck. At the middle of this fibre is attached a light glass blance-beam at right angles to the fibre. A small vertical mirror is attached just over the mid-point of the beam. Any displacement of the beam can be observed from the mirror by lamp and scale arrangement. A small mica damping vane has also been attached to the beam. From one end of the beam is suspended the crystal system. The lower portion of the suspension consists of a stout glass fibre in low temperature measurements and a copper wire in case of high temperature measurements, the central portion is of quartz fibre and the upper portion a small length of a glass rod, the upper end of which has been bent into the form of a hook so that the whole system can be suepended from the balance beam. In the present measurements the suspension system has been attached rigidly with the balance beam by means of shellac. The length of the suspension system is so adjusted that the crystal which has been attached to the glass rod or the copper wire with basal plane vertical always remains within the cryostat or the heating chamber, in a non-homogeneous magnetic field—the gradient being in a vertical direction. Small aluminium and copper riders are placed at the other end of the beam until the beam becomes horizontal. When the field is switched on the crystal after taking up its natural setting position will move vertically along the gradient of the field. The resulting displacement of the beam can be very accurately observed by the lamp and scale arrangement. By rotating the torsion head, the beam and with it the crystal can be brought back to their original positions. The angle of torsion necessary for this purpose is evidently proportional to the susceptibility of the crystal. The room temperature value of the susceptibility being previously known, the values at any other temperatures can be extrapolated by simply observing the angle of torsion necessary at that temperature to bring the crystal back to its original position.

RESULTS

The results of these measurements are shown in Table I and II. These values are the mean of a number of observations taken with crystals from different specimens. The magnetic susceptibilities are expressed in E.M.C.G.S. units. From the tables it is evident that while $\chi_{\perp} - \chi_{\parallel}$, the magnetic anisotropy changes considerably from the highest to the lowest temperature, the variation of $\chi_{\perp}$, the susceptibility perpendicular to the principal axis, within the same range of temperature is extremely slow. These results are shown diagrametically in Fig. I.

TABLE I

T°K	$(\chi_\perp - \chi_\parallel) \times 10^6$ per gram mol.	T°K	$(\chi_\perp - \chi_\parallel) \times 10^6$ per gram mol.
90	46.4	255.5	43
113	45.4	298	42.7
127	44.8	334	41.6
146	44.5	384	40.8
160	44.3	462	40.3
172.6	44.2	482	40
190	44	566	39.4
229	43.4	730	36.8

TABLE II

T°K	$-\chi_\perp \times 10^6$ per gram mol.	TK°	$-\chi_\perp \times 10^6$ per gram mol.
90	45	384	44
183	44.6	462	43.8
306	44.4	570	43.4

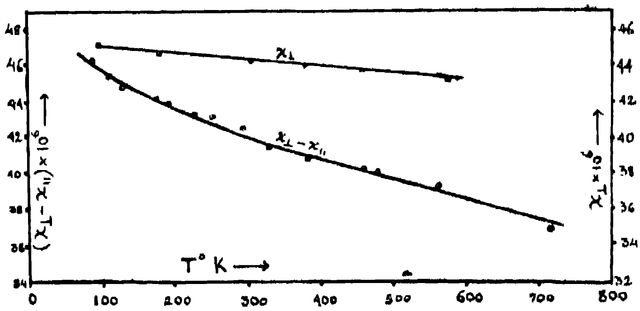

FIG. 1

CONSIDERATION OF THE STRUCTURE OF MOLYBDENITE

Molybdenite is a hexagonal crystal, with perfect basal cleavage. The molybdenum and sulphur atoms in it are arranged in parallel layers, each layer of molydenum atoms being sandwitched between two layers of sulphur atoms and these three layers form a composite layer by the repetition of which the whole structure is built. The various interatomic distances are represented as follows

Mo – Mo = 3.15 A.U. S – S = 3.15 A.U. Mo – S = 2.41 A.U.

and the distance between the two composite parallel layers of molybdenite has been found to be 3.66 A.U. The large distance between the adjacent layers shows that the binding between them is extremely loose and is probably of the Van der. Waals type. The binding between M_0 and S has heen proved to be of the covalent type (Hultgren, *loc. cit.*). But the bindings along the directions parallel to the basal plane seem to be of a partially metallic character. This view is supported by the metallic lustre of the cleavage face, appreciable electrical conductivity along directions parallel to the basal plane and the metallic reflection from its surface (*loc. cit.*). The interatomic distances along the basal plane also lends support to this view. The presence of metallic binding along directions in the basal plane postulates the existence of a free election gas having the motion of the electrons restricted along planes perpendicular to the hexagonal axis of the crystal. Consequently we should expect a temperature sensitive diamagnetic contribution perpendicular to the basal plane.

The diamagnetic properties of this crystal has recently been studied in this laboratory (1944). The susceptibility per gram molecule of the crystal perpendicular to the hexagonal axis, $\chi_{\parallel}$, is about -44.3×10^{-6}. On the other hand, the susceptibility along the hexagonal axis, $\chi_{\parallel}$, is about -87.1×10^{-6}, *i.e.*, the anisotropy is about 72 per cent. Thus the diamagnetic anisotropy is directed along the hexagonal axis of the crystals. The numerical value of the anisotropy, which may be taken to be equal to $\chi_{\parallel} - \chi_{\perp}$, and which will be denoted by χ_{e}, appears to be the contribution from the mobile electrons in molybdenite, having their mobility restricted along the basal plane only.

TEMPERATURE VARIATION OF THE ANISOTROPY

The values of $(\chi_{\parallel} - \chi_{\perp})$ per gm. mol. of molybdenite at different temperaures have been plotted against the reciprocal of the temperature in Fig. 2.

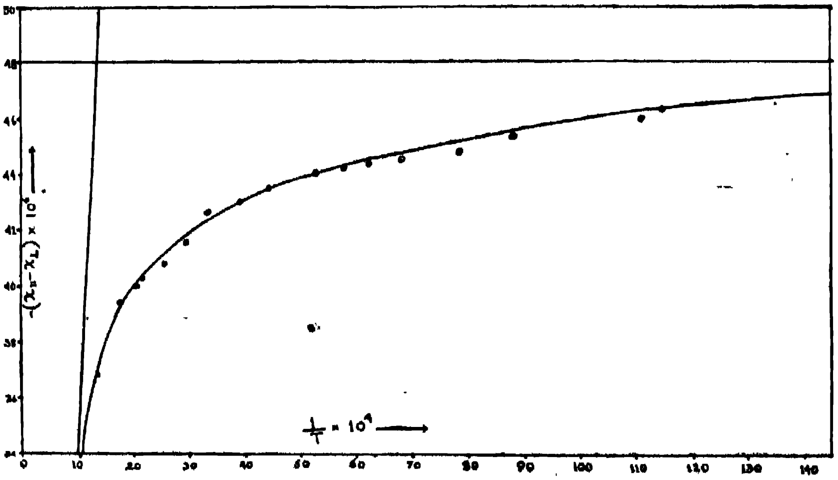

FIG. 2

It is observed that at low temperatures, the anisotropy tends to reach the temperature independent value of -48×10^{-6} per gm. mol. and at high temperatures it tends to reach asymptotically the value $\chi_e = \chi_{\parallel} - \chi_{\perp} = -\frac{.036}{T}$. From the nature of variation of the anisotropy with temperature, it seems that the magnetic anisotropy in molybdenite is a diamagnetic contribution from the free-electrons that might be present in it. Consequently it seems worthwhile to study the behaviour of these electrons in detail after the method developed by Ganguly and Krishnan (1941) in their investigations of the diamagnetic susceptibilities of graphite.

FREE ELECTRON SUSCEPTIBILITY IN MOLYBDENITE

Landau has shown that free-elections should have besides their spin paramagnetism an appreciable amount of diamagnetism also and the numerical value of the diamagnetic susceptibility should be one third that of the paramagnetic one. At a temperatures very much lower than the degeneracy temperature, T_0, the diamagnetic susceptibility $(\chi_e)_d$ is given by

$$(\chi_e)_d = -\frac{nN\mu^2}{2kT_0} \text{ per gram atom} \quad \ldots \quad (2)$$

And at a temperature $T^\circ >> T_0$

$$(\chi_e)_d = -\frac{nN\mu^2}{3kT} \text{ per gram atom} \quad \ldots \quad (3)$$

where n is the number of free electrons per atom, N, the Avoradro number and the rest of the symbols have their usual significance. Stoner (1935) has further shown that when $T << T_0$

$$(\chi)_e)_d = -16.1\left(\frac{n}{V_0}\right)\left\{1 - 6.11 \times 10^{-9}\left(\frac{T}{V_0}\right)^2\right\} \text{ per gram atom} \quad \ldots \quad (4)$$

and when $T >> T_0$

$$(\chi_e)_d = -\frac{124n}{T}\left\{1 - 3.23 \times 10^{-5}\left(\frac{V_0}{T}\right)^{\frac{3}{2}}\right\} \text{ per gram atom} \quad \ldots \quad (5)$$

where V_0 is the maximum kinetic energy of the electrons in the completely degenerate state.

Now from fig. 2, it is seen that at very high temperatures the susceptibility $\chi_e = \chi_{\parallel} - \chi_{\perp}$ tends to reach asymptotically the value

$$\chi_e = -\frac{.036}{T} \text{ per gram mol.}$$

But from (3) $\quad (\chi_e)_d = -\frac{nN\mu^2}{3kT} = -\frac{.12n}{T}$ per gram atom.

Comparing these two relations we find n to be equal to 0.3. Taking MoS_2 to be a complex atom, this means that, 0·3 electrons are free per MoS_2 atom. Also considering (4) we still get n to be equal to 0.3.

Again from fig. 2 we find that at low temperatures χ_e tends to reach the temperature independent value of -48×10^{-6} per gram molecule. Thus from (2), n and $(\chi_e)_d$ being known, T_0 comes out to be about 1100°K. From these observations it can be said that the observed electronic susceptibility of molybdenite is the same as the susceptibility of a free-electron gas having an electron density of 0.3 per atom and a degeneracy temperature of about 1100°K. The full line curve in fig. 3 is the theoretical curve of such an electron gas drawn according to the Stoner's Equation (*loc. cit.*). The straight line represents the line $(\chi_e)_d = -\dfrac{nN\mu^2}{3kT}$, which the theoretical curve tends to reach at high temperatures. It will be seen that the experimental values represented by circles lie close to the curve.

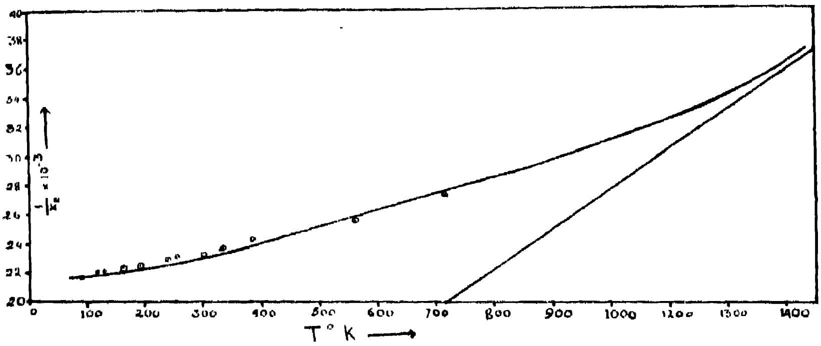

FIG. 3

In the above discussions no account has been taken of the effect due to the lattice field, which is generally very difficult, except, for the case dealt by Mott and Jones (1936), *i.e.*, when the surfaces of constant energy in K-space form a family of similar ellipsoids. For the present case, we shall proceed in a similar fashion, taking the magnetic field to be along the Z-axis of the energy ellipsoid. The diamagnetic susceptibility along the Z-axis may then be expressed as follows:

at high temperatures, $T>>T_0$

$$(\chi_e)'_d = -\frac{nN\mu^2}{3kT}\,\alpha_1\alpha_2 \text{ per gram atom} \tag{6}$$

and at low temperatures $T<<T_0$

$$(\chi_e)'_d = -\frac{nN\mu^2}{2kT_0}\left(\frac{\alpha_1^2\alpha_2^2}{\alpha_3}\right)^{\frac{1}{2}} \text{per gram atom} \tag{7}$$

where α_1, α_2 represent the ratio of the actual to effective mass of the electrons for motion along the x-y plane and α_3 that for motion in the perpendicular directions. Now, comparing (6) with the actual relation which the susceptibilities satisfy at high temperatures *i.e.* comparing

$$(\chi_e)'_d = \frac{n.12}{T}\alpha_1\,\alpha_2 \text{ with } \chi_e = -\frac{.036}{T}$$

we get

$$n\alpha_1\alpha_2 = 0.3 \qquad \ldots \ (8)$$

In view of the conclusion already obtained, the obvious solution that we get is

$$\alpha_1 = \alpha_2 = 1 \qquad \ldots \quad (9)$$

If we now calculate the degeneracy temperature of a free electron gas having 0.3 electrons per atom which has not been influenced by the effect of the lattice field, according to the usual relation

$$T_0 = \frac{\zeta_0}{k} = \frac{h^2}{2mk}\left(\frac{3n'}{8\pi}\right)^{\frac{2}{3}} \qquad (10)$$

where the various symbols have their usual significance, we get $T_0 = 14000°K$ approximately. But the degeneracy temperature which has been observed actually is about 1100°K. It is however known that the effect of the lattice field is to change the degeneracy temperature as follows

$$T'_0 = T_0(\alpha_1\alpha_3\alpha_2)^{\frac{1}{3}} \qquad \ldots \quad (11)$$

where T'_0 is the degeneracy temperature under the influence of the lattice field and T_0 that without the field. Thus we have

$$1100 = 14000\ (\alpha_1\alpha_2\alpha_3)^{\frac{1}{3}}$$

since

$$\alpha_1\alpha_2 = 1$$

we have

$$\frac{\alpha_1\alpha_2}{\alpha_3} = (13)^3 \qquad \ldots \quad (12)$$

which indicates a high eccentricity for the ellipsoidal surfaces of constant energy in K-space, being much elongated in directions perpendicular to the C-axis, their common axis being along the C-axis of the crystal.

Thus from the above considerations we see that the effective mass of the electrons for motion at right angles to the basal plane is enormous while that along the basal plane is just the actual mass. All these findings point to the fact that the mobility of these electrons is effectively restricted only in planes parallel to the basal surface.

DIAMAGNETIC ANISOTROPY IN MOLYBDENITE—A CONTRIBUTION FROM THE 'OVERLAPPING' ELECTRONS

If we now consider the nature of the Brillouin zone for this structure we find that there is a Zone which can accommodate all the valency electrons per atom in it (*viz.*, 6 per atom, since electron atom ratio of MoS_2 is 6) bounded by planes $(\bar{2}11,0)$ and $(000,6)$, which are planes of large energy discontinuity. It is a hexagonal prism with its axis along 'c' of height $\frac{6}{c}$ and side $\frac{2}{a\sqrt{3}}$. The diamagnetism is then to be attributed to the few electrons that overlap beyond this Zone, *i.e.* whose Fermi surfaces extend slightly beyond the planes of energy discontinuity.* Since the planes bounding the Brillouin Zone are planes of large energy discontinuity causing the overlap to be very small and since these planes occur symmetrically with respect to the origin, it is possible to regard the overlapping electrons as forming a number of ellipsoidal distribution in k-space having the origin still at the centre.

From the nature of the Brillouin Zone and in view of the small value of α_3, it is evident that the band width in the direction of the principal axis is very small *i.e.* electrons can take up all permitted values k_z. Similarly it is evident that along directions in the basal plane very high values for either α_1 or α_2 is not possible. Thus the electrons along the basal plane behave as though they are free, whereas at right angles to the plane their motion is highly restricted.

EXPLANATION FOR THE ABSENCE OF THE SPIN-PARAMAGNETISM

Normally the spin paramagnetism should predominate over the diamagnetism of the free electrons except when $\frac{1}{3}\alpha_1\alpha_2$ is very great causing the spin paramagnetism to be insignificant. But according to our previous findings $\alpha_1=\alpha_2=1$. However an explanation of the type offered by Ganguli and Krishnan (1941) in the case of graphite is also applicable here for explaining the absence of any spin of the free electrons at ordinary temperatures. It can be assumed that each of the energy levels are either occupied by an electron pair of opposite spins or not occupied at all. In the occupied levels the energy of the coupling between the spin-moments may be assumed to be large in comparison with the energy corresponding to temperatures ordinarily attainable. Thus the spins remain balanced for ordinary temperatures. If in addition, the occupied energy levels are so closely spaced that they may be regarded as almost continuous, the energy of distribution will be practically the same as when the spin-spin coupling is absent. The coupling will not therefore affect the diamagnetism of the electron gas and the temperature variation of the diamagnetism will be in accordance with the theory postulated for the purpose. When the temperature of the electron gas is very high—so high that the corresponding energy attains a value sufficient to cause the dissociation of the components of a pair of electrons with opposite spins. Above this temperature the diamagnetism is expected to be completely masked by the spin-paramagnetism.

In conclusion the author wishes to express his best thanks to Prof. K. Banerjee for his keen interest in the work, to Prof. A. Mookerjee for helpful discussions and to Mr. L. J. D. Fernando, Government Minerologist at Ceylon for his kind present of some of the molybdenite crystals with which the measurements described in this paper were made.

Indian Association for the
Cultivation of Science
210, Bowbazar Street, Calcutta.

REFERENCES

Bose, A., 1940, *Proc. 27th Indian Science Congress*, Part III, 41.

Coblentz, W. W. and Kahler, H., 1919-20, *Sc. Papers Bur. Std.* **16** 161.

Dutta, A. K., 1944, *Ind. Jour. Phys.*, **18**, 249

Ganguli, N. and Krishnan, K. S , 1941, *Proc. Roy. Soc. A.*, **177**, 168.

Hultgren, R., 1932, *Phys. Rev*, **40**, 291.

Mott, N. F. and Jones, H. 1936, The Theory of the Properties of Metals and Alloys, Oxford Univ. Press, pp. 207.

Stoner, E. C., 1935, *Proc. Roy. Soc. A*, **152**, 672.

"A SPECTROSCOPIC STUDY OF AN UNCONDENSED SPARK BETWEEN COPPER ELECTRODES IN THREE DIFFERENT CASES AT VARIOUS PRESSURES"

By JAGDEO SINGH AND SREE RAMULU

(Plate X)

ABSTRACT. A detailed study of the nature of the spectra at various portions of the spark in illuminating gas air and carbon dioxide at various pressures, the spark being excited by a large induction coil, is described.

The following are some of the more important observations and results obtained:—

(*a*) Most of the lines are due to the material of the electrode. They are prominent at higher pressures and decrease in intensity as the pressure decreases. At a pressure of 10 cms. practically all of them disappear. Even at higher pressures, where the lines are prominent, they are more concentrated at the two ends of the spark.

(*b*) Bands are practically absent from the atmospheric pressure up to 30 cms. of mercury. They appear at this pressure and gain in intensity as the pressure is further reduced. The optimum pressure at which the bands are developed with the greatest intensity shows practically no variation from gas to gas.

(*c*) A study of the bands due to CN and NO indicates that the formation of these molecules and their excitation to give their characteristic spectra is influenced by the neighbouring gases.

(*d*) It seems likely that the effective temperature of the spark is not constant throughout its length, the middle portion being cooler than the end portion. This statement requires confirmation by accurate methods of evaluating temperatures.

(*e*) One particular line, belonging to ionised oxygen exhibits a strong effect of pressure broadening in the illuminating gas.

INTRODUCTION

The selective excitation of lines and bands in spectroscopy has been studied in a number of cases. It mainly falls in three groups: (1) The effect of foreign gases on the nature of spectrum of a substance, (2) The method of excitation and (3) The effect of pressure. There are various cases of the first type specially in a discharge tube as for example (*a*) the behaviour of first positive nitrogen (Jevons, 1932) bands in the presence of high pressure inert gases, (*b*) the production of negative nitrogen (Jevons, *loc. cit.*) bands in high pressure helium containing a trace of nitrogen, (*c*) the intense development of the Swan band (Jevons, *loc. cit.*) system by a trace of carbon in high pressure helium or argon; (*d*) the development of Cameron bands (Jevons, *loc. cit.*) by a trace of cabon in high pressure neon; (*e*) the isolation of the high pressure carbon and the triplet carbon band systems under similar conditions; (*f*) the behaviour of mercury vapour (Wood, 1924) in the presence of foreign gases as revealed by Wood's investigations on mercury vapour in the presence of nitrogen at a pressure of 2 m.m. Kaplan (1930) observes that CO is more effective in quenching λ 2536 line than N_2.

Coming to the second case we have various methods of excitation as for example electro-luminescence, photo-luminescence, chemi-luminescence, thermo-luminescence, etc. In electroluminescence again there are many classes: *e.g.*, high frequency discharge, spark discharge, arc-discharge, etc. In a variety of cases the high frequency (Brasfeld, 1929) discharge gives rise to an intensity distribution different from that obtained from other types of excitation of spectra. In hydrogen (Asundi and Ors. 1942) it has been found that the primary spectrum is stronger than the secondary spectrum when excited by an ordinary induction coil and the secondary spectrum is stronger than the line spectrum when excited by the H.F. discharge. It has been found by Notingham that the relative intensities of the lines in the spectrum of the arc depends upon the current strength and in the case of the spark on the size and shape of the electrodes too. Peters and Mankoff found that in the case of low voltage arc using cathode layer, the line spectra of most elements are from 10 to 100 times stronger immediately in front of the cathode than in the arc gas column, this effect being stronger for elements of the first three groups of the periodic table. It has been found that the self induction and the capacity in the circuit cause considerable changes in the excitation of spectra. The introduction of an auxiliary spark gap in series with the analysis spark has three effects: (1) general increase in intensity. (2) selective increase in intensity and (3) stabilization of the spark. Lastly the investigations of Newmann on the arc discharge in gases and mixed gases at various pressures are among other sources of data on selective excitation. A detailed study of this nature of the uncondensed spark spectra of three gases namely the illuminating gas, the carbon dioxide and the air has been presented in this paper.

EXPERIMENTAL ARRANGEMENT AND PROCEDURE

The uncondensed spark was maintained in a glass tube of nearly 3 cms. in diameter which had copper electrodes fitted to it with sealing wax. The glass tube was blown in the form of a bulb in the middle where the spark used to occur and the whole thing was kept inside a water tight wooden trough such that the two side tubes and the front end of the tube with quartz window projected outside the trough. The inlet and outlet tubes were bent so that they might rest on the top of the trough when the tube was kept in position. A continuous flow of water through the wooden trough was arranged, care being taken to see that the water level in the trough was always 2 or 3 cms. above the main body of the discharge tube. This arrangement was made to avoid the discharge tube from being cracked by the heat of the spark. Two copper electrodes were inserted inside the tubes. They were completely insulated by rubber except at either ends, so that there might not be any sparking between the electrodes and the side tubes. The outer tube was connected to the Cenco-high-vacuum pump to exhaust the gas inside through a two-way glass tube, the other end of which was connected to a mercury manometer which could record pressures from 1 cm. of mercury up to the atmospheric pressure. All the joints were made air-tight with sealing wax. The tube was washed many times by the gas before the spark was passed. The discharge tube which was ultimately adopted is shown in Fig. 1.

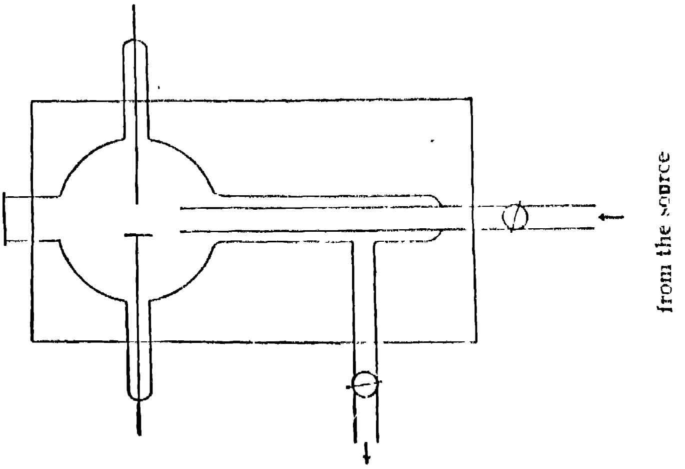

FIG. 1

A large induction coil of 10 in. spark-length was used so that a very high voltage was impressed. The current from the 220 D.C. mains regulated through a rheostat was supplied to a mercury interrupter whose base was 15 cms. in diameter. The interrupted current (6 to 9 amp) passed through the primary ends of the induction coil, the secondary ends of which were connected to the two electrodes of the experimental discharge tube. The interrupter used to stop functioning after some time and then the mercury was cleaned and replaced. Sometimes shaking the interrupter also helped in this direction.

The illuminating gas used was obtained from the main laboratory supply and had the constitution of 48% nitrogen, 12% oxygen, 24% methane, 4% hydrogen and 12% unsaturated hydro-carbons ; carbon dioxide was produced by the action of dilute hydrochloric acid on marble in a Woulf's bottle. In this way the spark discharge between copper electrodes in illuminating gas, carbon dioxide and air at the pressures 2, 5, 10, 20, 30. 40, 50, 60 and 75 cms of mercury was studied from the three parts of the spark, namely the central portion ; the stationary spot at the cathode and the moving spot at the other end of the spark and these are denoted by a, b, c respectively in the spectrograms (Plate IX).

A Hilger small quartz spectograph was used for photographing the spectra. Ilford H. P. 2 plates were used and the time of exposure in all cases was 10 minutes. Spectogram (1) and (2) are taken with the illuminating gas at the pressures of 40, 30, 20, 10, 10, 5 and 2 cms. of mercury. Spectogram (3) is taken the pressure of 40, 30, 20, and 10 cms. and plates (4) and (5) are taken with air at carbon dioxide at the pressures of 75, 60, 50, 40, 40, 30, 20 and 10 cms. of mercury. In all these a, b, c are marked for the three spots.

RESULTS AND DISCUSSIONS

The intensity of bands and lines has been estimated visually from the blackening on the plates without taking into account many other well-known factors such as the sensitivity of the plate, etc. modifying the blackening. Because of this fact much importance has not been attached to the observations of the individual bands, but only systems of bands as a whole are taken into account. This is summarised in Table I.

The spectra of the spark in various gases have been found to show widely different intensity distribution in the case of bands, lines and continuum present. As will be seen from Table I, pressure has a marked effect on the excitation of bands, the lines and the continuous spectra also. Various portions of the spark give rise to widely different spectra. The nature of spectra appears to be dependent mainly upon three factors, namely (1) the gas in which the spark is excited; (2) the pressure of the gas and (3) the portion of the spark photographed.

The present investigation, however, confines itself only to the mention of some very striking differences and it is believed that for such observations, the visually estimated intensities can be relied upon :

(1) *Bands.*—The observation in the case of first negative nitrogen, second positive nitrogen, cyanogen violet, NOγ and OH are summarised in the Table I.

(2) *Lines.*—From the Spectograms we see that the lines present are almost all those of the Cu electrodes. They are intense at higher pressures and decrease in intensity as the pressure decreases, so much so that in air a pressure of 10 cms. of mercury all the lines except the two strongest copper lines at $\lambda\lambda$ 3247, 3274 have disappeared completely. Same is found to be the case in carbon dioxide and illuminating gas. Further in general the lines when present are more prominent at the two ends of the spark and weak at the central portion of the spark. This is true for all the three gases investigated.

(3) The continuous spectrum is present with weak intensity only in the case of the illuminating gas.

Thus from the results given above we can conclude that the various lines present except a very few, namely carbon line at λ2478 and some oxygen lines, are all due to the material of the electrodes of the spark. It can be seen that the lines are more prominent at the atmospheric pressure and decrease in intensity as the pressure of the gas surrounding decreases and nearly disappear at a pressure of 10 cms. of mercury. This is true in the case of almost all the three gases investigated. On the other hand the bands show variations in intensity in the reverse direction. They are absent at the atmospheric pressure and as the pressure decreases they make their appearance at a particular pressure which we may say is the characteristic of the system excited as well as of the gas surrounding the spark. At pressures lower than this optimum pressure the system may become weak as has been found firstly in the case of first negative nitrogen bands excited in the illuminating gas (41% of N_2), where they become prominent at a pressure of 10 cms. and become weaker at still lower pressures, or the system

SPECTROGRAM 1

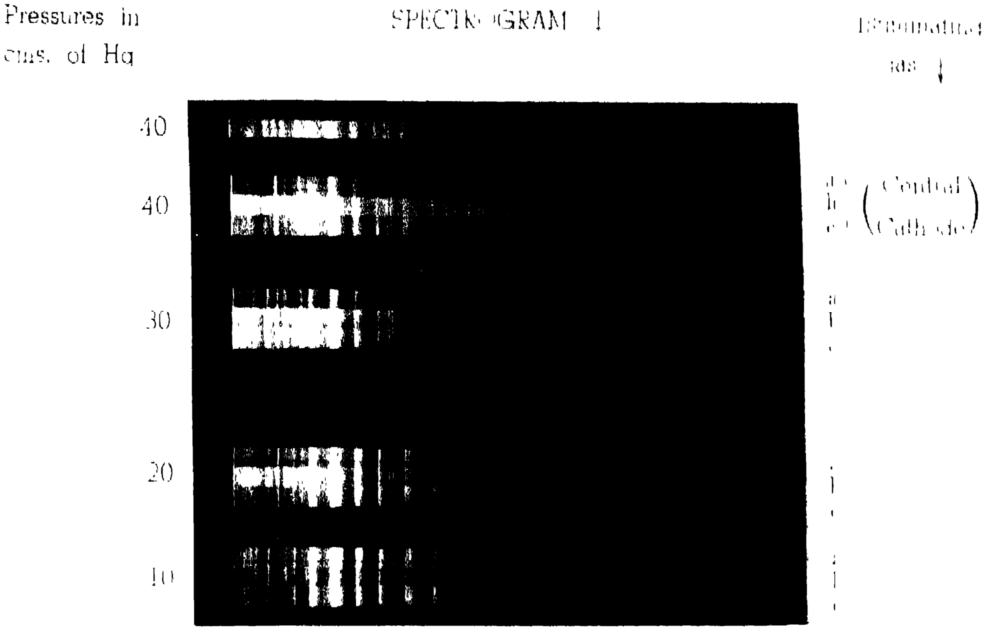

SPECTROGRAM 2

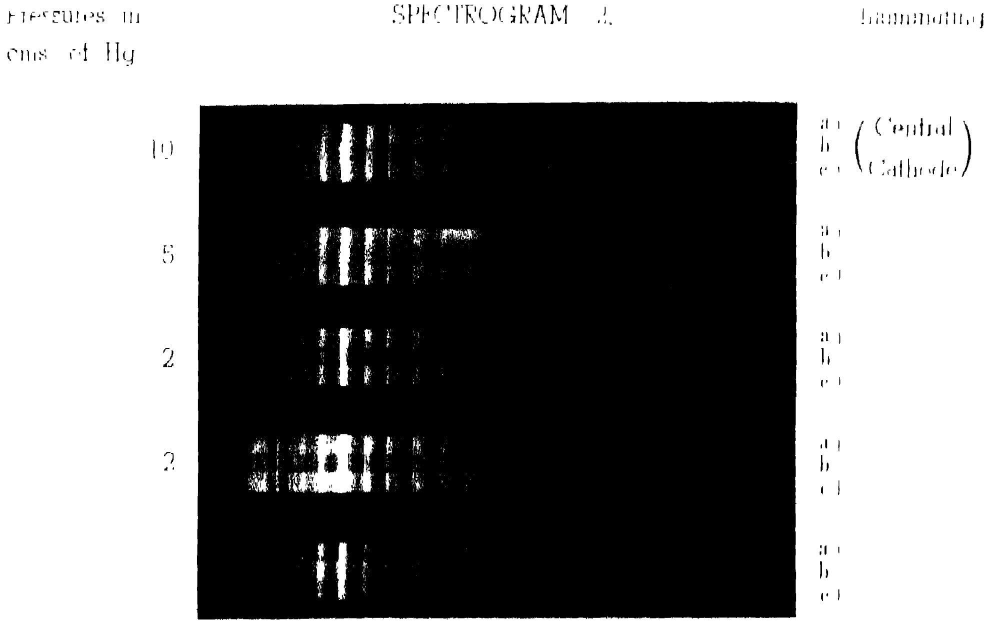

SPECTROGRAM Air ↓

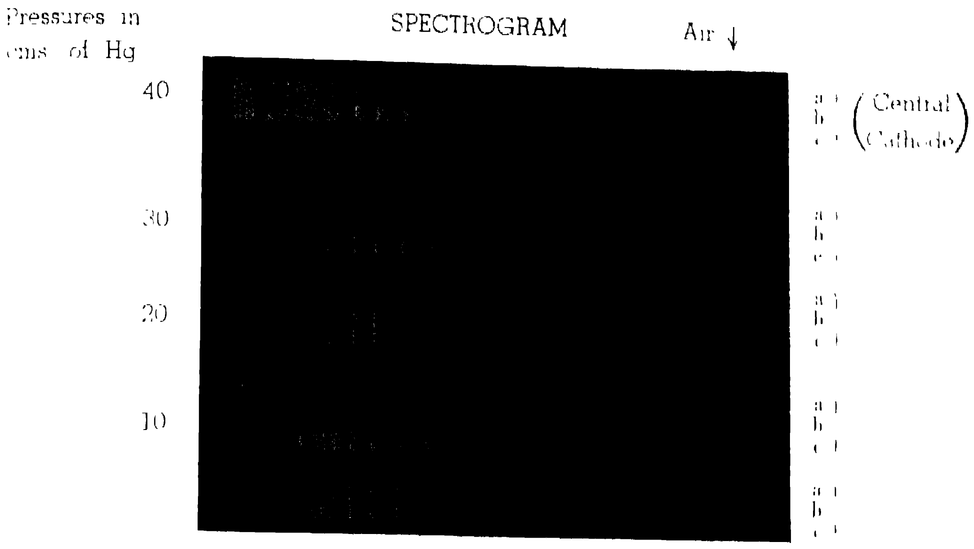

SPECTROGRAM 4. CO_2 ↓

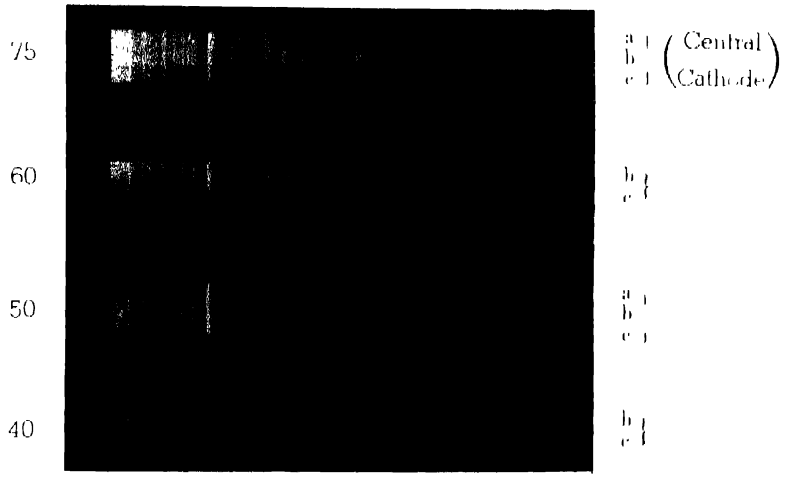

SPECTROGRAM 5. CO_2 ↓

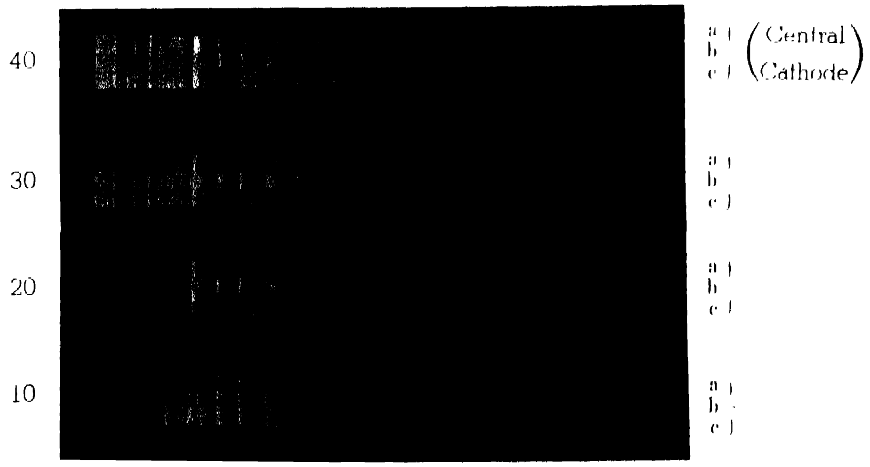

may become strong at pressures lower than the characteristic pressures for excitation as has been found in the case of second positive nitrogen bands developed in air when they appear at a pressure of 40 cms. and become stronger at still lower pressure or the system may remain with the same intensity at pressures lower than the characteristic pressure as has been found in the case of cyanogen violet system developed both in the case of CO_2 and illuminating gas but not in air. So we can generalise and say that under the conditions of the present experiments it is possible to excite the molecules of the surrounding gas in the spark discharge between the electrodes almost free from the characteristic lines of the electrodes. This happens when the pressure of the surrounding gas is near about 10 cms. of mercury. There appears to be a very slight variation in this pressure depending upon the nature of the gas.

We wish to point out another striking peculiarity. The first negative nitrogen bands as produced in the illuminating gas and in air are present only at the stationery spot of the spark in the illuminating gas while in the case of the air they are strong at the moving spot of the spark. It is difficult to understand this phenomenon. It would be very interesting if a more detailed investigation of this particular phenomenon is undertaken employing accurate methods of intensity measurements.

Another interesting observation concerns NOγ bands. Since nitric oxide is not present as such in any of the three gases, the presence of these bands is indicative of the conditions suitable for their development. Again the NOγ (Bair, 1920) bands are particularly weak in the illuminating gas, which contains as has been mentioned above a fairly large amount of nitrogen and oxygen. These bands are strong both in air and CO_2 in the latter of which nitrogen and oxygen can only be in small amounts as impurities. This is rather interesting when we contrast it with the complete absence of cyanogen bands in air, which must presumably contain traces of carbon. Probably it will be correct to say that whereas for the production of NOγ bands traces of nitrogen and oxygen if avilable in the presence of other gases are more favourable, a much higher concentration of carbon is necessary for the development of cyanogen bands in the presence of other gases. In this respect, however, Newmann (1929) has obtained cyanogen bands when an intermittent arc discharge is passed through hydrogen at a pressure of 10^{-3} mm. in the presence of helium and neon, where also therefore carbon and nitrogen must have been present only as impurities in small quantities. Newmann explains the presence of these bands as due to the effect of temperature being responsible for the production and excitation of CN bands. This is in contradiction to the observation made here. The effective temperature is roughly of the same order of magnitudes in both cases. Hence the absence of CN bands in the sparks in air is not explained on the temperature hypothesis. We have to conclude that the presence of helium and neon is responsible for the production of these bands in Newmann's experiment.

TABLE I

System of bands.	Illuminating gas (investigated at prs. 40-2 cms.)		Air (investigated at prs. 40-10 cms.)		Carbon dioxide (investigatsd at pressures 75-10 cms)	
	At different pressures	At various portions of the spark	At different pressures	At various portions of the spark.	At different pressures	At various portions of the spark
First negative nitrogen bands	Completely absent at pressures higher than 10 cms. They also decrease in intensity at still lower pressures.	Present only at the stationary spot of the spark (one end of the spark commonly known as the cathode.	They appear at all pressures and increase in intensity as the pressure decreases, but the change is not so well marked.	The system as a whole is very strong at the moving spot of the spark (may be called anode)	Appear at all pressures but become weak as the pressure decreases.	Equally intense at all portions of the spark.
Second positive nitrogen bands	Appear at all pressures become more intense as the pressure decrease.	Equally strong at all portions of the spark, but with this difference that at pressures lower than 10 cms. they are slightly less intense at the stationary spot.	Appear at all pressures and become prominent as the pressure decreases, the effect being marked this system is more prevalent in air than in illuminating gas at all pressures.	Less intense at the central portion of the spark.	Become prominent at pressure = 30 cms. the system as a whole increases in intensity as the pressure decreases. The increment being gradual and marked so much so that the 0, 0 band which is absent at pressure = 75 cms. makes its appearance at pressure = 10 cms. with intensity = 10	Intense at the stationary spot and weak equally both at the moving spot and the central portion of the spark.

TABLE I—(*contd.*)

System of bands.	Illuminating gas (investigated at prs. 40-2 cms.)		Air (investigated at prs. 40-10 cms.)		Carbon dioxide (investigated at pressures 75-10 cms.)	
	At different pressures	At various portions of the spark	At different pressures	At various portions of the spark.	At different pressures	At various portions of the spark
Cyanogen violet system.	Make their appearance at all prassures and do not show much variation with pressure.	Equally strong at all portions of the spark.	Completely absent at all pressures.	Completely absent at all portions of the spark.	The system as a whole appear even at pressure=75 cms. and shows practically no variation with the pressure.	The various portions of the spark are giving rise to the same intensity distribution.
$NO\gamma$ bands.	Very weak at all prestures.	Equally weak at all portions of the spark.	Make their appearance at all pressures and increase in intensity as the pressure decreases	At pressure=10 cms., they are very weak at the stationary spot, but at higher pressures equally intense at all portions of the spark.	Become prominent at pressure=20 cms.	Equally intense at all portions of the spark
OH bands	Make their appearance at pressure—20 cms, becoming stronger at still lower pressures.	Weak at the cathode.	The system is more prominent in air than in the illuminating gas at all pressures Makes its appearance at pressure=40 cms.	At pressures=40 cms. and 30 cms. equally strong at all portions. At pressure=20 cms. were at the moving spot and at pressure=10 cms. weak at the stationary spot.	Make their appearance at pressure=20 cms. and increase in intensity as the pressure decreases.	equally strong at all portions of the spark.

From the observations of the intensity distribution of nitrogen bands obtained by the spark in air Tawde (1934) evaluated a temperature of 7200°K. The present experiments do not allow us to evaluate the effective temperature with any confidence. But it is interesting that values obtained by using the visually estimated rough intensities for the band heads, are of the same order of magnitude as that obtained by accurate measurements of intensity. Thus for the spark in air at a pressure of 20 cms. a temperature of 8160°K is derived as the mean of the values for the three parts of the spark. In general we find that at the same pressure in different gases the temperature is the lowest in the illuminating gas, whereas in air and carbon dioxide they are of higher magnitude, but roughly coincident with the values obtained by previous workers. Also the middle portion of the spark gives a temperature lower than the two ends of the spark. No quantitative significance can obviously be attached to the values thus obtained but from the right order of magnitude it seems likely that the differences in temperature along the length of the sparks are real. It would be interesting to test this by accurate methods of intensity measurements.

There is one particular line which has been marked in the Spectrogram 1 as O^+. This is one of the three or four lines of ionised oxygen which lie at about λ 4870A. This line is very broad and appears as a band at a pressure of 40 cms. It gradually becomes less broad with decrease in pressure and at 10 cms. it is almost sharp like a line. This line is, therefore, pressure sensitive. It, however, is present in the spark spectra of illuminating gas and absent in other spectra.

In conclusion the results show that it is not improbable to arrange the conditions of the spark in various media in such a way that not the lines characteristic of the electrodes but the bands characteristic of the molecules of the vapour can be excited. This observation is rather interesting and further work will show whether the method cannot be employed to bring about an excitation of multiatomic molecules.

ACKNOWLEDGEMENT

Our thanks are due to Dr. R. K. Asundi, Benares Hindu University for the guidance in the work and for the innumerable help during the course of the investigation.

Hindu University,
Benares.

REFERENCES

Asundi, Singh and Singh, 1942, *Proc. Ind. Sci. Cong*, 35.
Bair, 1920, *Astro. Phy. Jour.*, **52**, 301.
Brasefield, 1929, *P.R.*, **34**, 431.
Jevons, 1932, Report on Band Spectra.
Kaplan, 1930, *P.R.*, **35**, 788.
Newmann, 1929, *Phil. mag.* **7**, 1084.
Tawde, 1934, *Proc. Phy. Soc.*, **46**, 333.
Wood, 1924, *P.R.S.*, **106**, 679.

ELECTRON DENSITY MAP OF ANTHRAQUINONE CRYSTAL

By S. N. SEN

ABSTRACT. It was shown by the author (Sen, 1940) that anthraquinone really belongs to the monoclinic class and not to the orthorhombic class as was assumed to be previously. A revised projection of electron density on the (001) plane of anthraquinone crystal by the two-dimensional Fourier analysis method has been carried out in the light of the new space group derived after re-classification of the crystal into monoclinic system. Much larger number of reflecting planes have been taken into account in the present analysis to make the Fourier series more convergent Co-ordinates of atomic centres in the projection have been obtained with greater accuracy. Fresh calculation of structure factors have shown much better agreement with the observed values. Observed difference in intensities of h_0k_0o and $h_0\bar{k}_0o$ reflections (referred to orthorhombic ones), which are not possible for an orthorhombic crystal, are found to be of real significance in the light of the present analysis.

In an earlier communication, it was shown by the author (Sen, 1940) that anthraquinone really crystallises in the monoclinic class having a space group $C_{2h}^5P2_1/a$. Previously the crystal had been assumed to be orthorhombic. Banerjee and Sen (1938) had obtained a projection of electron density on the (001) plane of anthraquinone crystal by the two-dimensional Fourier analysis method, but in that analysis the crystal was assumed to be orthorhombic in accordance with the space group as determined by the previous workers. But when it was found that the anthraquinone crystal was really monoclinic with $C_{2h}^5P_1^2/a$ as its space group, it was primarily important to revise the electron density projection on (001) plane obtained on the basis of the orthorhombic hypothesis in the light of the new space-group of the crystal. The origin of pseudo-symmetries observed in the planes of reflection in the older orthorhombic system will be readily found by transforming the older indices $h_0k_0l_0$ into their corresponding indices in the monoclinic system. It can easily be shown that a plane $h_0k_0l_0$ on the older orthorhombic nomenclature corresponds to $h_mk_ml_m$ in the new monoclinic system, where $h_m=(h_0+k_0)/2$, $k_m=l_0$ and $l_m=(h_0-k_0)/4$. For h_0k_0o planes it was found that (*i*) h_0+k_0 is divisible by 4 which means h_m is divisible by 2, (*ii*) h_0-k_0 is divisible by 4 means that l_m may have any value for h_mol_m planes. Also for ool_0 planes, l_0 is found to be even, *i.e.*, in ok_mo planes, k_m is even. These are in fact the criteria for space group $C_{2h}^5P2_1/a$. The pseudo-symmetries in the orthorhombic cell actually appeared for taking a bigger unit cell (orthorhombic) while the real fundamental cell (monoclinic) in the crystal is much smaller.

For obtaining the electron density map projected along the symmetry axis we may retain the pseudo-orthorhombic system of co-ordinates because this direction happens to be a crystallographic axis in both the systems and the other two pseudo-orthorhombic axes are the diagonals of the fundamental monoclinic lattice which may be approximately regarded for the purpose of the Fourier summation to be mutually perpendicular, the actual angle between them as calculated from the measured dimensions of the cell being 90°42′. There is, however, a fundamental difference between the summations carried out on

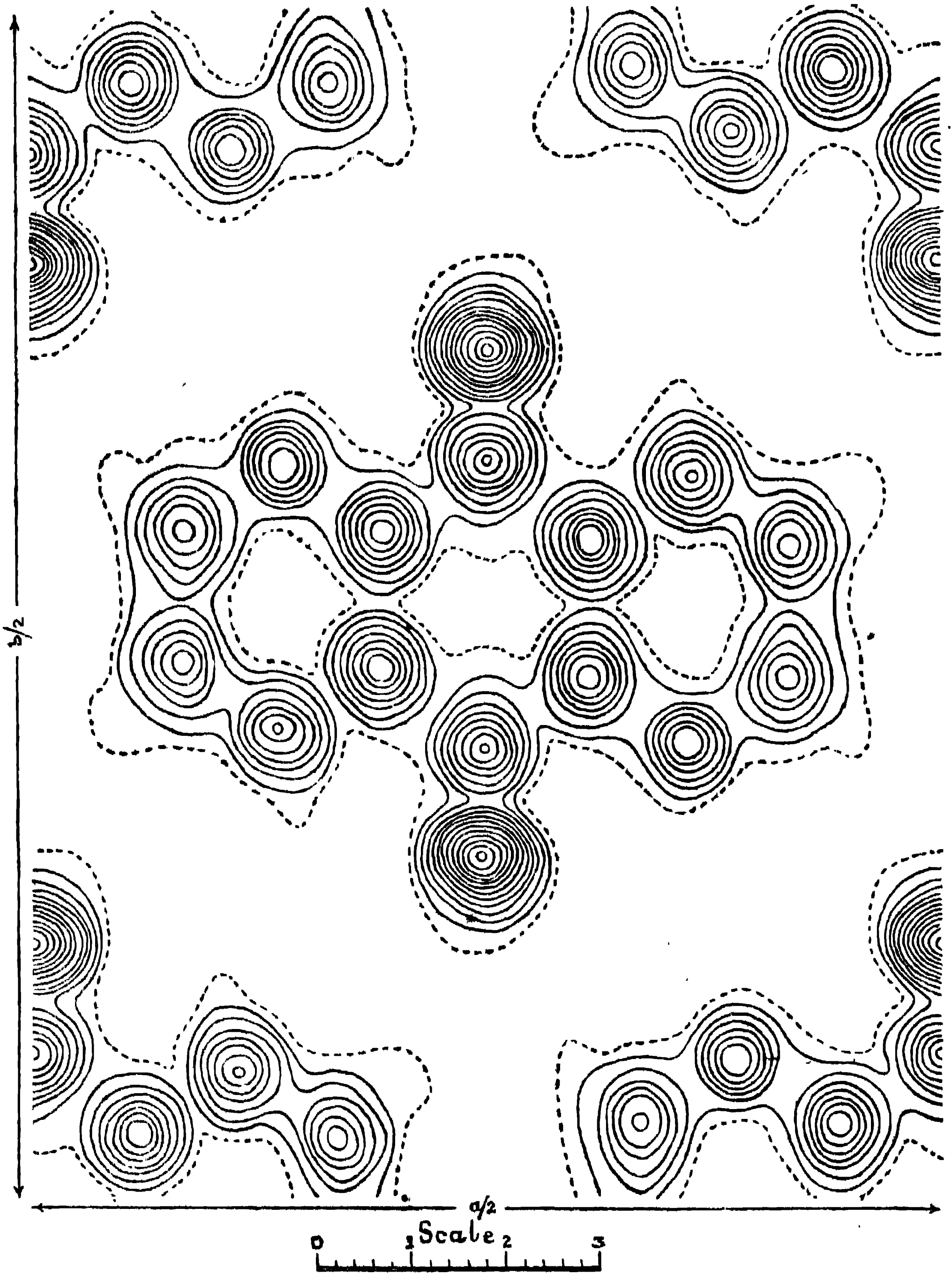

Projection along the c-axis. The dotted line represents the one electron line, the other lines are drawn at intervals of one electron per A³.

FIG. 1

the assumption of an orthorhombic cell and those according to the correct monoclinic cell. That is due to the difference in the structure factors of h_0k_0o and $h_0\bar{k}_0o$ planes. In evaluating electron density on the symmetry plane, the mean of structure factors for h_0k_0o and $h_0\bar{k}_0o$ planes were taken on the basis of the earlier assumption of orthorhombic lattice. The actual differences observed in the intensity measurements of those planes were then believed to be spurious or due to experimental errors and hence the mean of the two values were used for both h_0k_0o and $h_0\bar{k}_0o$ planes in the Fourier summation. The observed difference in the intensities of h_0k_0o and $h_0\bar{k}_0o$ reflections were later found to be of real significance as the h_mk_mo and $h_m\bar{k}_mo$ planes when transformed to the new monoclinic system represent different planes altogether, reflections from which cannot be expected to be of the same intensities. So the contributions of the h_mk_mo and $h_m\bar{k}_mo$ planes towards Fourier summation were worked out separately on the basis of their respective intensity measurements. Further, a highly overexposed Weissenberg photograph was taken round the old c-axis in order to take the weaker reflections also into account and thereby make the Fourier series more convergent. Structure factors of 92 planes have been used in the present Fourier summation while those of only 44 planes were used in the previous summation to obtain the electron density map published before.

The Fourier summation was carried out over a half of one molecule which forms the asymmetric unit of structure, the axial subdivisions being $a_0/48$ and $b_0/48$. But for accurate location of the atomic centres, additional summations were carried out at closer intervals with axial subdivisions $a_0/96$ and $b_0/96$ round about the atomic centres. The electron density distribution thus obtained is shown in Fig. 1. The x and y co-ordinates finally obtained are given in Table I for which the key to the symbols for the atoms will be obtained from the structural formula given in Fig. 2.

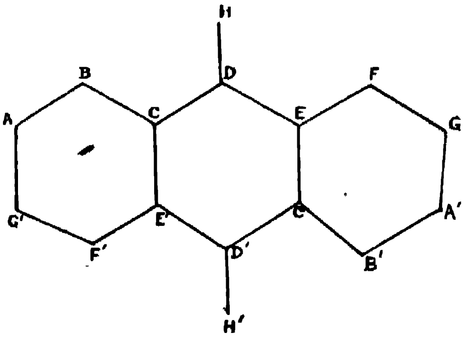

Structural formula of anthraquinone. ABCDEFG A'B'C'D'E'F'G' are carbon atoms and H and H' are oxygen atoms. H-atoms are not shown.

FIG. 2

TABLE I

Co-ordinates of Atoms referred to Orthorhombic cell
Molecular centre of symmetry at (000) as origin

Atom	x(in A.U.)	(in A.U.)
A (CH)	− 3.253	0.765
B (CH)	− 2.198	1.447
C (C)	− 1.115	0.745
D (C)	0.038	1.476
E (C)	1.164	0.649
F (CH)	2.236	1.311
G (CH)	3.308	0.615
H (O)	0.049	2.623

Fresh calculation of structure factors of all h,k,o planes were made with the final *x* and *y* co-ordinates of atoms obtained from the electron map. The agreement between the measured and calculated values of structure factors is considerably better as compared to those worked out with the structure obtained previously. The differences in the measured structure factors of certain pairs of hko and hko planes (arising from the observed differences in the intensities of their reflections) were found to be in very good agreement with the calculated values of structure factors obtained from the final structure. It is, therefore, worth noting that the final structure, owing to its slight deviation from the orthorhombic symmetries, have accounted for the observed differences of intensities between pairs of hko and $h\bar{k}o$ planes, which previously was thought to be spurious.

In conclusion I wish to express my sincere thanks to Prof. S. N. Bose for his keen interest in this work and to Prof. K. Banerjee for suggesting the problem and advice during the progress of the work.

METEOROLOGICAL OBSERVATORY,
ALIPORE.

REFERENCES

Banerjee, K. and Sen, S. N. (1938), *Science and Culture*, **3**, 570.
Sen, S. N. (1940), *Science and Culture*, **6**, 717